Bio-Based Dynamic Polymer Networks from Synthesis to Applications

Farhad Asempour

A thesis submitted in partial fulfillment of the requirements of the degree of

Doctor of Philosophy

Department of Chemical Engineering

McGill University

Montreal, Canada

August 2024

To my parents, ***Fatemeh*** *&* ***Mostafa***

for their endless love, unwavering support, and nourishing encouragement

Abstract

Plastic wastes and climate change pose significant challenges to our generation. Addressing these environmental concerns requires transitioning to a circular bio-economy and shifting away from conventional petroleum-based polymers to highly recyclable bio-based alternatives. In this doctoral thesis, novel bio-derived and reprocessable covalent adaptable networks (CANs) were developed. In the past decade, vitrimers, specifically associative CANs, have rapidly emerged as a new class of cross-linked networks bridging the gap between classical thermosets and thermoplastics.

In the first part of this doctoral work, rubbery vitrimers were synthesized utilizing β-myrcene, a commercially available plant-based monoterpene. Nitroxide mediated polymerization (NMP) of myrcene with (2-acetoacetoxy)ethyl methacrylate (AAEMA) yielding linear precursors was thoroughly examined. The β-ketoester functionality of AAEMA upon treatment with various di and tri-functional amines formed dynamic networks of vinylogous urethanes. The resulting rubbers exhibited weldability and excellent reprocessability. Furthermore, our approach of decoupling the networks' backbone structure and cross-linkers, allowed high tunability of the vitrimers' mechanical and rheological properties by adjusting prepolymer composition, molecular weight, cross-linkers and cross-linking density. It was demonstrated that combining vitrimer chemistry with myrcene is a facile and inexpensive, yet highly versatile method to modulate and compensate for the poorer mechanical properties of such brush-like terpene-based elastomers. In addition, shape memory effects were imparted by careful design of the network architecture, and their shape recovery and shape reprogramming were optimized.

In the second part of this thesis, a series of prepolymers of lignin-based vanillin methacrylate (VMA) with a mixture of vegetable oil-derived alkyl methacrylate (C13MA) were synthesized as precursors to form imine-based vitrimers. Reversible addition fragmentation chain-transfer (RAFT) afforded precise control over microstructure of statistical, di and tri-block copolymers, together with molecular weight (segment length) and composition. The vitrimers showed excellent retention of their thermomechanical properties after at least 3× reprocessing cycles. Microphase separation was confirmed in the "hard-soft" type block vitrimers. Self-assembly enhanced the dimensional stability and creep resistance of the vitrimers. Our findings suggest that by controlling the chain topology in block copolymers and optimizing the order disorder transition, we can both enhance vitrimers' creep resistance and tune their mechanical strength.

The vitrimeric systems developed in this doctoral research offer a promising platform for further advancements in the field of recyclable bio-based rubbers with highly tunable rheo-mechanical properties and shape memory effect functionalities.

Résumé

Les déchets plastiques et le changement climatique posent des défis significatifs à notre génération. Pour aborder ces préoccupations environnementales il est nécessaire de passer à une bio-économie circulaire et de s'éloigner des polymères conventionnels à base de pétrole au profit d'alternatives bio-sourcées hautement recyclables. Dans cette thèse de doctorat, de nouveaux réseaux adaptables covalents (CAN pour covalent adaptable networks en anglais) dérivés de la biomasse ont été développés. Au cours de la dernière décennie, les vitrimères, en particulier les réseaux associatifs, ont rapidement émergé en tant que nouvelle classe de réseaux réticulés comblant le vide entre les thermodurcissables classiques et les thermoplastiques.

Dans la première partie de ce travail de doctorat, des vitrimères élastomériques ont été synthétisés en utilisant le myrcène, un monoterpène d'origine végétale disponible commercialement. La polymérisation NMP de l'anglais Nitroxide-Mediated Polymerization (Modulation de la réactivité des radicaux propagateurs par des contre-radicaux nitroxydes) a été utilisé pour synthétiser différents polymères.La polymérisation de précurseurs linéaires de myrcène avec du méthacrylate de (2-acétoacétoxy)éthyle (AAEMA), a notamment été minutieusement examinée. La fonctionnalité β-cétoester de l'AAEMA peut régir avec diverses amines di et tri-fonctionnelles pour former des réseaux dynamiques d'uréthanes vinylogues. Les caoutchoucs obtenus présentaient une soudabilité et pouvait être usiné plusieurs fois sans pertes de propriétés. De plus, en jouant sur la structure du squelette des polymères et sur les agents de réticulation, nous avons puadapter les propriétés mécaniques et rhéologiques des vitrimères. En effet, en ajustant la composition des prépolymères, le poids moléculaire, les agents de réticulation et la densité de réticulation différentes propriétés ont ainsi pu être atteintes.Il a été démontré que l'association de la chimie des vitrimères avec le myrcène est une méthode facile, peu coûteuse ettrès polyvalente pour moduler et compenser les propriétés mécaniques moins bonnes des élastomères à base de terpènes en forme de brosse. De plus, des effets de mémoire de forme ont été conférés par une conception minutieuse de l'architecture du réseau. Leur récupération et leur reprogrammation de forme ont aussi été optimisées.

Dans la deuxième partie de cette thèse, une série de prépolymères à base de lignine de méthacrylate de vanilline (VMA) mélangés à du méthacrylate d'alkyle dérivé d'huile végétale (C13MA) ont été synthétisés en tant que précurseurs pour former des vitrimères à base d'imines. La réaction de

transfert de chaîne par fragmentation d'addition réversible (RAFT) a permis un contrôle précis de la microstructure des copolymères statistiques, di et tri-blocs, ainsi que du poids moléculaire (longueur de segment) et de la composition. Les vitrimères ont montré une excellente rétention de leurs propriétés thermomécaniques après au moins 3 cycles de ré-usinage. La séparation de phase microscopique de type "dur-mou" a été confirmée dans les vitrimères. L'auto-assemblage a amélioré la stabilité dimensionnelle et la résistance au fluage des vitrimères. Nos résultats suggèrent qu'en contrôlant la topologie de la chaîne dans les copolymères à blocs et en optimisant la transition ordre-désordre, nous pouvons à la fois améliorer la résistance au fluage des vitrimères et ajuster leur résistance mécanique. Les systèmes vitrimériques développés dans cette recherche doctorale offrent une plateforme prometteuse pour de nouvelles avancées dans le domaine des caoutchoucs recyclables à base de biomasse, dotés de propriétés rhéo-mécaniques hautement adaptables et d'effets de mémoire de forme.

Acknowledgments

I consider it a blessing that so many people in my life have supported me throughout my doctoral studies and made it possible for me to enjoy every step of the way.

I would like to express my sincere gratitude to my supervisor, Prof. Milan Maric, for introducing me to the fascinating word of controlled radical polymerization and sustainable polymers. I am grateful for his unwavering professionalism, patience, and guidance throughout my studies. Thank you for putting up with all the late-night emails and thank you for your prompt, early-next-day morning replies! I would like to thank Prof. Craig Hawker for his supervision and supporting my research on degradable bio-polymers at the University of California Santa Barbara. Also, special thanks to Profs. Christopher Bates and Javier Read de Alaniz for their invaluable contributions.

I thank all the funding agencies, including NSERC, FRQNT, and Mitacs, who enabled this work.

Many thanks to my great friends and collaborators in the research group. To Sharmaine Luk and Matt Halloran for their great friendship and supporting me at the beginning of my research works. To Eline Laurent and Yvan Ecochard, for our fruitful collaborations both in the lab and on the hiking trails! Masa Alrefai, Ruixuan Yang, Faezeh Hajiali, and Saeid Tajbakhsh, sharing an office with you and working along you has been an absolute pleasure. To Adrien Métafiot, Georges Younes, Ching Yang Du, Mary Hnatyshyn and Theo Bride, thank you for consistent humor and work ethic.

To my humorous and all together wonderful compatriots Phil Cimento, Dante Filice, and Lynn Hein, thank you for your invaluable friendship! Here's to many more late-night (sometimes afternoon) adventures at Thomson House! Special thanks to Joey Kim for her wonderful friendship and support during the COVID-19 pandemic!

I want to express my deepest love and appreciation to my family both here in Canada and at home. Thank you, Aunt Sedi, for making Montreal feel like home and thank you my dear sister Ladan for being always there for me!

Finally, to my beloved parents, thank you for your unconditional love and continuous encouragement, you are my anchor!

Thank you all from the bottom of my heart!

Table of Contents

List of Figures

List of Tables

List of schematics

Abbreviations

Acronym/symbol	Definition
AAEMA	(2- acetoacetoxy) ethyl methacrylate
AIBN	Azobisisobutyronitrile
AMS	α-Methyl-p-methylstyrene
ATRP	Atom transfer radical polymerization
BB	BlocBuilder-MA
BPO	Benzyl peroxide
CDCl3	Deuterated chloroform
CEF	Chain-end functionality
CRP	Controlled radical polymerization
CTA	Chain transfer agent
C13MA	13 carbons long methacrylic ester
DMF	Dimethylformamide
DMTA	Dynamic mechanical thermal analysis
DP	Degree of polymerization
DSC	Differential scanning calorimetry
EtOH	Ethanol
FRP	Free radical polymerization
f_i	Monomer composition of i
F_i	Polymer composition of i
G′	Shear storage modulus
G″	Shear loss modulus
GMA	Glycidyl methacrylate
GPC	Gel permeation chromatography
IBOMA	Isobornyl methacrylate
k_c	Recombination rate constant
k_d	Dissociation rate constant
K_{eq}	Activation-deactivation equilibrium constant
k_p	Propagation rate coefficient
$[M]_0$	Concentration of monomer at t = 0
M_e	Entanglement molecular weight
MeOH	Methanol
MMA	Methyl methacrylate
M_n	Number-average molecular weight
$M_{n,\ target}$	Target molecular weight at 100% conversion
M_w	Weight-average molecular weight
Myr	β-Myrcene
NHS-BB	Succinimidyl-modified BlocBuilder
NMP	Nitroxide-mediated polymerization

NMR	Nuclear magnetic resonance
PRE	Persistent radical effect
PE	Polyethylene
RAFT	Reversible addition-fragmentation transfer
RDRP	Reversible deactivation radical polymerization
r_i	Relative reactivity of monomer i
SAXS	Small angle X-ray scattering
SBR	Styrene butadiene rubber
SBS	Poly(styrene-b-butadiene-b-styrene)
Sty	Styrene
SFRP	Stable free radical polymerisation
$T_{10\%}$	Decomposition temperature at 10% weight loss
T_g	Glass transition temperature
TEMPO	(2,2,6,6-tetramethyl-piperidin-1-yl)oxyl
TEMPS	(2,2,6,6-tetramethylpiperidin-1-yl)disulfide
TGA	Thermogravimetric analysis
THF	Tetrahydrofuran
T_{onset}	Onset decomposition temperature
Tol	Toluene
TPE	Thermoplastic elastomer
Tren	Tris(2-aminoethyl)amine
VMA	Vanillin methacrylate
VOC	Volatile organic compound
UV	Ultraviolet
X	Conversion
$Đ$	Dispersity (Mw/Mn)
$Tan(\delta)$	Damping factor (G″/G′)
E_a	Apparent activation energy
τ	stress relaxation time
χ	Flory-Huggins enthalpic interaction parameter
δ_i	Solubility parameter of monomer i

Contributions of authors

This thesis is presented in a manuscript-based format comprising 4 manuscripts where I, Farhad Asempour, am the first author and have done the majority of the work. In all cases, I did the main conceptualization of the research ideas, developed the methodology, formulated the polymers and vitrimers, and conducted most of the synthesis, characterization and interpretation of the results. In all cases, I wrote the majority of the manuscripts. Prof. Milan Maric is a coauthor and the principal investigator of all publications.

The list of coauthors and their help and contributions for each chapter are as follows.

Chapter 3

Milan Maric: supervision, data analysis, funding, writing review & editing.

Chapter 4

Ruixuan Yang: helping with polymer synthesis and analyzing the reactivity ratios.

Milan Maric: supervision, data analysis, funding, writing review & editing.

Chapter 5

Eline Laurent: synthesis of VMA and help with polymer synthesis, characterization, data collection, analysis, with writing, reviewing, and editing.

Yvan Ecochard: synthesis of VMA and its characterization.

Milan Maric: supervision, data analysis, funding, writing review & editing.

Chapter 6

Eline Laurent: synthesis of VMA and help with polymer synthesis, characterization, data collection, analysis, with writing, reviewing, and editing.

Theo Bride: helping with characterization and data collection.

Milan Maric: supervision, data analysis, funding, writing review & editing.

Chapter 1: Introduction and objectives

1.1. Motivation

The year 2020 marked an important milestone for polymer science. Almost 100 years ago, Hermann Staudinger published the very first article on the concept of macromolecules consisting of long chains of covalently linked building blocks [1]. Ever since, polymers have undergone exponential growth and tremendously impacted society, technology in generally positive ways, and the environment, more recently in negative ways. Plastics are vital materials in our modern way of life and economy [2,3] . Plastics increase fuel efficiency of cars, help cure disease, protect food, provide clean water, and enable renewable energy technologies [4]. Clearly to promote and enable a sustainable society we need plastics. On the other hand, the ubiquitous use of plastics has led to significant waste pollution and has become a global environmental priority. Many countries and municipalities, including Canada and Quebec have introduced ambitious "zero-plastic waste" policies to move towards a circular plastic economy [5,6]. Currently, about 8% of the total fossil oils are used for manufacturing and processing of polymers. By 2050, it is projected that this value will increase to as high as 20% with about 15% of the annual carbon emissions budget. There is a growing international momentum to enhance all stages of the plastics lifecycle from design, manufacture, use, recycling and end-of-life management. Unfortunately, only about 9-15% of plastics are presently recycled [7,8]. These statistics underscore the need to redesign polymers using renewable resources and more sustainable processes to enhance their recyclability and reduce their carbon footprint.

Utilizing plant-derived building blocks for production of polymers can be an attractive route to reduce our dependence on fossil-based plastics. An abundant supply of renewable carbon is embedded in bio-based macromolecules, including cellulose, and lignin, as well as in small molecules and monomers including vegetable oils and terpenes [4]. Nonetheless, the challenge persists in creating economically viable pathways to transform such resources into useful materials. It is particularly difficult for new bio-based materials to compete with well-established and financially amortized fossil-based polymers solely based on price [4,9]. To rival fossil-based polymers at scale, bio-based polymers need to demonstrate performance advantages in production, processing, physicochemical properties, and end-of-life considerations [9,10].

In this context, the emergence of dynamic networks and vitrimers in the past decade has offered new tools to enhance and modulate the properties of bio-based polymers. These new technologies not only overcome some of the mechanical shortcomings of bio-derived macromolecules, but also, they afford incorporation of advanced and "smart" functionalities, including self-healing, shape-memory, and improved recyclability into them [11].

1.2. Objectives

The main goal of this thesis is to tackle the aforementioned challenges through the development of novel dynamically networked polymers sourced from plant-based raw materials. These polymers are intended to have performance advantages of being recyclable (contrary to classical thermoset networks) and exhibit some "smart" functionalities. Furthermore, to comprehensively understand their rheological properties, the polymers will feature controlled molecular architectures, enabling systematic studies aimed at controlling processability and strain over time under stress (creep) at service conditions. The primary objectives are outlined as follows.

1. Enhance the thermomechanical properties of bio-based β-myrcene (myrcene or Myr) while ensuring its recyclability. Myrcene is a conjugated diene monomer derived from terpenes with a bottle brush-like structure. This objective will be achieved by employing nitroxide-mediated polymerization (NMP) to synthesize statistical copolymers of myrcene and β-ketoester functional (acetoacetoxy)ethyl methacrylate (AAEMA) as prepolymers. Bio-based cross-linkers will be utilized to fabricate dynamic and recyclable vinylogous urethane vitrimeric networks. The study will investigate the impact of factors such as molecular weight, cross-linking density, and hybrid static-dynamic cross-linking on the mechanical and rheological properties of the resulting vitrimers . **(Chapter 3)**
2. Investigate the copolymerization of myrcene and AAEMA across various feed ratios to analyze how feed composition influences the final copolymer composition and properties of the vitrimers. Synthesize myrcene/AAEMA copolymers with controlled microstructures of random, alternating, and block types. Additionally, explore copolymerization with styrene to modulate thermomechanical properties of the terpolymer. The aim is to impart programmable shape memory effect while retaining recyclability. **(Chapter 4)**
3. Investigate alternative chemistries with superior control over the polymer microstructure. The novel copolymers will be synthesized using methacrylated bio-based monomers such as

C13MA, which contains a long olefin side chain and offers flexibility, in combination with vanillin methacrylate (VMA), which offers hardness and aldehyde-functionality for further dynamic cross-linking. Employ reversible addition−fragmentation chain-transfer (RAFT) polymerization for precise control of molecular architecture to synthesize block copolymers and terpolymers containing epoxy functionality. Fabricate vitrimers based on imine exchange chemistry. Control rheological properties of the resulting vitrimers through microphase separation and hybrid static-dynamic networks. Impart temperature triggered programmable shape memory effect. All the mentioned works will be done while maintaining high reprocessability **(Chapter 5)**.

4. Utilize RAFT polymerization to synthesize statistical, and "soft-hard" type diblock, and triblock terpolymers consisting of methyl methacrylate (MMA), C13MA and VMA; more specifically to fabricate poly[(MMA)-*block*-(C13MA-co-VMA)] and poly[(MMA)-*block*-(C13MA-co-VMA)-*block*-(MMA)]. The prepolymers will be dynamically cross-linked using aldehyde/amine (imine exchanges) chemistry. The integration of block copolymer architecture aims to facilitate microphase separation. This allows for the application of thermoplastic elastomers with vitrimers which compensates for the comparatively high entanglement molecular weight (M_e) of poly(C13MA) and enables the investigation of their impact on the rheological and tensile properties of the resulting vitrimers. **(Chapter 6)**

Chapter 2: Literature review

2.1. Preamble to Chapter 2

In this chapter, the polymerization techniques employed in this thesis are examined. To gain a deeper understanding of such controlled polymerizations, their historical context, practical applications, strengths, and limitations are reviewed. Additionally, dynamic networks are briefly explored, emphasizing their distinctions from classical thermosets and a wide range of available chemistries for their synthesis.

2.2. Chain polymerization

Polymerization is the process of joining many (~ few tens to thousands of) small molecules by covalent bonds to produce high molecular weight macromolecules. In general, polymerization methods can be generally categorized in two methods: step (sometimes called condensation polymerization) and chain polymerization [12]. Chain growth polymerization involves repeated addition of monomer units in a chain reaction. In this method monomers have a similar and single reactive function per unit; the reactive chain site can be a cation, anion, or a radical [12,13]. In this work, chain reactions were mostly utilized; thus, we review them in this chapter.

2.2.1. Free radical polymerization (FRP)

The most prevalent method of chain polymerization is free radical polymerization (FRP). Many of the commodity polymers that we use in everyday life, including polystyrene, polyethylene, polypropylene, and polyvinyl chloride are synthesized using FRP [14]. The name and concept of FRP was first reported in the literature by Paul Flory in the 1930s [15]. Flory received the Nobel Prize in Chemistry in 1974 "for his fundamental achievements both theoretical and experimental, in the physical chemistry of macromolecules". FRP, from an industrial perspective, is versatile as it can be carried out under relatively undemanding conditions; it is inexpensive and simple to carry out. FRP is tolerant towards impurities, that is, high molecular weight polymers can be often produced without removal of the stabilizers present in commercial monomers, in the presence of trace amounts of oxygen, or in solvents that have not been rigorously dried or purified [16]. FRP can be applied to a wide range of vinyl-containing (-CH=CH_2) monomers including styrenics, (meth)acrylates, (meth)acrylamides, acrylonitrile, dienes, and is tolerant of unprotected functionalities. Also, a range of reaction conditions and solvents including bulk, solution, suspension, emulsion, and homogeneous aqueous media are commonly applied to FRP [14,17].

These advantages make conventional free radical, alongside Ziegler-Natta catalyzed polymerization for polyolefins, the most widely used industrial methods [14,17].

FRP consists of a sequence of reactions: initiation, propagation, chain transfer, and termination. The initiation step is considered to involve two steps. First, the production of free radicals, usually a homolytic dissociation of an initiator species, by thermal decomposition or radiation, which yields a pair of radicals (R·). Second, addition of a monomer molecule to the formed radical is done to yield a chain initiating radical (M·). Propagation reactions consist of growth of the M· by the successive and repetitive addition of a high number of monomer molecules. In general, the propagation and growth of the chain to high degrees of polymerization takes place very rapidly. Values of the propagation rate constant (k_p) for most monomers are of the order of 10^2 - 10^3 L/mol·s which are much higher than those usually encountered in step polymerization. Besides monomer addition, radicals can undergo other reactions such as chain transfer and inhibition. Chain transfer can occur between radical chains and many other species such as monomers, initiator, solvent, and polymer, causing branching and backbiting reactions. Dissolved oxygen in the polymerization system can often act as inhibitor by reacting with radicals and forming stable species. For this reason, FRP is often carried out under inert atmosphere [12]. At some point, a propagating polymer chain stops growing and terminates, forming "dead" chains. Termination occurs by mutual annihilation of two radical centers. Two radicals react with each other by combination or, more rarely, by disproportionation, and often a mixture of the two happens [16].

Despite the practicality and scalability of conventional FRP, it also possesses significant drawbacks. The most important disadvantage is the inability to regulate the molecular weight, the architecture, and the topology of the resulting polymers. This led to the development of living polymerization methods.

2.2.2. Living polymerization

Termination and chain transfer are always present in radical polymerization which limit the lifetime of propagating radicals. Chain polymerizations without chain-breaking reactions are referred to as "*living*" polymerizations. In living polymerization, active sites are not lost and will continue to propagate if monomer is present, and no impurities are introduced to terminate the active center. In FRP molecular architecture is dictated by the statistics of initiation, propagation, and termination which often yields a broad molecular weight distribution, and considerable

differences in chain-to-chain compositional homogeneity (in statistical copolymerization). In contrast, in living polymerization, architecture is controlled much better [12]. This affords production of polymers with narrow molar mass distributions, i.e. low dispersity $Đ = M_w/M_n < 1.1$, (a measure of the breadth of the molecular weight distribution) and a linear increase of the number-average molar mass (M_n), with monomer conversion [13]. Furthermore, living polymerization gives access to block copolymers that can be synthesized by polymerizing different monomers in sequence [12,13] . Thus, living polymerization is important in the synthesis of well-defined homopolymers and copolymers. Living polymerization was discovered by Szwarc in 1956 when he reported the polymerization of styrene via an anionic active center in the presence of sodium naphthalene [16,18]. His work opened an avenue to produce well-defined polymers and nano-structured morphologies which are considered foundational to modern nanotechnology [19]. Nevertheless, to fully prevent termination and achieve a highly living polymerization, stringent reaction conditions, specialized equipment, and rigorous purification of reagents with minimal traces (<1 ppm) of moisture and air are required. This makes the synthesis more costly, although anionic polymerization was quickly adapted on an industrial scale [13,20,21]. This has led to mass production of several commercial products such as block copolymer-based thermoplastic elastomers (e.g. Kraton) [19]. The high cost and exacting reaction conditions of anionic polymerization led to the development of living/ controlled radical polymerization (CRP) also more formally known as reversible deactivation radical polymerization (RDRP), which would mimic the features of living polymerizations with the tolerance to impurities afforded with FRP.

2.2.3. Reversible deactivation radical polymerization (RDRP)

The field of chain polymerization was revolutionized in the 1990s by the development of RDRP which allows better control over molecular weight, architecture, and chain functionality compared to conventional FRP. As mentioned before, the average life span of a propagating radical chain in FRP is very short (~ 0.1 to 1s) before termination, which is too short for any synthetic manipulation [19]. By extending the life of a propagating radical, a more living nature of the active center can be accomplished. This is achieved in RDRP by temporary protecting and deactivating (capping) the radicals to suppress termination i.e., *"dead"* chains, although it cannot be fully stopped. A dynamic equilibrium between propagating radicals and dormant species is established which is fundamental to all RDRP methods. In such systems, radicals can either be reversibly trapped in a deactivation/ activation equilibrium or they can be involved in a reversible *degenerative transfer*

exchange process, shown in **Figure 2.1**. IUPAC's definition of reversible chain deactivation is "deactivation of a chain carrier in a chain polymerization, reversibly converting an active center into an inactive one and then, within the average lifetime of a growing macromolecule, regenerating an active center on the same original carrier" [22].

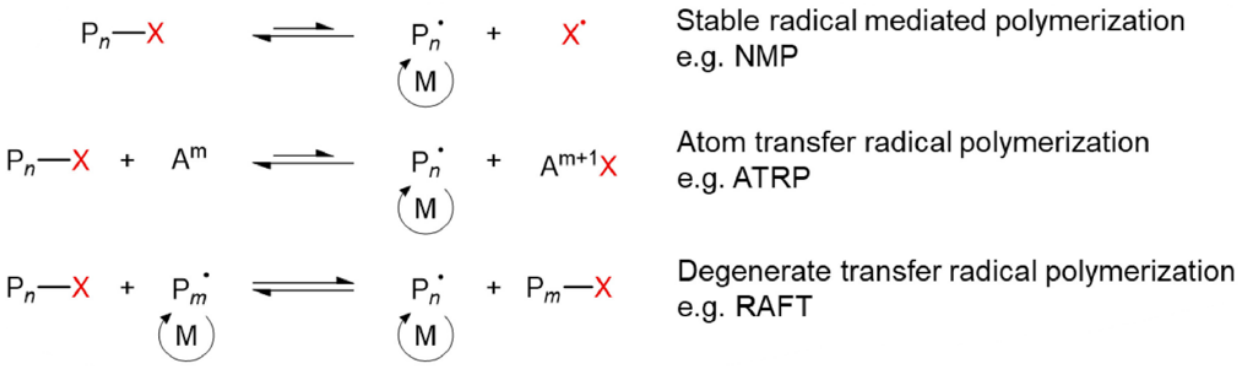

Figure 2.1 General mechanism of RDRP methods Pn•: propagating radical species, Pn-X: dormant capped polymer chains. Reprinted from [23]

As discussed by Matyjaszewski, there are three primary requirements for obtaining a highly living radical polymerization capable of a uniform molecular weight growth: (1) fast initiation relative to chain growth, that is rate of initiation >> rate of polymerization (2) low radical concentration compared to chain concentration, and (3) the on/off equilibrium between active and dormant species must be fast [24]. In a successful RDRP a linear relationship between polymer molecular weight and monomer conversion is obtained which is a direct result of high end-group fidelity [23]. It is noteworthy that the lifetime of a propagating radical in the active state in a RDRP process is comparable to the lifespan of a growing chain in FRP. However, since the whole propagation process may take up to ~1 day, various synthetic procedures, including chain-end functionalization or chain extension can be carried out [19,25]. **Figure 2.2** summarizes the benefits and characteristics of successful RDRP.

Controlled/living radical polymerization techniques can be broadly categorized into three distinct chemical mechanisms, as illustrated in **Figure 2.1**: (1) stable free radical-mediated polymerization (SFRP) which includes nitroxide mediated polymerization (NMP), (2) atom transfer radical polymerization (ATRP), and (3) degenerative- transfer radical polymerization including reversible addition-fragmentation chain transfer (RAFT) polymerization. The first two operate via a reversible termination mechanism, while RAFT relies on reversible chain transfer. In recent years,

ATRP and RAFT have generally emerged as the two most used RDRP techniques, both in scientific literature and industrial implementation [23]. However, NMP has recently improved its applicability to polymerize a wider range of monomers, while shortcomings in post-polymerization purification encountered by ATRP and RAFT have been addressed. In this thesis, NMP and RAFT polymerization were utilized for the synthesis of linear homo-, co-, and block-polymers; thus, we will examine these techniques in more detail here.

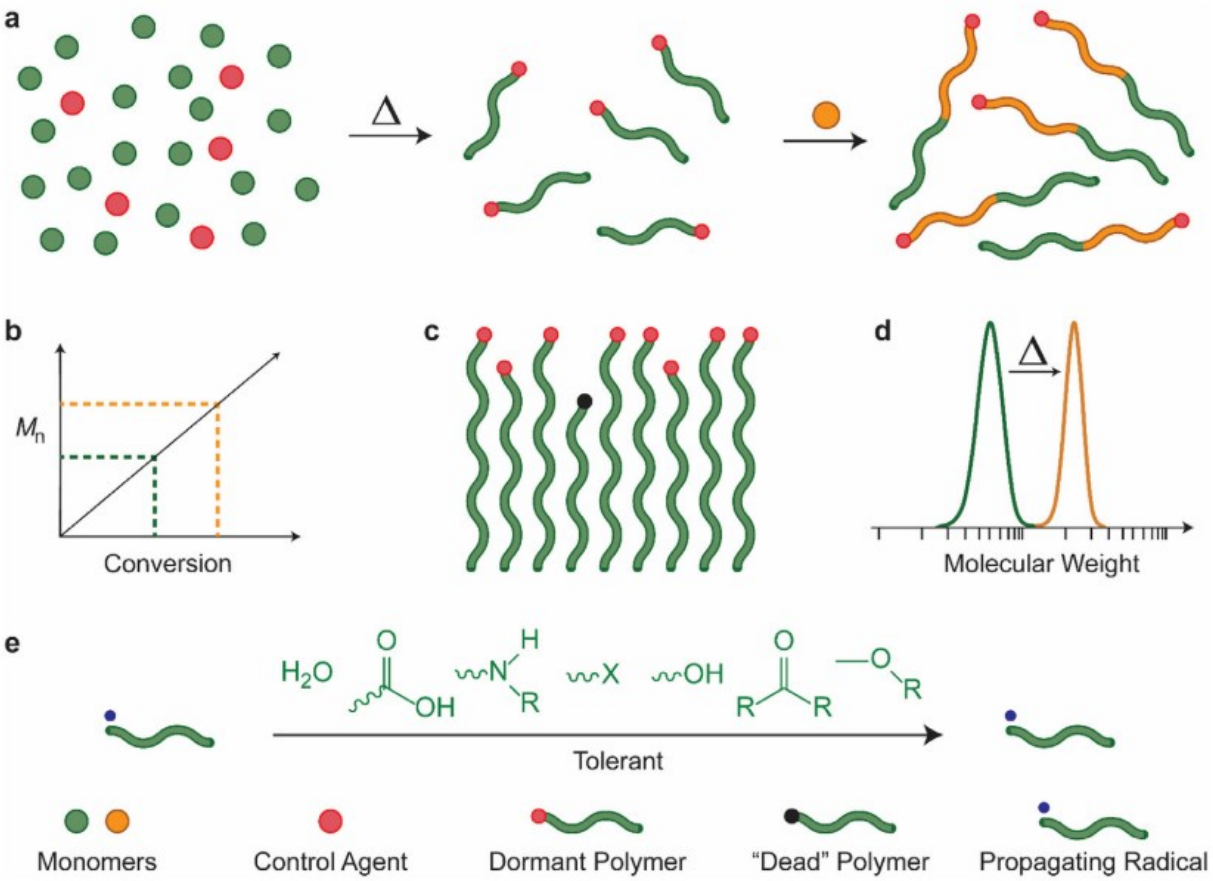

Figure 2.2 Capabilities of RDRP a) production of diblock copolymers; b) predictable molecular weight through linear relationship between monomer conversion and number average molecular weight (M_n); c) even chain length distributions and low $Đ$ <1.5; d) narrow molecular weight distributions and the complete shift in molecular weight upon chain extensions; e) high tolerance towards various functional groups. Reprinted from [23].

2.2.4. Nitroxide mediated polymerization (NMP)

In an SFRP process, the persistent radicals can undergo reversible termination (deactivation) without initiating a chain reaction themselves (mostly due to steric hindrance) [26]. Various stable

radicals have been reported as mediators (deactivator) in SFRP including verdazyl, substituted triphenyls, (arylazo)oxy, triazonilyn and nitroxides [16,26,27]. Nitroxides and their associated alkylated derivatives, known as alkoxyamines, are more successful in mediating polymerizations. **Figure 2.3** shows homolysis of an alkoxyamine producing a highly reactive radical and one stable nitroxide radical.

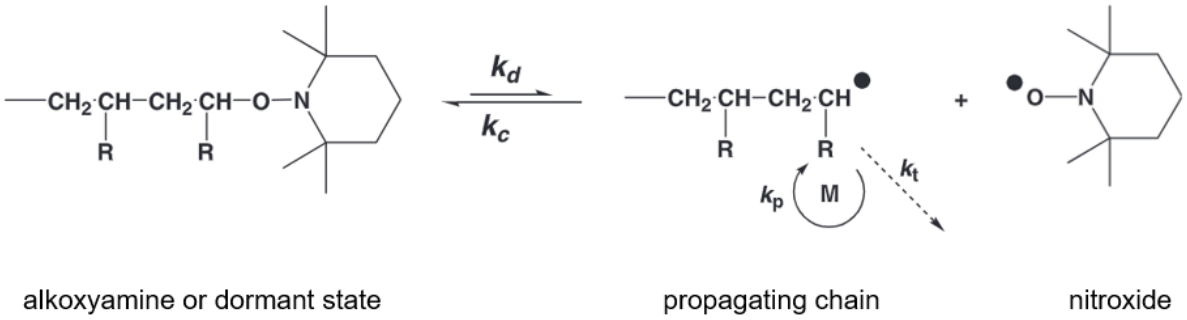

Figure 2.3 Dynamic equilibrium between propagating chain and dormant alkoxyamine. Homolysis of the alkoxyamine produces a reactive radical and a stable nitroxide radical, TEMPO in this case. Here, k_d stands for dissociation, k_c for combination, k_p for propagation, and k_t for irreversible bimolecular termination rate constants.

NMP is commonly considered to be historically the first reported RDRP method. The use of nitroxides as mediators was patented by Solomon and Rizzardo in 1986 at *Commonwealth Scientific and Industrial Research Organisation (CSIRO)* in Australia [28] . However, the major breakthrough took place in 1993 when Georges at al., at the *Xerox Research Center Canada* in Mississauga, Ontario reported a successful polymerization of styrene using benzoyl peroxide (BPO) as the initiator and 2,2,6,6-tetramethyl-l-piperidinyloxy (TEMPO) as the stable radical nitroxide with low $Đ < 1.3$ and M_n up to 150,000 g/mol [29]. Later, Fischer showed that the kinetics of NMP is based on the persistent radical effect, which served as the foundation for future development of polymerization kinetic models [30]. Accordingly, the NMP equilibrium constant ($K_{NMP} = k_d/k_c$), conversion profile via concentration of initial and instantaneous monomers ($[M]_0$ and $[M]_t$ respectively) and degree of polymerization ($\overline{DP}$) can be estimated as follows. Equation 3 can be used to design an ideal NMP reaction and targeting a certain molecular weight. Here $[M\cdot]$ is the concentration of radicals, $[\cdot ONR_1R_2]$ is the concentration of the stable nitroxide, and $[P\text{-}ONR_1R_2]$ is the concentration of the alkoxyamine or dormant polymer chain, and p is the conversion.

$$K_{NMP} = \frac{[M\cdot]\,[\cdot\ ONR_1R_2]}{[P-ONR_1R_2]} \qquad \text{(eq 1)}$$

$$ln\ \frac{[M]_0}{[M]_t} = \frac{3\,k_p}{2}\left(\frac{K_{NMP}\ [P-ONR_1R_2]_0}{3k_t}\right)^{1/3} t^{2/3} \qquad (eq\ 2)$$

$$\overline{DP} = \frac{p\,[M]_0}{[P-ONR_1R_2]_0} \qquad (eq\ 3)$$

Figure 2.4 shows the structures of some common alkoxyamine mediators for NMP. TEMPO forms relatively strong covalent bonds in alkoxyamines. Thus, it requires high temperatures for effective polymerization, for example, 120 °C for styrene [19]. Also, TEMPO-based NMP is restricted to the polymerization of styrenics [31]. In the past two decades, other nitroxides have been developed with more labile C–ON bonds which have greatly expanded the range of monomers to which NMP can be successfully applied. Bulkier nitroxides can decrease the dissociation energy of C–ON bonds formed during polymerization and require lower polymerization temperatures. Two such nitroxides are 2,2,5-trimethyl-4-phenyl-3- 10 azahexane-N-oxyl (TIPNO or so-called *universal*) developed by Hawker and coworkers [27], and N-tert-butyl-N-[1-diethylphosphono-(2,2-dimethylpropyl)] or so called SG1 (initials of Sandra Grimaldi) developed by Grimaldi, Gnanou, and Tordo and others [32,33]. TIPNO and SG1-based alkoxyamines have enabled the homopolymerization of acrylates, acrylamides, dienes, and are available commercially. MAMA-SG1, marketed with the trademark name of *BlocBuilder-MA* by Arkema (2-([tert-butyl[1- (diethoxyphosphoryl)-2,2-dimethylpropyl]amino]oxy)-2-methylpropionic acid) is one of the most successful alkoxyamines allowing polymerization reactions at temperatures as low as 71 °C [34].

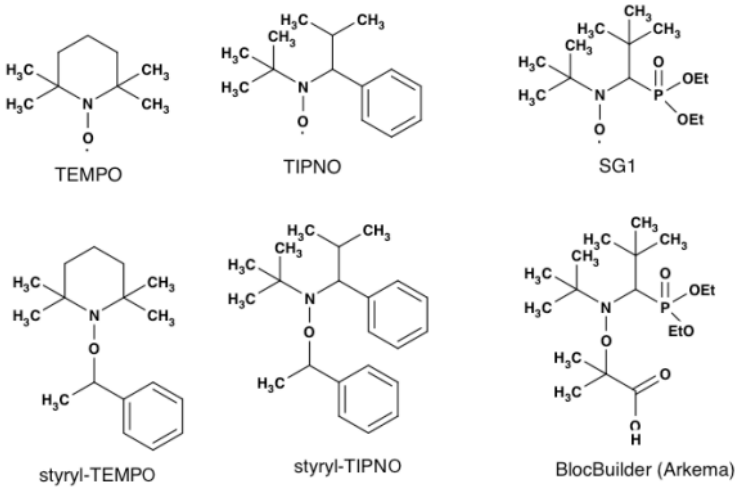

Figure 2.4 Structures of some common alkoxyamine mediator for NMP [34,35]

NMP can be initiated in two different methods. Conventional radical initiators can be used in the presence of the persistent radicals (nitroxides), or alternatively, by dormant (alkoxyamine) species, such as in BlocBuilder, which can be prepared in advance and used as both initiators and mediator, so-called unimolecular initiators, or macroinitiators for block copolymerization. In general, these well-defined unimolecular initiators afford much better control over polymer molecular weight and architecture than the aforementioned nitroxide persistent radicals used separately and in conjunction with the free radical initiators. Until 2008, NMP of methacrylates (an important group of monomers industrially) remained a challenge due to cross-disproportionation and a high activation-deactivation equilibrium constant (K). Charleux et al. reported a simple method to circumvent this limitation and effectively control SG1-based NMP of methacrylates by using 5-10 mol% of a comonomer with low K such as styrene or acrylonitrile to reduce the overall K of the polymerization [36]. In 2016, Asua's group reported successful nitroxide mediated homopolymerization of methacrylates by using a new class of alkoxyamine called 3-(((2-cyanopropan-2-yl)oxy)(cyclohexyl)amino)-2,2-dimethyl-3-phenylpropanenitrile (the so called Dispolreg) [37]. They reported an efficient NMP of methyl methacrylate with relatively narrow molecular weight distributions and a good retention of reactive chain ends capable undergoing chain extension [38–41]. These advances in NMP are the subject of many excellent reviews [31,34,42].

2.2.5. Reversible Addition Fragmentation Chain Transfer (RAFT) Polymerization

RAFT polymerization was first developed at the Commonwealth Scientific and Industrial Research Organization (CSIRO) Australia in 1998 by Moad, Rizzardo and Thang [43] . In the past 25 years, RAFT has rapidly grown to a versatile and powerful polymerization technique for the synthesis of complex polymeric architectures [21,23,44,45]. One of the main advantages of RAFT is its compatibility with most monomers capable of undergoing radical polymerization and good tolerance of functional groups [44,46]. More recently and with lapsing of the foundation patents, a range of versatile RAFT agents are commercially available rendering RAFT more industrially relevant [47].

In a degenerative transfer-type polymerization system, there is no change in the overall number of radicals during the activation−deactivation process. Therefore, a source of radicals is required; typically, conventional radical initiators such as peroxides and diazenes or photo induced initiators

are utilized [46,48,49]. The initiation, propagation, and termination steps in RAFT occurs similarly to conventional radical polymerization [50]. **Figure 2.5** shows the mechanism of RAFT polymerization. First, radical species are added to the system via initiation. Afterwards, the active centers are added to the RAFT agents, which are essentially chain transfer agents (CTA) [46]. This is followed by addition of propagating macroradicals to the CTA (often via carbon sulfur-double bond) to enter equilibrium between active ($P_n\cdot$ and $P_m\cdot$) and dormant species (R-X, P_n-X, P_m-X, where X is the thiocarbonylthio CTA). In an effective and well-controlled RAFT polymerization, equilibration between the active and dormant polymer is so rapid that ensures all chains possess an equal chance for growth [35,40]. This process makes all chains continue to grow, albeit intermittently, so all chains will essentially have a similar degree of polymerization (DP) at a given time and provide low dispersity ($Đ = M_w/M_n$) [46,50].

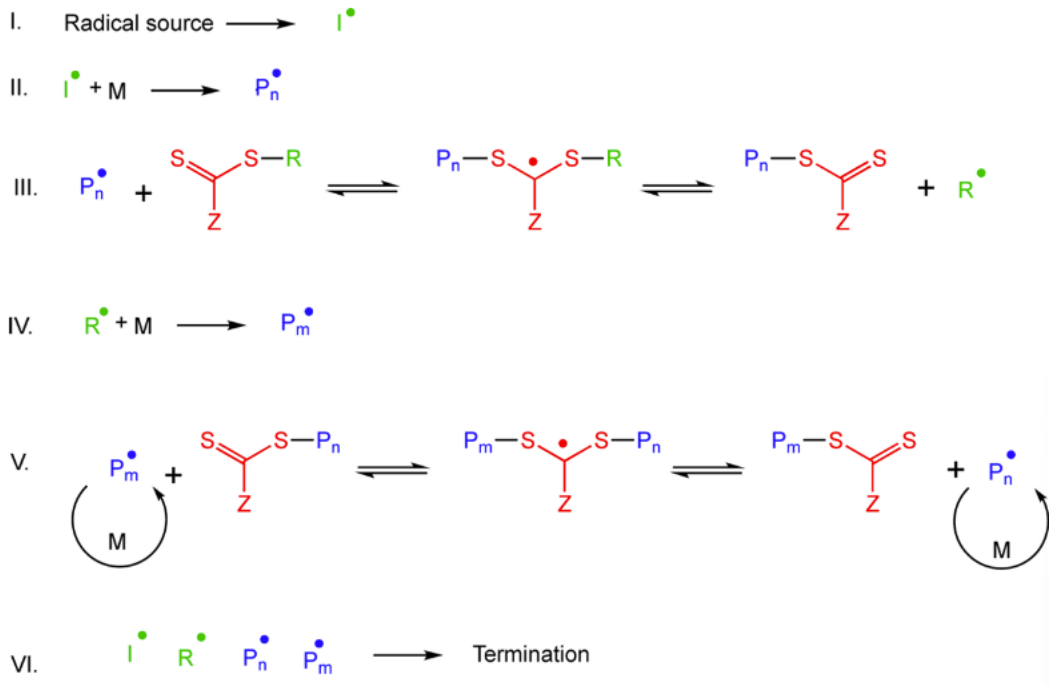

Figure 2.5 Generic mechanism of a RAFT polymerization, adapted from [46].

The molar mass of the polymer synthesized by the RAFT method can be estimated using the simple following relationship.

$$M_{n,theory} = \frac{p[M]_0}{[CTA]} M_M + M_{CTA} \qquad (eq.4)$$

Here, p is monomer conversion, $[M]_0$ and [CTA] are the concentration of the consumed monomer, and chain transfer agent (CTA) while M_M and M_{CTA} are the molar masses of the monomer and the CTA respectively [46].

Monomers and CTAs in RAFT

Monomers in RAFT polymerization are generally categorized into two groups: "more activated monomers' (MAMs) and "less activated monomers" (LAMs). In MAMs, the vinyl (double bond) group is conjugated to aromatic rings (e.g., styrene), or a carbonyl group (e.g., methacrylates, acrylates, acrylamides, N-acryloyl morpholine, maleic anhydride), or a nitrile (e.g., acrylonitrile) [51]. LAMs on the other hand, have the double bond adjacent to oxygen, nitrogen, halogen, sulfur lone pairs, or saturated carbons such as in vinyl acetate, N-vinylpyrrolidone, vinylchloride, 1-alkenes [46].Vast majority of RAFT literature, including the current thesis, is focused on the polymerization of acrylates, methacrylates, and styrenics (MAMs) [46].

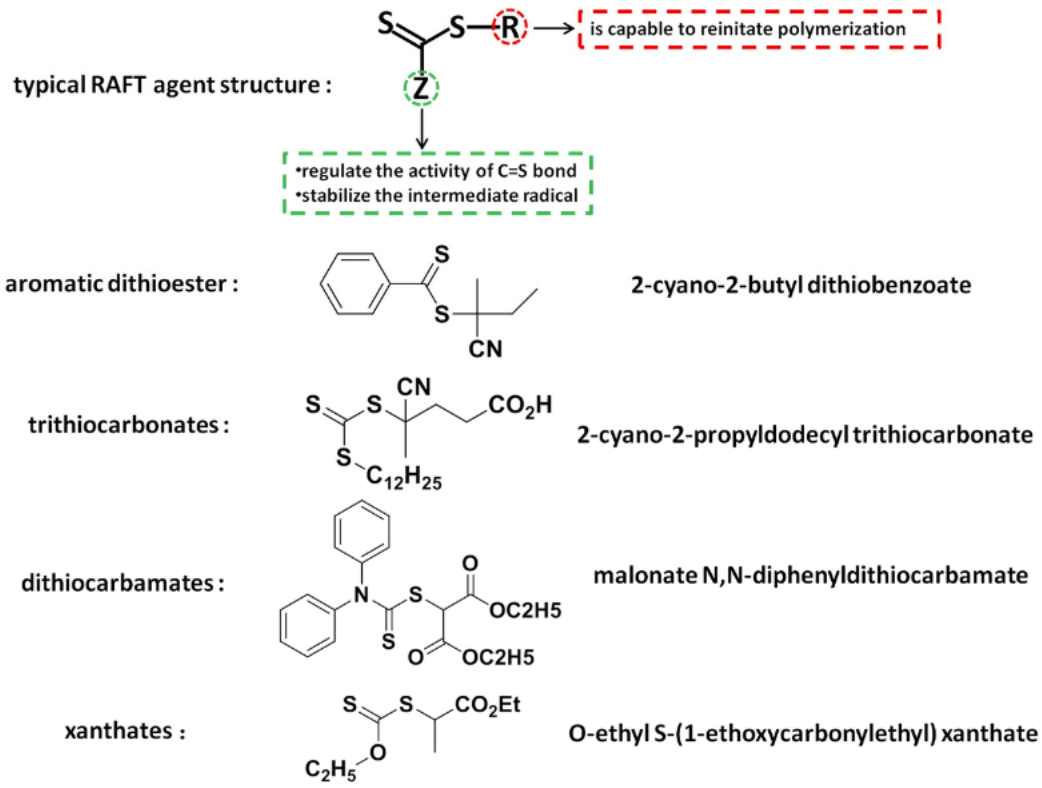

Figure 2.6 Four different generic types of common CTAs for MAMs and LAMs, copied from [52].

As shown in **Figure 2.6**, the activity of the C=S group in CTAs plays a key role regulating the polymerization process. To ensure a successful RAFT polymerization, the C=S bond of the CTA must be more reactive to radical addition than the C=C bond of the monomer. This is achieved by careful selection of the Z- and R-group of the CTA. The Z-group is mostly responsible for regulating the reactivity of the C=S bond toward radical addition and for stabilization of the intermediate radical [52]. On the other hand, the R-group should be excellent at leaving the CTA when the C=S bond of RAFT agent undergoes the addition of propagating radical, and it also must reinitiate polymerization rapidly and efficiently [53]. In other words, the leaving R-group should have same function and efficiency with the initiator and monomer radical [52]. In general CTAs can be categorized into dithiobenzoates, trithiocarbonates both of which are suitable for MAMs and xanthates and dithiocarbamates which are mostly used for LAMs and can provide relative control over MAMs [46,53,54].

Table 2.1 List of commonly used RAFT CTA with their suitability for various monomer types selected by Moad and Rizzardo. **A**: excellent control of molecular weight with low dispersity **B:** excellent control of molecular weight with moderate dispersity **C:** good control of molecular weight with high dispersity ($Đ$ >1.3), and **X**: not suitable [51,53].

	Styrenes	Acrylate	Methacrylates	Acrylamides	Methacrylamides	Vinyl esters	Vinyl amides
	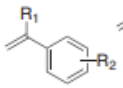	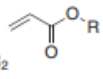	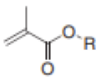	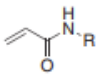	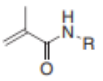	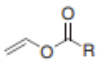	
RAFT agent							
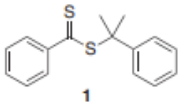 1	**A**	**A**	**A**	**A**	**A**	**X**	**X**
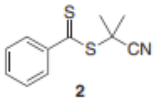 2	**A**	**A**	**A**	**A**	**A**	**X**	**X**
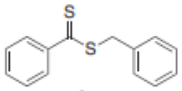 3	**B**	**B**	**X**	**B**	**X**	**X**	**X**
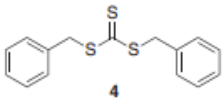 4	**B**	**B**	**X**	**B**	**X**	**X**	**X**
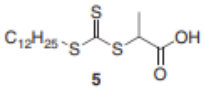 5	**B**	**B**	**X**	**B**	**X**	**X**	**X**
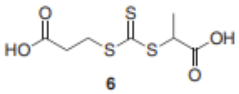 6	**B**	**B**	**X**	**B**	**X**	**X**	**X**
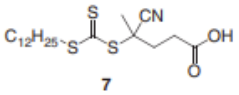 7	**A**	**A**	**A**	**A**	**A**	**X**	**X**
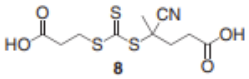 8	**A**	**A**	**A**	**A**	**A**	**X**	**X**
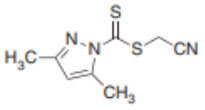 9	**A**	**A**	**X**	**A**	**X**	**B**	**B**

2.3. Covalent Adaptable Networks and Vitrimers

Polymeric materials are traditionally categorized into two primary classes: thermosets and thermoplastics, according to their thermal characteristics [55]. Thermosets, as the name implies, are permanent, insoluble, and predominantly inert polymer networks of covalent crosslinks. These

properties render them well-suited for a wide array of high-temperature, structural, or composite applications, spanning from wind turbine blades to adhesives [56]. Due to their permanent networked molecular architecture, thermosets, when fully cured, are physically and chemically stable and cannot be reshaped, processed, or recycled [55]. In contrast, thermoplastics can flow upon heating, which affords multiple and easy processing, such as by extrusion, as well as recycling [55,57]. The distinction between thermosets and thermoplastics blurs when the covalent cross-linking bonds in thermosets become dynamically reversible. If there are enough reversible bonds in the network, it can be rearranged, providing a molecular-level mechanism for macroscopic flow without risking structural damage [55,58,59]. This practically eliminates the barrier to reprocessing or reshaping of thermosets [60]. Such polymer networks containing exchangeable bonds are known as covalent adaptable networks (CANs) a term coined by Kloxin and Bowman [56]. CANs may be also divided into two subcategories of associative and dissociative networks based on the nature of the exchange mechanism of the dynamic covalent bonds [58]. In the dissociative cross-link exchange mechanism, chemical bonds are first broken and then reformed again at another place. Hence, the polymer network experiences a sudden reduction in cross-linking density between states, resulting in a viscosity drop, rapid topology rearrangements, and stress relaxation [56,58,61]. A prime example of such dissociative reversible chemistry is the Diels–Alder reaction between furans and maleimides, as shown in **Figure 2.7** [62,63].

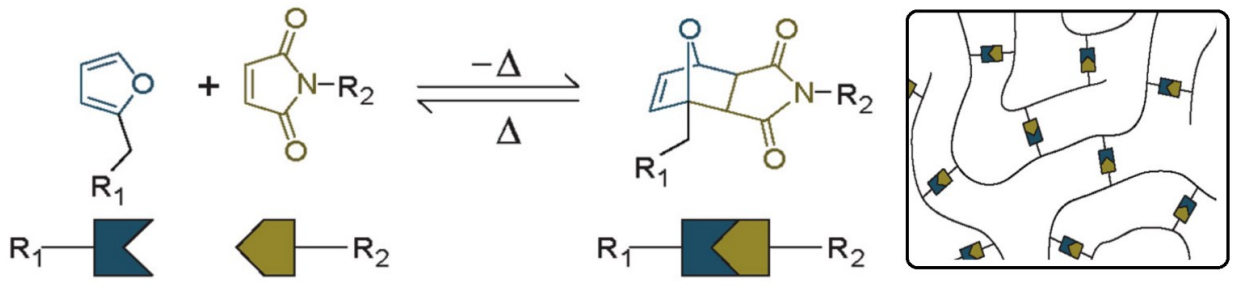

Figure 2.7 Example of dissociative reversible Diels-Alder reaction in a CAN; furans (blue) and maleimides (golden) in a CAN (right), adapted from [64].

Associative bonds

The second subcategory of CANs relies on associative exchange mechanisms. In such materials, depolymerization does not occur upon heating since the covalent bonds are only broken when new bonds are formed, shown in **Figure 2.8**. This leads to retention of the number of cross-links in the

network [58]. In 2011, Leibler's group in their seminal work developed a thermally triggered catalytic transesterification for epoxy/acid or epoxy/anhydride in polyester networks [65]. The networks showed a gradual decrease in viscosity when heated which is a distinctive feature of vitreous silica. Leibler coined the term vitrimer (glass or silica-like) for such dynamic networks with associative covalent bond exchanges [65]. Vitrimers are expected to maintain a constant rubbery plateau modulus during topological rearrangement and in ideal networks do not dissolve but swell [66]. Since the relaxation of polymer networks in vitrimers happens due to chemical reaction of dynamic covalent bond exchanges an Arrhenius behavior of stress relaxation times or viscosities versus temperature has been observed. The activation energies (E_a) typically span ~30 −160 kJ/mol and addition of a catalyst decreases the relaxation time and can also change the activation energy. It should be noted that there are many inconsistencies in the literature regarding E_a and the temperature dependence of relaxation modulus and this is still an active area of research [67,68].

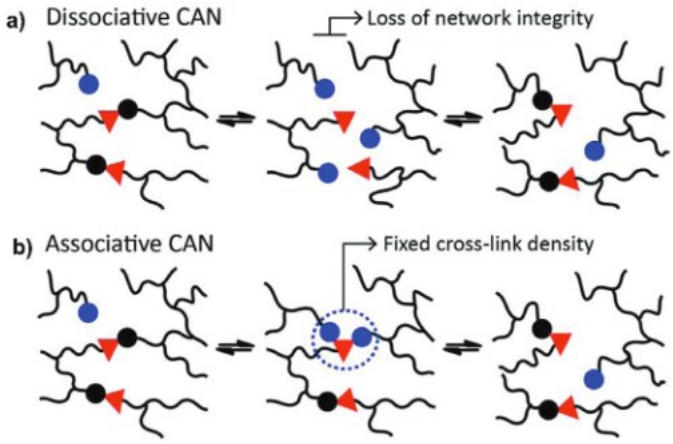

Figure 2.8 Two mechanisms of network rearrangements in CANs: a) dissociative b) associative (vitrimers) [58]

In the past decade, a wide array of catalyzed and catalyst-free associative dynamic covalent chemistries have been reported including transesterification [69–71], olefin metathesis [72], dioxaborolane exchange and boronic esters [73–85], silyl ether exchange [86,87], vinylogous urethanes [55,88–91], disulfides [92,93] imines exchanges [94–97], and several others [11,11,57–59,98] as demonstrated in **Figure 2.9**. It is well-established that increasing the cross-link density increases the rubbery modulus [99].

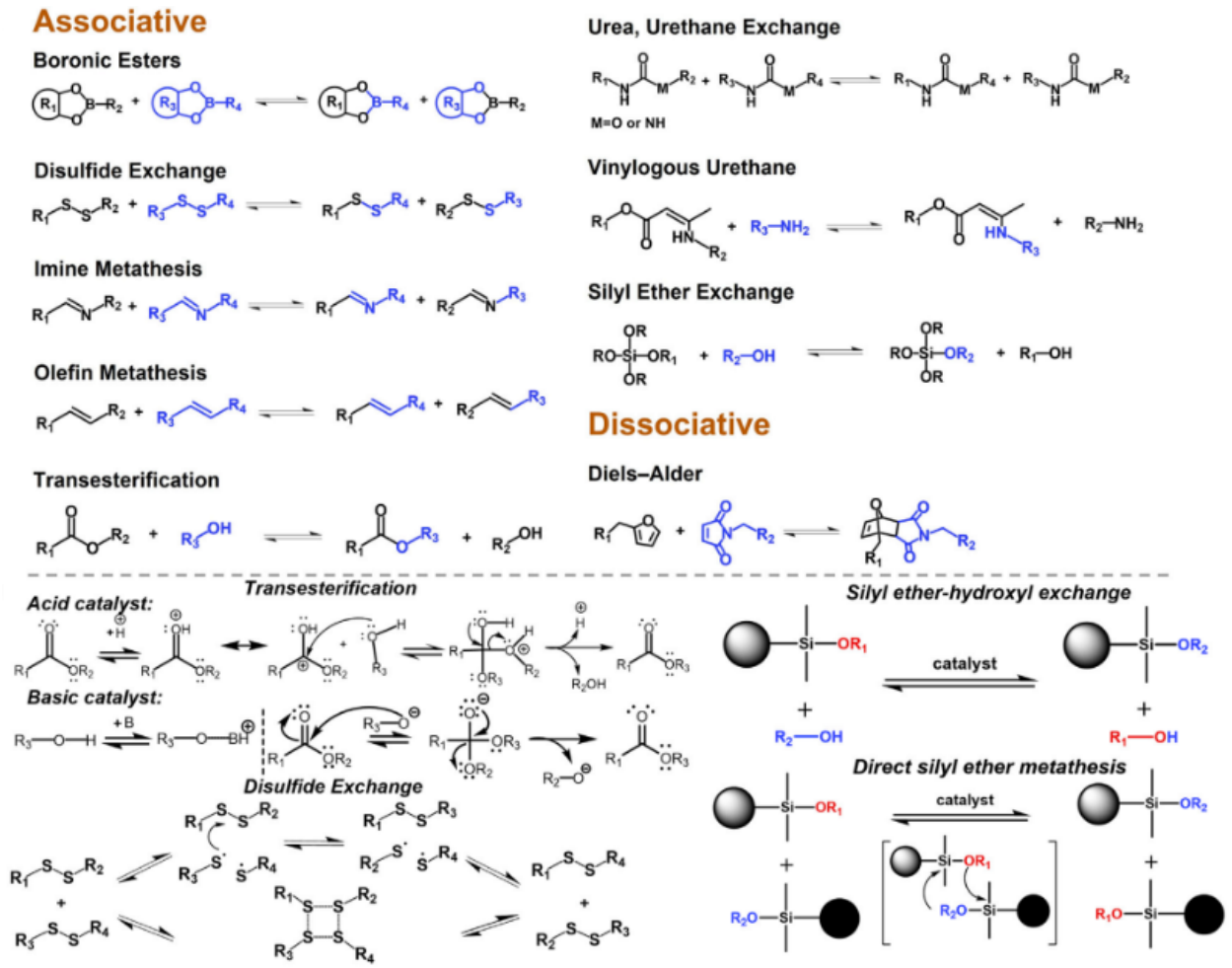

Figure 2.9 Various dynamic covalent bonds in CANs and Mechanism of several dynamic exchange reactions used for elastic vitrimers synthesis, from [100].

A hypothetical topology freezing temperature called T_v has been suggested for vitrimers. At temperatures below T_v the bond exchanges occur slowly enough such that the network is essentially frozen and exhibits a solid-like behavior [67]. At T > T_v, vitrimers will flow like viscoelastic liquids due to the topological rearrangement which are enabled by the dynamic bond exchange with Arrhenius-type behavior [101]. Therefore, in the case of $T_v > T_g$ determination of T_v is important for practical application of the vitrimers [102]. Leibler et al., have proposed the viscosity of 10^{12} Pa.s which is analogous to the definition of the glass transition temperature T_g for network glasses and small molecular systems [65,68]. However, more recently, many researchers have questioned this definition of T_v. More studies are required for better understanding of the viscoelastic behavior of vitrimers and T_v [68,100–102].

Building upon on the concepts of controlled polymerization and vitrimers, in this doctoral work, we began by synthesizing linear vinyl or diene-based prepolymers from bio-derived monomers using NMP and RAFT methods. Applying RDRP methods allowed for precise control over polymer microstructure, M_n, $Đ$, and composition, which allow for clearer linkages of structure with performance. Afterwards, the prepolymers were appropriately cross-linked to form dynamic networks and their thermomechanical properties were subsequently characterized.

Chapter 3: Vitrification: a versatile method to modulate properties of myrcene-based rubbers

This chapter is presented as an article published as the following with the same title and authors.

Farhad Asempour and **Milan Marić**

ACS Applied Polymer Materials, 5, 6364–6376

https://doi.org/10.1021/acsapm.3c00914 [103]

3.1. Preamble to Chapter 3

Using the concepts of RDRP, first several copolymers of myrcene, a bio-based diene, and β-ketoester functional methacrylate AAEMA were synthesized via NMP. Subsequently, the prepolymers were treated with di and tri-functional amine cross-linkers to form dynamic vinylogous urethane vitrimers. To impart shape memory effects and further modulate rheological properties of the vitrimers, a terpolymer of myrcene/AAEMA/GMA was also studied. The GMA (glycidyl methacrylate) epoxy functionality was used to form static cross-links with the amine cross-linkers.

In this chapter, we not only developed a novel terpene-based rubbery vitrimer but also demonstrated the effectiveness of vitrification as a method to enhance and customize the properties of brush-like bio-based monomers while maintaining their reprocessability. This initial study showed how a bio-based replacement's shortcomings can be accounted for by applying vitrimer chemistry. This concept was also applied in Chapters 6.

3.2. Abstract

We report bio-derived vitrimeric rubbers with weldability and excellent reprocessability. Reversible deactivation radical copolymerization of the commercially available terpene-based β-myrcene with 10 to 30 mol% (2-acetoacetoxy)ethyl methacrylate (AAEMA) afforded linear prepolymers which were cross-linked in a single step treatment with difunctional amine, the vegetable oil-derived Priamine 1075, or trifunctional amine tris(2-aminoethyl)amine (TREN). Decoupling the networks' backbone structure and cross-linkers led to high tunability of the vitrimers' final mechanical and rheological properties using prepolymer composition, molecular weight, nature and concentration of cross-linker and cross-linking density. The glass transition temperature (T_g) of the vitrimers ranged between -49 to -5 °C while the average elongation and stress at break ranged from ~83% and 0.18 MPa to ~30% and 1.68 MPa respectively from the lowest, 0.12 mol/L, to the highest, 0.98 mol/L, cross-linking densities. Characteristic features of dynamic vinylogous urethane-vitrimers were confirmed over at least 3 reprocessing cycles by grounding and hot pressing at 110 °C. No appreciable change in the ATR-FTIR spectra, T_g, decomposition temperatures, tensile properties and storage modulus were observed due to the reprocessing. Furthermore, incorporation of 5 mol% epoxy-based glycidyl methacrylate into the prepolymer led to the formation of a network with dual static and dynamic cross-links. Compared to the counterpart network with solely dynamic cross-links, the addition of static cross-links decreased creep by 75% and imparted shape memory effects. This work shows that combining vitrimer chemistry with myrcene is a facile and inexpensive, yet highly versatile method to not only modulate and compensate for the poorer mechanical properties of brush-like terpene-based elastomers but also provides a potential platform for recyclable bio-based rubbers with more sophisticated functionalities.

3.3. Introduction

Global warming and plastic waste pollution are considered planetary threats [3]. As a result, there is a growing interest in shifting from petroleum-based single-use polymers towards renewably sourced plastics with improved recyclability [9]. In this work, we are particularly focusing on the development of "greener" alternatives for thermosetting elastomers. Given the massive size of the synthetic rubber industry, with the current estimation of 15 to 20 million metric tons (MMT) per year, even small improvements can have significant environmental benefits [93].

Thermosets and elastomers are an irreplaceable category of polymers with substantial advantages associated with their mechanical, thermal, and chemical resistant properties [88]. However, due to their cross-linked molecular structure, they are commonly difficult to (re)process and recycle [104]. This issue has historically drawn a lot of attention from the polymer community. In the past two decades, covalent adaptable networks (CANs) exhibiting reversible covalent chemistry have appeared to offer a possible solution [105]. However, CANs can undergo depolymerization under certain conditions and temperatures, limiting their applications [93]. This has led to the development of vitrimers, first reported in 2011, as a new category of polymeric materials bridging the gap between thermosets and thermoplastics [93,106] . Vitrimers are permanently cross-linked networks with thermally induced "associative" dynamic covalent bonds [58,107]. This provides them with a unique ability to behave like thermosets at service temperatures but can change topology and be reprocessed without decreasing connectivity and dissolution at elevated temperatures [73,88] Several catalyst-free chemistries such as exchanges of silyl ethers [87], imines [108], vinylogous urethanes [40,55,88], disulfides [93], dioxaborolane metathesis [75,77,109], hydroxy urethanes [69] and metathesis of cyclic acetals [110] have been reported, showing great potential for malleability, shape memory, and weldability [57,59,99,111,112]. Despite these advantageous properties, it has been commonly reported that vitrimers undergo substantially higher creep compared to their static thermosetting counterparts [88,113]. Improving the dimensional stability of vitrimers is still an evolving area of research. It has been shown that a vitrimer's molecular architecture greatly influences its malleability and rheological properties [114–116].

In addition to reprocessability and recyclability, renewability plays a key role in the development of more sustainable polymeric materials [117]. Aside from natural rubber, various bio-based platforms such as itaconic acids, vegetable oils, lactides, norbornenes, and terpenes have shown much potential to produce rubbers [118]. Terpenes are particularly promising candidates as they can undergo radical polymerization with comparatively higher efficiencies [118–120]. Terpenes are made from highly abundant forestry feedstocks and are composed essentially of isoprenic motifs. Specifically, β-Myrcene (Myr) is a readily available acyclic monoterpene with a conjugated diene structure [121]. Myr can be isolated from pine, hops, bay leaves, lemongrass, celery, nutmeg, and rosemary [122,123]. Myrcene is industrially produced by pyrolysis of β-pinene, a major constituent of natural turpentine oil [123]. Similar to other 1,3-dienes, such as butadiene and isoprene, poly(Myr) also forms low glass transition temperature (T_g) (~ -75 °C) rubbery polymers [124]. In addition to renewability, an advantage of Myr over butadiene and isoprene is its lower volatility with a boiling point of 167 °C, meaning that Myr does not require pressurized equipment to handle [125]. However, the longer pendant side chain in poly(Myr) results in a higher entanglement molecular weight of ~ 18 kg/mol compared to that of polybutadiene and polyisoprene with ~ 3 and ~ 6 kg/mol respectively [124,126]. This in general can result in lower tensile strength, elongation, and toughness of poly(Myr), potentially limiting its applications [121,127]. Although some in-depth studies involving various polymerization techniques and properties of poly(Myr) have been reported, thorough investigations on the applications of poly(Myr)-based elastomers in the rubber industry are generally lacking in the literature [126–128]. Some works have investigated applications of vulcanized poly(Myr) as well as Myr-based thermoplastic elastomers with styrene and isobornyl methacrylate (IBOMA) [119,119,125,129,130]. Bhowmick's and Gong's groups have also reported Myr-based CANs using Diels-Alder chemistry via Myr copolymerizations with furan-based monomers. The resulting elastomers exhibited self-healing and shape memory properties [131,132].

Recently several works have reported promising results combining renewability and recyclability via vitrimer chemistry to produce elastomers [133]. Kölsch et al. synthesized poly(itaconate) elastomers with catalytic transesterification [134]. Feng et al. prepared photothermally induced self-healable and shape memory epoxidized natural rubber-based elastomers using catalytic transesterification [135]. Liu et al. reported the development of a cross-linker with triple dynamic

covalent bonds (boroxine, disulfide bond, imine bond) for the vitrification of epoxidized natural rubber, imparting self-healing and recyclability [136].

In this study, we report a facile method to produce thermally reprocessable bio-derived vitrimeric rubbers based on catalyst-free vinylogous urethane exchanges. Well-defined copolymers of inexpensive and commercially available Myr with a monomer containing a reactive β-ketoester moiety, 2-acetoacetoxy)ethyl methacrylate (AAEMA), were synthesized using nitroxide mediated polymerization (NMP). Two different cross-linkers, Priamine 1075 (referred to simply as Priamine hereafter), a long-chain dimer diamine with 100% bio-based carbon content, as well as tris(2-aminoethyl)amine (TREN), a smaller triamine molecule, were utilized to tailor cross-linking density. Thermomechanical tests showed that the resulting vitrimers had excellent reprocessability after three cycles of grounding and hot pressing. Moreover, to suppress creep and eventually impart shape memory effects, terpolymers of Myr, AAEMA, and glycidyl methacrylate (GMA), the latter containing an epoxy moiety, were synthesized. Upon reactions with amines, a dual static and dynamic network was formed. The use of different prepolymer compositions, cross-linkers, and the addition of the low number of static cross-links provided a versatile toolbox to tune the final mechanical and rheological properties of the vitrimers.

3.4. Experimental

3.4.1. Materials

All chemicals were of reagent grade and used as received unless otherwise stated. β-Myrcene (Myr, Sigma-Aldrich, ≥90%), (2-acetoacetoxy)ethyl methacrylate (AAEMA, TCI, 95%), glycidyl methacrylate (GMA, Sigma-Aldrich, 97%) were purified by passing through columns of basic alumina (Al_2O_3, Brockmann, Type I, Sigma-Aldrich) mixed with 5 wt% calcium hydride (90-95%, Sigma-Aldrich) and stored in a refrigerator under a head of nitrogen until needed. Priamine 1075 (Priamine) was procured from Cargill and tris(2-aminoethyl)amine (TREN, 97%) was purchased from Alfa Aesar. Butylamine (99%) was purchased from Sigma-Aldrich. Tetrahydrofuran (THF, HPLC grade), toluene (>99%), chloroform (>99%), N,N- dimethylformamide (DMF, >99%), acetone (>99%), reagent alcohol (anhydrous ethanol 90% v/v; methanol 5% v/v; 2-Propanol 5% v/v), methanol (>99%) were purchased from Fisher Scientific. Deuterated chloroform ($CDCl_3$, ≥99%) was purchased from Cambridge Isotopes Laboratory for ^1H NMR analyses.

BlocBuilder ^{TM} (BB, also known as MAMA-SG1, is the alkoxyamine for NMP, and SG1 is the free nitroxide, see Figure 1 and S1 for more details) was obtained from Arkema. 2-Methyl-2-[N-tert-butyl-N-(1-diethoxyphosphoryl-2,2-dimethylpropyl)-aminoxy]–N-propionyloxy-succinimide (NHS-BB, also known as NHS-BlocBuilder) was synthesized according to the previous literature [137], N,N'-dicyclohexylcarbodiimide (DCC), N-hydroxysuccinimide (NHS) were procured from Sigma Aldrich.

3.4.2. Polymer synthesis

We synthesized three different statistical copolymers of Myr with 10, 20, or 30 mol% AAEMA content with similar molecular weights. NMP with BlocBuilder, an SG1-based alkoxyamine, was used to initiate and control the synthesis of well-defined prepolymers. All polymerizations were performed in bulk. Métafiot et al., reported that polymerization of Myr in bulk was more effective in terms of polymerization kinetics and control [125]. Table 1 summarizes the copolymerization formulae and reaction conditions for prepolymers. As an example, for the synthesis of MyrAA-20 prepolymer, Myr (56.45 g, 414.3 mmol), AAEMA (22.2 g, 103.6 mmol), BlocBuilder (1.2 g, 3.145mmol), and a magnetic stir bar were added to a 250 mL three-neck round-bottom glass flask. The reactor was equipped with an overhead reflux condenser connected to a chiller (Fisher Scientific Isotemp 3016D) at 2 ˚C. The reaction solution was sparged with high-purity N_2 gas for 20-25 minutes prior to being heated at 125 ˚C for 8h using a heating mantle and a feedback temperature controller. Samples were periodically taken for ^{1}H NMR and GPC analyses. Afterward, the reaction was stopped by lowering the temperature, and the obtained viscous solution was three times (re)precipitated into a mixture of ethanol/methanol (70/30 v/v%) from THF. It should be noted that, the (re)precipitation and work up resulted in some polymer loss. Finally, the polymer was dried under a reduced pressure at 60 ˚C overnight, yielding 39.1 g of a yellow-colored viscous liquid. The overall monomer conversion from ^{1}H NMR was 88.2%, see Supporting Information section S2, and from gel permeation chromatography (GPC), the number average molecular weight (M_n) was 12,800 g/mol with the dispersity ($Đ$) of 1.49 relative to PMMA standards.

We also studied the effects of physical molecular entanglements on the rheological properties of vitrimers. To do so, we synthesized a prepolymer with a molecular weight higher than the

entanglement molecular weight (M_e) of poly(Myr) homopolymer, MyrAA-30-Long, by increasing the theoretical target molecular weight to 60 000 g/mol at 100% monomer conversion. Furthermore, to incorporate static cross-links into the vitrimeric network, we prepared a terpolymer of Myr with 20 mol% AAEMA and 5 mol% GMA. For the synthesis of the GMA-bearing prepolymer, a different initiator with an SG1-based alkoxyamine initiator bearing an N-succinimidyl ester group was synthesized (NHS-BlocBuilder) and utilized according to the literature [138].

The prepolymers are coded as MyrAA-xx, where xx refers to the AAEMA mol% in the initial monomer mixture composition. The high molecular weight polymer was coded as MyrAA-30-Long, and the copolymer with 5 mol% GMA content was named MyrAA-20-GMA-5.

3.4.3. Formation of vitrimers and (re)processing

Vitrification of a prepolymer started with dissolving it in THF, 40% (w/v), followed by the addition of Priamine or TREN and stirring until gelation. The resulting gel was left overnight at room temperature in a fume hood and was further cured and dried at 75 ± 10˚C under reduced pressure in a vacuum oven for 8-12 h. The resulting vitrimer was ground up and hot pressed (Carver Manual Hydraulic Press with Watlow temperature controllers), while sandwiched between two Teflon plates, at 110 ± 5 ˚C under 6 ± 1 metric tons for 50 ± 5 min yielding a yellow and transparent shaped material. See Supporting Information and Figure S3 for each step. To further explore the effects of cross-linking density, two different ratios of β-ketoester : amine were studied; 1:1 and 0.7:1. Vitrified polymers are coded as "MyrAA-xx-P/T-yy" where xx is the rounded molar ratio of the AAEMA, P/T shows the type of cross-linker, T for TREN or P for Priamine, and yy indicates the molar ratio of β-ketoesters from AAEMA in the co/terpolymer to NH_2 from the cross-linker. As an example, *MyrAA-20-T-0.7* represents a vitrified polymer with 20 mol% AAEMA which is cross-linked with TREN with a 0.7:1 ratio of β-ketoesters to NH_2.

3.4.4. Characterization

Nuclear Magnetic Resonance (NMR) Spectroscopy

^{1}H NMR spectra were recorded on a Bruker AVIIIHD 500 MHz Spectrometer using 16 scans with $CDCl_3$ at room temperature. DOSY NMR measurements were performed in CDCl3 solution at 25°C on a Varian Inova 500 MHz NMR Spectrometer with stimulated echo sequence, 64 increments, and 4 scans per increment. The gradient strength of 51.4 G/mm was logarithmically incremented from 2 % up to 80 % of the maximum gradient strength. The gradient pulse length was 2 ms (one-half of bipolar pulse pair) in order to ensure full signal attenuation. All measurements were performed with a compromise diffusion delay D of 350 ms in order to keep the relaxation contribution to the signal attenuation constant for all samples. The DOSY maps were obtained with the MestReNova.

Gel Permeation Chromatography (GPC)

The number average molecular weight (M_n) and dispersity ($Đ = M_w/ M_n$) of the polymers synthesized were estimated using GPC (Waters, Breeze System) in THF (HPLC) at 40 °C and a flow rate of 0.3 mL/min. The GPC system was equipped with a guard column, a differential refractive index (RI 2414) detector and three Styragel HR columns (with a molecular weight measurement range of 10^2 to 5×10^3 g/mol for HR1, 5×10^2 to 2×10^4 g/mol for HR2 and 5×10^3 to 6×10^5 g/mol for HR4). Poly(methyl methacrylate) (PMMA) (Varian) standards were used for calibration of molecular weights ranging from 875 to 1,677,000 g/mol.

FT-IR Spectroscopy

Infrared spectra were collected on a Thermo Scientific Nicolet™ iS50 FTIR Spectrometer equipped with diamond attenuated total reflectance (ATR) accessory using 32 scans.

Differential Scanning Calorimetry (DSC)

DSC experiments were collected on a Discovery 2500 TA Instruments equipped with an autosampler and refrigerated cooling system (RSC 90) using aluminum hermetic pin-hole pans. Calibrations for temperature and heat flow were carried out using indium and benzoic acid standards. Temperature ramp experiments (cool/heat/cool/heat) were run from -90 to 30 °C under nitrogen with heating rate of 15 °C/min and cooling rate of 10 °C/min with 3-min isotherms at

each extreme. Experimental data were recorded and analyzed using TA instrument TRIOS software. The reported T_g were calculated using the curve inflection and only the second heating run was considered to remove any thermal history.

Thermal Gravimetric Analysis (TGA)

To study the thermal stability of the polymers, a TA Instrument's Discovery TGA 5500 with autosampler and platinum pans were used. All experiments were done under a nitrogen flow. The samples were heated to 100 °C for 30 min isotherms prior to each run to remove any moisture or residual solvent. Ramp experiments were performed with a heating rate of 15 °C/min until 650 °C. Isothermal experiments were done from room temperature up to 110 °C and remained at the temperature for a 6 h total run time.

Tensile Analysis Testing

Tests were performed on a universal Shimadzu Easy Test system with a 500 N load cell and a crosshead speed of 10 mm/min. Dog-bone shaped tensile specimen similar to ASTM D638 type V (overall length of 60 mm and respective neck thickness and width of approximately 2 and 3mm) were prepared using a Carver hot-press as described previously[23]. Reported results are the average of at least 3 specimens.

Dynamic Mechanical Analysis (DMA) and Rheology

All tests were done using an Anton Paar MCR 302. DMA tests were conducted using a solid rectangular fixture (SFR 12). Rectangular-shaped samples (60mm length, 10mm width, and 2mm thickness) were heated from room temperature to 130 °C with an average rate of 5 °C/min and at a frequency of 1 Hz. Rheological tests were done with a 25 mm parallel plates geometry. Strain sweep tests were carried out at 100-130 °C to determine the linear viscoelastic region (LVR) at 1 Hz. Stress relaxation experiments were conducted at 0.1 % strain at the desired temperatures. Creep recovery experiments were performed at 1000 Pa for 300 s followed by 0 Pa for 600 s, total experiment time of 900 s.

Gel fraction and swelling tests

Gel fraction was obtained by soaking the networks in excess amount of a desired solvent for 72 hours at room temperature. Next, the swelled samples were filtered, dabbed with delicate task

wipes to remove any excess solvent, and immediately weighed to find the samples' swelling ratio. This was followed by drying the samples in a vacuum oven at reduced pressure and 60 °C for a day, and finally weighing them. Gel fraction was calculated using m_2 / m_0 where m_0 is the original mass of the sample and m_2 is the mass of dried sample after swelling.

3.5. Results and discussion

3.5.1. Prepolymer synthesis and characterization

We anticipated that the thermomechanical properties of the final vitrimers would be dictated by those of the linear reactive precursors. Therefore, we commenced our studies by synthesizing statistical copolymers of Myr with AAEMA, which provides the functionality for amine-crosslinking. NMP with BlocBuilder was used to control the molecular weight of the prepolymers and minimize possible side reactions and cross-linking of Myr during the polymerization. Copolymerizations of Myr using reversible-deactivation radical polymerization (RDRP) have been reported [41,118]. For example, Pablo-Morales et al. and Hilschman et al. utilized reversible addition−fragmentation chain-transfer (RAFT) for copolymerization of Myr with GMA and styrene respectively [139,140]. Métafiot et al. showed effective copolymerization of Myr with methacrylates such as IBOMA and GMA with high regioregularity microstructure using NMP [125,141]. Herein, NMP was adopted since it does not rely on sulfur-based chain transfer agents or any metallic ligands [42,142]. This is particularly important since the thiocarbonylthio chain transfer agent moieties in RAFT are prone to rapid aminolysis upon treatment with primary amines and therefore chain end modification is required before further processing [40,112].

Three different prepolymers with initial AAEMA feed ratios of 10, 20 and 30 mol% were prepared to investigate the effects of cross-linking density. See Figure 1 and S1 for the synthetic route used to prepare these copolymers. Table 1 summarizes the overall monomer conversion, molecular and thermal characterization of all synthesized prepolymers. Characterization by GPC showed that the M_n of the MyrAA-10, 20 and 30 were predictable, ranging from 11.8 to 12.8 kg/mol with relatively low dispersities ($Đ$) of 1.38 to 1.51. It should be mentioned that some deviation from the theoretical M_n was observed which indicates divergence from the ideal persistent radical effect and the possibility of chain transfer and/or termination reactions [34]. Additionally, all M_ns reported were relative to PMMA standards, which may introduce some error as the copolymers were largely

Myr-based in composition. Figure 2 illustrates representative kinetic plots and molecular weight characterizations of MyrAA-10. From the ^{1}H NMR analyses, a pseudo-first-order linear monomer conversion over time was observed. Reasonable overall monomer conversion of 76 to 89% for Myr, and >95% for AAEMA were achieved. See Figures S4 and S5 for representative ^{1}H NMR spectra, calculations of conversion, and Figure S7 for GPC traces. The observed linear trend of chain growth combined with the low $Đ$ suggest that the possible side reactions and chain terminations were largely suppressed [34]. Figure S8 shows the ratio of unreacted AAEMA to Myr monomers as a function of the polymerization time of MyrAA-10. A decrease in the reactants' ratio from 0.11 to 0.01 over time suggests some compositional drift in the prepolymers. Further investigation on the reactivity ratios and compositional drift of Myr and AAEMA is out of scope of this work and is underway. Via ^{1}H NMR, the microstructure of the incorporated Myr was also determined. Myr can be polymerized into 3 different regioisomers: 1,4-, 3,4- and 1,2- vinyl addition [125,130]. All prepolymers had high regioregularity with >90% of the 1, 4-addition structure, which agrees with the literature [139]. In the DOSY maps, Figure S6, a single population of species with a diffusion coefficient of 6.3E-07 cm^2/s was observed. That is, statistical copolymers, and not distinct homopolymers, were synthesized.

In the second part of our study, we aimed to suppress creep in the vitrimers using two strategies: incorporating physical chain entanglements or adding chemically static cross-links. To achieve the first strategy, we synthesized a statistical prepolymer of Myr and AAEMA with M_n of 22 kg/mol (coded as MyrAA-30-Long) which is slightly higher than the critical entanglement molecular weight (M_e) of poly(Myr) homopolymer (M_e ~18 kg/mol) [124,143]. Figure S9 shows the GPC traces of all prepolymers. A clear shift towards higher molecular weights was observed for MyrAA-30-Long.

Moreover, we incorporated GMA in MyrAA-20-GMA-5 prepolymer, as seen in Figure 1. The epoxy group in GMA can react with amines and generate secondary chemically static cross-links. For the synthesis of the GMA-based prepolymer we used NHS-BlocBuilder instead of neat BlocBuilder. This was to avoid side reactions between the epoxy group and carboxylic acid groups from BlocBuilder [141]. Interestingly, MyrAA-20-GMA-5 had a comparatively lower $Đ$ of 1.29. This can be attributed to a higher dissociation rate and slightly lower activation energy of NHS-BlocBuilder, compared to BlocBuilder, which mimics the use of additional controlling SG1,

thereby providing more efficient control [137]. Incorporation of epoxy groups was confirmed by ^{1}H NMR, Figure S5.

From the DSC traces, T_g of the prepolymers systematically increased from -63 °C to -49 °C by increasing the AAEMA and GMA content; see Figure S10 for the DSC experiments. The measured T_gs are in good agreement with the estimates from the Flory-Fox equation [14,144] , see Table S2 for the details.

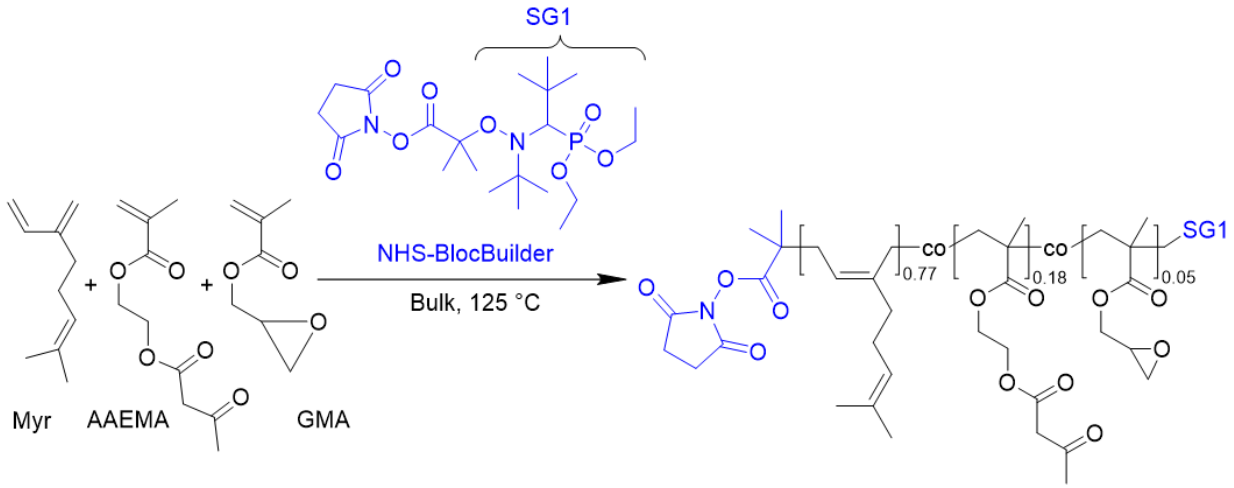

Figure 3.1 Statistical copolymerization of MyrAA-20-GMA-5 with NHS-BlocBuilder. A controlled radical polymerization was achieved using NMP.

Table 3.1 Molecular and thermal characterizations for various synthesized prepolymers

code	X (%) [a]	M_n (g/mol) [b]	$Đ$ [b]	F_{Myr} [c]	1,4 addition	F_{AAEMA}	F_{GMA}	T_g (°C) [d]
MyrAA-10	70.0%	11,800	1.38	90%	93.5%	10%	—	-63
MyrAA-20	88.2%	12,750	1.49	82%	89.6%	18%	—	-62
MyrAA-30	92.6%	12,650	1.51	69%	93.6%	31%	—	-53
MyrAA-30-Long	90.2%	22,060	1.45	70%	92.3%	30%	—	-54
MyrAA-20-GMA-5	79.5%	13,860	1.29	77%	92.4%	18%	5%	-49

[a] Overall monomer conversion determined by ^{1}H NMR

[b] Number average molecular weight (M_n) and dispersity ($Đ$) from GPC relative to PMMA standard in THF at 40 ˚C

[c] Molar fraction of monomers in the final polymer determined by ^{1}H NMR

[d] Percentage of 1,4 addition microstructure in poly(Myr)

[e] Determined by DSC

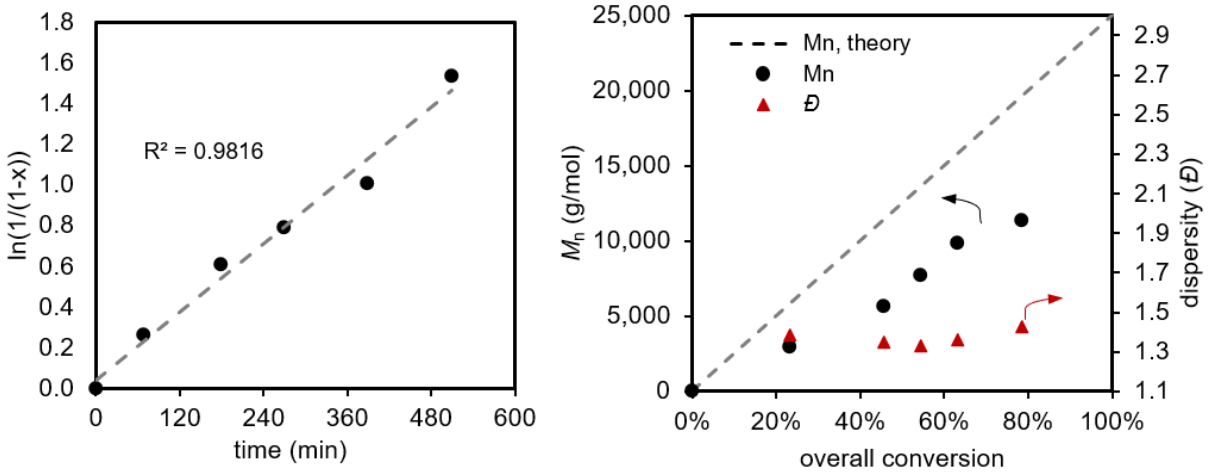

Figure 3.2 Representative polymerization data of MyrAA-10 prepolymer: left) linearized overall monomer conversion versus time and right) evolution of M_n and $Đ$ against overall monomer conversion.

3.5.2. Vitrimer network synthesis and characterization

Once the prepolymers were prepared, vitrification was performed by simple solution casting, as seen in Figure S3. Two different cross-linkers were used. TREN, a small trifunctional molecule and Priamine, a difunctional vegetable oil-based molecule with relatively longer arms, are shown in Figure 3. Due to the associative nature of transamination, a stoichiometric imbalance is required to have an effective cross-linking exchange [106,145]. However, the effects of cross-linking ratio on the rheological properties and dimensional stability of vitrimers have generally been limited [88,116].Therefore, we prepared networks with two different ratios of amine to β-ketoester for each cross-linking system to test for sensitivity. We were able to study the mechanical and rheological properties of the resulting vitrimers over a wide range of cross-linking densities by

decoupling the structure and composition of the prepolymers from the nature and ratio of the cross-linkers.

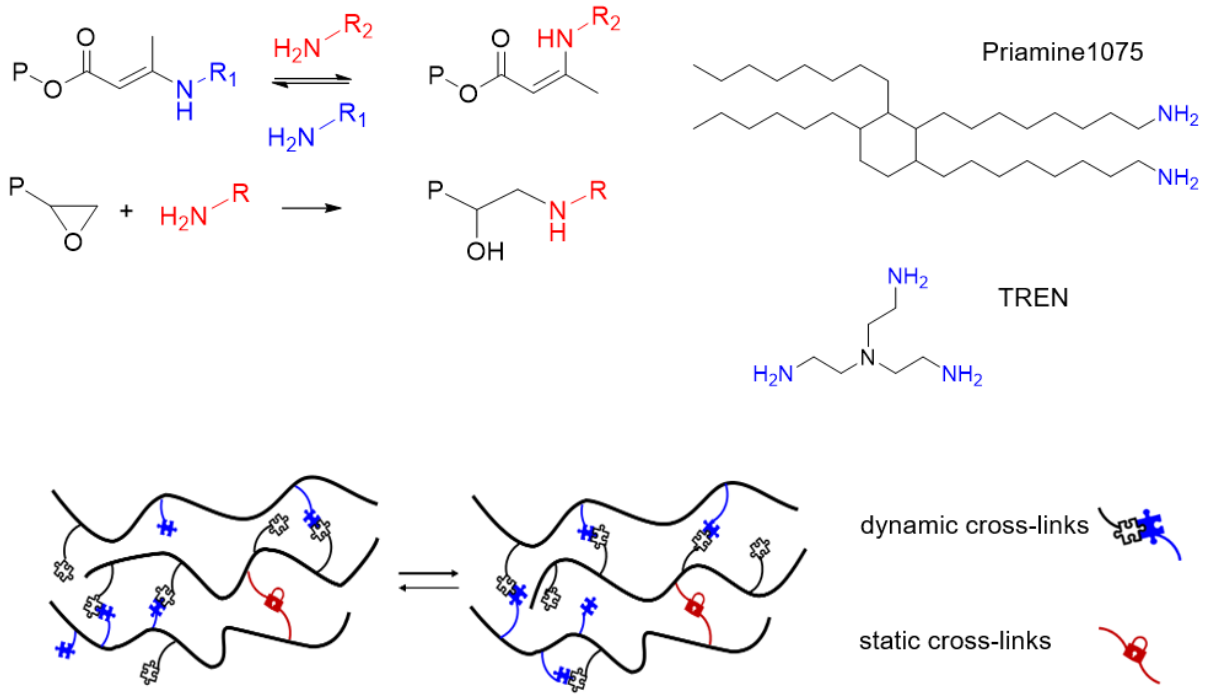

Figure 3.3 Cross-linking of MyrAA-20-GMA-5 prepolymer with Priamine or TREN. Both dynamic and static cross-links are present, enabling exchange and incorporation of shape memory behavior.

3.5.3. Swelling test

Due to the associative nature of the reversible cross-links in vitrimers, the networks do not dissolve in solvents but swell [98,107,115]. Indeed, this was evident for all synthesized vitrimers. The results of swelling tests for various networks and solvents are summarized in Table 2. A compromise between the gel content and swelling ratio was observed. Swelling ratio increased with looser networks by shifting from TREN to Priamine. Expectedly, MyrAA-30-T-1, with the tightest network, had the lowest swelling ratio while MyrAA-10-P-0.7 exhibited the highest one, as it had the lowest b-ketoester concentration and higher free amine chain ends (β-ketoester/NH_2

= 0.7). Also, MyrAA-20-GMA-5-P-0.7 showed an intermediate value of cross-linking density between MyrAA-20-P-0.7 and MyrAA-30-P-0.7 as expected.

Table 3.2 Swelling results of various vitrimers in toluene and gel content of MyrAA-20-T-0.7 in THF

Vitrimer	**MyrAA-30 -T-1**	**MyrAA-30 -T-0.7**	**MyrAA-30 -P-1**	**MyrAA-30 -P-0.7**	**MyrAA-20 - P-0.7**	**MyrAA-10 -P-0.7**	**MyrAA-20-GMA-5 -P-0.7**
Gel Content*	95%	95%	95%	93%	91%	87%	96%
Swelling ratio*	202%	235%	242%	261%	361%	692%	294%
Solvent	THF	Toluene	Chloroform	DMF	Methanol		
Gel Content**	92%	89%	91%	93%	93%		

* in toluene

** Tests done with MyrAA-20-T-0.7

The cross-link densities (υ_e) of equilibrated swollen networks were estimated using the Flory-Rehner equation (eq 1):

$$\upsilon_e = -\frac{ln(1-V_r)+V_r+\chi_{12}\,V_r^2}{V_s\left(V_r^{\frac{1}{3}}-\frac{V_r}{2}\right)} \qquad \text{(eq 3.1)}$$

in which V_s is the molar volume of solvent (106.5 cm^3/mol for toluene [146]) and V_r is the volume fraction of polymer network in the swollen sample, calculated using equation 2) [14]. χ_{12} is the Flory-Huggins polymer-solvent interaction parameter and is estimated using the Flory-Hildebrand equation (eq. 3)[14].

$$V_r = \frac{\frac{m_2}{\rho_2}}{\frac{m_1}{\rho_1}+\frac{m_2}{\rho_2}} \qquad \text{(eq 3.2)}$$

$$\chi_{12} = \frac{V_s}{RT}\,(\delta_s - \delta_p)^2 \qquad \text{(eq 3.3)}$$

Here, m_1 and m_2 are the mass of the swollen and vacuum dried samples and δ_s and δ_p are the solubility parameters of the solvent and polymer [130]. δ_p of different prepolymers were either taken from the literature or estimated using the group contribution method of Hoftyzer and van Krevelen with a weighted average of different comonomers using the volume fraction [129,147]. See section S5 in the Supporting Information for the details of calculations. Figure S15 compares the cross-linking density of the various networks studied ranging between the two extremes. As expected, the sample with highest AAEMA content and a balanced β-ketoester : amine ratio exhibited the highest cross-linking density of 0.98 mol/L. In contrast, MyrAA-10-P-0.7 which had the lowest AAEMA content and was cross-linked with excess Priamine expectedly showed lowest cross-linking density of 0.12 mol/L. This trend correlates with the results from the DSC analyses and the shift in the T_gs of the vitrimers discussed in Table 1.

3.5.4. Network disintegration and polymer recovery

Considering the dynamic nature of transamination in vinylogous urethanes, we hypothesized that by adding an excess amount of a monofunctional amine, the network can be disintegrated, and the prepolymer be chemically recovered [12,104]. Thus, MyrAA-20-P-0.7 with toluene and excess butylamine were added to a vial and sealed with a closed lid. Interestingly, the network did not dissolve after 24hr at room temperature; however, once the vial was placed in an oven at 110 ± 5 °C the vitrimer was fully dissolved in a few hours. Figure 4 compares the GPC traces and molecular weights of MyrAA-20 prepolymer and MyrAA-20-P-0.7 after disintegration and chemical recovery. These results confirm that the vitrimer processing, shaping, and chemical recovery of the prepolymer did not significantly degrade the polymer backbone.

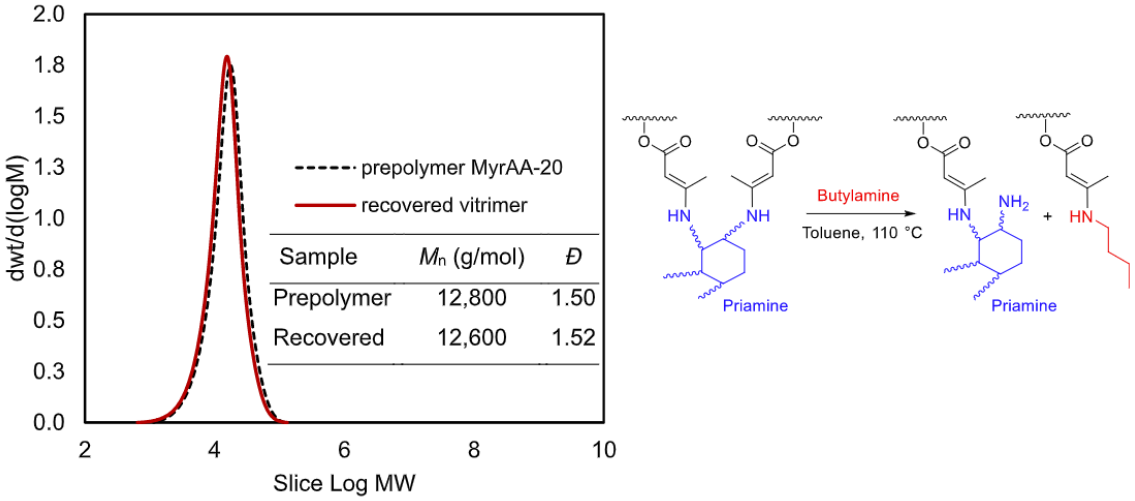

Figure 3.4 Polymer recovery using butylamine; right) Schematic of vitrimer disintegration left) Comparison of GPC traces, M_n (relative to PMMA) and $Đ$ of MyrAA-20 prepolymer and its recovered vitrimer.

3.5.5. Thermal and mechanical properties

The DSC traces of the MyrAA-30 prepolymer and its associated vitrimers are shown in Figure 5.a. A clear shift towards higher T_gs was observed after the network formation. Vitrimers cross-linked with TREN exhibited T_gs that were about 20 °C higher than those cross-linked with Priamine. This can be attributed to the higher cross-linking density of the TREN-based networks. However, it appears that changing the β-ketoester : amine ratios did not have a significant impact on the T_gs. Similar shift towards higher T_gs was observed for vitrified MyrAA-30-Long. Interestingly, although prepolymers of both MyrAA-30 and MyrAA-30-Long had similar T_gs of -53°C and -54 °C respectively, vitrified MyrAA-30-Long -T-0.7 had a T_g that was about 10 °C lower than that of the vitrified MyrAA-30-T-0.7. One possible explanation for this is that there may have been a compositional drift in the prepolymers during the synthesis, resulting in the formation of longer Myr-rich sequences in the chains of MyrAA-30-Long, as seen in section 3.1 and Figure S10. Determination of reactivity ratios for this system is underway to verify if compositional drift is significant.

Figure 5.b illustrates the results of tensile tests performed with the various vitrimers. The tensile strength at break of the vitrimers systematically increased by increasing the AAEMA content in the copolymer. For samples cross-linked with excess difunctional amine (P-0.7), an increase in tensile strength from MyrAA-10-P-0.7 with 0.18 ± 0.03MPa to MyrAA-30-P-0.7 with 0.48 ± 0.03

MPa was seen. Simultaneously, the opposite trend was observed for samples' elongation at break, as it decreased from 82.7 ± 18.6% for MyrAA-10-P.0.7 to 22.5±0.5% for MyrAA-20-P-0.7. In addition, The maximum tensile strength of 1.68 ± 0.02 MPa was observed for MyrAA-30-T-1.

From Figure S21, it is evident that replacing the diamine cross-linker with the triamine one, resulted in the formation of stiffer materials in case of MyrAA-20-P-0.7 and MyrAA-20-T-0.7. A similar trend was observed by DMTA with a systematic increase in modulus from MyrAA-10-P-0.7 to MyrAA-30-T-1. The tensile data closely follow the results of the swelling tests and cross-linking density calculations. These findings show that vitrification can be used as an effective tool to modulate the mechanical properties of terpene-based rubbers.

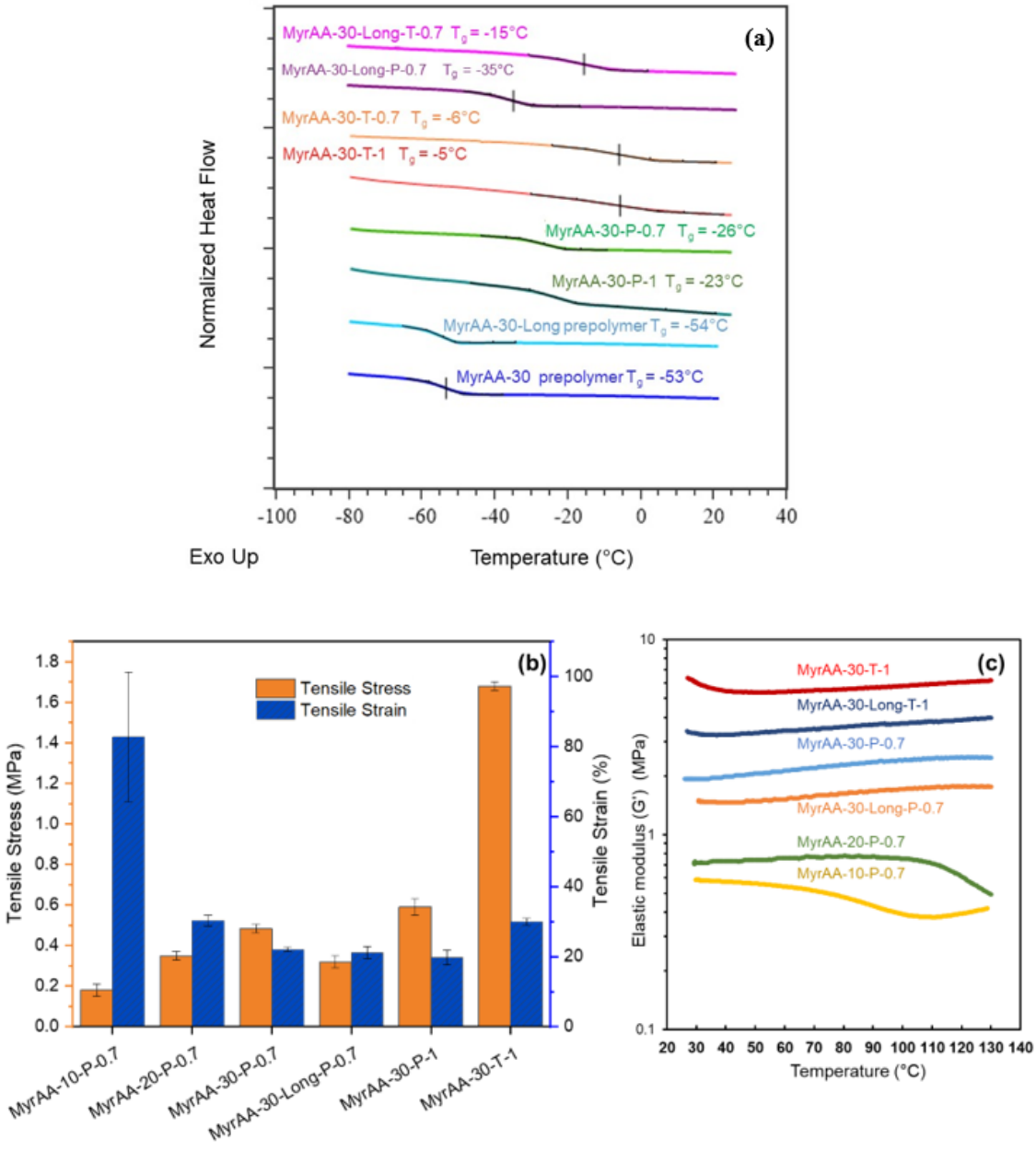

Figure 3.5 a) DSC traces of MyrAA-30 and MyrAA-30-Long prepolymer and their networks cross-linked with two ratios of TREN and Priamine; vitrification increased the glass transition temperature; **b)** Tensile data of various prepolymers cross-linked with Priamine with 0.7 to 1, and TREN with 1 to 1 β-ketoester : amine ratios. Increasing the network cross-linking density systematically reduced the elongation at break and increased tensile strength; **c)** representative DMTA data, elastic modulus and rubbery plateau of the vitrimers increased with cross-linking concentration.

3.5.6. Rheological properties

Stress-relaxation and creep

The recyclability of vitrimers is directly influenced by the exchange rate of the dynamic bonds due to their associative nature. The dynamic cross-link exchanges facilitate rearrangements in the network morphology, segmental healing, and reformation of a continuous material macroscopically [115]. We carried out stress-relaxation experiments to investigate the flow behavior of the vitrimers and quantify the timescale of the conformational rearrangements. Figure 6.a compares the normalized stress-relaxation spectra of various prepolymers vitrified with an excess amount of Priamine, P-0.7, at 130 °C. Increasing the AAEMA content systematically slowed down the stress-relaxation rate of the vitrimers which is in line with the networks' cross-linking density. Networks with 10 and 20 mol% AAEMA content showed fast and complete relaxation. Moreover, increasing the molecular weight of the prepolymer, in the case of MyrAA-30-Long-P, beyond the M_e, further slowed down the stress relaxation which suggests some restrictions in conformational rearrangements due to physical chain entanglements. Furthermore, addition of static cross-links via epoxy groups i.e., MyrAA-20-GMA-5, resulted in a significant increase of stress relaxation time with a portion of the stress never being fully relaxed after 1000 seconds.

Figure 6.b illustrates a typical normalized stress-relaxation i.e., G(t)/G(0), curve for MyrAA-30-T-0.7 in the temperature range of 90 to 130 °C. According to the single element Maxwell viscoelastic model, $G(t)/G(0) = -exp\ (t/\ \tau\ ^*)$, the characteristic relaxation time (τ*) is identified at the time when the normalized relaxation modulus reaches the value of e^{-1} (≈ 0.37) [115,148]. It is important to note that although the e^{-1} method is widely used in literature, it should be used with caution, as it may result in significant errors [68]. Nevertheless, with increasing cross-linking density some deviations from the ideal Maxwellian behavior were observed. To capture these deviations, a stretched exponential decay model was used according to equation 4. which permits the extraction of (τ*):

$$\frac{G\ (t)}{G\ (0)} = \ e^{-\left(\frac{t}{\tau^*}\right)^{\beta}} \qquad \text{(eq. 3.4)}$$

where, G(t) and G (0) are the relaxation moduli at time t and 0, τ* is the characteristic relaxation time and β ($0 < \beta \leq 1$) is a parameter related to the breadth of the relaxation distribution. For

MyrAA-30-T-0.7, β varies between 0.50 and 0.69 showing deviations from ideal Maxwellian behavior [149]. See Table S4 for detailed τ* and β values obtained by curve-fitting. As suggested by Leibler et al., since a chemical reaction is responsible for the dynamic exchanges in cross-linking, an Arrhenius relationship can be used to model the gradual decrease of viscosity with increasing temperature according to equation 5 [88].

$$\ln \tau^* = \frac{E_a}{RT} + \ln (\tau_0) \qquad \text{(eq. 5)}$$

Here, E_a is the viscous flow activation energy, R is the universal gas constant, T is temperature, and τ_0 is the Arrhenius pre-factor. The calculated E_a for MyrAA-30-P-0.7 and MyrAA-30-T-0.7 were 67 and 91 kJ/mol respectively, which is consistent with the literature; the observed increase in the activation energy can be attributed to the different nature of the cross-linkers and the higher T_g of the latter network [112]. Figure 6.c compares the Arrhenius plots of MyrAA-30-T-0.7 (with 0.7:1 β-ketoester : NH_2 ratio) and MyrAA-30-T-1 (with 1:1 β-ketoester : NH_2 ratio). In the latter case, decreasing the concentration of amine groups to a balanced stoichiometric ratio increased the E_a to 105 kJ/mol. Typically, higher values of E_a indicate a higher energy barrier of bond exchange which leads to a rapid decrease of viscosity upon increasing temperature. In contrast, vitrimers with low E_a show less pronounced viscosity change with temperature alterations [106]. This trend agrees with the observed flow behavior of MyrAA-30-P-0.7, MyrAA-30-T-0.7, and MyrAA-30-T-1. A practical manifestation of this phenomenon can be utilized in the design of vitrimers with enhanced dimensional stability at service temperatures and yet rapid viscosity decay with increasing temperatures which enables their fast processability [107]. Figure S20 compares the Arrhenius plots of MyrAA-30-P-0.7 and MyrAA-30-Long-P-30; a similar trend was observed with a slight increase of E_a value from 67 to 76 kJ/mol for the respective vitrimers.

Figure 6.d shows the results of creep-recovery experiments for 5 different prepolymers vitrified with excess β-ketoester : amine ratio of 0.7:1. As the cross-linking density increased, the creep systematically decreased. Networks with copolymer having 10 and 20 mol% AAEMA content exhibited similar creep behavior with 2.8% and 2.6% shear strain at 300 s followed by some limited strain recovery of 27% and 28%, respectively. Further increasing the AAEMA content in the copolymer to 30 mol%, MyrAA-30-P-0.7, led to lower shear strain of 1.3% at 300 s which had 52% lower deformation compared to MyrAA-10-P-0.7. In addition, a higher creep recovery of

56% at 900 s was observed for MyrAA-30-P-0.7. At the 300 s point, the creep-recovery analysis of the MyrAA-30-Long-P-0.7, with $M_n \geq M_e$, revealed a lower deformation of about 49% compared to its counterpart, MyrAA-30-P-0.7, with a shorter backbone and $M_n < M_e$. Furthermore, we studied the influence of additional static cross-links in MyrAA-20-GMA-5-P-0.7. The dual cross-linked network showed the lowest deformation until 300 s combined with the highest creep recovery of 83% at 900 s. The high creep recovery in MyrAA-20-GMA-5-P-0.7 indicates that less permanent deformation had occurred in the sample. This can be credited to the presence of static cross-links which restricts network strand deformation [109,150]. The results of creep-recovery are in good agreement with those of stress-relaxation tests, showing that dimensional stability of the vitrimers can be tailored by cross-linking density, increasing primary chain length, and addition of physical or chemical, static cross-links [106,145,149,150].

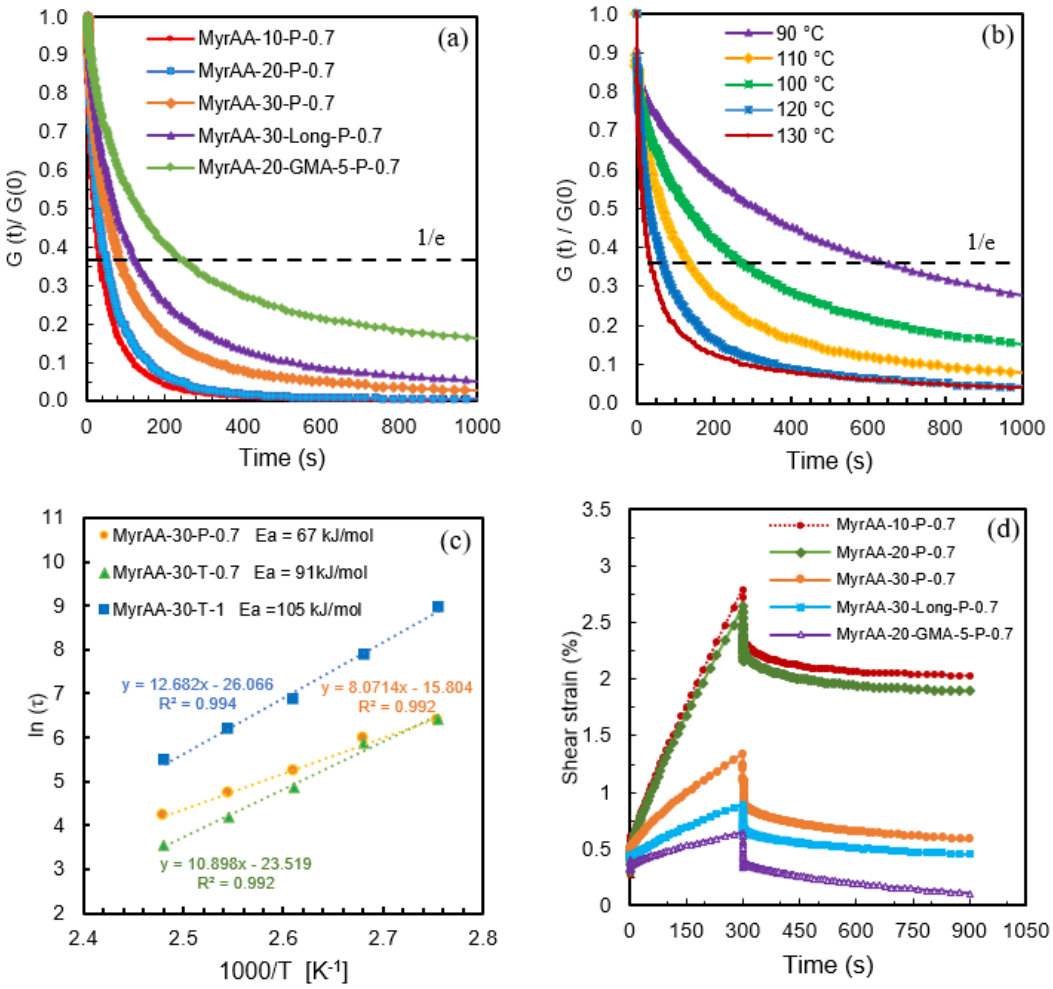

Figure 3.6 Stress-relaxation data **a)** Comparison of stress-relaxation behavior of various pre-polymers vitrified with an excess amount of Priamine (P-0.7) at 130 °C. Increasing AAEMA content and molecular weight of prepolymer ($M_n > M_e$) as well as incorporation of static cross-links systematically increased the relaxation time. **b)** Comparison of stress-relaxation behavior of MyrAA-30-T-0.7 from 90 to 130 °C. **c)** Arrhenius relationship between relaxation time and temperature obtained from the stress relaxation experiment of the MyrAA-30-T-1 (with 1:1 β-ketoester : NH_2) and MyrAA-30-T-0.7 (with 0.7 : 1 β-ketoester : NH_2) vitrimers using stretched exponential decay fit. **d)** Creep-recovery data of various vitrimers cross-linked with excess Priamine (P-0.7). Creep was decreased by increasing the cross-linking density (AAEMA content), increasing the M_n of prepolymer (>M_e), and incorporating 5 mol% GMA to impart dual static and dynamic networks.

3.5.7. Recycling of vitrimers

Vitrimer re-processability and ability to be remolded into new materials after curing is one of the most important properties of such polymer networks. This phenomenon is a direct consequence of the dynamic nature of the cross-links. Particularly, processability of vinylogous urethanes cured with TREN and Priamine were well-established by others [40,55,66,88,115]. Therefore, we mimicked similar recyclability tests by cutting the processed MyrAA-20-T-0.7 into small pieces and re- processing them via hot-pressing for 3 cycles. Figure S22 shows pictures of reprocessed and cut MyrAA-20-T-0.7 samples. We performed the compression molding at a relatively low temperature of 110 °C for 50 ± 5 min to minimize possible side reactions or degradation, and even though this temperature is lower than the values reported in the literature, well-formed samples were achieved. In addition, vitrified polymers showed high isothermal stability in a TGA test at 120 °C under nitrogen flow for 6 h (see Figure S12).

Figure 7 compares the thermomechanical and chemical properties of the original MyrAA-20-T-0.7 and those of the same sample after 3 recycling processes. ATR-FTIR spectra of the sample after each reprocessing cycle showed peaks attributed to the vinylogous urethanes at 1600 cm^{-1}, indicating N-H bending, and 1655 cm^{-1}, indicating C=C stretching, were retained and no other noticeable degradation was observed [55,107].

Thermal analyses by TGA and DSC show that thermal properties of the vitrimer essentially stayed intact after reprocessing. The onset degradation at 360 °C with $T_{5\%}$ = 196 °C and T_g = -48 ± 1 °C was observed for the original and the recycled (3×) samples. DMTA analyses showed that the rubbery plateau was retained after 3× reprocessing with elastic modulus (G′) of 1.8 ± 0.5 MPa. Most importantly, the tensile properties remained intact after each processing cycle.

Figure 7.d illustrates the stress-strain curves of the MyrAA-20-T-0.7 of the originally processed sample and its three consecutive reprocessed ones. Table S5 summarizes the results of tensile tests of reprocessed samples; respectively, average stress and elongation at break of 366 kPa and 21.7% were recorded for the (re)processed samples.

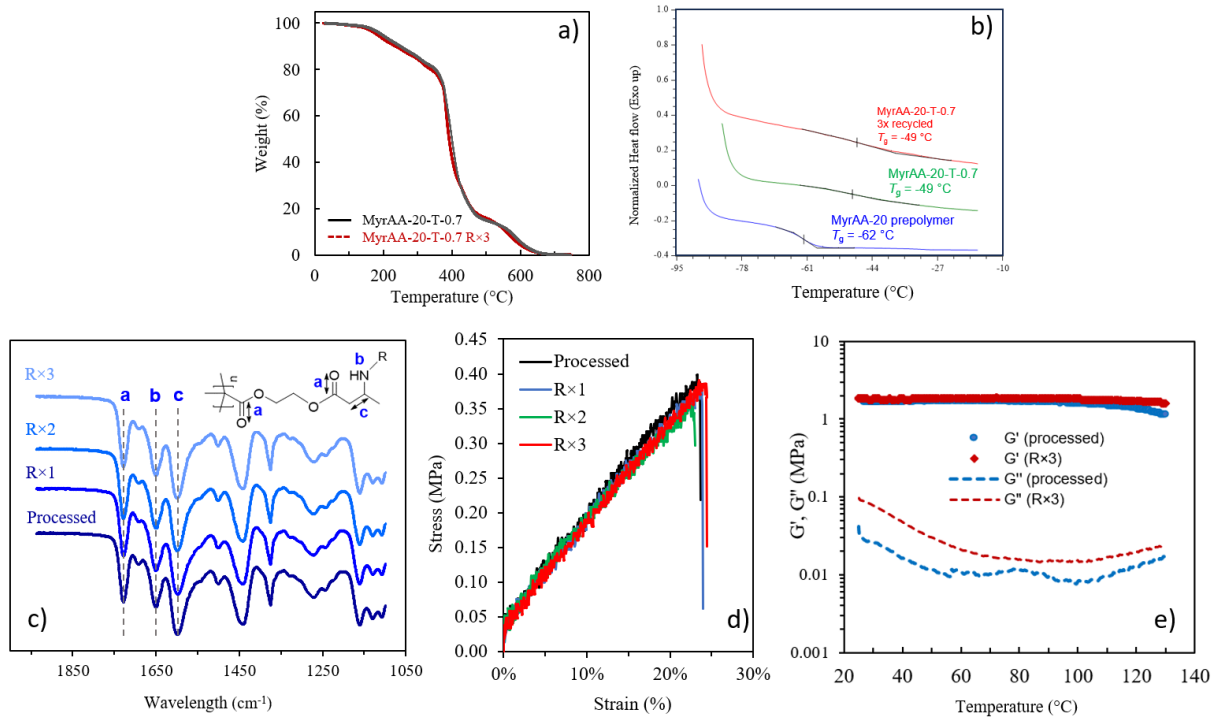

Figure 3.7 Properties of reprocessed MyrAA-20-T-0.7 vitrimer after 3 cycles **a)** TGA traces, thermal decomposition temperature with onset of 355 ± 5 °C did not change. **b)** DSC traces of MyrAA-20 prepolymer (blue line) with T_g of -61.8 °C, pristine processed Myr-AA-20-T-0.7 vitrimer (green line), and Myr-AA-20-T-0.7 vitrimer after 3 reprocessing cycles (red line); T_g was retained at ~ -48 ±1°C after vitrification and reprocessing. **c)** ATR-FTIR spectra, bands of N-H bending at 1600 cm^{-1} and C=C stretching at 1655 cm^{-1} corresponding to the vinylogous urethane cross-links retained. **d)** Stress-strain curves did not change **e)** Semi-logarithmic DMTA traces of originally processed vitrimer and after 3 reprocessing cycles (R×3), the rubbery plateau in elastic (G′) and loss (G″) was retained.

3.5.8. Welding

An interesting consequence of dynamic cross-linking is the ability of different cured samples to be welded together without using significant pressure. Inspired by Liu et al., we performed a welding experiment by dabbing 2-3 drops of butylamine on top of two different rectangular samples each with a size and weight of about 1.5×1×0.1 cm (length×width×thickness) and 0.15 g respectively [91]. Afterwards, the samples were quickly combined and placed in an oven at 115 °C for 20 min. An empty NMR tube was placed on top of the samples to physically secure them, and no extra pressure was applied. The welded sample could resist up to 23.5 g, which is more

than 60 times its weight, illustrated in Figure S23. Control samples without any butylamine could not resist any external weight after a similar welding procedure was applied. Thus, it appears that butylamine caused welding by either solvent welding via swelling of the surfaces and/or possible liberation of some functional groups on the vitrimers and promotion of transamination between the two surfaces which led to a relatively fast and effective welding.

3.5.9. Shape memory

As mentioned in section 3.5, we originally synthesized the dual-functionalized MyrAA-20-GMA-5 prepolymer to impart both static and dynamic cross-links with the goal of reducing creep. Additionally, we hypothesized that shape memory effects can be seen in this material as static epoxy-amine cross-links can "memorize" the permanent shape of the vitrimer while the dynamic vinylogous urethane can retain the temporary shape [135,151]. Therefore, we first vitrified the sample in a rectangular mold, i.e., the permanent shape. Afterwards, the sample was heated and carefully bent and reshaped, the temporary shape, and kept in an oven at 110 °C under vacuum for 1 h. This was followed by cooling of the sample under stress. The resulting sample's shape, Figure 8-b, was temporarily stable, at least for 48 h, until it was heated again in an oven at 120 °C. The full shape recovery was achieved in about 4 h. While good shape fixity and shape recovery ratio was observed, the rate of shape recovery was slow. These results are in line with the observed slower stress-relaxation and full creep-recovery, Figure 6, of MyrAA-20-GMA-5. Although a relatively simple shape recovery is reported, this initial exploration combining shape recovery with hybrid networks of static/dynamic cross-linking was promising.

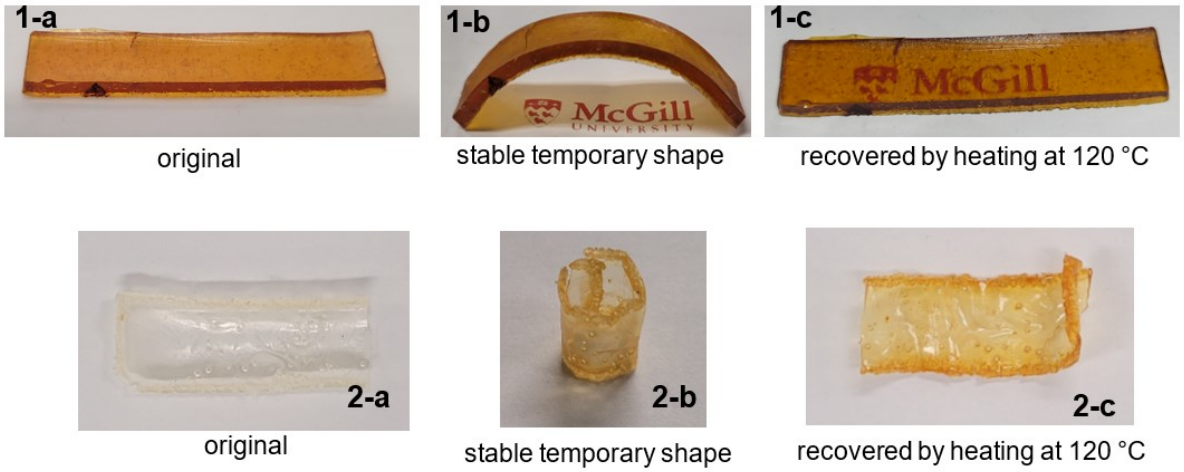

Figure 3.8 Shape memory effect of 2 different shapes of MyrAA-18-GMA-8-P-0.7 samples (the scale is in ~ 1-2 cm) **a)** original shape was formed after vitrification as described in section 2.3 **b)** temporary shape was formed after heating to 110 °C and cooling under stress; the shape was stable at room temperature for at least 24hr **c)** recovery of the original shape by reheating to 120 °C for 4 h.

3.6. Conclusions

Development of elastomers from renewable feedstocks with enhanced recyclability is a step forward towards a more sustainable rubber industry. We have demonstrated a straightforward approach to synthesize bio-based vitrimers using commercially available and relatively inexpensive myrcene with catalyst-free vinylogous urethane chemistry for the first time. Statistical prepolymers of Myr and AAEMA were prepared in a controlled fashion using NMP and afterwards cross-linked with biobased Priamine or TREN via solution casting and compression molding. The final mechanical and rheological properties of the networks could be effectively tailored by changing the prepolymers' composition, molecular weight, and the nature and ratio of the cross-linkers. The rubbery networks exhibited effective reprocessability by mechanical grinding and hot pressing at 110 °C in less than 60 min for at least 3 cycles. ATR-FTIR confirmed retention of the network while no change in the T_g, onset of decomposition, storage modulus as well as elongation and stress at break was observed after reprocessing. Although vitrimer-like insolubility of the networks in different solvents was confirmed, prepolymers could be chemically recovered by addition of excess monofunctional amines at 110 °C without degradation, confirmed by GPC. Also, Myr-based vitrimers could be welded to each other by using a few drops of n-butyl amine at

115 °C in 20 min. Increasing the prepolymer's molecular weight beyond its entanglement limit ($M_n > M_e$) led to decreased creep. In addition, dual networks with static and dynamic cross-links were formed by incorporation of 5 mol% epoxy-based GMA in the prepolymer. The resulting network exhibited significant reduction in creep in addition to shape memory effects.

Adopting vitrimer chemistry is a versatile and yet simple tool in tailoring the thermomechanical properties of poly(Myr) with excellent re-processability. We envision that this approach can be used as a platform to develop customized recyclable biobased elastomers with applications in rubbers, smart materials, wearable electronics, to name but a few.

3.7. Supporting Information for Chapter 3

3.7.1. Synthetic route of prepolymers and vitrimers

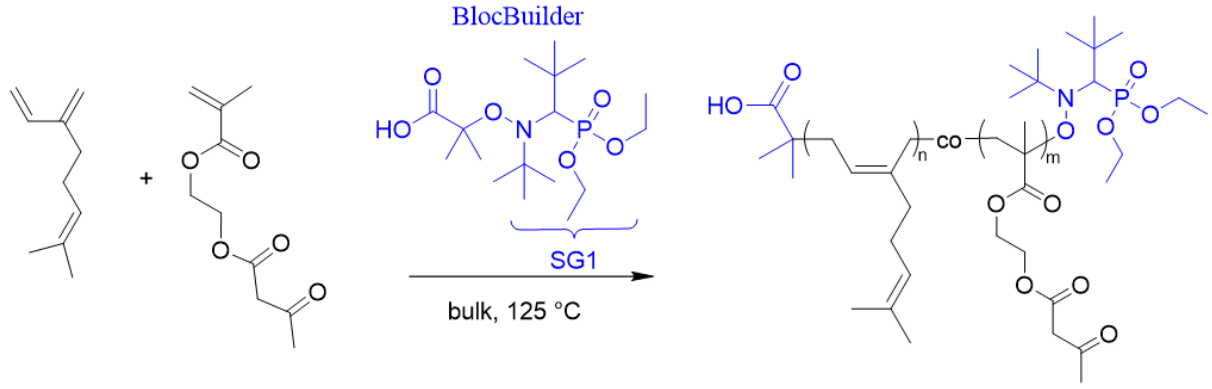

Figure S 3.1 Statistical nitroxide mediated polymerization (NMP) of Myr and AAEMA with BlocBuilder

The prepolymers are coded as MyrAA-xx, where xx refers to the AAEMA mol% in the initial monomer mixture composition. The high molecular weight polymer was coded as MyrAA-30-Long, and the copolymer with 5 mol% GMA content was named MyrAA-20-GMA-5.

Table S 3-1 Myrcene/ AAEMA/ GMA copolymerization formulae and synthesis conditions

prepolymer code [a]	$[Alkoxyamine]_0$ (M)[c]	$[Myr]_0$ (M)[d]	$[AAEMA]_0$ (M)	$[GMA]_0$ (M)	$M_{n,\,target}$ [e] (g/mol)	T (˚C)	time (h)
MyrAA-10 [a]	0.033	5.19	0.58	—	25,000	125	8.5
MyrAA-20 [a]	0.035	4.56	1.21	—	25,000	125	8
MyrAA-30 [a]	0.036	3.82	1.79	—	25,000	125	6
MyrAA-30-Long [b]	0.015	3.83	1.79	—	60,000	125	8
MyrAA-20-GMA-5	0.033	4.32	1.15	0.29	25,000	125	6

[a] Experimental identification of copolymers: MyrAA-xx, where xx referees to the initial molar ratio of AAEMA
[b] Long refers to prepolymer with higher target number average molecular weight (M_n)
[c] Molar concentration of BlocBuilder, or NHS-BlocBuilder in case of MyrAA-20-GMA-5
[d] Initial monomer molar concentration in the feed
[e] Target M_n at 100% conversion

3.7.2. Vitrification

As an example, for the synthesis of MyrAA-30-P-0.7 and MyrAA-30-T-0.7 vitrimers, 7 g and 8.5 g of each dried prepolymers were dissolved in 21 and 17 mL of THF respectively. Afterwards 5.03 g Priamine and 1.11 g TREN were added to each solution respectively.

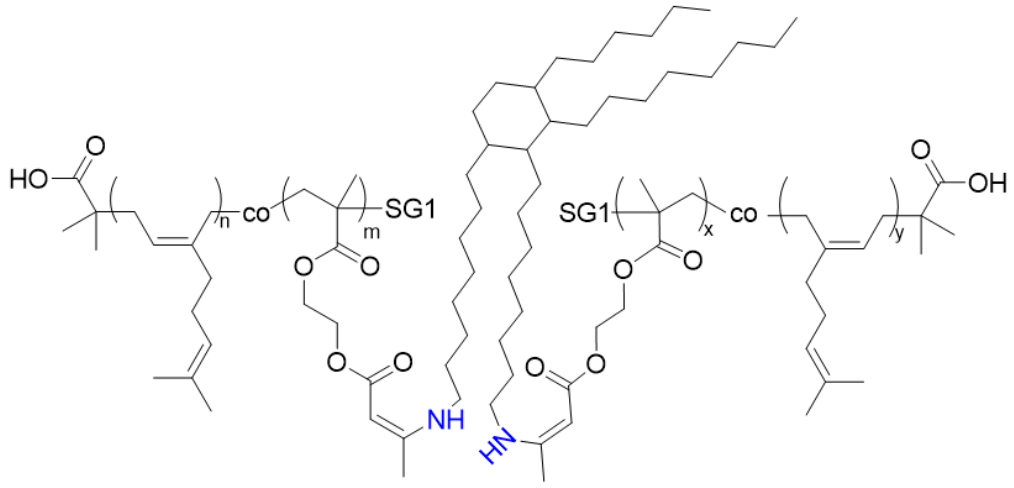

Figure S 3.2 Vitrified MyrAA-based prepolymer with Priamine

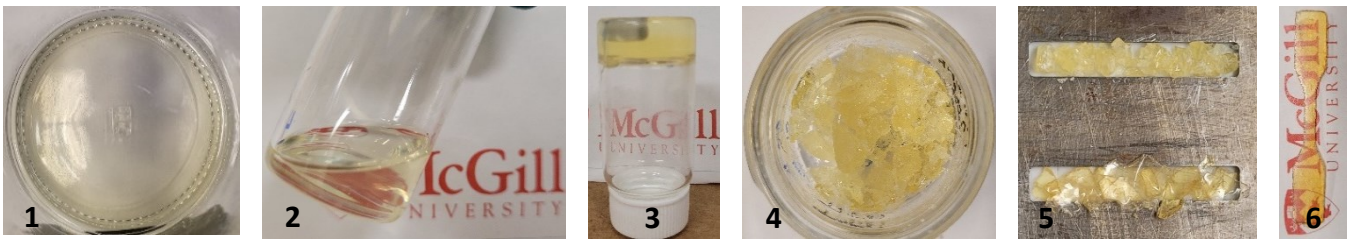

Figure S 3.3 Chronological synthesis and processing of vitrimers. 1) liquid like pre-polymer of p(Myrcene-co-AAEMA), 2) prepolymer dissolved in THF, 3) addition of cross-linker (Priamine or TREN) and gelation, 4) drying the network under reduced vacuum and elevated temperature, 5) compression molding, 6) shaped final samples

3.7.3. ^{1}H NMR spectra and analyses of prepolymers

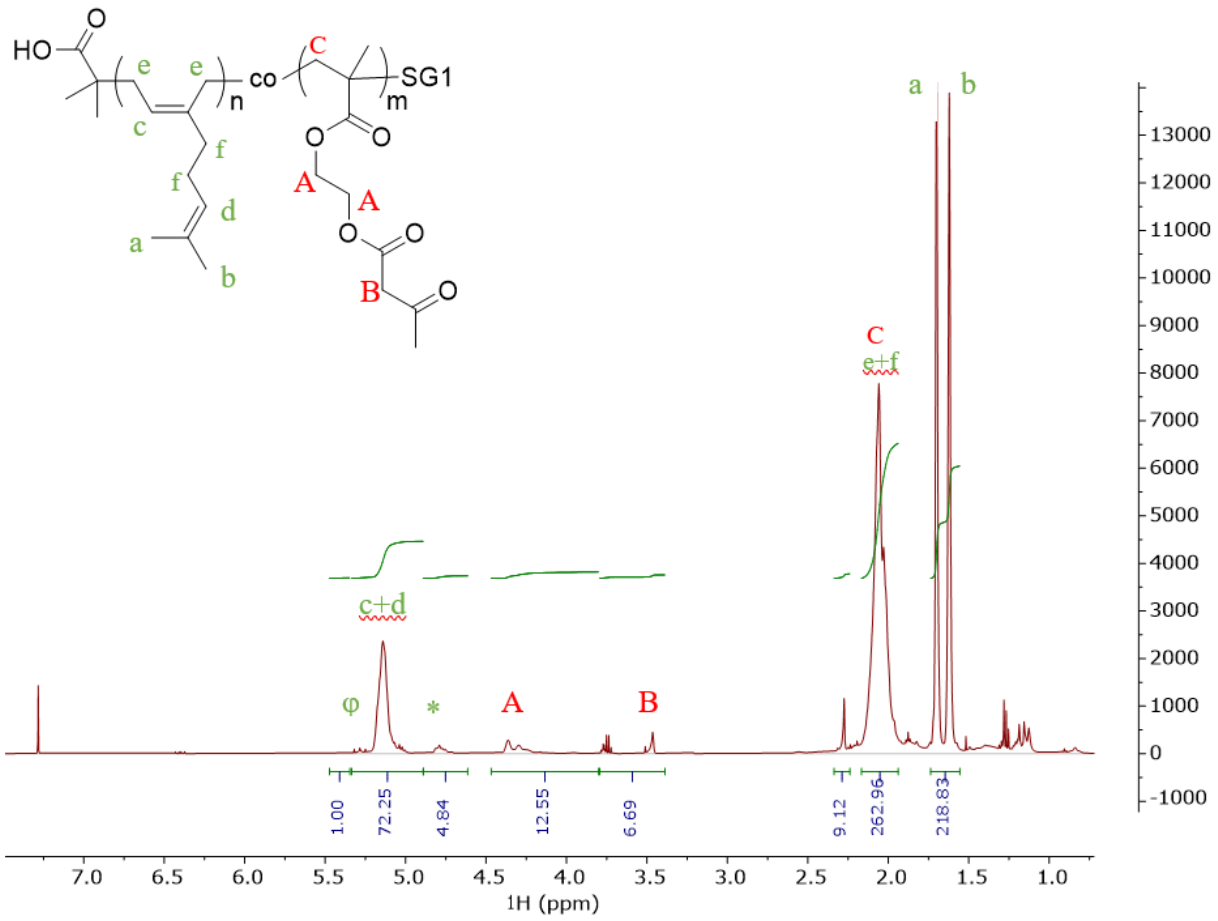

Figure S 3.4 ^{1}H NMR spectrum of dried poly(MyrAA-10) after precipitation and recovery in CDCl3 (500 MHz) at room temperature. poly(MyrAA-10): δ = 5.50-5.30 (t br, 1H ^{1,2}), 5.25-5.00 (t br, 1H^{1,2}, 1H^{3,4}, 2H ^{1,4}), 4.80-4.70 (m, 2H ^{1,2} 2H ^{3,4}), 4.44-3.85 (d br, 4H $^{poly(AAEMA)}$), 3.85-3.4 (s, br 2H $^{poly(AAEMA)}$), 2.27 (s, 3H $^{poly(AAEMA)}$), 2.25 -1.85 (m br, 8H $^{poly(Myr)}$),1.90-1.75 (m, 2H $^{poly(AAEMA)}$), 1.67 (s, 3H $^{poly(Myr)}$), 1.59 (s, 3H $^{poly(Myr)}$).

* Signal at 4.80-4.70 ppm corresponds to vinylic 2H ^{1,2} and 2H ^{3,4} and φ signal at 5.50-5.30 ppm correspond to olefinic 1H ^{1,2} (not shown in the chemical structure).

Monomer peaks (not shown): δ = 6.45-6.27 (m, 1H ^{Myr}), 6.15 (s, 1H ^{AAEMA}), 5.60 (s, 1H ^{AAEMA})

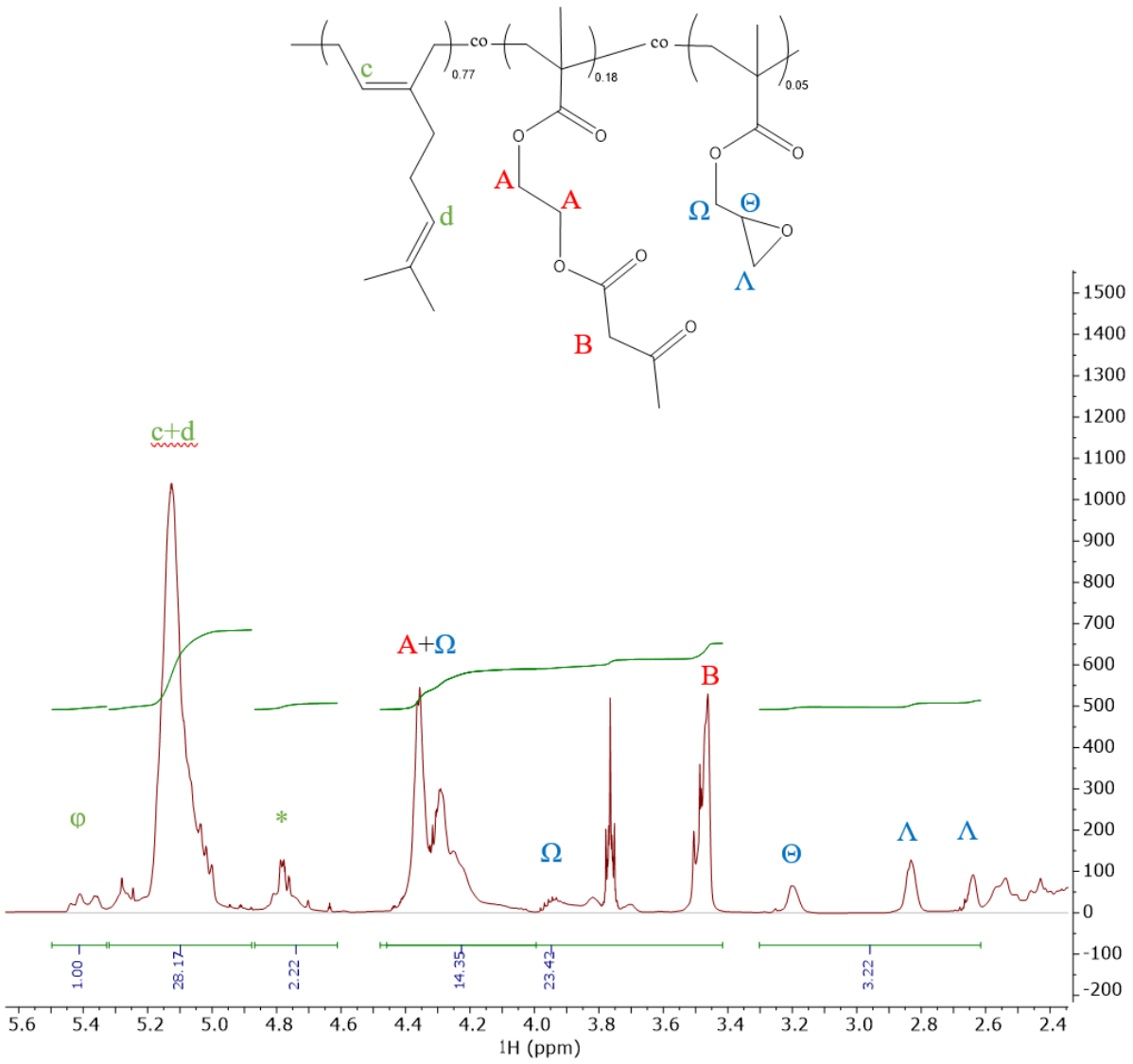

Figure S 3.5 ^{1}H NMR spectrum of dried poly(MyrAA-20-GMA-5) statistical terpolymer after precipitation and recovery in $CDCl_3$ (500 MHz) at room temperature. p(MyrAA-20-GMA-5): δ = 5.50-5.30 (t br, 1H ^{1,2}), 5.25-5.00 (t br, 1H^{1,2}, 1H^{3,4}, 2H ^{1,4}), 4.80-4.70 (m, 2H^{1,2} 2H^{3,4}), 4.45-3.85 (br, 4H $^{poly(AAEMA)}$ 1H $^{poly(GMA)}$), 3.85-3.4 (br, 2H $^{poly(AAEMA)}$, 1H $^{poly(GMA)}$), 3.25-3.13 (s, 1H $^{poly(GMA)}$), 2.95-2.75 (s, 1H $^{poly(GMA)}$)), 2.70-2.60 (s, 1H $^{poly(GMA)}$)), 2.27 (s, 3H $^{poly(AAEMA)}$), 1.90-1.75 (m, 2H$^{poly(AAEMA)}$, 2H $^{poly(GMA}$), 1.67 (s, 3H $^{poly(Myr)}$), 1.59 (s, 3H $^{poly(Myr)}$), 0.90-0.65 (m, 3H $^{poly(GMA)}$). * Signal at 4.80-4.70 ppm corresponds to vinylic 2H ^{1,2} and 2H ^{3,4} and φ signal at 5.50-5.30 ppm correspond to olefinic 1H ^{1,2} (not shown in the chemical structure).

Calculation of AAEMA and GMA incorporation

$n_{poly(GMA)} = (\text{Area}_{3.30\text{-}2.60ppm})/3$

$n_{poly(AAEMA)} = [\text{Area}_{4.5\text{-}3.4ppm} - 2\times(\text{Area}_{3.30\text{-}2.60ppm})/3] / 6$

$n_{poly(Myr)} = (\text{Area}_{1.75\text{-}1.69ppm})/6$

$\%\ poly(AAEMA) = [n_{poly(AAEMA)} / (n_{poly(GMA)} + n_{poly(AAEMA)} + n_{poly(Myr)})] \times 100\%$

$\%\ poly(GMA) = [n_{poly(GMA)} / (n_{poly(GMA)} + n_{poly(AAEMA)} + n_{poly(Myr)})] \times 100\%$

$\%\ poly(Myr) = [n_{poly(Myr)} / (n_{poly(GMA)} + n_{poly(AAEMA)} + n_{poly(Myr)})] \times 100\%$

For poly(MyrAA-20-GMA-5) we have:

$n_{poly(GMA)} = (3.22)/3 = 1.07$

$n_{poly(AAEMA)} = [23.42 - 2\times(3.22)/3] / 6 = 3.54$

$n_{poly(Myr)} = (\text{Area}_{1.75\text{-}1.69ppm} = 90.67)/6 = 15.11$

$\%\ poly(AAEMA) = [3.54 / (1.07 + 3.54 + 15.11)]\times 100\% \approx 18\%$

$\%\ poly(GMA) = [1.07 / (1.07 + 3.54 + 15.11)] \times 100\% \approx 5\%$

$\%\ poly(Myr) = [15.11/(1.07 + 3.54 + 15.11)] \times 100\% \approx 77\%$

Calculation of p(Myr) microstructure:

x, y, z are attributed to one ^1H of 1,4 and 1,2 and 3,4 addition respectively

$\text{Area}_{5.50\text{-}5.30\ ppm} = y$

$\text{Area}_{5.25\text{-}5.00\ ppm} = 2x + y + z$

$\text{Area}_{4.80\text{-}4.70\ ppm} = 2y + 2z$

The system of equations can be easily solved. The composition of the microstructure can be calculated as following.

$\%\ poly(Myr_{-1,4}) = [x/(x+y+z)] \times 100\%$

$\%\ poly(Myr_{-1,2}) = [y/(x+y+z)] \times 100\%$

$\%\ poly(Myr_{-3,4}) = [z/(x+y+z)] \times 100\%$

Sample calculation for poly(MyrAA-10):

Area $_{5.50\text{-}5.30\ ppm} = y = 1$

Area $_{5.25\text{-}5.00\ ppm} = 2x + y + z = 72.25$

Area $_{4.80\text{-}4.70\ ppm} = 2y + 2z = 2 + 2z = 4.84$

$y = 1$

$x = 34.91$

% poly(Myr $_{-1,4}$) = $[\ 34.91/\ (34.91+1+1.42)]$ ×100% ≈ 93.5%

% poly(Myr $_{-1,2}$) = $[\ 1/\ (34.91+1+1.42)]$ ×100% ≈ 2.7%

% poly(Myr $_{-3,4}$) = $[\ 1.42/\ (34.91+1+1.42)]$ ×100% ≈ 3.8%

Diffusion Ordered Spectroscopy (DOSY)

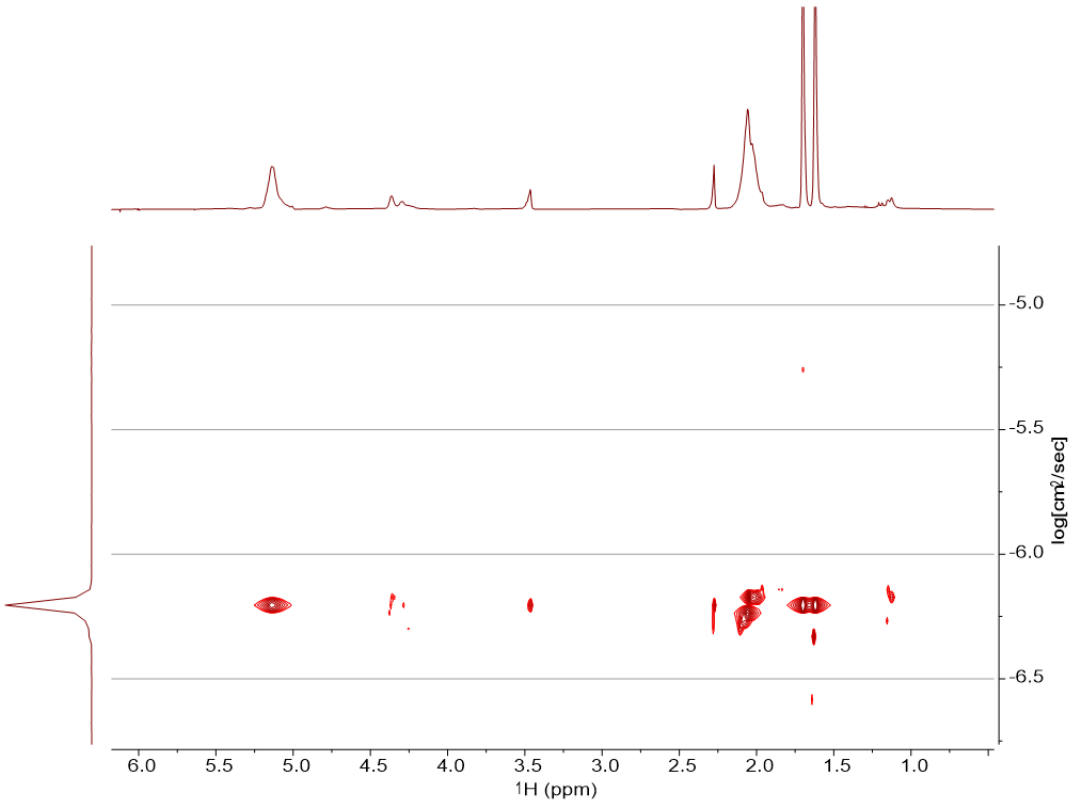

Figure S 3.6 2D DOSY NMR spectra of MyrAA-20 prepolymer obtained at 25°C in $CDCl_3$ solution. The existence of one vertical peak with the estimated diffusion coefficient of 6.3E-07 cm^2/s confirms formation of a single population of copolymers.

3.7.4. Kinetics of MyrAA-10 polymerization

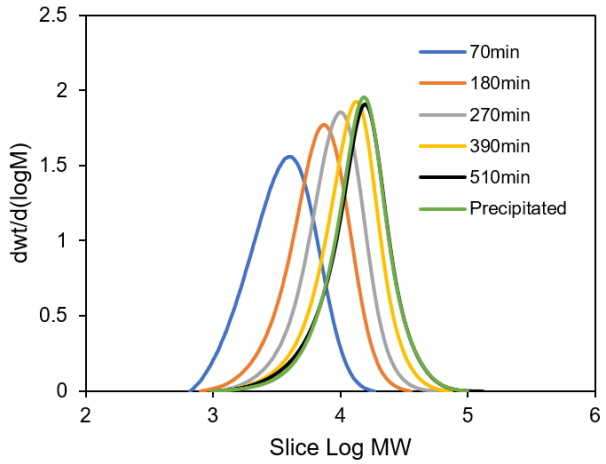

Figure S 3.7 GPC traces of MyrAA-10 from kinetic studies.

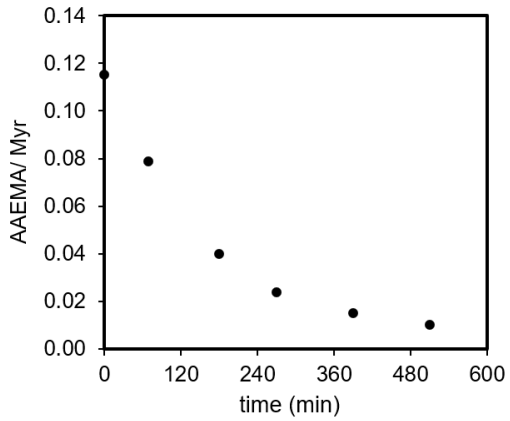

Figure S 3.8 Unreacted AAEMA to myrcene ratio during the synthesis of MyrAA-10 over time. The decline of the ratio suggests a compositional drift.

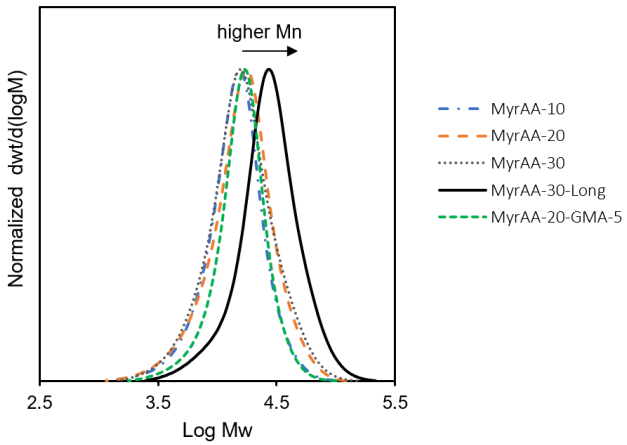

Figure S 3.9 GPC traces of various prepolymers. All prepolymers had similar Mn except MyrAA-30-Long.

3.7.5. DSC experiments and glass transition temperatures (T_g)

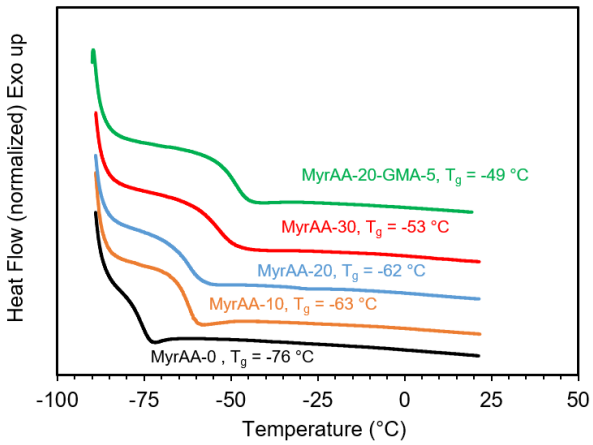

Figure S 3.10 DSC traces of prepolymers. Glass transition temperature (T_g) increased from -76°C for the poly(myrcene) homopolymer to -54°C for MyrAA-30 copolymer.

Using the Flory-Fox equation, theoretical T_g of the prepolymers ($T_{g,\,theory}$) can be estimated.

$$\frac{1}{T_{g,theory}} = \sum_i \frac{w_i}{T_{g,i}}$$

Here, w_i is the mass fraction of component i in the polymer resin and $T_{g,i}$ is the glass transition of the homopolymer of component i in K. Assuming T_g of homopolymers of Myr, AAEMA, and GMA to be -76 °C, 15 °C, and 85 °C respective, the estimated T_gs will be as follows [40,141].

Table S 3-2 Comparison of T_g from DSC and estimated by Flory-Fox equation

code	$T_{g\,DSC}$ (˚C)	$T_{g\,Fox}$ (˚C)
MyrAA-10	-63	-67
MyrAA-20	-62	-59
MyrAA-30	-53	-47
MyrAA-30-Long	-54	-47
MyrAA-20-GMA-5	-49	-53

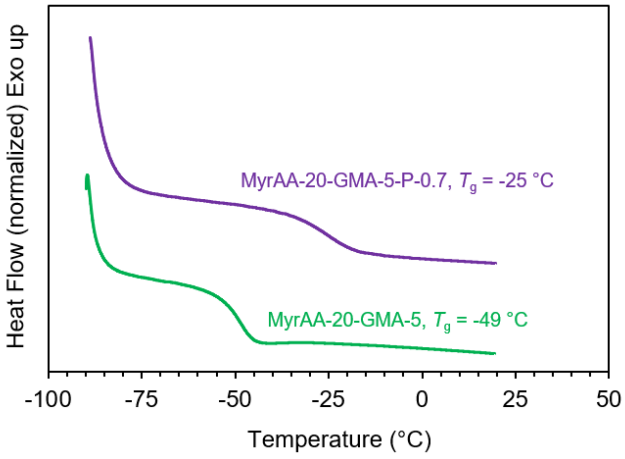

Figure S 3.11 DSC spectra of MyrAA-20-GMA-5 prepolymer and Myr-20-GMA-P-0.7 vitrimer. A shift toward higher T_gs is observed due to cross-linking and network formation.

3.7.6. Calculation of copolymers' solubility parameters (δ)

Solubility parameters of homopolymers of p(Myr) and p(GMA) were 16.8 and 18.2 $(MPa)^{0.5}$ respectively, according to the literature [130,141,152] The Hoftyzer and Van Krevelen method was used to estimate the solubility parameter of the p(AAEMA) homopolymer [147]: δ_{AA} = 19.0 $(MPa)^{0.5}$. The detailed calculations according to the group contribution method are as follows. δ_d, δ_p , δ_p are contributions from dispersion forces, polar forces and hydrogen bonding respectively. F_{di} and F_{pi} are the molar attraction constants for dispersion and polar forces while E_{hi} is the cohesive energy for hydrogen bonding. V_m is the molar volume of Myr, AAEMA, GMA and were assumed to be 170, 190, and 132 mL/mol, respectively using $V_{m,i} = Mw_i/\rho_i$ [146,147,153].

$$\delta_d = \frac{\sum F_{di}}{V_m} \quad ; \quad \delta_p = \frac{\sqrt{\sum F_{di}^2}}{V_m} \quad ; \delta_h = \sqrt{\frac{\sum E_{hi}}{V_m}}$$

$$\delta^2 = \delta_d^2 + \delta_p^2 + \delta_p{}^2$$

Therefore, δ_{AA} = 19.0 $(MPa)^{0.5}$.

The solubility parameter of the final copolymers ($\delta_{copolymer}$) was estimated using the volumetric average $\overline{V}_i$ of each homopolymer. F_i is the molar ratio of each co-monomer in the dried prepolymer.

$$\delta_{copolymer} = \frac{\overline{V}_i\, \delta_{homo\,,\,i}}{\sum \overline{V}_i\, \delta_{homo\,,\,i}} \qquad \overline{V}_i = \frac{F_i V_{m,i}}{\sum F_i V_{m,i}}$$

Table S 3-3 Group contributions of AAEMA

groups	#	F_{di} [MPa$^{1/2}$· mol^{-1}]	F_{pi}^2 [MPa· mol^{-2}]	E_{hi} [J·mol^{-1}]
-CH3	2	840	0	0
-CH2-	4	1080	0	0
>CH-	0	0	0	0
>C<	1	-70	0	0
-CO-	1	290	592900	2000
-COO-	2	780	960400	14000
Total		2920	1553300	16000

The Flory-Huggins solvent-polymer enthalpic interaction parameter (χ) and cross-linking density (υ_e) were calculated by the following equations.

$$\upsilon_e = -\frac{ln(1-V_r)+V_r+\chi_{12}V_r^2}{V_s\left(V_r^{\frac{1}{3}}-\frac{V_r}{2}\right)}$$

$$V_r = \frac{\frac{m_2}{\rho_2}}{\frac{m_1}{\rho_1}+\frac{m_2}{\rho_2}}$$

$$\chi_{12} = \frac{V_s}{RT}(\delta_s - \delta_p)^2$$

In which, V_s is the molar volume of toluene; V_r is the volume fraction of polymer network in the swollen sample; m_1 and m_2 are the mass of the swollen and vacuum dried samples, and δ_s and δ_p are the solubility parameters of the solvent and polymer, respectively.

3.7.7. TGA of various vitrimers

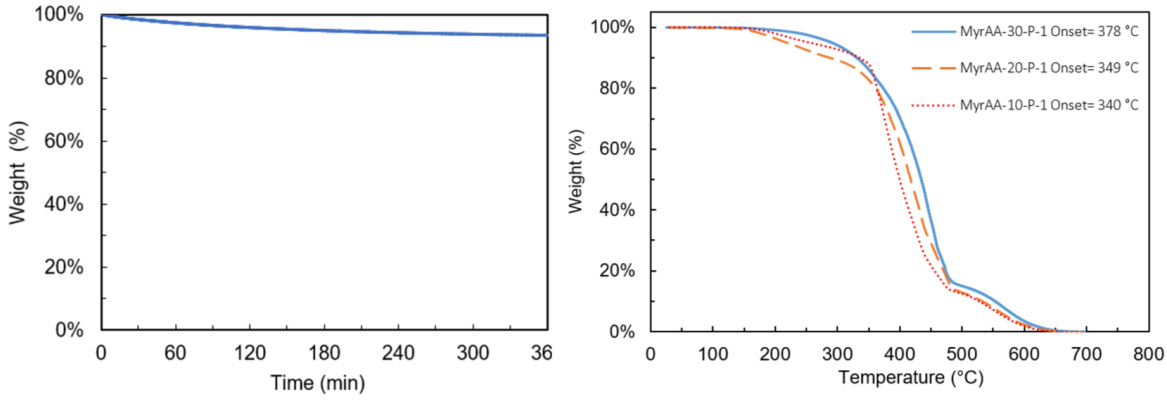

Figure S 3.12 TGA traces of: Left) MyrAA-T-0.7 vitrimer at 120°C isotherm for 6h; 6.43% weight loss was observed. Right) different networks with various AAEMA loadings and crosslinked using Priamine and 1 : 0.7 ratio of NH2 : β-ketoester. The onset of degradation was shifted to higher temperatures with increasing AAEMA loading

3.7.8. Swelling of vitrimers and chemical recycling

Figure S 3.13 Swelling of MyrAA-20-T-0.7 vitrimer in chloroform, toluene, THF, DMF, and methanol.

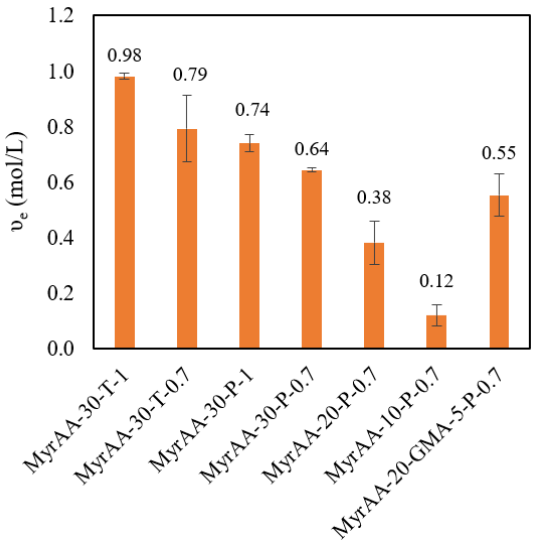

Figure S 3.14 Comparisons of the cross-link density of various networks from highest to lowest, calculated using the Flory-Rehner equation and swelling tests in toluene. A monotonic rise in cross-linking density was observed with increasing AAEMA content and balancing the stoichiometric cross-linking ratio.

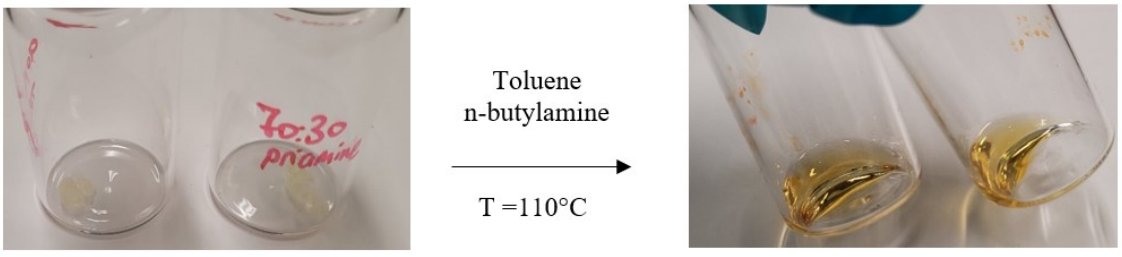

Figure S 3.15 Network disintegration of MyrAA-20-P-0.7 and MyrAA-30-P-0.7 vitrimers using excess n-butylamine in toluene at 110 °C.

3.7.9. Strain sweep tests and linear viscoelastic region

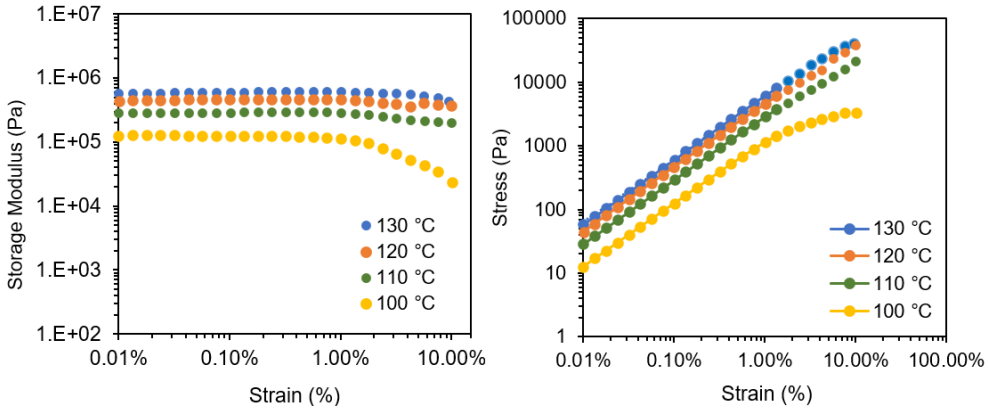

Figure S 3.16 Strain sweep (left) and stress-strain sweep (right) tests at 1Hz of MyrAA-30-P-0.7 at various temperatures. The linear viscoelastic regions in (right).

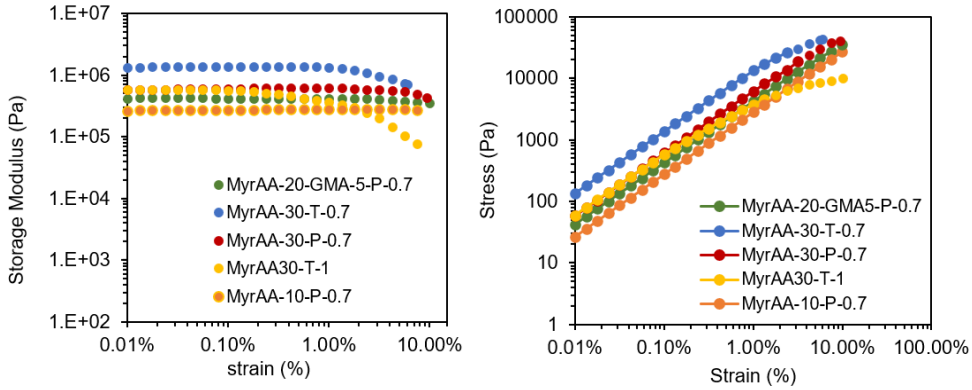

Figure S 3.17 Representative strain sweep (left) and stress-strain sweep (right) tests at 1 Hz of various vitrimers at 130 °C. The linear viscoelastic regions in (right).

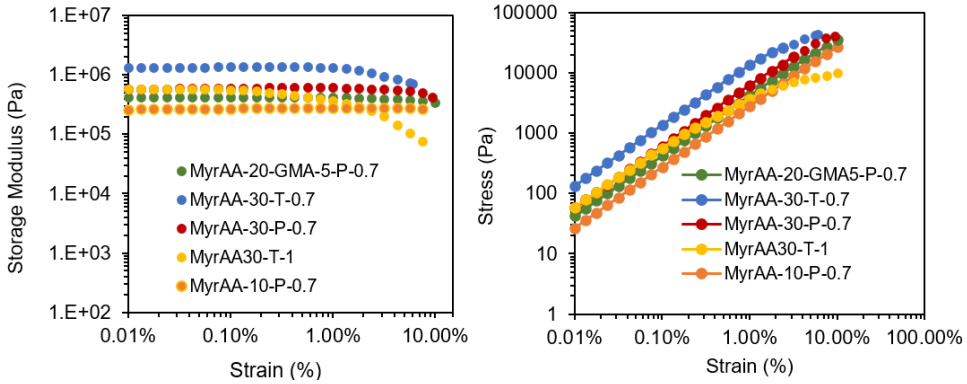

Figure S 3.18 Representative strain sweep (left) and stress-strain sweep (right) tests at 1 Hz of various vitrimers at 130 °C. The linear viscoelastic regions in (right).

3.7.10. Stress Relaxation

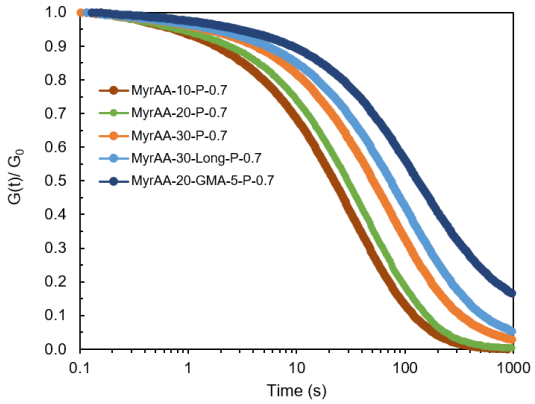

Figure S 3.19 Semi logarithmic graphs of stress-relaxation behavior of various pre-polymers vitrified with an excess amount of Priamine (P-0.7) at 130 °C. Increasing AAEMA content and molecular weight of prepolymer ($M_n > M_e$) as well as incorporation of static cross-links systematically increased the relaxation time.

Table S 3-4 Parameters obtained by curve fitting the stress relaxation curves using the stretched exponential model. The results show slower relaxation due to increasing the molecular weight of the prepolymer $M_n > M_e$ and having balanced 1:1 β-ketoester : NH_2.

MyrAA- 30-P-0.7			MyrAA-30-Long- P-0.7			MyrAA- 30-T-0.7			MyrAA- 30-T-1		
T (°C)	**τ***	**β**	**T (°C)**	**τ***	**β**	**T (°C)**	**τ***	**β**	**T (°C)**	**τ***	**β**
90	812.7	0.57	90	1655.0	0.61	90	755.7	0.57	90	7853.5	0.43
100	499.0	0.66	100	765.4	0.66	100	369.2	0.66	100	2713.4	0.42
110	253.1	0.43	110	423.1	0.66	110	131.4	0.43	110	968.8	0.52
120	148.6	0.44	120	236.1	0.67	120	64.6	0.44	120	499.7	0.56
130	89.7	0.40	130	132.8	0.68	130	36.5	0.40	130	242.6	0.58

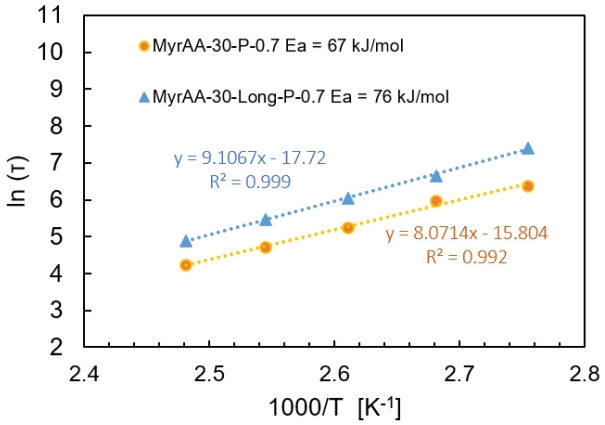

Figure S 3.20 Arrhenius relationship between relaxation time and temperature obtained from the stress relaxation experiment of the MyrAA-30-P-0.7 (with 1:0.7 NH2 : β-ketoester) and MyrAA-30-Long-P-0.7 (with 1:0.7 NH2 : β-ketoester) vitrimers. The figures show that increasing the M_n of the prepolymer ($M_n > M_e$) in case of MyrAA-30-Long-P-0.7 slightly increased the activation energy.

3.7.11. Tensile data of MyrAA-20 vitrimer

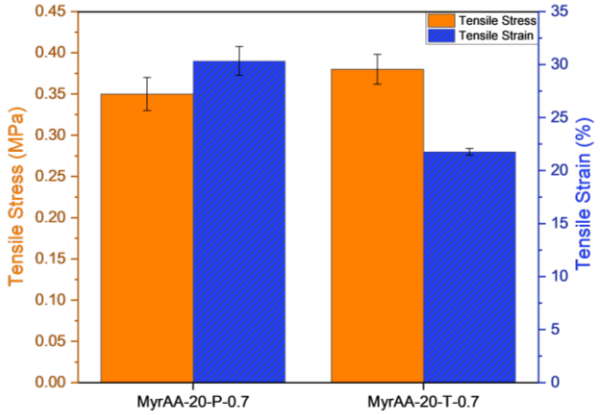

Figure S 3.21 Tensile data of MyrAA-20-P-0.7 and MyrAA-20-T-0.7 vitrimers. The use of triamine cross-linker resulted in a tighter and stiffer network.

3.7.12. Reprocessing of vitrimers

Figure S 3.22 Reprocessing of poly(myrcene)-based vitrimers. Cured and processed samples were cut into small pieces and hot-pressed for 3 cycles.

Table S 3-5 Tensile properties of reprocessed MyrAA-20-T-0.7. The results show that the tensile properties of the vitrimer did not deteriorate after at least 3 cycles of reprocessing.

MyrAA-30-T-0.7	Stress at break (kPa)	Strain at break (%)	Young's Modulus (MPa)
Original Processed	375.7 ± 22.7	22.1 ± 0.8	1.53 ± 0.04
Reprocessed ×1	362.6 ±29.0	22.6 ± 1.4	1.45 ± 0.02
Reprocessed ×2	348.3 ± 16.3	20.0 ± 2.1	1.54 ± 0.14
Reprocessed ×3	377.7 ± 52.4	22.3 ± 2.4	1.52 ± 0.09

3.7.13. Welding of two different vitrimer samples

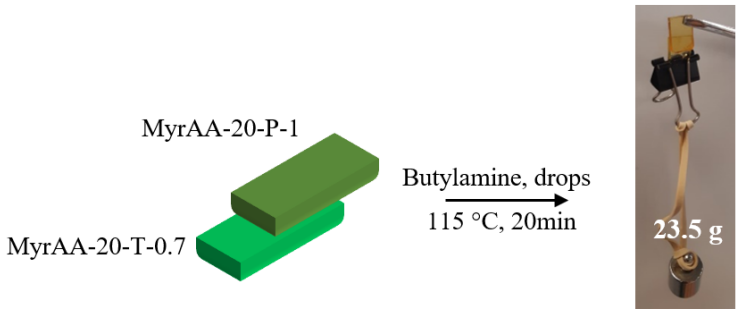

Figure S 3.23 Welding of two different vitrimeric samples: MyrAA-20-P-1 and MyrAA20-T-0.7. Samples were dabbed with a few drops of butylamine at the interface and then heated for 20 min under no added pressure. The welded sample could resist up to 23.5 g, which is more than 60 times its weight.

3.7.14. ATR-FTIR analyses

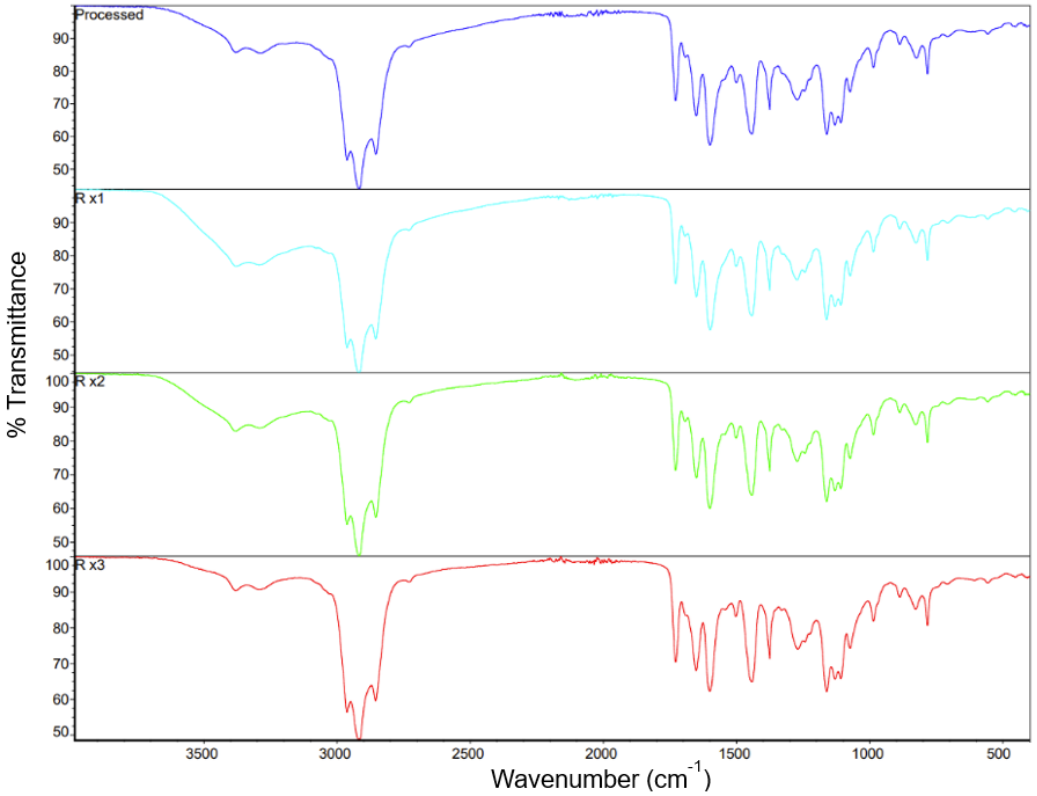

Figure S 3.24 Full ATR-FTIR spectra of the MyrAA-20-T-0.7 vitrimer after original processing and 3 cycles of reprocessing (each cycle denoted by R ×1, R×2, R×3) by mechanical grinding and hot pressing. No appreciable alteration in the spectra was observed due to reprocessing. Bands of N-H bending at 1600 cm^{-1} and C=C stretching at 1655 cm^{-1} corresponding to the vinylogous urethane crosslinks being retained [88,88,112].

Chapter 4: Thermadapt shape memory vitrimeric polymyrcene elastomer

Farhad Asempour, Ruixuan Yang, Milan Maric

This chapter is presented as an article published as the following with the same title and authors.

Reactive and Functional Polymers

Volume 201, August 2024, 105941

DOI: https://doi.org/10.1016/j.reactfunctpolym.2024.105941 [154]

4.1. Preamble to Chapter 4

In Chapter 3, we developed myrcene-based vitrimeric rubbers. However, a few questions remained unanswered. First, some evidence of compositional drift in the synthesis of myrcene/AAEMA copolymers was observed leading to ambiguity in their microstructure. Second, shape memory recovery times were excessively long, being > 1 h and were not efficient.

In this chapter, we addressed these issues by conducting a series of copolymerization experiments to find the reactivity ratios of myrcene/AAEMA system and allow for prediction of monomer sequences in the final copolymer. Our findings indicate that myrcene and AAEMA tend to react in an almost alternating manner. Additionally, we explored the use of T_g as a bulk material property for rapid induction of shape memory effects, instead of slower dynamic bond exchanges, through external stimuli.

4.2. Abstract

Earlier studies of β-Myrcene (Myr)/ β-ketoester functional (acetoacetoxy)ethyl methacrylate (AAEMA) copolymers exhibited compositional drift, leading to ambiguity in microstructure/thermomechanical property correlations while shape memory recovery times were excessively long > 1 h. The terpene-based 1,3-diene Myr and AAEMA were copolymerized via nitroxide-mediated polymerization (NMP) with an initial Myr molar feed ratio ranging from 0.1 to 0.9. Reactivity ratios estimated by the Meyer-Lowry method were $r_{Myr} = 0.20$ and $r_{AAEMA} = 0.22$ with respective 95% confidence intervals of [0.13, 0.37] and [0.15, 0.23], suggesting alternating copolymerization. Bulk terpolymerization with styrene (Sty) afforded linear poly(Myr-*stat*-Sty-*stat*-AAEMA) prepolymers designed to modulate glass transition temperature T_g and stiffness. Subsequent cross-linking with isophorone diamine (IPDA) formed catalyst-free vinylogous urethane dynamic linkages. ATR-FTIR, dynamic mechanical analysis (DMA), and tensile measurements confirmed the recyclability of vitrimers through hot pressing at 110 °C, demonstrating minimal changes in rheological and mechanical properties even after four cycles. By heating the vitrimers to above their T_g (to ~ 45°C), they exhibited a shape memory effect with high shape fixity and fast shape recovery (< 1 min). The vitrimers could undergo permanent shape reprogramming through reconfiguration of dynamic bonds at ~110 °C. This work shows the adaptability of Myr-based rubbers by vitrification and appropriate copolymerization for the synthesis of more sustainable elastomers with stimuli responsive properties.

4.3. Introduction

Elastomers and rubbers play an important role in modern technologies whenever flexibility is required [155]. Their low cost, light weight, facile processing, and overall durability render them ideal materials for tires, apparel, seals, damping systems, soft robotics, wearable electronics, and stretchable sensor [60]. Conventional elastomers are manufactured via vulcanization (curing) processes, which form covalently crosslinked networks to ensure elasticity, mechanical robustness, thermal and chemical stability [156]. However, crosslinking inherently limits their (re)processability and recycling. Recycling of waste rubber products has become a serious environmental problem [1,4]. With the paradigm shift of moving away from fossil-based materials and going towards a circular economy, there is also considerable interest in switching to biomass feedstocks with enhanced recyclability and closed loop production cycles [11,156–158].

In the past decade, vitrimers have emerged as a promising class of materials to address the recyclability of thermosetting elastomers [75,159]. Vitrimers are dynamically cross-linked macromolecules that can undergo network and topology rearrangement at elevated temperatures without disrupting the number of bonds and cross-linking density [73]. The associative nature of the dynamic bond exchanges makes vitrimers combine the flowability and reprocessability of thermoplastics with toughness and insolubility of thermosets [160] . Many dynamic cross-linking chemistries such as transesterification, vinylogous urethane, boronic ester, imine and urethane exchange reactions have been employed in the synthesis of rubbers [59,66,98,111,161]. Another interesting consequence of dynamic covalent bonds is the possibility of imparting stimuli-responsive properties such as self-healing and shape memory effects [161–163]. Shape Memory Vitrimers, sometimes called Thermadapts, exhibit permanent shape reconfigurability [164,165]. Their solid-state plasticity allows for sophisticated shape transformations without the constraints of molds.

In addition, numerous bio-sourced precursors, including derivatives of lignin, saccharides, furans, fatty acids, terpenes, and natural rubber, have been reported for elastomeric vitrimers [11]. Among the broad and diverse category of bio-monomers and polymers, terpenes stand out prominently, thanks to their abundance and distinctive chemical structure [166]. Terpenes are composed of essentially isoprene-based building blocks and are commonly found in plants and essential oils. Their unique natural fragrances make them valuable in a range of industries, such as perfumes,

cosmetics, and food additives [120]. β-Myrcene (Myr), the monomer of interest in this work, is an acyclic monoterpene with three double bonds which can undergo radical polymerization like other 1,3 diene monomers. Myr is commonly found naturally in essential oils of plants such as hops, cannabis, lemongrass, as well as in citrus fruits [123] Despite that, pyrolysis of β-pinene is currently the primary industrial method for Myr production [123,167]. With an approximate glass transition temperature (T_g) of −75 °C, poly(Myr) yields rubbery polymers similar to petroleum-based isoprene and butadiene polymers; hence, Myr has been targeted as a greener alternative [118,121]. Despite the promise of Myr, its polymer exhibits poorer mechanical properties compared to poly(isoprene) and poly(butadiene) due to Myr's comparatively higher entanglement molecular weight M_e of ~20,000 g/mol [121,124,168]. In contrast, poly(isoprene)'s M_e has been reported to be 4000-6000 g/mol) [168]. Many strategies have been reported to render poly(Myr)-based rubbers more industrially relevant including functionalization with reactive groups [20,141,146] copolymerization with ethylene and propylene [169,170] styrene (Sty) [119,125,171], isobornyl methacrylate (IBOMA) [129], α-methyl-p-methylstyrene (AMMS) [167] , hydrogenation [122], and dynamic cross-linking [103,131]. Recently, our group reported vitrification of poly(Myr) by copolymerization of Myr with 2-(acetoacetoxy)ethyl methacrylate (AAEMA) as a tool to tailor the properties of Myr-based rubbers [103]. It was found that vitrification can be a relatively inexpensive and facile method to improve the thermomechanical properties of poly(Myr) [103]. Despite these encouraging results, identification of the nature of copolymerization between dienes like Myr with AAEMA is needed to better understand the impact of copolymer microstructure on the vitrimer's thermomechanical properties. From our previous work, we found evidence of compositional drift which can play a role in the placement of the dynamic cross-linking on the chain [103].. Thus, herein, we endeavored to determine the reactivity ratios for the Myr/AAEMA system and kinetics versus composition relationships. We also used that data to synthesize statistical, gradient, and diblock copolymers of Myr/AAEMA.

Furthermore, inspired by butadiene/styrene (Sty) rubbers (SBR), we sought to enhance the mechanical properties of the Myr-based vitrimers through terpolymerization with Sty as the third monomer. This approach allowed tailoring of the mechanical and viscoelastic characteristics of the vitrimer by simple manipulation of the prepolymer's T_g. More significantly, by leveraging the control over the T_g, we intricately incorporated a shape memory effect into the Myr-based rubber. Our group previously introduced Myr-based shape memory vitrimers based on slow

reconfiguration of hybrid dynamic/static cross-linking to trigger the shape memory effect at high temperatures (T > 110 °C) [103]. In the current work, we demonstrate a shape memory effect with tunable triggering temperature, achieved by manipulating T_g, enabling fast shape recovery (< 1 min), excellent shape fixity, and the ability to undergo shape reprogramming—all while maintaining recyclability through dynamic covalent chemistry. Attacking these prominent issues will lead to improved design of Myr-based thermadapt rubber.

4.4. Experimental

4.4.1. Materials

Chemicals were of reagent grade and used as received unless otherwise stated. β-Myrcene (Myr, Millipore-Sigma, ≥90%), (2-acetoacetoxy)ethyl methacrylate (AAEMA, TCI, 95%), styrene (Sty, ≥90%, Millipore-Sigma) were purified by passing through columns of basic alumina (Al_2O_3, Brockmann, Type I, Millipore-Sigma) mixed with 5 wt% calcium hydride (90-95%, Millipore-Sigma) and stored under a head of N_2 in a refrigerator until use. Isophorone diamine (IPDA, ≥ 99.0%) was purchased from Millipore Sigma. High purity N_2 gas (99.998%) was purchased from Linde. Tetrahydrofuran (THF, HPLC grade),xylenes (>99%), toluene (>99%), chloroform (>99%), N,N- dimethylformamide (DMF, >99%), acetone (>99%), reagent alcohol (anhydrous ethanol 90% v/v; methanol 5% v/v; 2-Propanol 5% v/v), methanol (>99%) were purchased from Fisher Scientific. Deuterated chloroform ($CDCl_3$, ≥99%) was purchased from Millipore-Sigma for ^1H NMR analyses. BlocBuilder ™ (BB, also known as MAMA-SG1, alkoxyamine for NMP) was obtained from Arkema.

4.4.2. Characterization and instrumentation

Gel Permeation Chromatography (GPC)

A Waters Breeze GPC using HPLC-grade THF as the eluent at 40 °C and a flow rate of 0.3 mL/min was used to measure the molecular weight distributions. It was equipped with a guard column, a differential refractive index (RI 2414) detector, and three Styragel HR columns with a molecular weight measurement range of 10^2 to 5×10^3 g/mol for HR1, 5×10^2 to 2×10^4 g/mol for HR2, and 5×10^3 to 6×10^5 g/mol for HR4. Poly(methyl methacrylate) (PMMA) standards (Varian) were

used for calibration and estimation of number average molecular weight (M_n) and dispersity ($Đ = M_w/M_n$) of the prepolymers within the range of 875 to 1,677,000 g/mol.

Nuclear Magnetic Resonance (NMR) spectroscopy

^1H and ^{13}C NMR analyses were performed in $CDCl_3$ using a Bruker 500 MHz NMR spectrometer at a temperature of 25 °C with 16 and 1024, respectively, scans for the nuclei.

ATR-FTIR Spectroscopy

A Thermo Scientific Nicolet iS50 FTIR Spectrometer equipped with a diamond ATR was used. 32 scans over the range of 4000-400 cm^{-1} were performed for each sample.

Swelling Tests

To find the gel fraction of the vitrimers, four samples were soaked in excess toluene for 72 h at room temperature. The swelled samples were filtered and immediately weighed to find the samples' swelling ratio. Samples were dried in a vacuum oven at reduced pressure and 60 °C for a day and weighed again. Gel fraction was calculated by m_2/m_0; in which m_0 is the mass of the original sample and m_2 is the mass of dried sample after swelling and drying.

Differential Scanning Calorimetry (DSC)

A TA Instruments Discovery 2500 DSC equipped with refrigerated cooling system (RSC 90) with aluminum hermetic pin-hole pans was used. Calibrations for temperature and heat flow were conducted using indium and benzoic acid standards, respectively. Samples were analyzed with temperature ramps of -90 ℃ to 60 ℃ using a heat/ cool/ heat procedure at a rate of 15 ℃/min. The glass transition temperature (T_g) was calculated using the curve inflection of the second heating ramp using TA Instruments TRIOS software.

Thermal Gravimetric Analysis (TGA)

TGA was performed on a TA Instrument Discovery 5500 machine with ceramic pans. The prepolymers and vitrimers were heated at a rate of 10 ℃/min from 25℃ to 600℃. TA Instruments TRIOS software was utilized to record and analyze the data. An isothermal experiment was performed first for a 15 min at 105˚C to remove any moisture and/or solvents followed by an isothermal period at 120 °C for the total run time of 3 h.

Dynamic Mechanical Analysis (DMA) and Rheology

An Anton Paar MCR 302 rheometer was used for the various rheological tests. DMA tests were conducted using a solid rectangular fixture (SFR 12). Rectangular-shaped samples (60 mm length, 10 mm width, and 2 mm thickness) were heated from room temperature to 115 °C for the vitrimer at an average rate of 5 °C/min while being subjected to a sinusoidal 0.05% strain at a frequency of 1 Hz. Rheological tests were conducted using a 25 mm parallel plates geometry. Strain sweep tests were carried out at 110 –130 °C to determine the linear viscoelastic region (LVR) at 1 Hz. Frequency sweep tests were performed at 120 °C and 0.1% strain. Stress-relaxation experiments were conducted at 0.1% strain at 110 to 150 °C. Creep-recovery experiments were performed at 1000 Pa for 350 s, followed by 0 Pa for 350 s, with the total experiment time of 700 s.

Tensile Analysis Testing

The tensile tests were performed on a universal Shimadzu Easy Test system with a 500 N load cell and a crosshead speed of 10 mm/min. Vitrimer samples were hot-pressed (please see section 2.4 for details) into dog-bone shaped tensile specimens similar to ASTM D638 type V with overall length of 60 mm and respective neck thickness and width of 2 and 3 mm. The reported results are the average of at least 3 specimens.

4.5. Polymer synthesis

4.5.1. Myrcene/ AAEMA copolymerization

We synthesized a series of statistical copolymers of Myr and AAEMA to examine polymerization kinetics, monomers' reactivity ratios, and the influence of feed composition on the final copolymer composition. A general reaction schematic is shown in Schematic S1. Table 1 summarizes the experimental formulation of all reactions. Polymers are coded as "Myr XX-AAEMA YY, in which XX and YY denote the initial molar ratio of each monomer. Copolymerization reactions were initiated and controlled using NMP via BlocBuilder, an SG1-based alkoxyamine. For example, for the synthesis of Myr 50 AAEMA 50 polymer, the following components were added into a 100 mL three-neck round-bottom glass flask: Myr (5.10 g, 37.4 mmol), AAEMA (8.01g, 37.4 mmol), BlocBuilder (0.20 g, 0.5 mmol), and xylene (13.35 g, 15.5 mL). The reactor was equipped with an overhead reflux condenser connected to a chiller (Fisher Scientific Isotemp 3016D) at 2 °C and a

magnetic stir bar. The reaction solution was purged with N_2 gas for 20 min and heated at 120 °C for 8 h using a heating mantle and a feedback temperature controller. Samples were periodically collected for ^{1}H NMR to obtain conversion and composition, and GPC analyses for the molecular weight distributions. For all polymerizations, the reaction was stopped by reducing the temperature and the viscous solution was reprecipitated into methanol 3 times from THF. Afterwards, the resulting polymer was dried under vacuum at 60 °C overnight, yielding approximately 6.5 g polymer (~ 49 %) for this specific example. The overall monomer conversion $\left(X_{overall} = f_{0,Myr}X_{Myr} + f_{0,AAEMA}X_{AAEMA}\right)$ from ^{1}H NMR was 73%; please see Figure S1 to S5 for complete detailed calculations. It should be noted that reprecipitation and workup resulted in lower yield than the overall conversion from NMR analysis. From GPC, a dispersity ($Đ$) of 1.30 was achieved along with M_n of 13,300 g/mol relative to PMMA standards for the example cited. Note that in the copolymerization of Myr 10-AAEMA 90, a 50% v/v mixture of DMF and xylenes was used as the solvent to avoid precipitation of AAEMA-rich copolymer during the polymerization.

4.5.2. Semi-batch synthesis of statistical copolymers of Myrcene and AAEMA

A semi-batch mode was employed to synthesize a statistical (nearly random) copolymer of Myr 80-AAEMA 20 in bulk. The formulation for the semi-batch copolymerization is provided in Table 1.B. The required amount of the AAEMA monomer was split into two equal batches; one half was used to initially charge the reactor, and the other half was continuously fed into the reactor using the pump. A mixture of BlocBuilder initiator (0.40 g, 1.05 mmol), Myr (18.82 g, 138.1 mmol) and one half of the AAEMA (3.70 g and 17.3 mmol) were added to the reactor with a similar setup to the standard solution copolymerizations described previously and purged with N_2 for 20 min at room temperature prior to heating. The mixture was heated to 120 °C while maintaining the N_2 purge. After reaching the 120 °C setpoint, the other 50% of the previously purged AAEMA (3.70 g and 3.3 mL) was continuously pumped into the reactor at the rate of 0.4 mL/h using a New Era NE-1000 programmable single syringe pump. The polymerization was allowed to continue for 555 min at 120 °C. The yield was approximately 57 wt% after reprecipitation in methanol.

4.5.3. Chain extension and block copolymers of Myr/AAEMA

NMP, like other reversible deactivation radical polymerization (RDRP) processes, affords the retention of chain end fidelity and formation of block copolymers despite using essentially radical polymerization conditions [103]. We consequently studied synthesis of diblock copolymers

consisting of Myr and AAEMA to compare against their statistical copolymerization counterparts via NMP. To do so, two different synthetic routes were tested: chain extension from a poly(AAEMA) homopolymer macroinitiator to Myr, i.e. poly(AAEMA-*block*-Myr) as well as chain extension from a poly(Myr) macroinitiator to AAEMA, i.e. poly(Myr-*block*-AAEMA). Formulation and molecular characterization for the block copolymers are provided in Table 1.B and C. Regardless of the synthetic route, for the synthesis of the poly(AAEMA) block, 10 mol% Sty was initally used in the feed as a controlling comonomer as a low fraction is required for the NMP of methacrylates with BlocBuilder (SG1) type of initiators [34,138]. For the synthesis of poly(AAEMA-*block*-Myr), first a homopolymer of poly(AAEMA-*stat*-Sty) with target M_n of 15,000 g/mol at 100% conversion was synthesized as follows. AAEMA (28.20 g, 131.6 mmol), Sty (3.25 g, 14.6 mmol), BlocBuilder (0.8 g, 2.1 mmol) were mixed with 50% wt/wt dioxane solution (31.4 g, 30.5 mL). The experimental setup and procedure were similar to the statistical copolymers described earlier with the only differences being reaction temperature and polymerization time (90 °C and 70 min, respectively). After 3 reprecipitations and workup, the yield was approximately 12.5 g with M_n = 7,500 g/mol and $Đ$ = 1.33 relative to PMMA standards in THF at 40 ºC. To perform the chain extension with Myr, 2.1 g of the AAEMA-based macroinitiator was dissolved in 10.5 mL of a 2:1 v/v mixture of xylene:DMF to avoid precipitation of the block copolymers during the polymerization. Then, 8.4 g (61.6 mmol) of Myr was added to the solution via syringe and purged with N_2 for 20 minutes at room temperature, followed by heating and subsequent polymerization at 120 °C for 480 min. After stopping the polymerization by lowering the temperature below 40 °C, the mixture was reprecipitated into methanol. The polymer was reprecipitated two more times from THF into methanol to remove high boiling point solvents and unreacted monomer. From ^{1}H NMR, the conversion of Myr was 42%. Reprecipitation and workup resulted in a substantial loss of some polymer, yielding approximately 3.1 g (~30% yield) of product with M_n of 13,400 g/mol and $Đ$ = 1.82 relative to PMMA standards. For the synthesis of poly(Myr-*block*-AAEMA), first Myr (104.8 g, 769.6 mmol) was homopolymerized in bulk with BlocBuilder (0.8 g, 2.1 mmol) at 120 °C for 300 min resulting in approximately ~ 33 g of poly(Myr) homopolymer with M_n of 15,000 g/mol and $Đ$ = 1.31. For the chain extension, 4.3 g of the purified poly(Myr) macroinitiator (13 wt%) was dissolved in 18.5 mL of dioxane (ca 60 wt%) followed by addition of 8.16 g (38.2 mmol, 26 wt%) AAEMA and 0.44 g (4.2 mmol, 1 wt%) Sty controlling comonomer. The solution was purged with N_2 for 20 min prior to heating, and

polymerization ensued at 90 °C for 300 min, yielding approximately 7.1 g polymer with M_n of 24,500 g/mol and $Đ = 2.23$. At each step, the resulting polymer was precipitated and purified using the same methods as described above.

4.5.4. Synthesis of statistical poly(Myrcene-*co*-AAEMA-*co*-Styrene) prepolymer and vitrification

To synthesize the vitrimer, first a terpolymer of Myr, Sty, with 10 mol% AAEMA was synthesized as a prepolymer, as shown in Schematic 1 and S1. A similar reaction setup to the statistical and block copolymer synthesis was applied using the BlocBuilder alkoxyamine with target $M_{n,\,100\%}$ of 15,000 g/mol. The initial molar composition of Sty was 55 mol% to make the resulting polymer stiffer and increase its T_g. The polymerization reaction was performed in bulk at 120 °C for 400 min. From ^{1}H NMR, the $X_{Myr} \approx 88\%$ and $X_{AAEMA} \approx 73\%$ while X_{Sty} was only 42%. The relatively low conversion of Sty can be explained by the Myr/Sty copolymer reactivity ratios. Trumbo studied Myr/Sty copolymerization and reported that the growing polymer chains strongly favor Myr monomer, leading to formation of relatively long sequences of Myr [172]. This also corroborates with Figure S7 in which an increase in instantaneous f_{Sty} from ~ 0.55 to ~ 0.78 was observed while f_{Myr} and f_{AAEMA} steadily decreased to 0.2 and 0.02, respectively after 400 min of reaction. The overall conversion from NMR was 56% and from GPC, M_n of 13,500 g/mol and $Đ$ = 1.53 was estimated, relative to PMMA, shown in Figures S4-5. The polymer was then (re)precipitated 3 times in methanol from THF and yield was ~ 38 wt%.

To form the vitrimer, 13.31 g of p-MyrStyAAEMA prepolymer (p indicates the polymer in the un-cross-lnked state) was dissolved in THF, 50% (w/v). Afterwards, IPDA, with β-ketoester : amine ratio of 1 : 0.85 (0.65 g IPDA in ~20% w/v THF), was added and the solution was stirred until gelation occurred, which took less than 15 min. The resulting gel was left overnight at room temperature in a fume hood and was further cured and dried at 80°C under reduced pressure in a vacuum oven for ~12 h. The resulting vitrimer was hot pressed using a Carver Manual Hydraulic Press with Watlow temperature controllers. The steel mold was sandwiched between two Teflon plates, at 110 ± 5 °C under 6 ± 1 metric tons for 60 ± 5 min yielding a yellow and transparent shaped material for tensile and rheological tests. Vitrified polymer is coded as "v-MyrStyAAEMA", where v indicated cross-linked vitrimer.

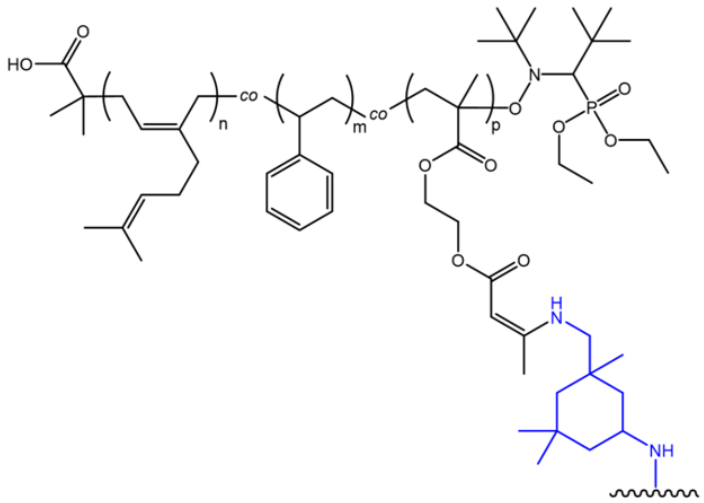

Figure 4.1 Structure of v-MyrStyAAEMA vitrimer with IPDA and formation of vinylogous urethane cross-links

4.6. Results and discussion

4.6.1. Poly(Myr-*stat*-AAEMA) synthesis and characterization

Initially, we studied the copolymerization kinetics of Myr/AAEMA mixtures and the effects of feed composition on the copolymer's composition and microstructure. Previously, we found Myr/AAEMA copolymerization was prone to compositional drift, which influenced the properties of their corresponding vitrimers [103]. Thus, determining monomer sequences in poly(Myr-*co*-AAEMA) (i.e. determination of reactivity ratios) is crucial towards optimizing properties. To that end, a set of Myr/AAEMA copolymerizations with various initial AAEMA molar ratios $f_{AAEMA,0}$ ranging from 0.1 to 0.9, were synthesized via NMP in solution at 120 °C. ^{1}H NMR and GPC were used to estimate the monomer conversion, polymer composition, M_n and $Đ$, as summarized in Table 1.A. The kinetic plots (Figure S3) confirm that the copolymerization was well-controlled in terms of linear progression of M_n versus conversion ($X_{overall}$) and $Đ$ ranging from 1.26 to 1.59. As evident in Table 1.A, with increasing AAEMA content, the $Đ$ of the copolymers tends to broaden. This can be attributed to the challenges encountered with NMP of methacrylate-rich compositions with BlocBuilder type of initiators, derived from the SG1-based nitroxide. It has been shown that the slow recombination of nitroxides and sterically-hindered growing poly(methacrylate) radicals lead to a high average activation–deactivation equilibrium constant K [36]. Recently, 3-(((2-cyanopropan-2-yl)oxy)-(cyclohexyl)amino)-2,2-dimethyl-3-phenylpropanenitrile (known as Dispolreg 007) has emerged as a robust alkoxyamine to control nitroxide-mediated homo and co

polymerization of methacrylates and styrene [38,142,173]. Another method to effectively control the NMP of methacrylates is using BlocBuilder with the addition of a low concentration of a co-monomer with a much lower *K*, such as Sty. The role of controlling monomer is to decrease the overall concentration of propagating radicals by decreasing *K* and allowing the preferential formation of styrene-terminated macroalkoxyamines. Previously, Myr and isoprene were reported to control NMP of isobornyl and glycidyl methacrylate, respectively when using SG1-based nitroxides [129,141]. Herein, the copolymerization of AAEMA at 120 °C with 30 mol% Myr resulted in copolymers with $Đ \leq 1.39$ and linear increase of M_n vs $X_{overall}$ and quasi-linearity of $\ln(1\text{-}X)^{-1}$ versus reaction time with regression coefficient $R^2 = 0.995$, as indicated in Figure S3. These results suggest that addition of Myr in the AAEMA-rich feed can decrease the *K* and be an effective NMP controller. Nevertheless, at higher conversions, $X > 25\%$, some deviation from the theoretical M_n was observed. This trend is commonly reported in methacrylate-rich copolymerizations by NMP which can be attributed to irreversible termination or chain transfer [174].

Table 4.1 Formulation of all polymerization reactions with molecular characterization

(A) Formulation for poly(Myr-*co*-AAEMA) synthesis and molecular characterization

Reaction ID	$[Myr]_0$ (M)	$[AAEMA]_0$ (M)	$M_{n,\,100\%}$ ($g\ mol^{-1}$)	T (°C)	time (min)	Solvent	F_{Myr} (%)	F_{AAEMA} (%)	$X_{overall}$ (%)	$Đ$	M_n ($g\ mol^{-1}$)*
Myr 90:10 AAEMA	5.30	0.59	25,000	120	480	Xyl	77	23	45.4	1.27	8,100
Myr 80:20 AAEMA	4.47	1.12	25,000	120	480	Xyl	76	24	54.2	1.33	8,500
Myr 70:30 AAEMA	3.72	1.59	25,000	120	500	Xyl	71	29	64.5	1.26	10,000
Myr 60:40 AAEMA	3.04	2.03	25,000	120	450	Xyl	61	39	68.8	1.32	10,600
Myr 50:50 AAEMA	2.42	2.42	25,000	120	480	Xyl	51	49	72.6	1.30	13,300
Myr 40:60 AAEMA	1.85	2.78	25,000	120	480	Xyl	43	57	78.2	1.31	12,800
Myr 30:70 AAEMA	1.33	3.11	25,000	120	435	Xyl	34	66	73.1	1.39	12,500
Myr 20:80 AAEMA	0.85	3.42	25,000	120	480	Xyl	22	78	79.8	1.59	15,500
Myr 10:90 AAEMA	0.41	3.70	25,000	120	360	Xyl +DMF	13	87	81.0	1.57	14,900

[a] Experimental identification given My XX -AAEMA YY where XX and YY are % of initial molar fraction of respective monomers
[b] $M_{n,\,100}$% is the targeted molecular weight for 100% monomer conversion
[c] Polymer composition from ^{1}H NMR
[d] From GPC, compared to PMMA standards at 40˚C in THF

Table 4.1 (continued) Formulations of all polymerization reactions with molecular characterization

(B) Formulation for statistical copolymer – semi-batch

Reaction ID	$[Myr]_0$ (M)	$[AAEMA]_0$ (M)	feed rate (mL/h)	$M_{n,\,100\%}$ ($g.mol^{-1}$)	T (˚C)	time (min)	Solvent	F_{Myr} (%)	F_{AAEMA} (%)	$X_{overall}$ (%)	Đ	M_n ($g\ mol^{-1}$)
SB-Myr 80-AAEMA 20	5.1	0.6	0.4	25,000	120	555	—	16	84	73	1.34	12,000

(C) Formulation for poly[Myr-*block*-(AAEMA-*co*-Sty)]

Reaction ID	$[Myr]_0$ (M)	$[AAEMA]_0$ (M)	$[Sty]_0$ (M)	$[(macro)initiator]_0$	T (˚C)	time (min)	Solvent	F_{Myr} (%)	F_{AAEMA} (%)	F_{Sty} (%)	$X_{overall}$ (%)	Đ	M_n ($g\ mol^{-1}$)
poly(Myr)	5.83	—	—	0.016 mol/L	120	300	—	100	—	—	44	1.31	15,000
Poly[Myr-*block*-(AAEMA-*co*-Sty)]	—	26 wt%	1 wt%	13 wt%	90	300	Dioxane	53	42	6	55	2.23	24,500

(D) Formulation for poly[(AAEMA-*co*-Sty)-*block*-Myr]

Reaction ID	$[Myr]_0$ (M)	$[AAEMA]_0$ (M)	$[Sty]_0$ (M)	$[macroinitiator]_0$	T (˚C)	time (min)	Solvent	F_{Myr} (%)	F_{AAEMA} (%)	F_{Sty} (%)	$X_{overall}$ (%)	Đ	M_n ($g\ mol^{-1}$)
poly(AAEMA-*co*-Sty)	—	1.96	0.49	—	90	70	Dioxane	—	83	17	51	1.33	7,500
Poly[(AAEMA-*co*-Sty)-*block*-Myr]	2.76	—	—	0.28 wt%	120	300	Xyl +DMF	77%	19	4	42	1.82	13,000

(E) Formulation for vitrimer prepolymer

Reaction ID	$[Myr]_0$ (M)	$[AAEMA]_0$ (M)	$[Sty]_0$ (M)	$[initiator]_0$	T (˚C)	time (min)	Solvent	F_{Myr} (%)	F_{AAEMA} (%)	F_{Sty} (%)	$X_{overall}$ (%)	Đ	M_n ($g\ mol^{-1}$)
poly(MyrStyAAEMA)	2.54	0.73	4.00	0.033	120	400	—	51	9	40	56	1.53	13,500

* All M_n and $Đ$ values are compared to PMMA standards

To comprehensively study the microstructure of the synthesized copolymers and predict the copolymer composition based on the initial monomer concentrations, the reactivity ratios of Myr and AAEMA were determined. Various methodologies for ascertaining reactivity ratios are widely used in the literature, including traditional linear regression approaches such as the Fineman–Ross (FR) and Kelen–Tüdös (KT), direct non-linear least square (NLLS) analysis of the Mayo-Lewis equation, and various integrated methods [14]. However, discrepancies persist in these approaches resulting in inconsistent results. Lynd et al. compared these methodologies in a comprehensive

analysis of 560 data sets, underscoring the inaccuracies often encountered when non-integrated methods like FR and KT are used [175]. Conversely, integrated methods demonstrated a consistent accuracy in reactivity ratio determinations. Therefore, we employed an integrated approach by using the Meyer-Lowry (ML) analytical interpretation of Skeist's equation for binary copolymerization, yielding the reactivity ratios of Myr/AAEMA, as outlined in Eq .1 [176].

$$\frac{M}{M_0} = 1 - \left(\frac{f_A}{f_{A,0}}\right)^{\frac{r_B}{1-r_B}} \left(\frac{1-f_A}{1-f_{A,0}}\right)^{\frac{r_A}{1-r_A}} \left(\frac{f_A(2-r_A-r_B)+r_B-1}{f_{A,0}(2-r_A-r_B)+r_B-1}\right)^{\frac{r_A r_B-1}{(1-r_A)(1-r_B)}} \quad (1)$$

Here, M/M_0 is the overall molar conversion, f_1 and f_2 represent the molar compositions of monomer 1 and 2 in the reaction mixture, and $f_{1,0}$ and $f_{2,0}$ denote the initial molar ratios of these monomers in the feedstock.

Figure 2 shows the experimental data with the fitted curves derived through the integrated method. MATLAB was utilized for curve-fitting by minimizing the total difference between the experimental and model-predicted conversions. The analysis showed the reactivity ratios of $r_{Myr} = 0.20$ with a 95% confidence interval of [0.13, 0.37], and $r_{AAEMA} = 0.22$ with a 95% confidence interval of [0.15, 0.23]. Both r_{Myr} and r_{AAEMA} are significantly less than 1, suggesting a strong preference of the propagating chains ended with $-Myr^{\cdot}$ and $-AAEMA^{\cdot}$ radicals for incorporating the alternate monomer. Furthermore, the similar propagation rate as inferred from $r_{Myr} \approx r_{AAEMA}$, and the product $r_{Myr}r_{AAEMA} = 0.044$ which is close to zero, signifying a tendency for an alternating copolymer sequence. Such behavior is typically observed in systems where the monomers exhibit vastly different polarities or form complexes that hinders polymerization of one monomer with its own type [14]. The alternating tendency is further verified by the observation that the f_{AAEMA} remained nearly constant throughout the reaction with a 50 mol% initial feed, whereas f_{AAEMA} decreased when the initial feed composition was below 50 mol% and increased when the initial composition was above 50 mol%, as illustrated in Figure 2. With no previously reported reactions between a diene and AAEMA other than our study, references for reactivity ratios are limited. Métafiot et al, (using NMP) and Pablo-Morales et al. (using RAFT), delved into the copolymerization of Myr with glycidyl methacrylate (GMA) [139,141]. In addition, Trumbo conducted a series of studies examining copolymerization of Myr with methyl methacrylate (MMA) [172]. Notably, the three mentioned studies concluded that copolymerization tends to occur in an alternating fashion, based on both reactivity ratios being much less than unity.

Furthermore, with the recent developments in neural networks, Farajzadehahary et al., have developed a model capable of predicting reactivity ratios with considerable precision based solely on the chemical structures of the monomers, and they have generously offered a web application for the prediction of monomer reactivity pairs [177]. According to their model, the predicted reactivity ratios for Myr and AAEMA are 0.34 and 0.44, respectively, which align closely with our findings [177]. It should be mentioned that ^{13}C NMR analyses, Figure S2, for definitive determination for non-azeotropic compositions were not conclusive and dyads/triads could not be determined in the composition and conversion ranges studied here.

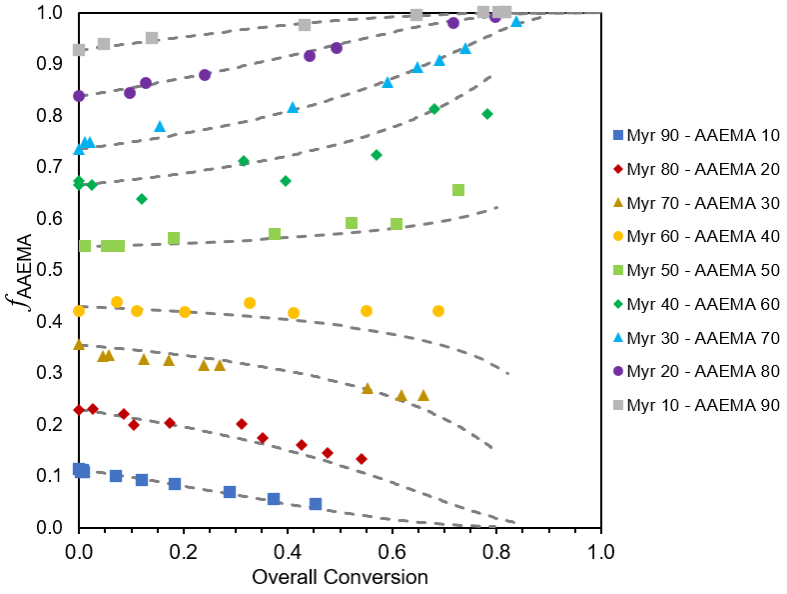

Figure 4.2 Curve fitting of AAEMA composition (f_{AAEMA}) in the monomer mixture versus overall conversion ($X_{overall}$) for different reactions with varied initial feed compositions, using the Meyer-Lowry method. Experimental data points are represented by markers, while the black dashed lines correspond to the fitted curves derived from the model.

Table 4.2 Reported reactivity ratios of Myr in the literature.

Monomer $_1$	Monomer $_2$	r_1	r_2	$r_1 \cdot r_2$	ref.
Myr	AAEMA	0.20	0.22	0.04	This work
Myr	MMA	0.44	0.27	0.12	[172]
Myr	GMA	0.52	0.30	0.16	[141,170]
Myr	IBOMA	2.07	0.05	0.05	[129]
Myr	Styrene	1.36	0.27	1.20	[172]

r values are within 90-95% confidence

Synthesis of poly(Myr-*ran*-AAEMA) in semi-batch mode

As shown in the previous section, Myr/AAEMA systems tend to copolymerize in an alternating fashion. To synthesize random copolymers without compositional drifts, a semi-batch copolymerization of Myr 80-AAEMA 20 was studied. Using a syringe pump, 50% of the total AAEMA monomer was added at a constant rate to the reacting bulk solution of BlocBuilder, Myr and the remaining 50% of the AAEMA. No solvents were added to minimize the use of volatile organic compounds. The kinetic plots are summarized in Figure 3. A linear growth of M_n versus $X_{overall}$ with relatively low $Đ \leq 1.34$ suggests a well-controlled polymerization. Figure 3.b shows the evolution of instantaneous AAEMA mol fraction ($f_{AAEMA,\,t}$) with $X_{overall}$. In the semi-batch mode, $f_{AAEMA,\,t}$ stayed at 0.12 ± 0.01 until $X_{overall}$ = 45% (t ≈ 360 min) and slightly increased to 0.19 ± 0.01 afterwards. In contrast, in the counterpart Myr 80-AAEMA 20 batch mode polymerization, due to the alternating copolymerization, $f_{AAEMA,\,t}$ continuously decreased from 0.23 to 0.13 with increasing $X_{overall}$ (at t ≈ 320 min, X_{AAEMA} ≈ 90% while $X_{overall}$ ≈ 60%) as shown in Figure 2. This also corroborates with the previous reports of Chapter 3 regarding Myr/AAEMA copolymerizations in which a compositional drift was observed.

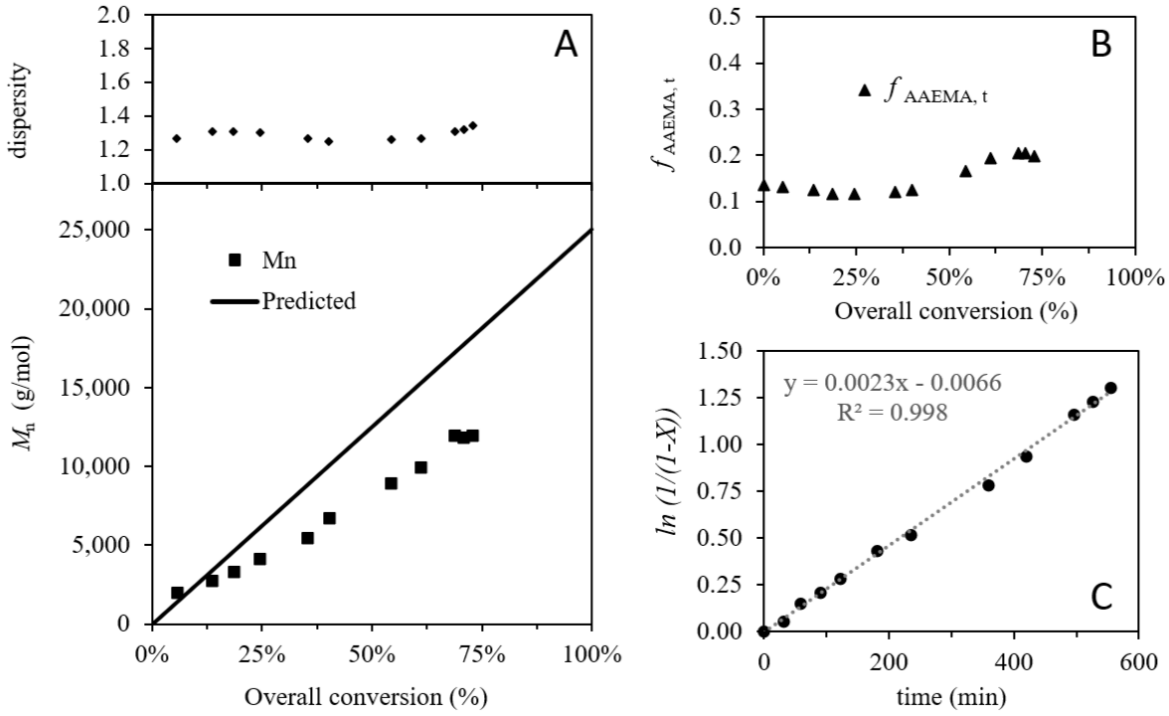

Figure 4.3 Semi-batch synthesis of Myr 80-AAEMA 20 with AAEMA injection. Semi-batch synthesis of Myr 80-AAEMA 20 with AAEMA injection**.** A) Molecular weight (M_n) and dispersity

versus overall conversion ($X_{overall}$), B) instantaneous feed composition ($f_{AAEMA,\ t}$), and C) semi-logarithmic kinetic plots of $X_{overall}$ versus reaction time.

The satisfactory results from the SG1-based NMP of Myr/AAEMA copolymerization prompted us to study the synthesis of their block copolymers. An important consequence of NMP is the formation of polymer chains capped with nitroxides which can be reactivated. Four extra statistical copolymerization reactions were conducted to synthesize two block copolymers with two different synthetic routes: poly(Myr-*block*-AAEMA) and poly(AAEMA-*block*-Myr). For the synthesis of the former, first a homopolymer of poly(Myr) was synthesized in bulk followed by chain extension with AAEMA and Sty (10 mol% eq of AAEMA) as a controlling comonomer required for SG1-based NMP. The reaction was performed in dioxane at 90 °C. Figure 4.A illustrates the evolution of the molecular weight distribution through GPC traces of the chain extension polymerization of poly(Myr-*block*-AAEMA). High $Đ$ of 2.23 and a bimodal molecular weight distribution was observed, indicating contamination of the block copolymer with unreacted macroinitiator. The low efficiency in converting from the macroinitiator to the chain-extended species can be explained by the existence of a high concentration of dead chains in the poly(Myr) macroinitiator and/or unfavorable kinetics of chain extension of p(Myr) with AAEMA [178]. On the other hand, the chain extension of poly(AAEMA) with Myr, was more successful according to the GPC results and formation of block copolymers with monomodal distributions. In the second synthetic route, a copolymer of AAEMA with controlling Sty comonomer, was first synthesized. Again, in the synthesis of the macroinitiator, modest conversion ($X_{overall} \sim 50\%$) was aimed to maximize the chain-end fidelity. Afterwards, the poly(AAEMA-*co*-Sty) was dissolved in a mixture of xylenes and DMF and reacted with Myr at 120 °C. The GPC traces of the poly(AAEMA-*co*-Sty) and poly[(AAEMA-*co*-Sty)-*block*-Myr)] are compared in Figure 4.B. A clear shift towards higher molecular weights was observed. However, the M_n stopped increasing after about 200 min at 13,000 g/mol and $Đ$ increased to 1.82 suggesting formation of some dead chains. Further investigation is necessary to optimize and obtain a deeper understanding of the AAEMA/Myr chain extension but does not impede the with the desired studies involving the ensuing rheological and mechanical properties.

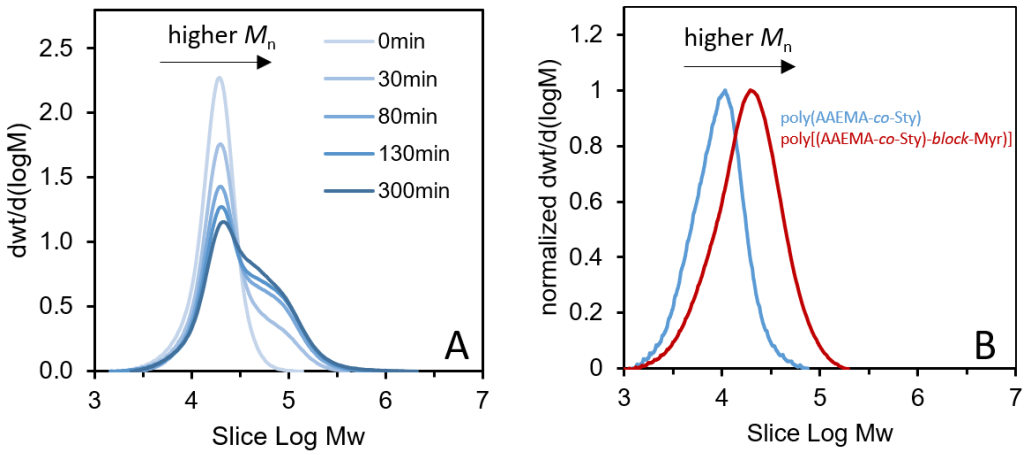

Figure 4.4 GPC traces of A) poly[Myr-block-(AAEMA-co-Sty)] and B) poly[(AAEMA-co-Sty)-block-Myr)]. The molecular weight distribution in A showed a significant shoulder suggesting contamination with macroinitiator. In the case of B, a monomodal curve was observed suggesting a more successful chain extension reaction.

In the initial section of this study, we focused on the copolymerization of Myr and AAEMA, revealing an alternating microstructure with an azeotropic composition between 45% to 55% of the feed molar composition. With this insight into the kinetics and composition of the copolymers, we have a clearer ability to control the microstructure and enhance the resulting vitrimer mechanical properties.

4.7. Vitrimer synthesis and characterization

Given the data about the microstructure, our focus now shifted towards enhancing the mechanical properties and functionality of poly(Myr) rubbers with a primary aim to impart reprogrammable rapid shape memory effects. To achieve this objective, we employed a dual strategy. First, inspired by styrene-butadiene rubbers (SBR), we modulated the T_g and stiffness of the prepolymer through terpolymerization with Sty. Second, we incorporated a low concentration of the β-ketoester functional AAEMA which enables formation of vinylogous urethane-based vitrimers. The linear terpolymer of Myr/AAEMA/Sty prepolymer, coded as p-MyrStyAAEMA, was synthesized in bulk to minimize solvent usage, with an initial feed composition of 10 mol% AAEMA and 55 mol% Sty. The terpolymerization kinetic plots and molecular characterization are shown in Figure 5 and Table 1.E, respectively. The polymerization was relatively well-controlled by NMP in terms of linear M_n versus X up to nearly 70% conversion and $Đ \sim 1.4$.

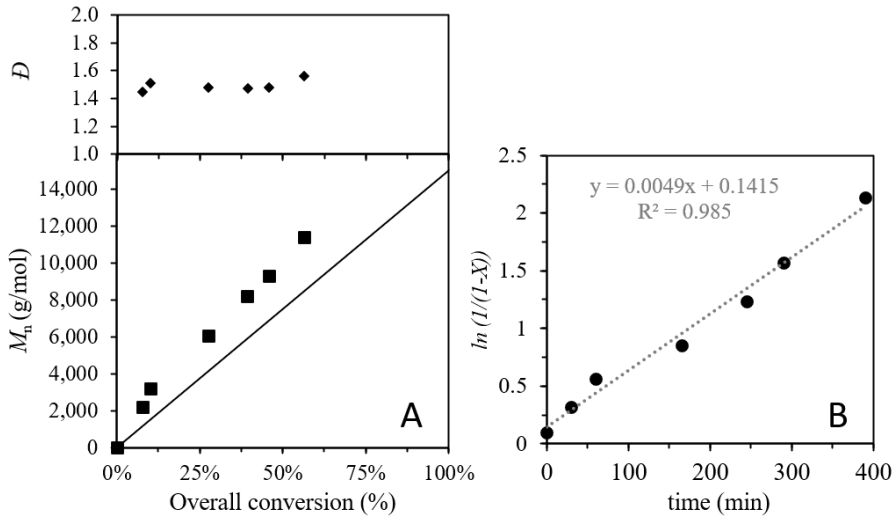

Figure 4.5 NMP of poly(Myr-stat-Sty-stat-AAEMA) (p-MyrStyAAEMA) in bulk with initial feed composition of $f_{Myr,0}$=0.35, $f_{Sty,0}$ =0.55 ,and $f_{AAEMA,0}$ =0.1. A) M_n and $Đ$ versus $X_{overall}$ and B) linearized semi-logarithmic kinetic plots of $X_{overall}$ versus reaction time.

The vitrification was carried out by cross-linking with difunctional IPDA, a widely used hardener that can increase the T_g and improve mechanical properties of the final vitrimers [179].The resulting vitrimer, v-MyrStyAAEMA, was transparent with a slightly yellowish color. Formation of vinylogous urethanes were confirmed by ATR-FTIR by the appearance of peaks at 1600 cm^{-1}, and 1655 cm^{-1} indicating N–H bending and C═C stretching, respectively, as illustrated in Figure 6.A [112]. Formation of a cross-linked network was confirmed by swelling tests in toluene on at least 3 samples. The average gel content was 90 ± 1% and the swelling ratio was 269 ± 10%.

Thermomechanical properties of the vitrimer

The DSC traces of the prepolymer and its associated vitrimer are shown in Figure S8. The p-MyrStyAAEMA prepolymer had a T_g = -19 ˚C which is in good agreement with estimates using the Flory-Fox equation, as shown in Supporting Information Eq S1 [144].Cross-linking by IPDA resulted in T_g increasing from -19 to 22 ˚C. Figures 6C and S8 show the TGA traces of the v-MyrStyAAEMA vitrimer. From TGA tests under nitrogen, onset thermal degradation of 363 ˚C and $T_{5\%}$ of 240 ˚C were estimated for the vitrimer. In addition, after 180 min of the isothermal TGA test at 120 ˚C, less than 4% weight loss was observed, confirming thermal stability of the vitrimers was sufficient for (re)processing.

To better understand the effects of cross-links and flow behavior of the vitrimer, we carried out rheological studies. The linear viscoelastic region was first determined by amplitude sweep tests, shown in Figure S10. Frequency sweep tests at 120 ˚C also showed a plateau with elastic (G′) and loss (G″) modulus of 153.1 and 1.8 MPa respectively, as seen in Figure S11, confirming the cross-linked and elastic nature of the vitrimers. Thermomechanical properties of the vitrimer were further studied by DMTA as shown in Figure 6.B. With increasing temperature from 25 °C, an initial sharp decrease in G′ and G″ was observed. This is due to the T_g of the vitrimer at ~ 22 °C observed from DSC. The vitrimer showed a plateau at ~ 0.6 MPa, above its T_g, which is typical of cross-linked systems [145].

Vitrimer flowability at higher temperatures and their ability to be reprocessed, despite their cross-linked nature, originate from the dynamic exchange reactions within the network [59]. The rate constant of the dynamic chemical bonds, together with functional group concentration and mobility, determines the net exchange reaction within the network. As a result, for a vitrimer, with a given dynamic bond and precursor, the viscoelastic properties are influenced by the cross-linking density and the temperature [59]. Stress relaxation experiments were conducted to study the flow behavior of the v-MyrStyAAEMA vitrimer at 110 to 150 °C. The normalized relaxation modulus of the vitrimers is shown in Figure 6.E. Although full relaxation was not observed within 1000 s, the stress-relaxation time systematically decreased by increasing temperature and could be fit to an Arrhenius-type relationship, Eq 2 and Figure S 12, modelling the gradual decrease of viscosity with temperature [73]. The characteristic relaxation time (τ*) was extracted using a stretched exponential decay model Kohlrausch–Williams–Watts equation (KWW) (Eq 3) [115].

$$ln(\tau^*) = \frac{E_a}{RT} + ln\,(\tau_0) \qquad \text{(Eq 2)}$$

$$\frac{G\,(t)}{G_0} = \exp\left(-\left(\frac{t}{\tau*}\right)^{\beta}\right) \qquad \text{(Eq 3)}$$

Here, E_a is the viscous flow activation energy, R is the universal gas constant, T is temperature, G(t) and G_0 are the relaxation moduli at time t and initial time t_0, and β is a parameter related to the breadth of the relaxation distribution. For the stress-relaxation test at 150 °C, τ* and β were 2881s and 0.58, respectively, Table S1. The E_a can be roughly estimated as 235 kJ/mol. The higher relaxation time and E_a in this work compared to those of the previously reported Myr/AAEMA

based vitrimers can be attributed to the effects of copolymerization with Sty, higher T_g, and the use of IPDA [55,91].

A critical drawback of vitrimers is their susceptibility to creep. Creep is the continuous deformation during exposure to stress at service temperatures. Traditional thermosets show almost no creep [150]. The creep-recovery experiments were conducted at two different temperatures shown in Figure 6.F. The vitrimers underwent ~ 0.6% deformation under 1 MPa stress after 350 s at 150 °C (~130 °C above the T_g). This was followed by reaching the residual deformation of 0.06% , 350 s after removal of the stress.

Comparing the viscoelastic properties of the v-MyrStyAAEMA with a similar previously reported vinylogous urethane-based Myr vitrimer, we observed slower stress-relaxation and lower level of creep at similar cross-linking density and T_g [103].. This trend can be attributed to lower flowability of the v-MyrStyAAEMA, due to copolymerization with Sty. This also corroborates with the slightly higher estimated activation energy in this work (E_a of ~ 235 kJ/mol) compared to previous chapter of Myr/AAEMA based vitrimers (~ 70 kJ/mol) [103].

We also studied the uniaxial tensile properties of the v-MyrStyAAEMA vitrimer at room temperature. Table S.1 summarizes the results of the tensile experiments. The v-MyrStyAAEMA vitrimer exhibited tensile strength and elongation at break of 0.73 ± 0.07 MPa and 146 ± 14%, respectively. Compared to previously reported work on Myr/AAEMA based vitrimers with comparable cross-linking density, terpolymerization with Sty and vitrification with IPDA led to much higher toughness and elongation at break. Table 3 summarizes the tensile properties of reported recyclable Myr-based rubbers in the literature. The table constitutes either hard-soft type thermoplastic elastomers of Myr or networks with reversible cross-linking. It should be noted that direct comparison of the tensile properties should be carried out with caution as the M_n, T_g, composition, and cross-linking density of the reported polymers varies. The M_n in this work is designed to be less than the M_e of poly(Myr) to ensure reporting the effect of vitrification via dynamic covalent cross-linking. Later, using the reactivity ratio information and the terpolymerization approach to improve creep performance indicated in this report, we will examine polymers above the poly(Myr)'s M_e and expect much better stress/strain properties.

Table 4.3 tensile properties of recyclable thermoplastic or CAN Myr-based rubbers in literature.

polymer	F_{Myr} [a]	M_n Myr [kg/mol] [b]	M_n overall [kg/mol]	σ [c] [MPa]	ε [c]	ref.
p(AMMS-*b*-Myr-*b*-AMMS)	75%	77.4	115	9.9	973%	[167]
p(AMMS-*b*-Myr-*b*-AMMS)	88%	146.1	165.5	0.5	1340%	[167]
p(IBOMA-*b*-Myr-*b*-IBOMA)	59%	52.7	94.7	3.9	490%	[129]
p(Myr-*b*-Sty)	73%	30.4	42.6	0.4	14%	[125]
p(Sty-*b*-Myr-*b*-Sty)	78%	48.7	62.2	3.4	620%	[180]
p(Myr-*co*-Myr/furan/hydroxy) XL bismaleimide [d]	96%	—	70.6	4	1597%	[132]
p(Myr-*co*-Myr/pyridine/hydroxy) XL Zn acetate [d]	95%	—	67.9	0.75	950%	[132]
p(Myr-*co*-AAEMA) XL Priamine	90%	—	12	0.18	80%	[103]
p(Myr-*co*-AAEMA) XL TREN [f]	70%	—	12	1.68	30%	[103]
p(Myr-*co*-Sty-*co*-AAEMA) XL IPDA	51%	—	13.5	0.73	146%	this work

[a] fraction of Myr in mol% or wt%
[b] estimated M_n of the Myr block
[c] stress or strain at break
[d] Myr copolymerized with either furan and hydroxy functionalized-Myr or pyridine and hydroxy-Myr
[e] "XL" stands for cross-linked with
[f] Tris(2-aminoethyl)amine

Recycling

Reprocessability and recyclability are viewed as key properties of vitrimers [181]. Here, dynamic exchanges of the vinylogous urethane bonds allow network rearrangement. The v-MyrStyAAEMA vitrimer was reprocessed by mechanical cutting and hot-pressing, as shown in Figure 7. Samples were easily reshaped and formed into molds in about 60 min. ATR-FTIR spectroscopy confirmed the retention of the characteristic vinylogous urethane linkages at ~ 1600 and 1650 cm^{-1} after 4 reprocessing cycles, as shown in Figure 6.A. TGA showed very similar decomposition behavior with T_{onset} *and* $T_{d\text{-}5\%}$ of 361 °C and 236 °C, respectively (Figure 6.C). To further validate the reprocessability of the vitrimer, DMTA was performed on the R×4 sample

(Figure 6.B). The R×4 vitrimer exhibited similar thermomechanical behavior to the original sample with similar T_g and rubbery plateau (G′ ~ 0.6 MPa), confirming the cross-linked nature of the vitrimers. More importantly, we examined the tensile properties of the vitrimer at each reprocessing step, with the data summarized in Table S1. Figure 6.D also shows the representative stress-strain behavior of the vitrimer. Effectively, no meaningful change in the tensile properties were observed after 4x cycles with stress and strain at break of 0.88 ± 0.08 MPa and 169 ± 33% for the R×4 sample.

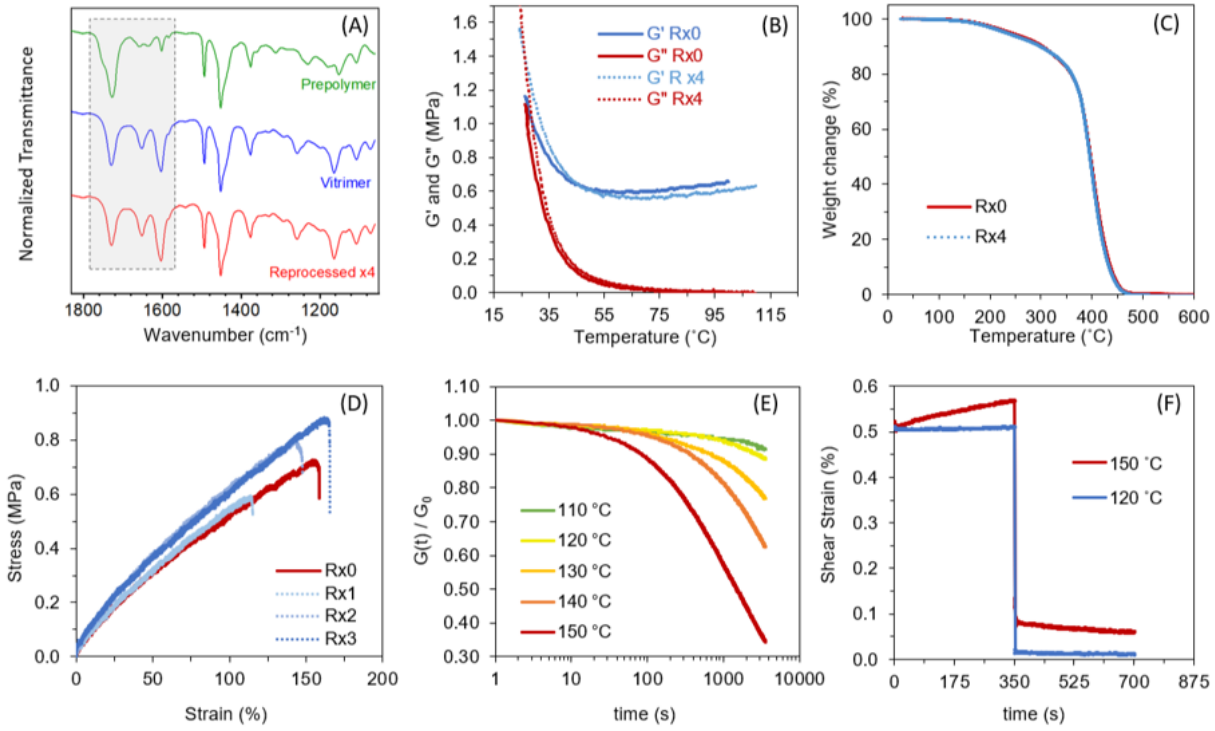

Figure 4.6 A) ATR-FTIR spectra of prepolymer, vitrimer and reprocessed vitrimer (Rx4), B) DMTA of vitrimer before and after recycling, C) TGA curves of the vitrimer before and after recycling, D) axial tensile test data of the vitrimers and after 4 processing cycles, E) Stress-relxation curves of vitrimer F) creep-recovery of the vitrimer at two different temperatures.

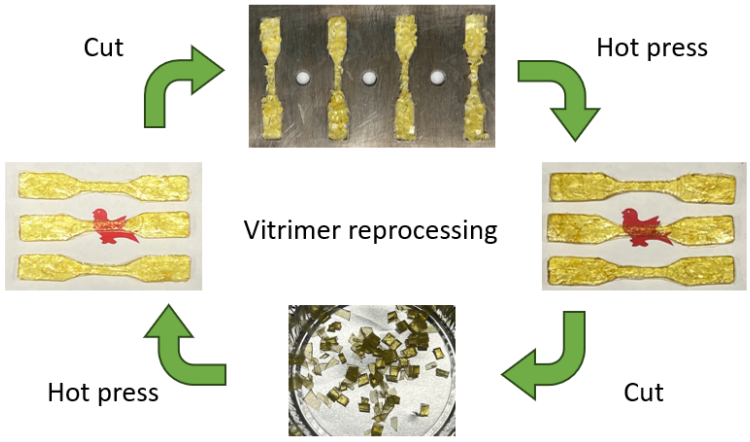

Figure 4.7 Reprocessing of vitrimers by multiple cycles of mechanical cutting and hot pressing.

4.7.1. Shape memory effect

The potential to develop stimuli responsive networks is a significant implication from dynamic bonds. For vitrimers, temperature triggered shape memory effects have been reported in several studies by careful programming and optimization of the polymeric network. Shape memory is not unique to a specific chemistry or microstructure; it is a consequence of molecular architecture, reversible mobility, conformational entropy and programming [182]. The shape memory effect refers to a material's ability to be programmed into a metastable temporary shape which can be triggered to return to its original shape through a specific stimulus [183]. For a polymer to demonstrate shape memory properties, two key structural elements are required: permanent net-points and a reversible molecular switching segment [182].. The net-points serve the purpose of storing and memorizing the permanent shape. On the other hand, the reversible molecular switching segments function to either fix or release the temporary shape upon triggering with the stimulus. Thus, in the case of v-MyrStyAAEMA, the cross-links can function as the net-point and T_g of the bulk material would act as the molecular switches. Since T_g of the v-MyrStyAAEMA was near room temperature, temperature could effectively be used as the trigger ($T > T_g$) for the shape recovery. In addition, due to the dynamic nature of the vinylogous urethanes, the net-points could be rearranged at high temperatures and new "permanent" shapes be programmed. Figure 8 shows the evolution of the shape memory effect in this work. Initially, a flat shape (permanent shape #1) sample was formed. Afterwards the temperature was increased to ~ 45 °C ($> T_g$) and the sample was rolled (temporary shape #1) and then cooled down to room temperature ($T \leq T_g$) under maintained stress. In the glassy state, at room temperature, the temporary rolled sample was stable.

Only upon reheating the sample to T > T_g the sample rolled open and the initial permanent shape #1 was recovered. The shape recovery happened instantaneously. Additionally, due to the dynamic bonds when the sample was heated to higher temperatures than the activation of vinylogous urethanes cross-linking i.e., the net point, it would be rearranged and the permanent shape would be reprogrammed. To illustrate, the flat sample was heated to 110 °C, folded, while maintaining the temperature for ~1.5 h to allow sufficient network rearrangement to the new permanent shape #3. The new shape could then undergo similar shape change recovery as depicted in Figure 8. The solid-state plasticity enabled shape transformations without being limited to the original mold i.e., thermadaptability [164]. As mentioned before, our group recently developed a shape memory poly(Myr)-based rubber based on a hybrid network of dynamic/static cross-links using a vinylogous urethane/epoxy system (Chapter 3). Although shape memory effects were observed, the shape transformation was slow and inefficient. The temporary shape reversibility was based on vinylogous urethane exchanges (as the molecular switches) and limited by the kinetics of the

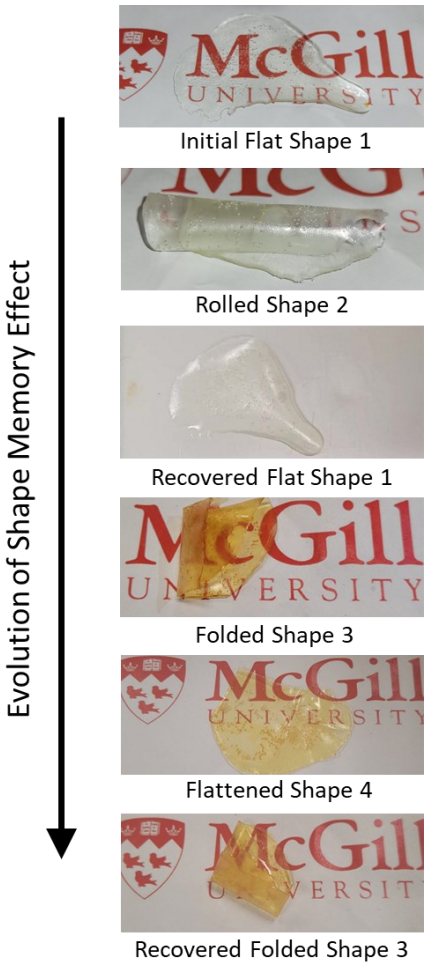

Figure 4.8 Evolution of shape memory effect: the permanent shape was reprogrammed confirming the thermadapt properties of the rubber. The temporary shape in "Rolled shape 2" and "Flattened Shape 4" were formed by heating at ~ 45 °C followed by cooling under applied

exchange rates. Also, the permanent shape was not reconfigurable at all as it was based on the static epoxy/amine cross-links (as the net points). Compared to the aforementioned work, here the reversible molecular switches were activated by T_g, which is a bulk property. Therefore, the shape recovery occurred within seconds and was more efficient. It is worth noting that a color change was observed in the second shape memory cycle. This can be attributed to the possible thermo-oxidative degradation of aliphatic amides [184].

4.8. Conclusions

We demonstrated a catalyst-free vinylogous urethane bio-based vitrimeric rubber from AAEMA and Myr. First, we explored statistical copolymerization of Myr and AAEMA via NMP. The reactivity ratios of the monomers pair in xylenes at 120 °C were found to be $r_{Myr} = 0.20 \pm 0.17$ $r_{AAEMA} = 0.22 \pm 0.07$, suggesting a nearly alternating copolymerization. In addition, semi-batch polymerization in bulk at 120 °C allowed synthesis of random copolymers of Myr and AAEMA. NMP allowed synthesis of diblock copolymers of poly(AAEMA-block-Myr) with M_n and $Đ$ of 13 kg/mol and 1.82.

A linear prepolymer of poly(Myr-*co*-Sty-*co*-AAEMA) was synthesized to mimic SBR rubbers and crosslinked by solution casting with IPDA. ATR-FTIR, DMTA and tensile results confirmed the recyclability of vitrimers by hot pressing at 110 °C without appreciable changes in the properties after at least 4 cycles. Furthermore, the vitrimers exhibited shape memory properties with good shape fixity and fast shape recovery. The thermadapt vitrimers could undergo permanent shape reprogramming. This work illustrates the adaptability of Myr-based rubbers by vitrification and copolymerization for the synthesis of sustainable elastomers with versatile properties.

4.9. Supporting information for Chapter 4

4.9.1. S1. Polymer Synthesis

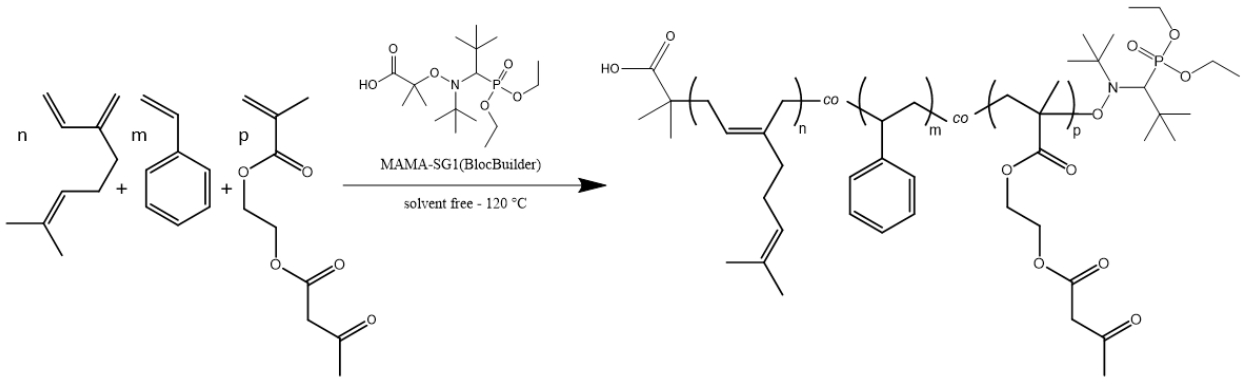

Figure S 4.1 Nitroxide mediated terpolymerization of myrcene (Myr), styrene (Sty) and (acetoacetoxy)ethyl methacrylate (AAEMA) with SG1-based BlocBuilder alkoxyamine to form poly(Myr-*co*-Sty-*co*-AAEMA) prepolymer, coded as p-MyrStyAAEMA. The resulting polymer had F_{AAEMA} = 0.09 and F_{Myr} =0.51 from ^{1}H NMR and M_n = 13,500 g/mol with $Đ$ = 1.54 from GPC (please see Table 1.a).

4.9.2. ^{1}H NMR spectra and molecular characterization of the polymers

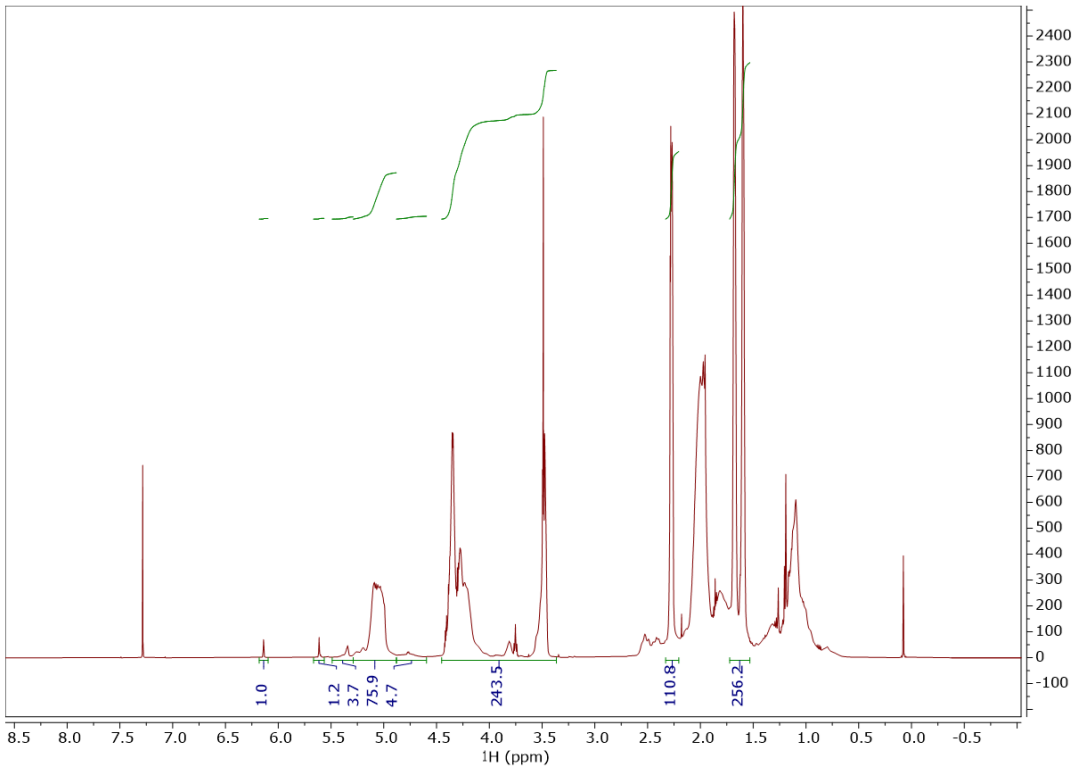

Figure S 4.2 ^{1}H NMR spectrum of dried poly(Myr 50 – AAEMA 50) after precipitation and recovery. The spectrum was taken in $CDCl_3$ (500 MHz) at room temperature. For poly(Myr 50 -

AAEMA 50): δ = 5.50-5.30 (t br, 1H [1,2]), 5.25-5.00 (t br, 1H[1,2], 1H[3,4], 2H [1,4]), 4.80-4.70 (m, 2H [1,2] , 2H [3,4]), 4.44-3.85 (d br, 4H poly(AAEMA)), 3.85-3.4 (s, br 2H poly(AAEMA)), 2.27 (s, 3H poly(AAEMA)), 2.25 -1.85 (m br, 8H poly(Myr)),1.90-1.75 (m, 2H poly(AAEMA)), 1.67 (s, 3H poly(Myr)), 1.59 (s, 3H poly(Myr)).

* The signal at 4.80-4.70 ppm corresponds to vinylic 2H [1,2] and 2H [3,4] and φ signal at 5.50-5.30 ppm correspond to olefinic 1H [1,2]. Monomer peaks (not shown): δ = 6.45-6.27 (m, 1H Myr), 6.15 (s, 1H AAEMA), 5.60 (s, 1H AAEMA)

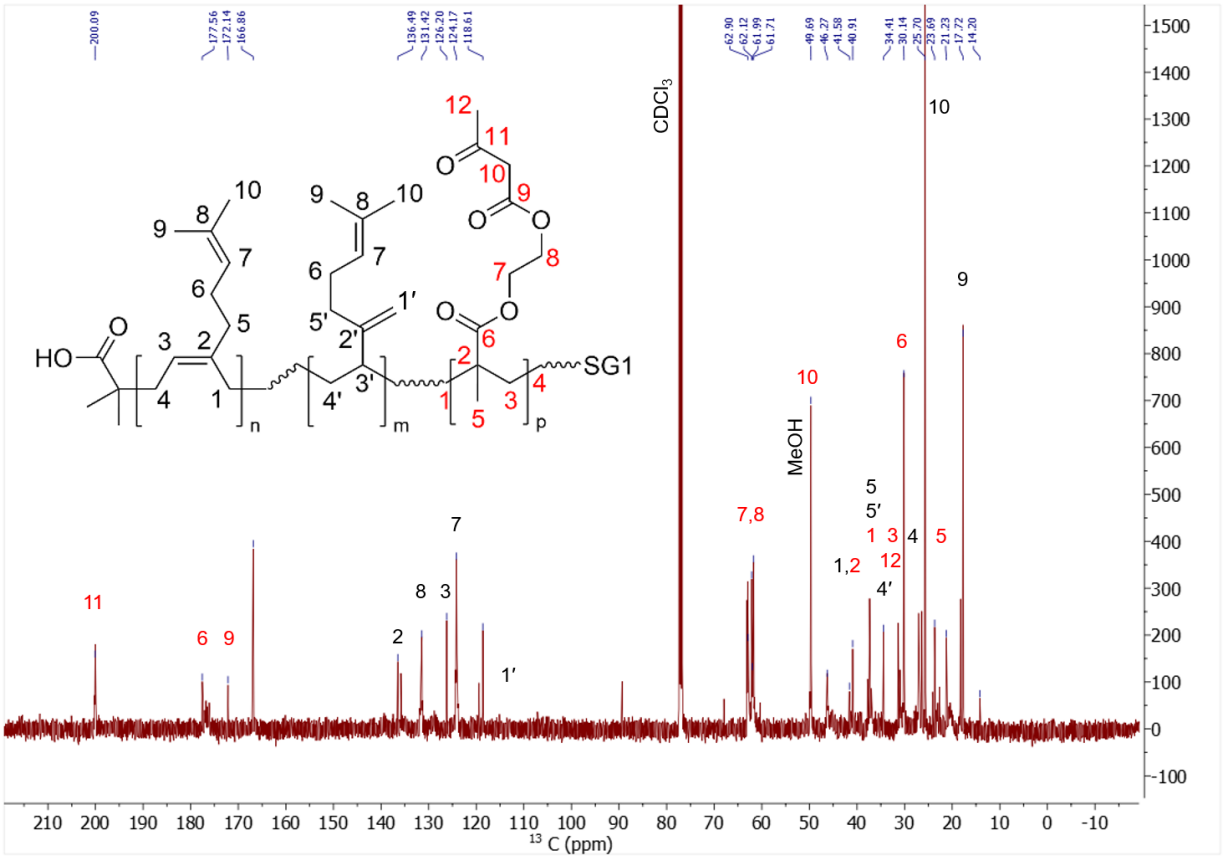

Figure S 4.3 [13]C NMR spectrum of dried poly(Myr 50–AAEMA 50) after precipitation and recovery. The spectrum was taken in $CDCl_3$ (500 MHz) at room temperature [132,180,185].

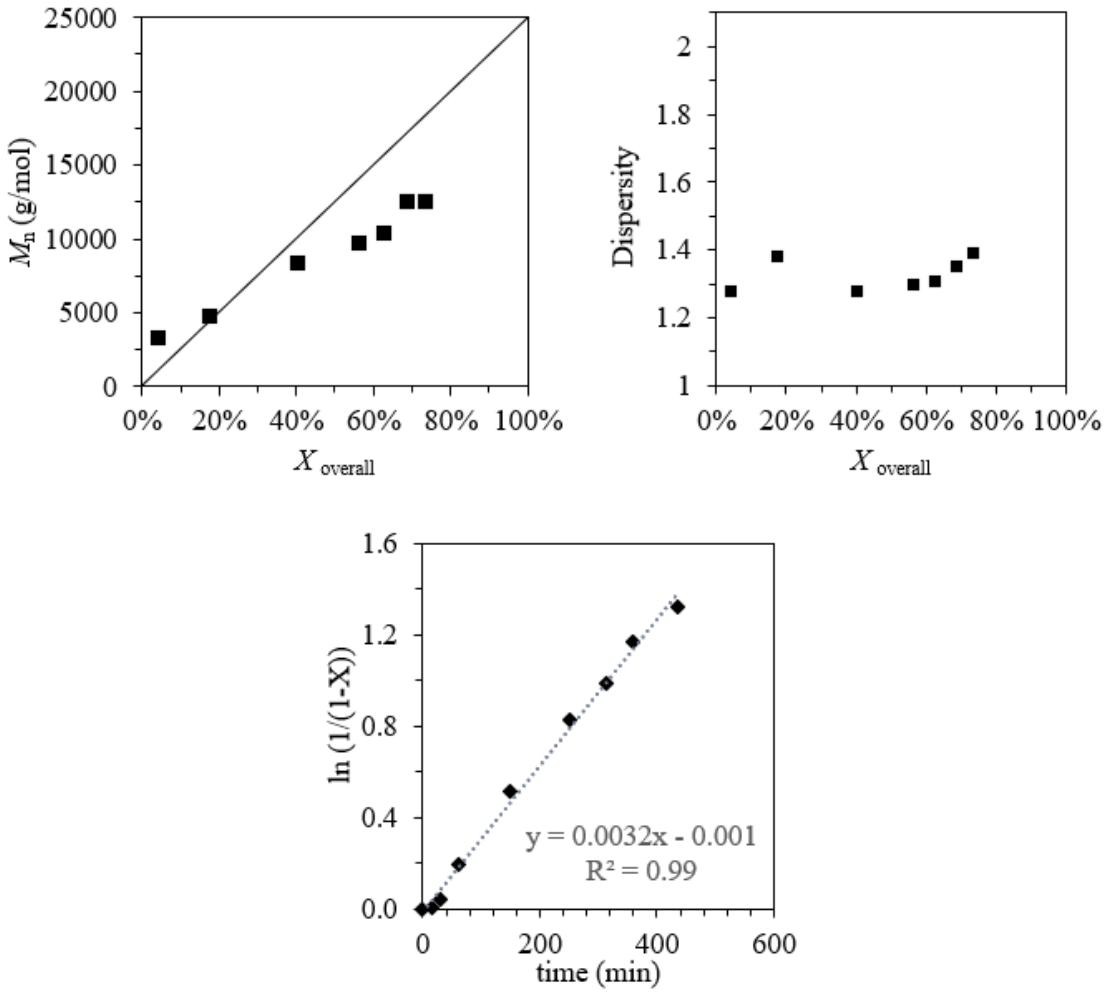

Figure S 4.4 Representative kinetic plots of Myr 30 – AAEMA 70 polymerization in 50 wt% xylene at 120 °C. The plot shows relatively well-controlled polymerization in terms of predictable chain growth with conversion and low dispersity ($Đ \leq 1.39$).

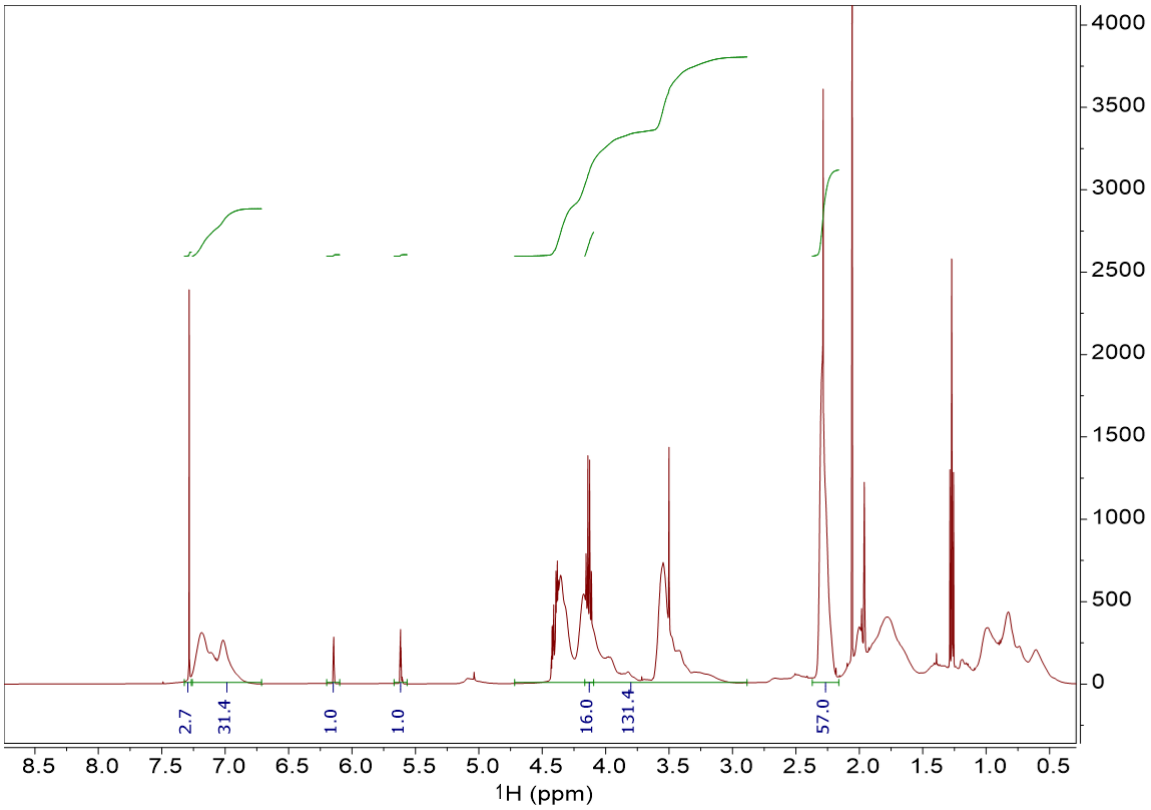

Figure S 4.5 ^{1}H NMR spectrum of dried poly(AAEMA-co-Sty) after precipitation and recovery. The NMR was done in $CDCl_3$ (500 MHz) at room temperature. For poly(AAEMA-*co*-Sty): δ = 7.26-6.30 (m, br, 5H poly(Sty)), 6.15 (s, 1H AAEMA), 5.60 (s, 1H AAEMA), 4.44-3.85 (d br, 4H poly(AAEMA)), 3.85-3.4 (s, br 2H poly(AAEMA)), 2.27 (s, 3H poly(AAEMA)), 1.90-1.75 (m, 2H poly(AAEMA))

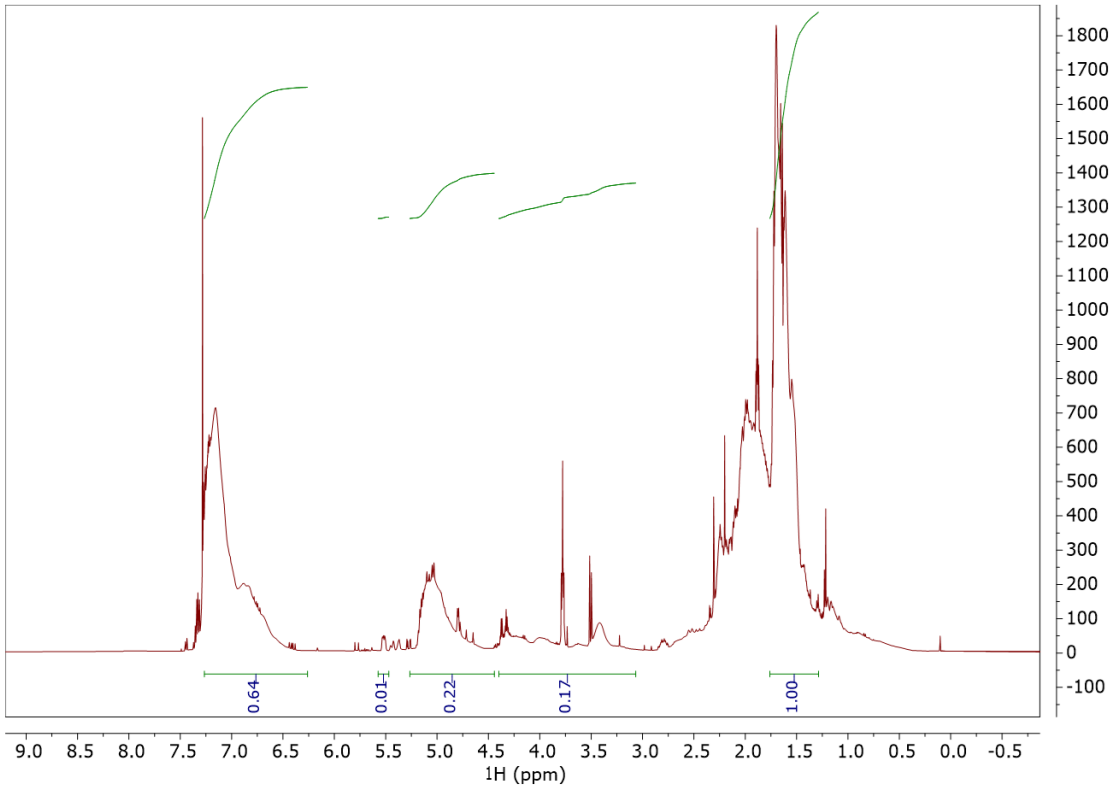

Figure S 4.6 ^{1}H NMR spectrum of dried poly(MyrStyAAEMA) terpolymer after precipitation and recovery. The spectrum was taken in $CDCl_3$ (500 MHz) at room temperature. poly(MyrStyAAEMA): δ = 7.26-6.30 (m, br, 5H poly(Sty)) δ = 5.50-5.30 (t br, 1H ^{1,2}), 5.25-5.00 (t br, 1H^{1,2}, 1H^{3,4}, 2H ^{1,4}), 4.80-4.70 (m, 2H ^{1,2} , 2H ^{3,4}), 4.44-3.85 (d br, 4H poly(AAEMA)), 3.85-3.4 (s, br 2H poly(AAEMA)), 2.27 (s, 3H poly(AAEMA)), 2.25 -1.85 (m br, 8Hpoly(Myr)),1.90-1.75 (m, 2H poly(AAEMA)), 1.67 (s, 3H poly(Myr)), 1.59 (s, 3H poly(Myr)). The signal at 4.80-4.70 ppm corresponds to vinylic 2H ^{1,2} and 2H ^{3,4} and at 5.50-5.30 ppm corresponds to olefinic 1H ^{1,2} (not shown in the chemical structure). Monomer peaks (not shown): δ = 6.45-6.27 (m, 1H Myr), 6.15 (s, 1H AAEMA), 5.60 (s, 1H AAEMA).

Calculation of F_{AAEMA}, F_{Myr} and F_{Sty}

$n_{poly(AAEMA)} = [Area_{4.5\text{-}3.1ppm}] /6 \approx 0.028$

$n_{poly(Myr)} = [Area_{1.75\text{-}1.69ppm}] /6 \approx 0.167$

$n_{poly(Sty)} = [Area_{7.26\text{-}6.30ppm}] /5 \approx 0.128$

$mol\ \%poly(i) = [n_{poly(i)} / \sum n_{poly\ (i)}] \times 100\%$

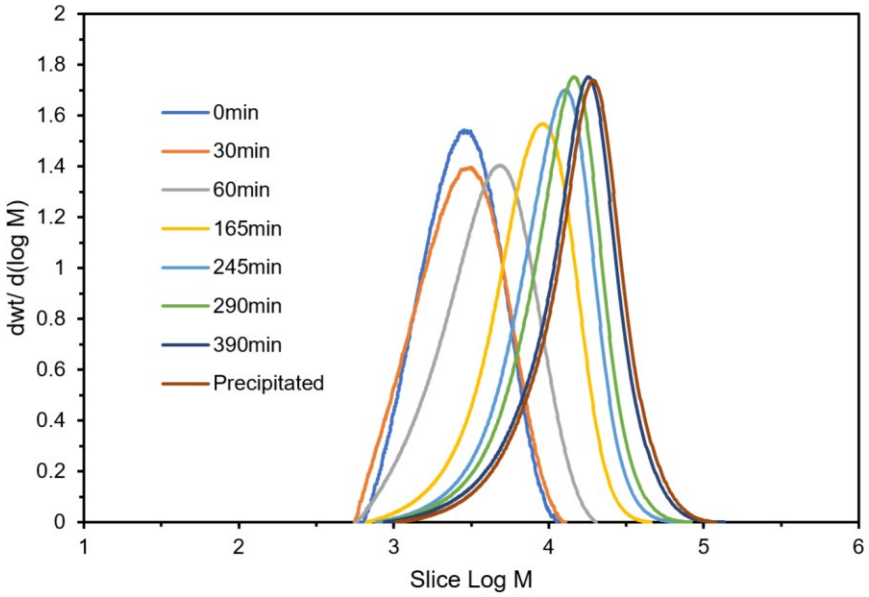

Figure S 4.7 GPC traces of p-MyrStyAAEMA

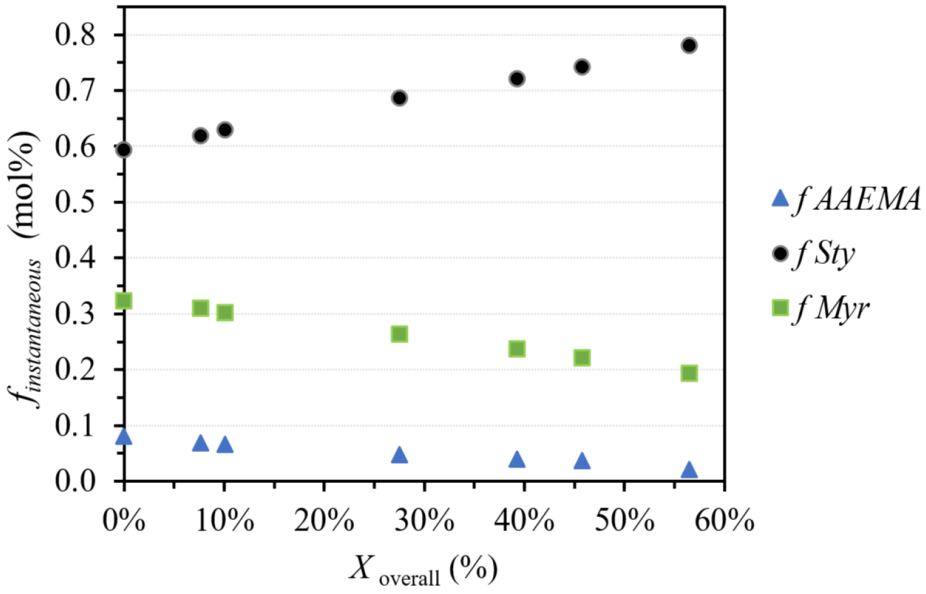

Figure S 4.8 Instantaneous composition ($f_{instantaneous}$) of unreacted monomers with $X_{overall}$ during the terpolymerization of Myr/Sty/AAEMA to form the p-MyrStyAAEMA prepolymer.

4.9.3. DSC and TGA

The T_g of the p-MyrStyAAEMA (see Table 1.E for details of composition) prepolymer can be estimated using the Fox equation.

$$\frac{1}{T_g} = \sum \frac{W_i}{T_{g_i}} \quad \text{(Eq S1)}$$

Here, w_i and T_{gi} are the weight fraction and T_g (in K) of each comonomer. $T_{g,\,AAEMA}$= 2 ˚C, $T_{g,\,Myr}$= -75 ˚C and $T_{g,\,Styrene}$ = 100 ˚C [125,141]. The estimated T_g of p-MyrStyAAEMA from the Flory-Fox equation is $T_{g,\,Fox}$ = -28 ˚C which is in good agreement with the DSC data, $T_{g,\,DSC}$ = -19 ˚C shown below. After the vitrification the T_g of the v-MyrStyAAEMA increased to 22 ˚C.

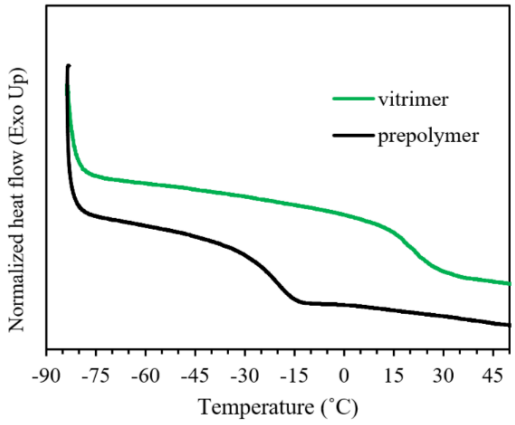

Figure S 4.9 DSC traces of p-MyrStyAAEMA prepolymer and its corresponding vitrimer. Vitrification with IPDA increased the glass transition (T_g) of the material from -19 ˚C to 22˚C.

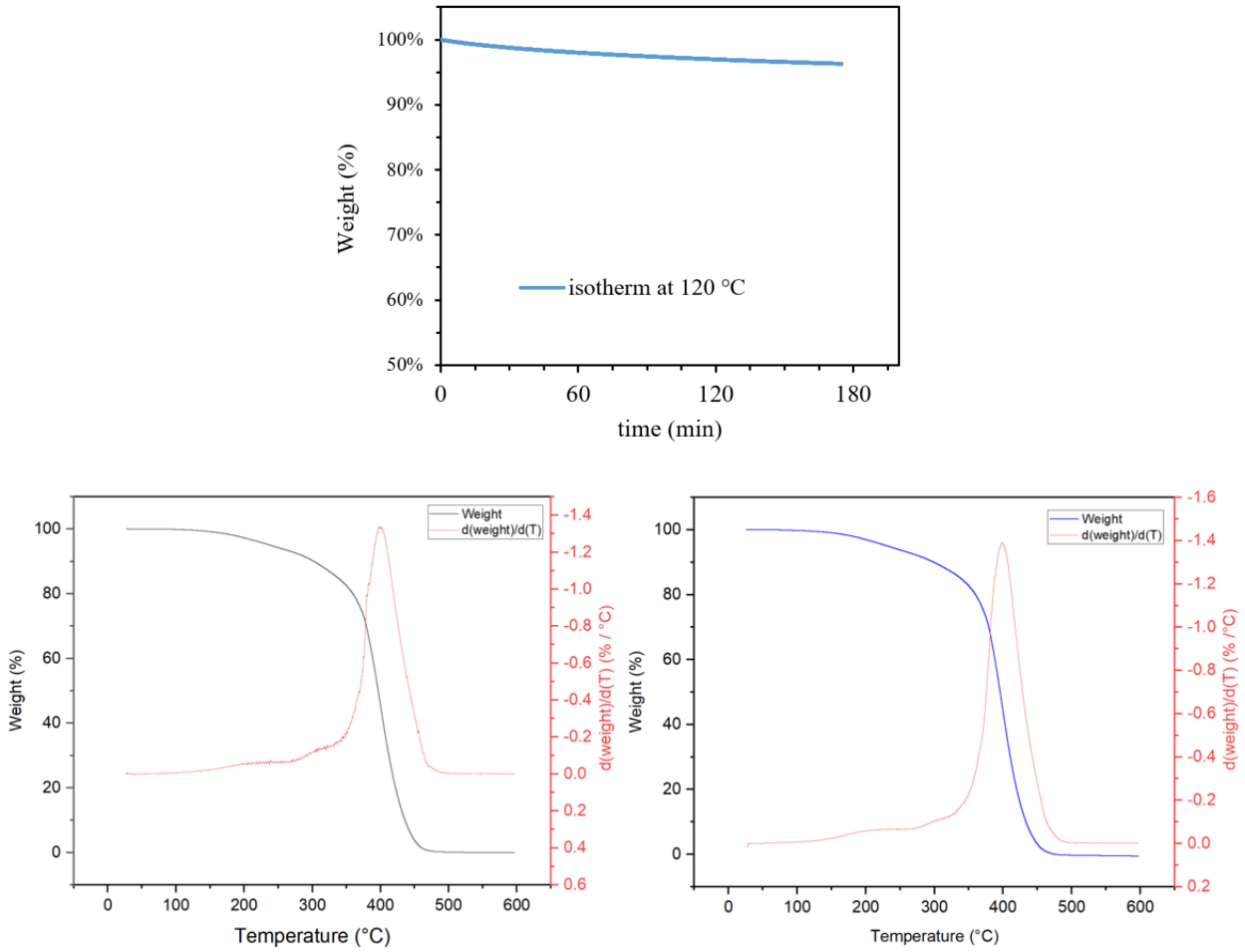

Figure S 4.10 Top: TGA trace of the vitrimer v-MyrStyAAEMA at 120°C isotherm. Less than 4% weight loss was observed after 180 min. Bottom: TGA traces of the v-MyrStyAAEMA and its derivative of pristine vitrimer (left) and four times recycled (R×4) (right).

4.9.4. S4. Rheology

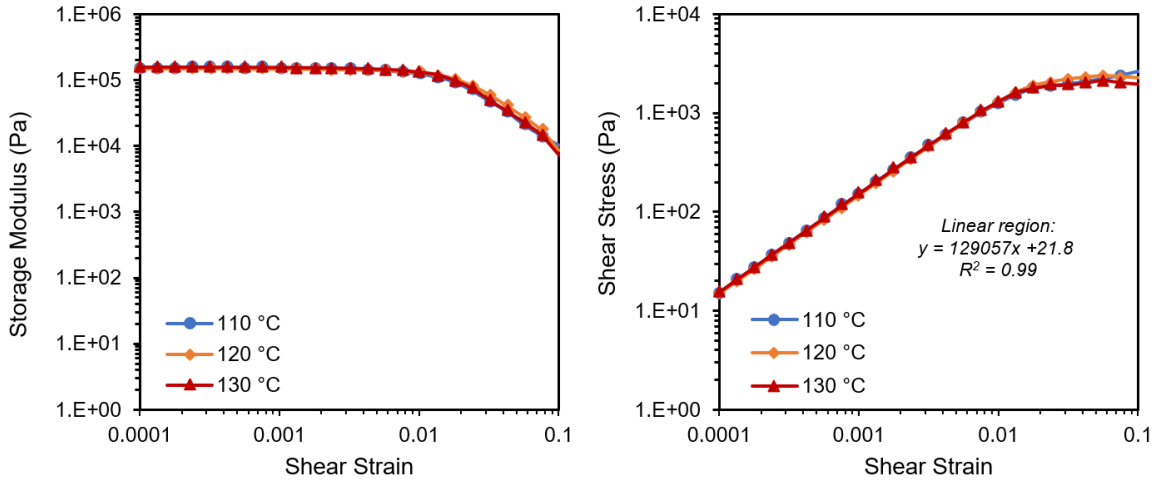

Figure S 4.11 Strain sweep (left) and stress-strain (right) tests at 1 Hz for v-MyrStyAAEMA vitrimer at 110 ˚C, 120 ˚C, and 130 ˚C. The linear viscoelastic region is fitted by linear regression (shear strain < 0.01).

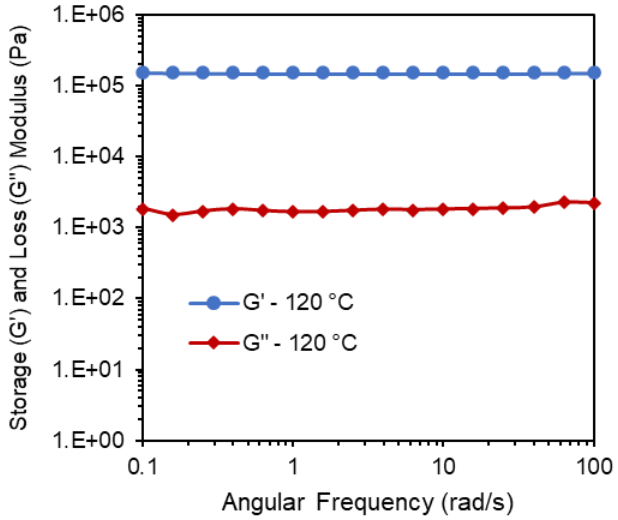

Figure S 4.12 Frequency sweep with constant strain of 0.1% at 120 ˚C. The v-MyStyAAEMA vitrimer exhibits typical elastomer behavior with a linear modulus and G′ > G″.

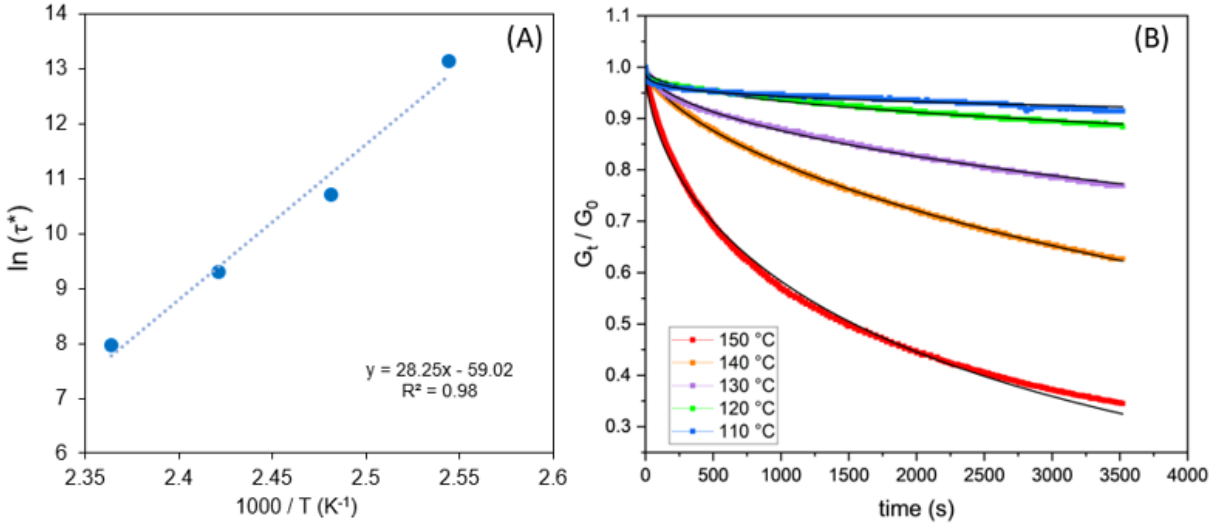

Figure S 4.13 A) Arrhenius relationship between the relaxation time and temperature from stress-relaxation experiments. The estimated E_a is 235 kJ/mol B) Curve fitting of stress relaxation tests with the stretched exponential decay Kohlrausch–Williams–Watts equation (KWW) model, shown in black solid lines.

Table S 4-1 Curve fitting of characteristic relaxation time (τ*) and β at various temperatures.

Model	Kohlrausch–Williams–Watts equation (KWW)				
Equation	$G/G_0 = \exp(-(t/\tau^*)^{\beta})$				
temperature	150 °C	140 °C	130 °C	120 °C	110 °C
τ* (s)	2880 ± 9	11020 ± 15	44500 ± 310	513800 ± 16600	8.85E7 ± 8.5E6
β	0.584 ± 0.001	0.655 ± 0.001	0.534 ± 0.001	0.433 ± 0.002	0.250 ± 0.002
Reduced Chi-Sqr	1.13E-04	2.38E-06	7.67E-06	1.18E-05	1.02E-05
R-Square (COD)	0.99652	0.99978	0.99781	0.98269	0.95293
Adj. R-Square	0.99652	0.99978	0.9978	0.98267	0.95287

Table S 4-2 Tensile properties of vitrimer before and after recycling

Sample	Stress at break (MPa)	Strain at break (%)
Vitrimer R×0	0.73 ± 0.07	146 ± 14
Reprocessed R×1	0.55 ± 0.05	104 ± 9
Reprocessed R×2	0.74 ± 0.05	136 ± 9
Reprocessed R×3	0.88 ± 0.08	169 ± 33

Chapter 5: Reprocessable bio-based statistical and block copolymer methacrylic vitrimers with shape memory effect

This chapter is presented as an article published as the following with the same title

Farhad Asempour, Eline Laurent, Yvan Ecochard, Milan Maric

ACS Applied Polymer Materials

2024, 6, 1, 956–966

https://doi.org/10.1021/acsapm.3c02515 [161]

This chapter also includes two videos on the shape memory:

Video 1: Evolution of shape memory effects of the vitrimer of the statistical copolymer consisting of C13-methacrylate/vanillin methacrylate (v-s-CV). Video shows the shape recovery after heating with a heat gun.
https://pubs.acs.org/doi/suppl/10.1021/acsapm.3c02515/suppl_file/ap3c02515_si_002.mp4

Video 2: Evolution of shape memory effects of the vitrimer of the statistical copolymer consisting of C13-methacrylate/vanillin methacrylate (v-s-CV) showing the transition from the deformed flat shape to a curved upward "recovered" shape with heating.
https://pubs.acs.org/doi/suppl/10.1021/acsapm.3c02515/suppl_file/ap3c02515_si_003.mp4

5.1. Preamble to Chapter 5

Building upon the lessons learned from myrcene based vitrimers, in this chapter, myrcene is replaced with methacrylate bio-based monomers. An alkyl methacrylate with an average side chain length of 13 CH_2 units (termed C13MA, derived from vegetable oils) was used. Compared to dienes, methacrylates require relatively lower polymerization temperatures and offer high efficiency. In addition, their RAFT polymerization affords high chain end fidelity essential for the synthesis of block copolymers. Also, poly(C13MA) provides better thermal stability than polymyrcene which is advantageous for thermal reprocessing. Similar to poly(myrcene), poly(C13MA), has a high M_e. Thus, based on the findings of Chapter 3, it was hypothesized that vitrification can modulate its mechanical properties. Based on the findings of Chapter 4, it was hypothesized that shape memory effects will be induced more efficiently using T_g as a trigger. In

addition, two strategies for improving the dimensional stability of the resulting vitrimer were directly compared: 1) by static-dynamic cross-links (from Chapter 3) and 2) by employing segmented diblock copolymers.

5.2. Abstract

Transitioning to a circular bioeconomy requires shifting away from conventional petroleum-based thermosets to recyclable biobased materials. We developed reprocessable and shape-memory bio-based vitrimers with controlled architecture and enhanced creep resistance. A series of prepolymers of lignin-based vanillin methacrylate (VMA), with a mixture of vegetable oil-derived methacrylic esters with an average alkyl side chain length of 13 units (C13MA), and glycidyl methacrylate (GMA) were synthesized: statistical copolymer poly(C13MA-*co*-vMA), block copolymer poly(C13MA-*block*-VMA), and statistical terpolymer poly(C13MA-*co*-VMA-*co*-GMA). Reversible addition fragmentation chain-transfer (RAFT) polymerization allowed control over backbone structure of statistical and block copolymers with similar overall molecular weight and composition. Vitrification via aldehyde-functional VMA units with isophorone diamine enabled dynamic imine cross-linking while adding the epoxy-functional GMA into the statistical terpolymer precursor enabled hybrid static-dynamic cross-linking networks. Vitrimers showed excellent retention of thermomechanical properties after 4× reprocessing cycles. Microphase separation was confirmed in the "hard-soft" type block vitrimers. While statistical vitrimers showed comparable tensile properties, self-assembled block vitrimers exhibited poor tensile strength. Additionally, we compared the creep control using microphase separation and hybrid network. Both methods reduced creep (up to 84%), but hybrid cross-linking caused significantly slower stress relaxation. A temperature-triggered shape memory effect was incorporated in the statistical vitrimer with two shape programming cycles. Combining C13MA and VMA presents a rich platform for greener vitrimers with highly tunable properties and functionalities.

5.3. Introduction

Since the pioneering works of Staudinger in the 1920s, plastic production has seen exponential growth. However, a mere 10% of polymers are currently being recycled [186]. Most consumed polymers are heavily linked to fossil feedstocks and mostly consist of stable C-C and C-H bonds, which in turn attain desirable properties at service time but limit their degradation at end-of-life [160]. In particular, the family of permanently cross-linked thermosets constitute an extraordinary challenge for recycling and participating in a circular economy [187,188].

An emerging strategy to address this issue is through the introduction of dynamic bonds which has led to the emergence of a new class of polymeric materials called Covalent Adaptable Networks (CANs) and their thermo-responsive subgroup known as vitrimers [64,65]. In addition to enhanced (re)processability and recyclability of CANs and vitrimers, incorporation of exchangeable bonds can provide advanced characteristics such as self-healing and responsiveness to external stimuli [57,189].Vitrimers encompass associative dynamic cross-links, where the rupture of dynamic bonds takes place only after another covalent cross-link has been formed. Thus, vitrimers bridge the gap between thermosets and thermoplastics. That is, vitrimers maintain their cross-linked structure when undergoing swelling and heating, like thermosets, yet they retain the capacity to be reshaped and mended like thermoplastics [58,59].

Despite the promise associated with vitrimers, a major practical issue with non-glassy vitrimers is creep [150]. Creep refers to the tendency of a viscoelastic solid to undergo continuous and permanent strain when subjected to mechanical stress. Many strategies have been proposed to suppress creep in vitrimers [187,190]. For example, the groups of Torkelson [150], Sumerlin [109] , and Nicolaÿ [75] have reported that incorporation of static cross-links with dynamic ones can improve creep resistance of the vitrimers. We followed a similar strategy to good effect with rubbery Myr-based vitrimers in Chapter 3 and 4 [103,154]. Although this method suppresses creep, it cannot stop it without losing reprocessing. Another strategy for controlling creep in vitrimers involves utilizing phase separation. Although the influence of phase separation on viscoelastic properties of polymers is well-known, only a handful of studies have explored it [94,115,191,192]. For example, Epps' and Sumerlin's groups investigated block copolymer vitrimers based on vinylogous urethane acrylates [114]. They reported that compared to homogenous counterparts, the microphase separated vitrimers exhibited lower creep due to lower network strand diffusion.

Apart from addressing polymer's end-of-life issues, the development of polymers obtained from sustainable resources is also relevant. Bio-based polymers not only help reduce the dependency on fossil feedstocks but also contribute to a reduced carbon footprint, owing to their closed carbon cycle [146,193]. Nevertheless, it is essential to consider the entire life cycle of such polymers to ensure true sustainability [194]. The combination of bio-based building blocks and dynamic covalent chemistry can play a significant role in the development of greener polymeric materials with lower environmental impact [11].

With this in mind, we propose a study based on three main objectives. First, we aim to increase the bio-based content of these networks while maintaining control on the polymer microstructure. We used C13-methacrylate (C13MA) and vanillin methacrylate (VMA) as monomers. C13MA is a soft methacrylate with an average pendant chain of 13 alkyl groups and is sourced from vegetable oil [174,195]. VMA was synthesized from methacrylation of vanillin, a natural phenolic aldehyde which can be extracted from vanilla beans and depolymerization of lignin [196]. VMA will provide both stiffness and reactivity for the vitrification process [197]. The aldehyde functionality of VMA reacted with free amines, resulting in the formation of reversible Schiff base imine cross-links [198]. Although many works have used vanillin to synthesize vitrimers via various polymerization strategies, only a few studies have reported the radical polymerization of VMA [96,199]. Recently, Gao *et al.*, and Gong *et al*., synthesized starlike Schiff base vitrimers of VMA and lauryl methacrylate which were grafted from lignin and ethyl cellulose macroinitiator, respectively [200,201].

The second goal of this work is to investigate the impact of network architecture on vitrimer properties and creep control. Block copolymer vitrimers reported earlier mainly focused on low T_g precursors [114,115]. Notably, only a limited number of studies have investigated the use of high T_g blocks, in our case the VMA-containing block segment, as possible anchors for creep control in such systems [90]. Holmberg et al. prepared diblock copolymers consisting of VMA and lauryl methacrylate. They observed self-assembly in the resulting block copolymer [195]. Additionally, we aimed to directly compare the effects of phase separation and the incorporation of dual dynamic/static cross-links on the overall properties of a system with similar composition and vitrimer chemistry. Here, we conducted a comparative analysis involving three distinct systems, encompassing a statistical vitrimer, a phase-separated block copolymer vitrimer, and a vitrimer

with a dual static and dynamic cross-linking network. To have a reasonable comparison, in all cases, the number average molecular weight (M_n), and overall composition (F) of C13MA and VMA were kept similar. However, for the third system with dual cross-linking, 2 mol % of glycidyl methacrylate (GMA) was copolymerized in the statistical prepolymer. GMA is an epoxy bearing repeating unit which can permanently react with free amines. Schematic 5-1 summarizes the schematic of the 3 vitrimeric systems studied in this work.

Finally, we aimed to extend the functionalities of the bio-based vitrimers by incorporating shape memory effects. Shape memory polymers (SMPs) can recover their original "permanent" shape upon activation by an external stimulus, heat in our case [151,182,183]. SMPs have the potential to be used in a wide range of applications including packaging, sensors, aerospace, biomedicine, and smart textiles [151,182,183]..

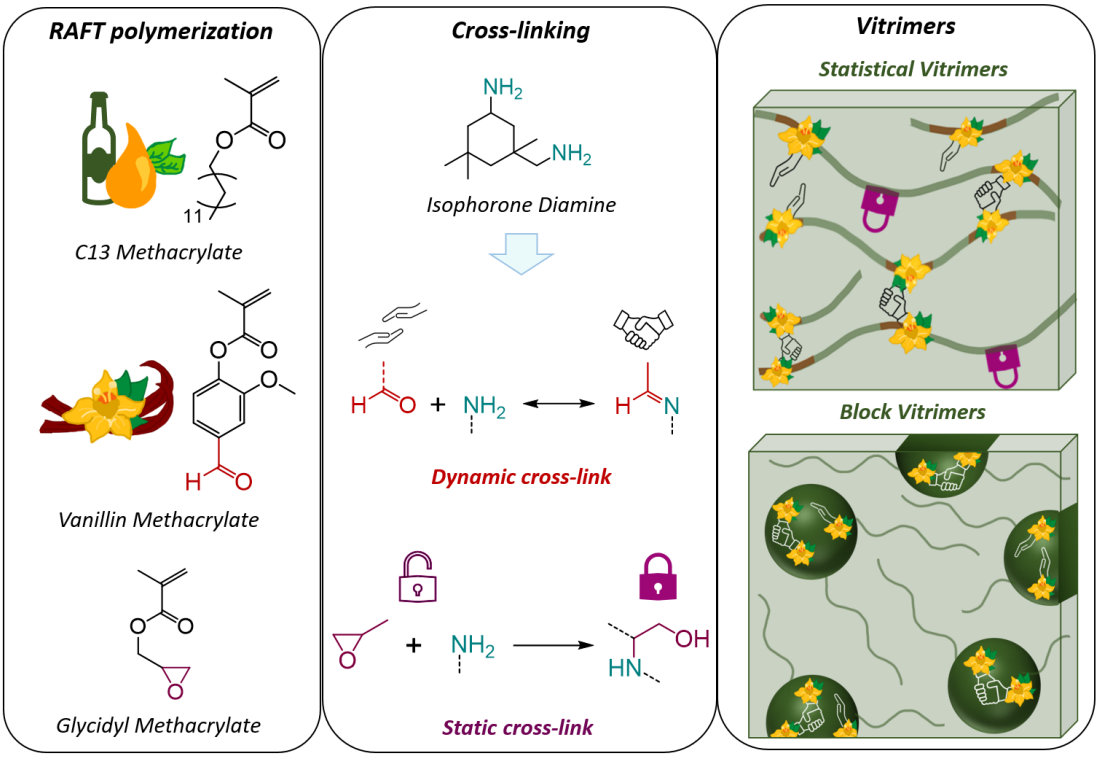

Schematic 5-1 Structures of C13 methacrylate (C13MA), vanillin methacrylate (VMA), and glycidyl methacrylate (GMA) monomers. Middle) Structure of isophorone diamine (IPDA) with the two types of incorporated cross-linking: dynamic or hybrid static-dynamic. Right) Schemes of statistical and block copolymer vitrimers.

5.4. Results and discussion

5.4.1. Synthesis of prepolymers

We employed reversible addition−fragmentation chain transfer (RAFT) polymerization to synthesize the prepolymers, as it is a well-suited platform for the synthesis of vinyl-derived vitrimers. RAFT polymerization enabled effective control over polymer architecture, with similar overall molecular weight targeted at 35,000 g/mol, and composition, with 80 mol% of C13MA, across the three reactions. Synthesis of VMA and all polymerization procedures is described in the Supporting Information (Sections S2.1 and S2.2 and Schematics S1 to S4).

The statistical poly(C13MA-*co*-VMA) is termed "p-s-CV" while the block copolymer, poly(C13MA-*block*-VMA), is coded as "p-b-CV". The statistical terpolymer poly(C13MA-*co*-VMA-*co*-GMA) is abbreviated as "p-s-CVG". Here, "p" stands for prepolymer, "s" or "b" specify statistical or block microstructure, and "C", "V", and "G" indicate C13MA, VMA, and GMA monomers, respectively. After the vitrification "p" is exchanged with lowercase "v". The chemical structures of p-s-CV and p-b-CV are illustrated **Figure 5.1.a**.

The polymerization kinetics were studied for the statistical copolymers to determine if a random incorporation of the monomers over time occurred. From ^{1}H NMR spectroscopy, it was confirmed that the molar ratio of unreacted monomers remained almost constant throughout the polymerization, as shown in **Figure S 5.3** and **Figure S 5.14**. This suggests that the monomers were evenly distributed along the polymer chains with a low gradient at the beginning of the reaction where the VMA was incorporated at a slightly faster rate but followed by a relatively equal incorporation of the two monomers. Gel permeation chromatography was used to measure the M_n and dispersity ($Đ$) of the prepolymers (summarized in **Table 5.1**). M_n values were corrected using the Mark–Houwink–Sakurada equation relative to poly(dodecyl methacrylate), shown in the Supporting Information Section 2.3 **Table S 5-1**. A linear increase of M_n versus conversion confirmed a well-controlled polymerization, please see **Figure S 5.2** and **Figure S 5.13**. Concerning the block copolymer synthesis, first a homopolymer of poly(C13MA), p-s-C, was synthesized with M_n = 28,000 g/mol and $Đ$ = 1.11. The macro-initiator was then chain extended by reacting with VMA i.e., p-b-CV; see **Figure S 5.6** and **Figure S 5.9** for the evolution of M_n and $Đ$ as a function of conversion for the first and second block respectively. As shown in **Figure**

5.1.b, a clear monomodal shift towards higher M_n (up to 35,200 g/mol) without a significant increase in $Đ$ (= 1.25) confirmed a successful chain extension reaction.

ATR-FTIR and ^{1}H NMR analysis were used to confirm the presence and the ratio of each monomer in the prepolymers. **Figure S 5.4**, **Figure S 5.8**, **Figure S 5.11**, and **Figure S 5.15** display the ^{1}H NMR spectra of the prepolymer showing the specific peak for each monomer. **Figure 5.2.a**, and **5.2.b** and S19 present the FTIR spectra where peaks at 733 cm^{-1} for –C-O-C, 1705 cm^{-1} for the formyl, 1758 cm^{-1} for -C=O and 2735 cm^{-1} for –CHO are attributed to VMA in p-s-CV and p-b-CV while the peak at 910 cm^{-1}, corresponding to the stretching C-O of oxirane group, confirms the incorporation of GMA into the p-s-CVG [202,203].

Table 5.1 Composition, molecular weight (M_n) and glass transitions temperature (T_g) of the three synthesized prepolymers.

Prepolymer	$F_{(C13MA)}$ [a]	$F_{(VMA)}$ [a]	$F_{(GMA)}$ [a]	M_n (g/mol)[b]	$Đ$	T_g (°C) [c]	Bio-Carbon content [d]
p-s-CV	82%	18%	0%	37,200	1.28	0	75%
p-b-CV	83%	17%	0%	35,200	1.25	-44 and +119	75%
p-s-CVG	83%	15%	2%	40,200	1.21	0	74%

[a] Molar fraction obtained by NMR [b] M_n obtained by GPC after chain-end removal. Numbers were obtained compared to PMMA standard and corrected with Mark–Houwink–Sakurada equation using dodecyl methacrylate parameters. [c] From DSC analysis. [d] see Supporting Information section 4 for calculations.

For all prepolymers, the chain-end from the RAFT benzodithioate moiety was removed and replaced with a non-reactive 2-cyanopropyl moiety, to avoid possible side-reactions with the amine-functional cross-linkers [112,114]. This was done by reacting solely the polymer with an excess of azobis(isobutyronitrile) (AIBN) initiator in 1,4 dioxane. UV-VIS analysis confirmed a successful chain-end removal by disappearance of the absorption band at 500 nm, corresponding to the $\pi \rightarrow \pi^*$ electronic transition of the benzodithioate (**Figure S 5.18**). ^{1}H NMR and ATIR-FTIR analyses still confirmed the presence of the aldehyde function with the same integration peaks in ^{1}H NMR, **Figure S 5.5**, **Figure S 5.12**, and **Figure S 5.16**, and bands in ATR-FTIR spectra, shown in **Figure S 5.19**. As summarized in **Table 5.1** Composition, molecular weight (Mn) and glass transitions temperature (Tg) of the three synthesized prepolymers., all the prepolymers had relatively low $Đ$ with a similar M_n and composition, ensuring a reasonable

comparison between the resulting vitrimers. In particular, p-s-CV and p-b-CV were quite different in physical appearance, as depicted in **Figure 5.1.d**. While p-s-CV was a highly viscous liquid, the block copolymer p-b-CV appeared more like a solid material. This can be attributed to the differences in their architecture and existence of a phase separated poly(VMA) hard domain.

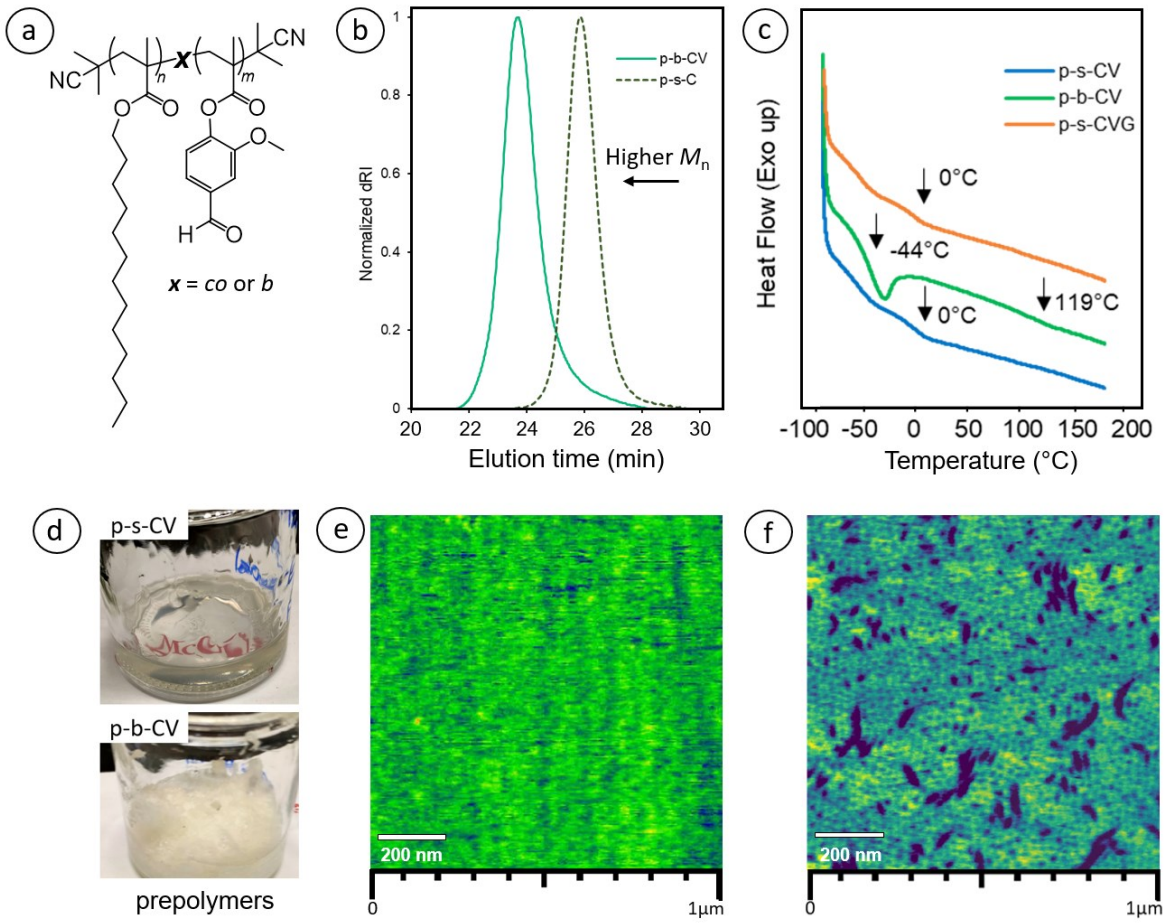

Figure 5.1 **a)** Chemical structure of statistical (p-s-CV) or block (p-b-CV) prepolymer. **b)** GPC traces of the first block of homo(C13MA) (p-s-C) and after chain-extension with VMA (p-b-CV) **c)** DSC traces of the 3 prepolymers; while the statistical prepolymer showed a single T_g at ~ 0 °C and the block copolymer (p-b-CV) showed 2 distinct T_gs corresponding to poly(C13MA) and poly(VMA) blocks. **d)** Pictures of p-s-CV and p-b-CV after chain end removal; while the prepolymers have similar compositions, they have distinctive properties **e)** AFM image of p-s-CV in phase mode **f)** AFM image of p-b-CV in phase mode; in the latter microphase separation into spheres and/or cylinders can be seen.

5.4.2. Microphase separation

After obtaining the prepolymers, we proceeded to investigate their thermal properties and formation of phase-separated microdomains within them. DSC traces of the prepolymers are shown in **Figure 5.1.c.** In the case of statistical prepolymers, a single T_g around ~ 0°C was observed. However, when examining the block copolymer (p-b-CV), two separate T_g values were evident, corresponding to the T_gs of poly(C13MA) and poly(VMA) blocks. The presence of distinct T_g values suggests the occurrence of microphase separation within the block copolymer structure.

In addition, we performed AFM on solvent cast films of both the statistical and block prepolymers. **Figure 5.1.e** and **f** compare the AFM images of the p-s-CV and p-b-CV using the phase channel from tapping mode. While a uniform morphology is seen for p-s-CV, the p-b-CV exhibited a microphase-separated structure typically associated with continuous sphere and/or cylinder morphologies.

To further investigate the microphase separation in p-b-CV, we estimated the segregation strength χN at the order disorder transition (ODT) temperature; where χ denotes the monomer-monomer Flory-Huggins interaction parameter and N represents the total degree of polymerization. The enthalpic part of χ can be estimated using equation 1 [204].

$$\chi = \frac{\overline{V}}{RT}(\delta_{VMA} - \delta_{C13MA})^2 \qquad \text{(Eq. 1)}$$

Here, δ is the solubility parameter, R is the universal gas contsatant, $\overline{V}$ is the reference molar volume and calculated by $\overline{V} = \sqrt{V_{VMA}\, V_{C13MA}}$, V_i is a molar volume of each constituent monomer i, and T is temperature given in an absolute temperature scale. Liebler, using a mean-field approximation, predicted that a symmetric monodisperse diblock copolymer undergoes microphase separation into lamellar geometries when $(\chi N)_{ODT} > 10.5$ [204,205]. Therefore, based on our calculations (detailed in the Supporting Information Section S3.2. and S3.3), the $(\chi N)_{ODT}$ values for this system at temperatures of 25 °C and 160 °C are approximately an order of magnitude higher than 10.5, respectively. This suggests substantial segregation between the blocks. More importantly, our observation corroborates with the findings of Holmberg *et al*., who synthesized similar diblock copolymers of poly(VMA)-*b*-poly(lauryl methacrylate) with higher M_n of 60,000 g/mol and similar composition of 17 vol % of the poly(VMA) block. They reported

that the block copolymer self-assembled into a body-centered cubic array of vanillin-based nanospheres in a poly(lauryl methacrylate) matrix, similar to our AFM observations [195].

5.4.3. Vitrification and (re)processing

As illustrated in Schematic S5, vitrification and network formation started with dissolving the prepolymers in THF (50 w/v%). Then, isophorone diamine (IPDA) crosslinker was added from THF to the solution with the ratio of 0.9 equivalent of NH_2 to the aldehyde of VMA for v-s-CV and v-b-CV. In the case of epoxy functionalized v-s-CVG, the ratio was 0.9 equivalent of NH_2 to the sum of aldehyde and epoxy functions. It should be noted, since each amine can react more than once with epoxides (i.e., as primary or secondary amine), tighter networks can be formed with smaller stoichiometry imbalance. The stoichiometry imbalance is well reported in the literature, and it is reported to promote associative crosslinking exchanges [40,55]. Gelation occurred within minutes, and the solution was capped and placed in a fume hood overnight. This was followed by vacuum drying at 120 ± 5 °C for 2 hours and then at 80 ± 5 °C for about 12 hours. Afterwards, the resulting yellowish solid was molded into tensile bars or disks using a hot press at 130 ± 5 °C and 6 metric tons pressure for 75 ± 5 min. The dynamic cross-links allowed fabrication of uniform shapes.

5.4.4. Network properties

After cross-linking, we probed the properties of the resulting networks. **Figure 5.2.a** and **b** show the ATR-FTIR spectra of the prepolymers and their associated vitrimers. For all samples, the disappearance of the characteristic peak of the aldehyde group of VMA at 1705 cm^{-1} and emergence of a new peak at 1648 cm^{-1}, corresponding to the imine bonds, strongly suggest formation of imine bonding networks [203]. In the case of GMA-based vitrimers, the disappearance of the characteristic oxirane peak at 910 cm^{-1} also confirms the reaction of IPDA with GMA [202].

Solubility tests were performed in THF at room temperature for 48 h. The high gel content of more than 90% for all samples verified the successful formation of cross-linked networks, shown in **Figure 5.2.c.** Due to the associative nature of the crosslinks, vitrimers do not dissolve in (nonreactive) solvents; however, their shape can significantly change following swelling. The v-s-CV and v-b-CV exhibited similar solubility behaviour in THF. In contrast, the dual cross-linked network, v-s-CVG, exhibited the highest gel content of 99 ± 1 % and lowest swelling ratio of 156

± 40 %. It appears that additional of static cross-links, by incorporation of 2 mol% GMA in the prepolymer, improved the network integrity. This was also confirmed by estimation of cross-linking density using the Flory-Rehner equation, in which a tighter network was calculated for v-s-CVG, please see details in S3.4 and **Figure S 5.20** [14].

As observed in the DSC curves (**Figure 5.2.d**), vitrification increased the T_g of the samples in all cases. For the statistical co/terpolymers, v-s-CV and v-s-CVG, the T_g increased from 0 °C to 30 °C and 35 °C, respectively; however, in the case of the v-b-CV, only the T_g associated with the poly(VMA) block increased, from 119 °C to 180 °C and the T_g of the poly(C13MA) block remained intact. This increase in the T_g of the poly(VMA) block can be attributed to cross-linking of VMA with the cyclic IPDA [95]. Again, appearance of 2 distinct T_gs can be a strong indication of microphase separation in v-b-CV [114]. TGA analyses showed slight improvements in the thermal stability of the samples due to vitrification, **Figure S 5.21**. The thermal stability of the v-s-CV was further investigated via TGA under isothermal conditions at 160 °C for 6 hours in a nitrogen atmosphere. The vitrimer exhibited high thermal stability, as it experienced less than a 2.2 % weight loss as shown in **Figure S 5.22**.

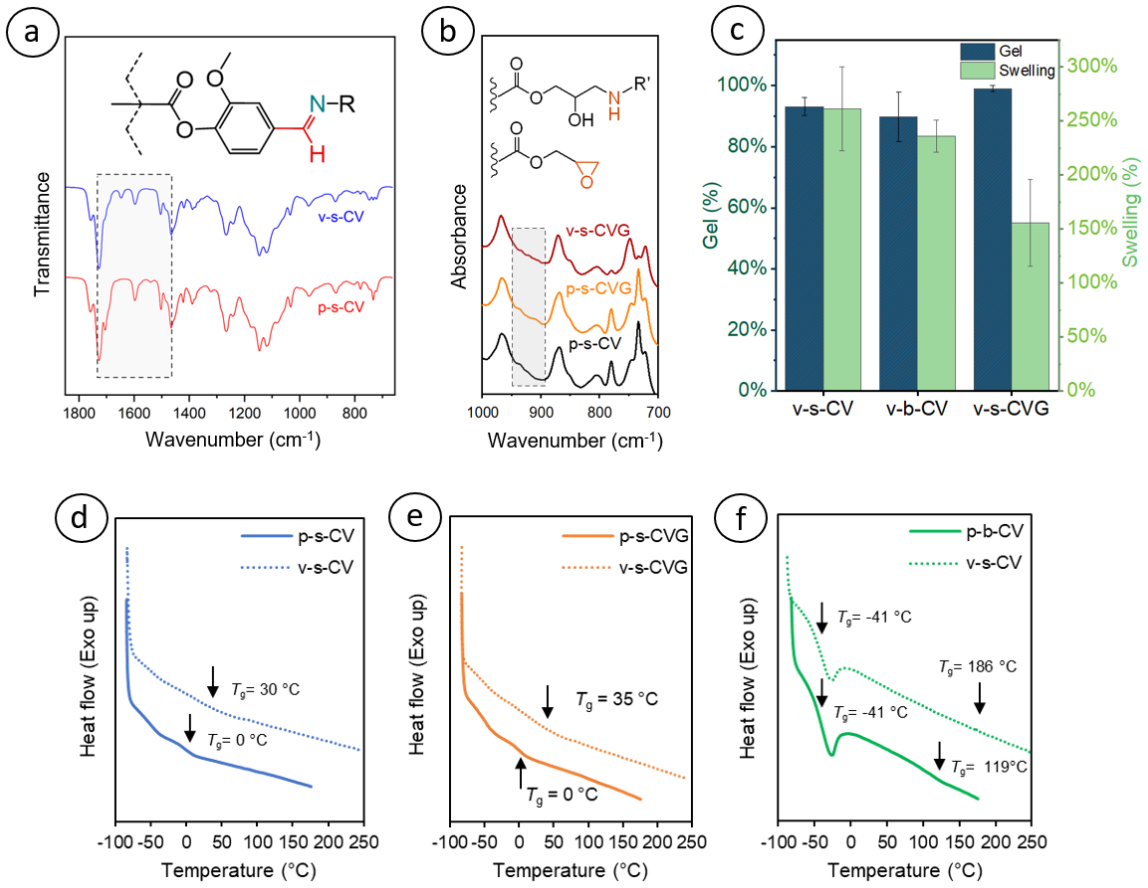

Figure 5.2 a) ATR-FTIR spectra of statistical prepolymer, p-s-CV, and its associated vitrimer, v-s-CV. **b)** Comparison of ATR-FTIR spectra of epoxy-based v-s-CVG vitrimer with its prepolymer **c)** Solubility tests of statistical, block and epoxy based vitrimers in THF after 48h. DSC curves of prepolymers and vitrimers: **d)** p-s-CV and v-s-CV (blue), **e)** p-s-CVG and v-s-CVG (orange) , **f)** p-b-CV and v-b-CV (green). Existence of 2 T_gs strongly suggest microphase separation. Vitrification increased the T_g in all cases.

To explore the occurrence of microphase separation in the vitrified block copolymer, we conducted AFM on v-b-CV. The sample was prepared by casting from THF prior to complete gelation. **Figure 5.3.a** shows an AFM image of solvent-cast v-b-CV. The characteristic microphase separated domains can be seen. Uniaxial tensile tests were performed to probe the mechanical properties of the vitrimers depicted in **Figure 5.2.b**. The statistical v-s-CV and v-s-CVG showed comparable elongation and stress at break. v-s-CV exhibited the highest elongation at break of 40 ± 4 % while v-s-CVG had the highest stress at break of 3.5 ± 0.1 MPa. In contrast, the block copolymer, v-b-CV, exhibited very different tensile behavior and was surprisingly brittle with tensile strength and elongation at break of 0.99 MPa and 5.3 % respectively. The difference in the

tensile properties of the block vitrimer compared to the statistical analogs can be related to microphase separation. One possible reason for the brittleness of the v-b-CV can be attributed to the high entanglement molecular weight (M_e) of poly(C13MA). The reported M_e of poly(lauryl methacrylate) is 225,000 g/mol which is much higher than the M_n of the poly(C13MA) block in this work [206,207]. The lack of cross-linking and physical entanglement results in domains with poor mechanical properties rendering v-b-CV incapable of withstanding uniaxial stress.

Nanoindentation with a Berkovich tip (three-sided pyramid) was used to generate the force-displacement curves illustrated in **Figure 5.3.c** from which the modulus and hardness was calculated. In contrast to the tensile modulus, the block copolymer vitrimer showed the highest hardness. Moreover, the v-b-CV exhibited the lowest creep among the vitrimers. It appears that the high T_g of poly(VMA) domains could effectively act as anchors to stabilize the dimensional stability of the vitrimers [90].

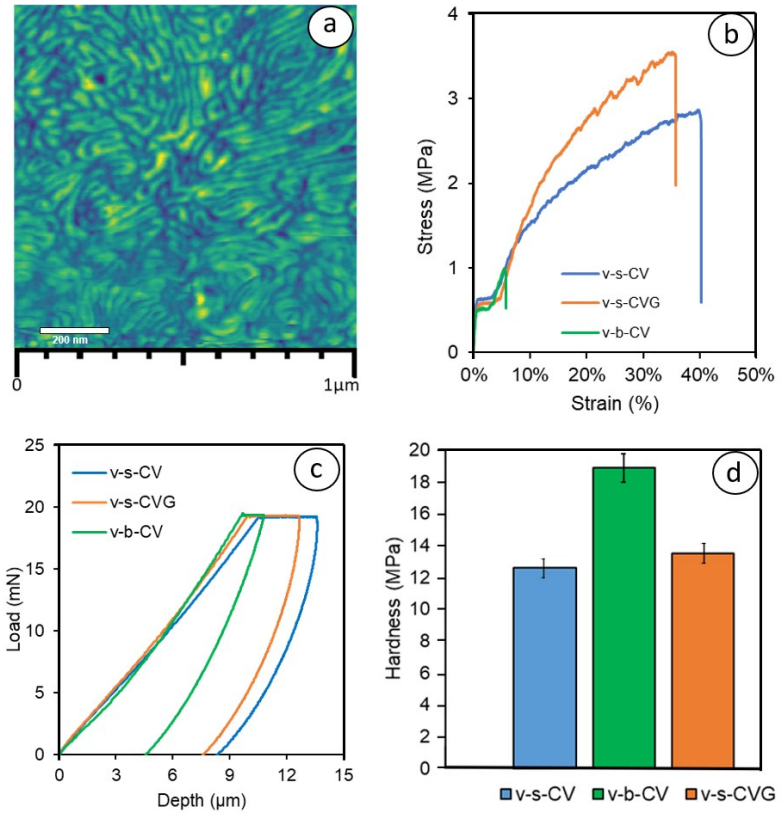

Figure 5.3 a) AFM image of v-b-CV and microphase separated domains. The lighter colors are attributed to the microphase with higher energy dissipation, i.e. the poly(C13MA) block. **b)** Tensile stress-strain of the vitrimers; while v-s-CV and v-s-CVG showed comparable tensile properties, the block vitrimer, v-b-CV showed much lower stress and elongation at break. **c)** Load-

displacement (depth) curves from nanoindentation with a Berkovich tip, block vitrimer showed lowest creep **d)** Calculated hardness from nanoindentation. Block vitrimer showed highest hardness. (Calculated modulus from nanoindentation can be seen in **Figure S 5.29**)

We investigated the rheological behavior of the vitrimers by dynamic mechanical thermal analysis (DMTA), shown in **Figure 5.4** and in the Supporting Information, section 3.7. In the case of the statistical vitrimers, v-s-CV and v-s-CVG, increasing the temperature above 25 °C resulted in a sharp drop in storage modulus followed by a rubbery plateau. However, the block vitrimers exhibited a different behavior; the storage modulus of v-b-CV slightly decreased until about 175 °C and a sharp decrease was only observed after that which can be contributed to the T_g of the VMA block. These results corroborate with the observed T_g values from DSC analyses and suggest microphase separation in the block vitrimers.

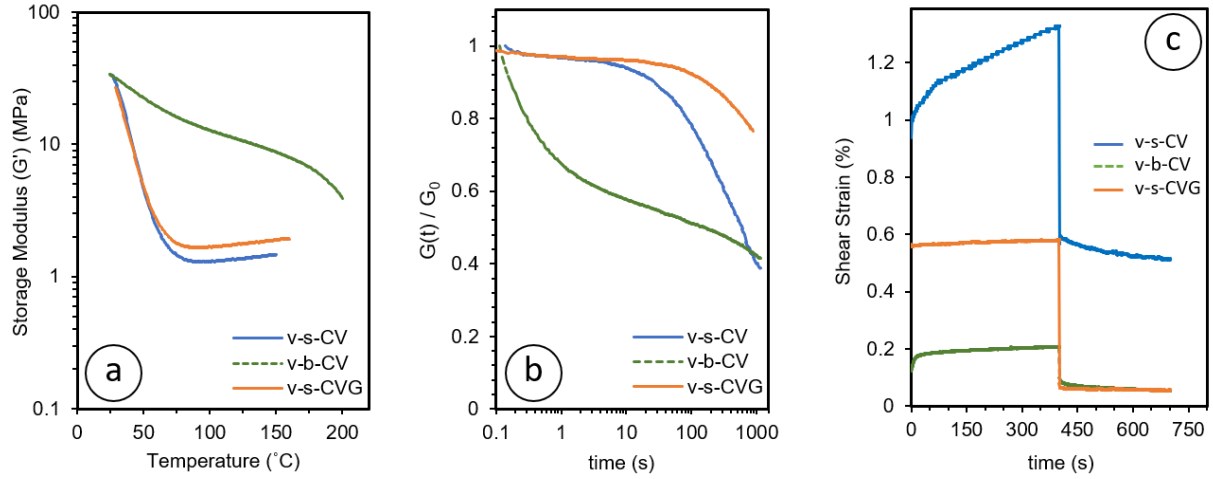

Figure 5.4 a) DMTA, temperature sweep curves of vitrimers **b)** Stress-relaxation curves of the vitrimers at 160 °C. c) Creep-recovery curves at 120 °C.

Figure 5.4.b and **Figure S 5.27** illustrates the stress-relaxation properties of the vitrimers. At 160 °C, the statistical vitimers, v-s-CV and v-s-CVG, showed similar behaviors at time scales shorter than 10 s; however, they diverged at longer time scales. It is suggested that an Arrhenius relationship (Eq. S7) can model the gradual decrease of viscosity with increasing temperature. As shown in the Supporting Information, a stretched exponential decay model (Eq. S6) was used to find the statistical vitrimers characteritic relaxation time (τ*) and subequently their viscous flow activation energy (E_a). With rising test temperature the beta values also increased which signifies less deviation from ideal Maxwellian behavious at higher temperatures. The calculated E_a of v-s-CV was 185 kJ/mol. The epoxy-based vitrimer with dual static and dynamic cross-links, v-s-CVG,

exhibited the slowest stress-relaxation behaviour with the apparent E_a of 230 kJ/mol (**Figure S 5.28**). This result highlights that even a low concentration of static cross-links can effectly restrict polymer chain movement. Interestingly, the block vitrimer, v-b-CV, displayed different behavior compared to the statistical vitrimers. Below the T_g of the hard block, the stress-relaxation of v-b-CV was dominated by the stress-relaxation of poly(C13MA) block and did not follow an Arrhenious type correlation which can be attrubited to the phase separation and existance of glassy poly(VMA) block. At time scales shorter than 650 s, v-b-CV underwent faster relaxation. Interestingly, at temperatures below the T_g of poly(VMA), after 650 s the stress-relaxation rate of v-s-CV surpassed that of the v-b-CV. Ricarte and Shanbhag conducted a study using an inhomogeneous Rouse model to simulate the rheological behavior of unentangled vitrimer melts with different distributions of cross-linkers [208]. They reported that vitrimers with blocky distributions of cross-links exhibit faster stress-relaxation compared to those with a uniform distribution of cross-links, which corroborates with what we see at shorter time scales, thus possibly for C13MA. Our observation of stress-relaxation at longer time scales (after 650 s) aligns also with the results of Lessard *et al.*, and Ishibashi *et al.* works who reported that vitrimers made of block copolymer have slower relaxation rate at longer time scales, which they attributed to higher restriction in polymer chain movements and diffusion [114,115]. In both previous studies, phase-separated diblock copolymers with vinylogous urethane chemistry and relatively soft acrylic backbone were investigated. The main distinction between the mentioned works and the present study is that, herein a hard-soft diblock copolymer was synthesized the stress-relaxation tests shown in **Figure 5.4.b** were conducted at a temperature below the T_g of the hard section of the vitrimer. To better study the influcence of phase separation on the stress-relaxation of v-b-CV, a relaxation test was performed at 200 °C which is higher than the observed T_g of poly(VMA) at ~180 °C, illustrated in **Figure S 5.27**. At 200 °C, v-b-CV showed a different behavior and can reached full relaxation.

The creep recovery data of the vitrimers are illustrated in **Figure 5.4.c**. The statistical v-s-CV exhibited the highest creep; however, the epoxy-based and block vitrimer exhibited improved creep resistance. This improvement can be attributed to the existence of static cross-links, in the case of v-s-CVG, and microphase separation with a hard domain in case of v-b-CV. The creep data from the rheometer also corroborates with that of the nanoindentation tests (**Figure 5.3.c**).

5.4.5. Reprocessing

An important consequence of vitrification is the ability of the resulting networks to be reprocessed and healed through the reconfiguration and exchange of cross-links. Herein, all vitrimer samples could be effectively shaped using the hot-press. However, due to the low tensile modulus and fragility of v-b-CV, we only studied the reprocessability of the statistical vitrimers in detail. To do so, samples went through at least 4 cycles of compression molding and deconstruction. **Figure 5.5.**a shows the ATR-FTIR spectra of the v-s-CV before and after 4 cycles of reprocessing. No appreciable change in the spectra was observed and the peak at 1648 cm^{-1}, attributed to the imine bonds, stayed intact after reprocessing [203]. In addition, no significant change in the thermal properties of v-s-CV was observed after 4 reprocessing cycles with the $T_g = 30$ °C, $T_{onset} = 355$°C, *and* $T_{5\%} = 285$ °C for the v-s-CV Rx4, as illustrated in **Figure 5.5. b** and **c.** Representative stress-strain curves of the v-s-CV after 4 (re)processing cycles are also depicted in **Figure 5.5.d.** The tensile strength and elongation at break for each cycle are summarized in **Table S 5-4**. Moreover, **Figure 5.5.e** presents the elastic and loss moduli traces from the DMTA of v-s-CV, collected using disk-shaped samples (unlike **Figure 5.4.a** where torsion bars were used). For v-s-CVG, similar retention of properties was observed after 3 reprocessing cycles as provided in **Table S 5-4**. These findings suggest that the vitrimers can maintain their structural integrity after repeated reprocessing cycles of deconstruction and compression molding. The illustrated recyclability of the studied C13MA/VMA based vitrimers combined with their bio-derived content suggest promising metrics for improved sustainability of these systems [209,210].

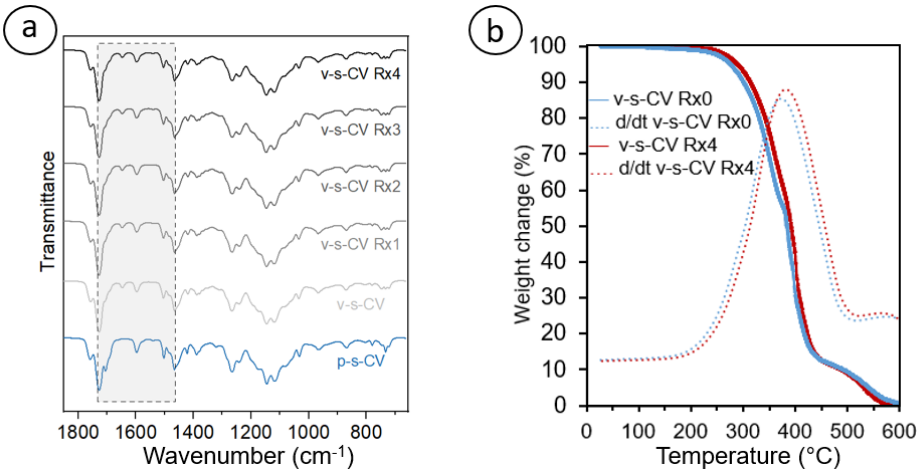

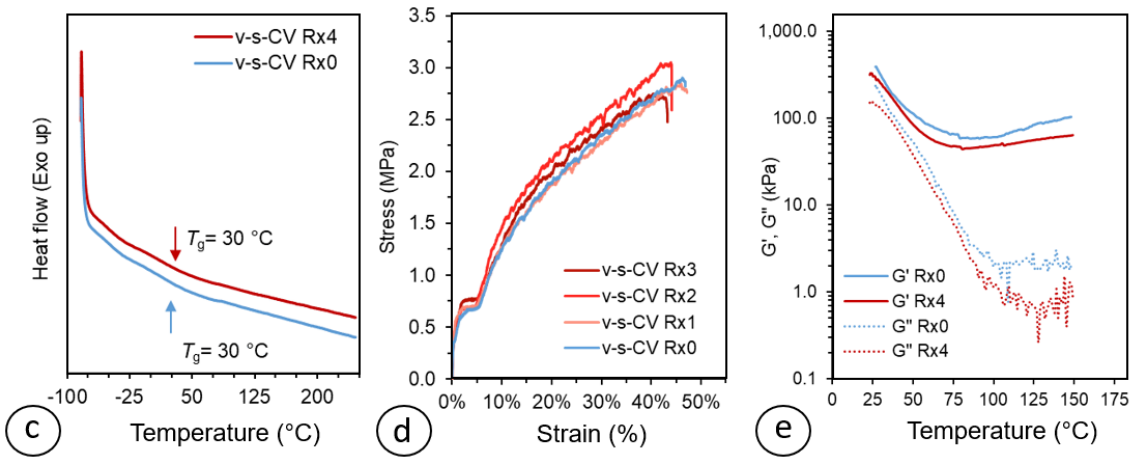

Figure 5.5 a) ATR-FTIR spectra of p-s-CV prepolymer and v-s-CV vitrimer after 4 cycles of reprocessing. **b)** TGA curves of weight change (solid lines) and its associated derivative (dotted lines) of the statistical vitrimer before and after 4 cycles of reprocessing **c)** DSC spectra of v-s-CV before and after reprocessing. **d)** Stress-strain curves of v-s-CV for 4 reprocessing cycles **e**) DMTA traces of v-s-CV before and after 4 reprocessing. The data shows that the vitrimer largely retained its chemical and thermomechanical properties after 4 reprocessing cycles.

5.4.6. Shape memory effect

Shape memory is a consequence of molecular architecture, reversible mobility changes and conformational entropy [182]. For a polymer to be capable of undergoing shape memory programming, two structural elements are required: permanent net-points and reversible switching segments [211]. The net-points create a three-dimensional network architecture that allows for storage and memorizing a permanent shape while reversible switching segments act to fix or release a temporary shape when triggered by stimulus through changes in molecular mobility [182]. Here, in the case of v-s-CV, we hypothesized that the cross-links can act as net-points while the T_g (~ 30 °C) could be used as the thermally triggered reversible switching segments. **Figure 5.6** depicts a complete evolution of shape memory effect of v-s-CV. First, we reprocessed the sample into a flat shape. Note that there are two arrows and sign "vs" written on the sample to show the concave sample, **Figure 5.6.c.** To program the shape memory effect, the sample was heated to ~ 70 °C (> T_g), bent and cooled down to room temperature while still under the applied load. This led to the formation of the temporarily deformed shape #1 which was stable at room temperature (< T_g). To recover the "fixed" shape #1, the sample was again heated using a heat gun (T > T_g). The shape recovery was fast and happened in less than 1-2 min, **Figure 5.6.e** and video 1. A consequence of dynamic covalent cross-linking in vitrimers is that the net-point can be also reshaped to reprogram the shape memory effect. To do so, we heated the sample to 125 °C at

which the dynamic bond exchanges are effectively activated and stress-relaxation is more significant. Afterwards, the sample was bent, this time concave up, while at 125 °C for about 3 h to ensure reconfiguration of cross-links, i.e., the net-points. The "fixed" shape #2 was achieved by cooling down the sample. Again, similar heating, deformation and shape recovery was repeated and achieved in steps f to h. The transition of the flat shape, **Figure 5.6.g** to an upward curve, **Figure 5.6.h**, is shown in video 2. The sample showed great retention of the deformed shapes and the shape recovery was achieved almost completely.

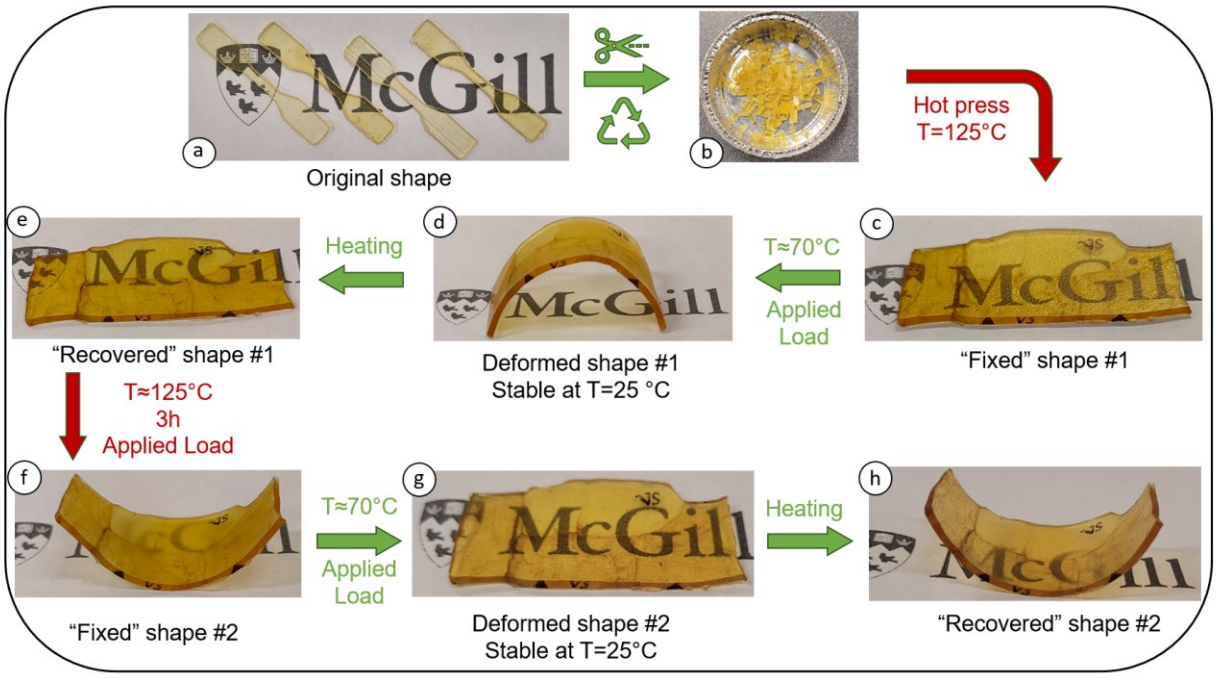

Figure 5.6 Evolution of shape memory effects of v-s-CV **a)** Original tensile samples. **b)** Cutting and reprocessing. **c)** Hot pressed flat sample, fixed shape #1, arrows were drawn on the edge of the sample to show the concave. **d)** Deformed shape #1 with concave down, sample was heated and deformed at ~ 70 °C and cooled down after ~ 5 min. **e)** "Fixed" sample #1 was recovered after heating with a heat gun in less than 2 min. **f)** "Fixed" shape #2, the shape was changed to concave up by heating the samples to 125 °C while applying load for 3 h. **g)** Flattened deformed shape #2 sample was heated and deformed at ~ 70 °C and cooled down after ~ 5 min. **h)** "Fixed" shape#2 with concave up was recovered after heating with a heat gun in less than 2 min. Fixed and deformed sample shapes were stable at room temperature for at least 48 h.

5.5. Conclusions

Combing polymer recyclability with bio-based raw materials can be an effective way to address the environmental issues of plastic waste. We developed thermally reprocessable Schiff base vitrimers made of copolymers of VMA, derived from lignin and vanilla, and C13MA, from vegetable oil, with 70% bio-based carbon content. RAFT polymerization allowed high control over the prepolymer topology, M_n and composition. Prepolymers were subsequently cross-linked with the diamine IPDA. We investigated the influence of network architecture on the viscoelastic characteristics of the resultant vitrimers with the goal of supressing creep. To do so, three distinct copolymer precursors with similar composition and overall M_n were synthesized: one with a statistical microstructure, another with a block microstructure, and a third employing an epoxy-based statistical configuration with 2 mol % GMA. Through DSC, DMTA and AFM analyses microphase separation was confirmed in the block vitrimer while ^{1}H NMR and ATR-FTIR proved formation of dual static dynamic cross-linking in the case of epoxy-based vitrimer.

The reprocessability of the statistical vitrimers was examined, revealing that their chemical and thermo-mechanical properties remained intact after undergoing four cycles. Tensile tests showed comparable properties for statistical vitrimers while the block vitrimer exhibited a notably weaker modulus. The poor ultimate stress and strain of block copolymer was linked to microphase separation and the high M_e of soft poly(C13MA) block. In contrast, phase separation led to enhanced hardness and reduced creep. We believe this can be attributed to the high stiffness and T_g of the poly(VMA) microdomains anchoring the network. Introduction of a small number of static cross-links via GMA copolymerization led to supress creep but also significantly reduced the rate of stress-relaxation. In addition to the development of shape memory bio-based vitrimers, this report directly compares creep control through microphase separation via hard blocks with hybrid static-dynamic networks. Based on our findings, while self-assembly can be leveraged for the development of creep resistant diblock copolymer vitrimers, it is equally important to optimize the interplay of glass transition, mechanical and viscoelastic properties of each individual constituent microdomains with the resulting network.

5.6. Supporting information for Chapter 5

5.6.1. Experimental part

Materials

All chemicals were of reagent grade and used as received unless otherwise noted. Azobisisobutyronitrile (AIBN, Millipore Sigma, 98%) was recrystallized from methanol and dried in vacuum prior to use. 2-cyano-2-propyl benzodithioate (CPB, RAFT agent) was purchased from Sigma Aldrich. C13-methacrylate (C13MA, Evonik) and glycidyl methacrylate (GMA, Millipore sigma) were passed through a column of basic alumina with ca. 5 wt% calcium hydride to remove inhibitors and acidic impurities prior to use. 1,4-dioxane (≥ 99.0%), dichloromethane (DCM, (≥ 99.0 %), hexanes (≥ 99.0 %), anhydrous magnesium sulfate ($MgSO_4$), tetrahydrofuran (THF, HPLC grade), methanol (≥99.8%) were purchased from Fisher. 4-dimethylaminopyridine (DMAP), methacrylic anhydride, vanillin, isophorone diamine (IPDA, ≥ 99.0%) were purchase from Millipore Sigma.

Instrumentations and methods

Nuclear Magnetic Resonance (NMR)

^1H NMR analyses were performed in deuterated chloroform ($CDCl_3$) using a Bruker 500 MHz NMR spectrometer at a temperature of 25 °C with 16 scans.

Attenuated total reflection (ATR)-Fourier Transform Infrared (FTIR)

ATR-FTIR spectroscopy was performed on a Thermo Scientific Nicolet iS50 FTIR Spectrometer equipped with a diamond ATR. For each sample, 32 scans were performed over the range of 4000-400 cm^{-1}.

Atomic Force Microscopy

AFM was performed on a Cypher VRS SPM (Asylum Research – Oxford Instruments) in air and tapping mode for phase imaging.

Gel Permeation Chromatography (GPC)

The number average molecular weight (M_n) and dispersity ($Đ = M_w/M_n$) of the polymers were estimated with a Waters Breeze instrument using HPLC-grade THF as the eluent at 40 °C and the flow rate of 0.3 mL/min. The GPC system was equipped with a guard column, a differential

refractive index (RI 2414) detector, and three Styragel HR columns. Poly(methyl methacrylate) (PMMA) standards (Varian) were used for the calibration of molecular weights. The reported M_n values were adjusted using the Mark–Houwink–Sakurada parameters for poly(dodecyl methacrylate).

Thermogravimetric Analysis (TGA)

TGA was performed on a TA Instrument Discovery 5500 machine with platinum pans. The prepolymers and vitrimers were heated with a rate of 10 ℃/min from 25 ℃ to 600 ℃. TA Instruments TRIOS software was utilized to record and analyze the data. In addition, isothermal experiments were done from room temperature up to 160 °C and remained at the temperature for the total run time of 6 h.

Differential Scanning Calorimetry (DSC)

DSC was performed on a TA Instruments Discovery 2500 machine equipped with refrigerated cooling system (RSC 90) using aluminum hermetic pin-hole pans. Calibrations for temperature and heat flow were conducted using indium and benzoic acid standards. Samples were analyzed with temperature ramps of -90 ℃ to 120 ℃ using a heat/ cool/ heat procedure with a heating rate of 15 ℃/min and cooling rate of 10 ℃/min. The glass transition temperature (T_g) was calculated using the curve inflection of the second heating ramp.

Dynamic mechanical analysis (DMA) and Rheology:

An Anton Paar MCR 302 machine was used for all tests. DMA tests were conducted using a solid rectangular fixture (SFR 12). Rectangular-shaped samples (60 mm length, 10 mm width, and 2 mm thickness) were heated from room temperature to 160 °C for the statistical v-s-CV and v-s-CVG, and 200 °C for v-b-CV vitrimer with an average rate of 5 °C/min and at a frequency of 1 Hz. For the reprocessability of v-s-CV, a 25 mm parallel plates geometry of thickness of 1 mm was used with the heating rate of 5 °C/min and at a frequency of 1 from 25 to 150 °C.

Rheological tests were conducted using a 25 mm parallel plates geometry. Strain sweep tests were carried out at 100–150 °C to determine the linear viscoelastic region (LVR) at 1 Hz. Frequency sweep tests were performed at 120 °C and 0.1% strain. Stress-relaxation experiments were

conducted at 0.1% strain at the desired temperatures. Creep-recovery experiments were performed at 1000 Pa for 400 s, followed by 0 Pa for 300 s, total experiment time being 700 s.

Nanoindentation

Tests were performed on a Nanovea M1 Hardness Tester instrument. All samples were characterized using a Berkovich tip with the load of 20 mN and approaching loading rate and unloading rate of 40 mN/min and 20 mN/min respectively. The approach speed was of 1 μm/min with contact load of 0.3 mN, with a pause of 30 s between the loading and unloading. The experiments were conducted at four different locations separated from each other of at least 1 mm. The hardness was calculated by Nanovea's software.

Swelling and gel fraction

Vitrimer gel fraction was obtained by soaking them in excess THF for 48 h at room temperature. Afterwards, the swelled samples were filtered, dabbed with delicate task wipes to remove excess THF, and weighed to find the samples' swelling ratio. This was followed by drying the samples in a vacuum oven at reduced pressure and 60 °C for a day, and finally weighing them. Gel fraction was calculated using equation Eq. S1 in which m_0 is the original mass of the sample and m_2 is the mass of dried sample after swelling.

$$Gel\ \% = \frac{m_2}{m_0} \times 100 \qquad \text{(Eq. S1)}$$

The swelling ratio was calculated using equation Eq. S2 in which m_0 and m_1 are the original and swollen mass of the sample.

$$SR\ \% = \frac{m_1 - m_0}{m_0} \times 100 \qquad \text{(Eq. S2)}$$

5.6.2. Monomers and polymers synthesis and characterizations

5.6.2.1 Synthesis of vanillin methacrylate

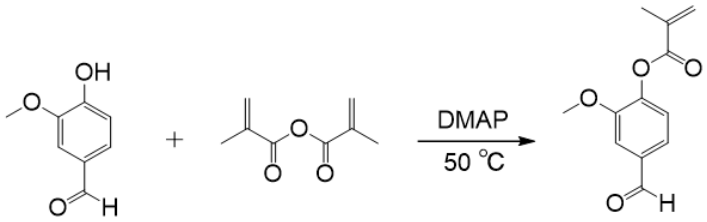

Schematic S 5-1 Synthetic route of vanillin methacrylate (VMA) from vanillin and methacrylic anhydride.

Vanillin Methacrylate (VMA), was synthesized through a Steglich esterification reaction following a procedure described by Zhang *et al*. [196]. Accordingly, in a round bottom flask, vanillin (1 eq., 32.8 mmol, 5 g), methacrylic anhydride (1.01 eq., 33.2 mmol, 5.12 g) and 4-dimethylaminopyridine (DMAP, 0.05eq., 9.8 mmol, 0.2g) were added, stirred, and sparged with nitrogen for 2 hours. While still under nitrogen atmosphere, the system was stirred overnight at room temperature. Afterwards, the temperature was increased to 50 °C and the solution was stirred vigorously for 24 additional hours. The final mixture was dissolved in dichloromethane and washed four times with saturated sodium bicarbonate aqueous solution. The separated organic phase was washed with a solution of NaOH (1 M), then with an aqueous solution of HCl at 5 wt% and finally with brine. After drying the organic solution over $MgSO_4$, filtration, concentrate with rotary evaporation and drying in a vacuum oven at 50 °C overnight, the obtained solid was recrystallized in hot hexane to obtain VMA as a white flaky powder.

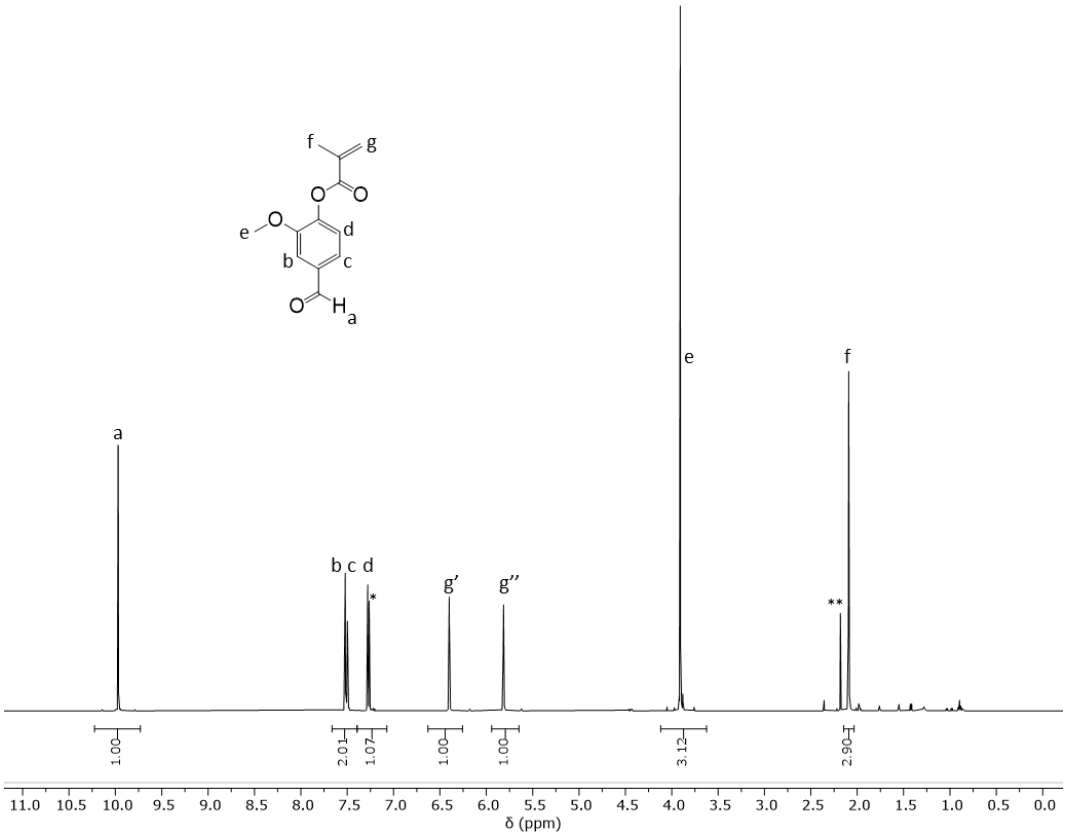

Figure S 5.1 ^{1}H-NMR spectrum of vanillin methacrylate (VMA). (* $CDCl_3$, ** acetone, from 0.83 to 2 ppm impurities from methacrylic anhydride).

Polymer synthesis

5.6.2.2 Statistical copolymer: poly(C13MA-co-VMA): p-s-CV

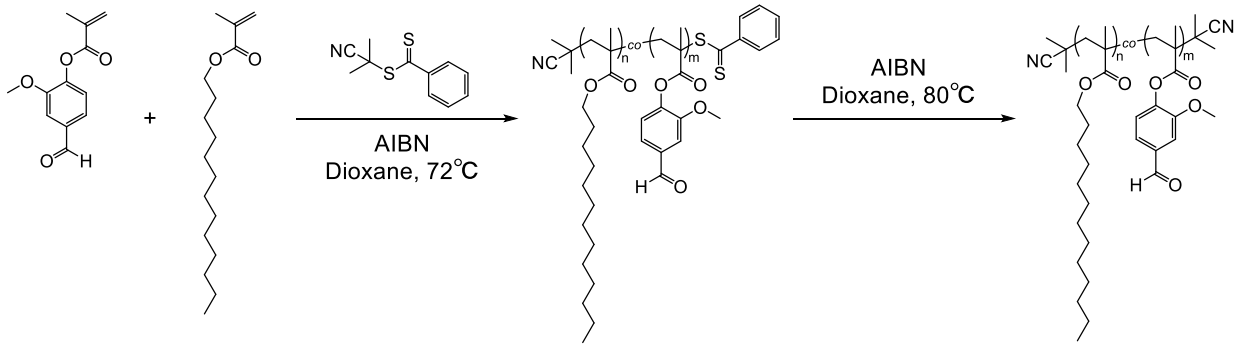

Schematic S 5-2 Synthesis of p-s-CV via RAFT and subsequent chain end removal using AIBN.

C13MA (16 g, 100 eq.), vanillin methacrylate (VMA, 4 g, 25 eq.), 2-cyano-2-propyl benzodithioate (CPB, 0.127 g, 0.8 eq.), and azobisisobutyronitrile (AIBN, 18.9 mg, 0.12 equiv., $\frac{n_{AIBN}}{n_{CPB}} = 0.2$) were added to a Schlenk flask containing 1,4-dioxane (40 mL). The solution was purged with nitrogen (N_2) and submerged into a preheated oil bath at 72 °C for 7 h. The obtained polymer was precipitated into methanol resulting in a pink viscous liquid (16.4 g, yield = 82%). p-s-CV (5.04 g, 1 eq.) terminated with the benzodithioate moiety was dissolved in 1,4-dioxane (50 mL) prior to the addition of AIBN (0.71 g, 20 eq.). The solution was heated at 80 °C under N_2 overnight, and p-s-CV was precipitated into methanol yielding a white viscous liquid.

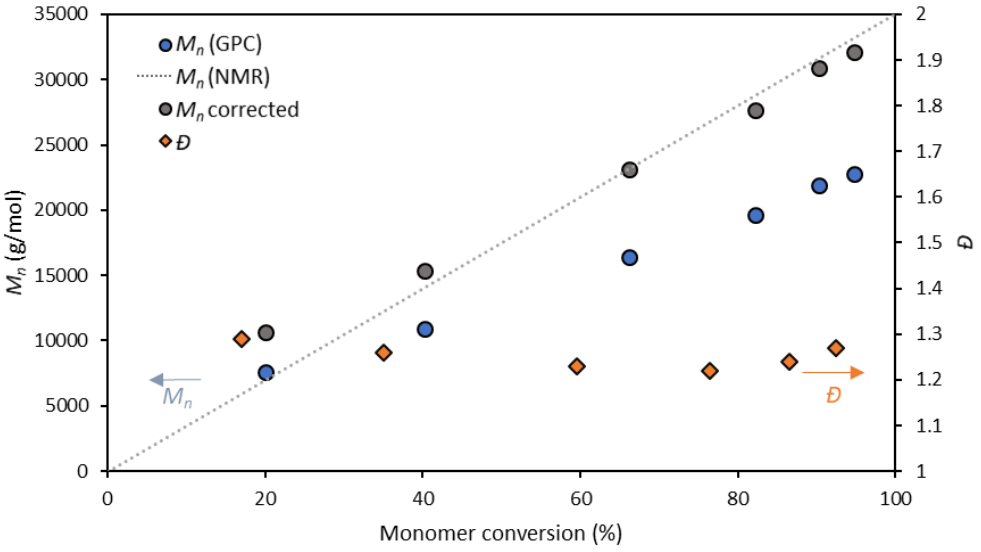

Figure S 5.2 M_n (blue circles), theoretical molecular weight (grey line, calculated from conversion obtained by NMR), corrected molecular weight calculated from Mark-Houwink coefficients of poly(dodecyl methacrylate) (grey circles) and *Đ* (orange diamonds) versus monomer conversion for the polymerization of p-s-CV.

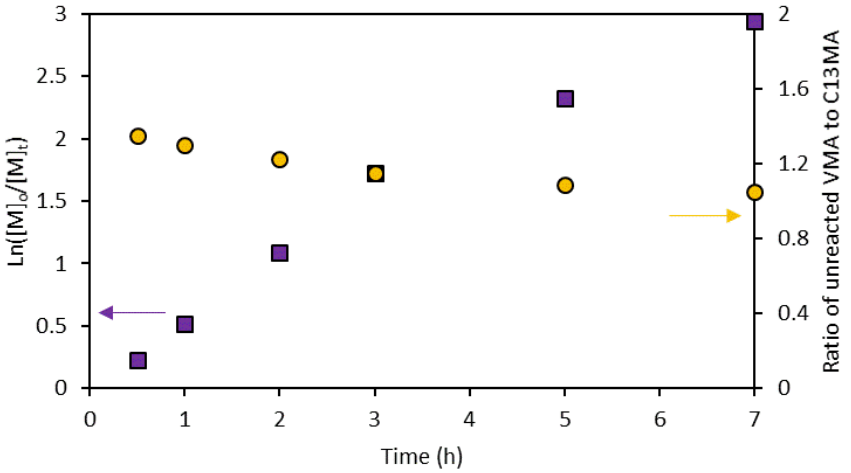

Figure S 5.3 Pseudo-first order kinetics plot for the polymerization of p-s-CV (purple square) and ratio of unreacted VMA to C13MA throughout the polymerization (yellow sphere).

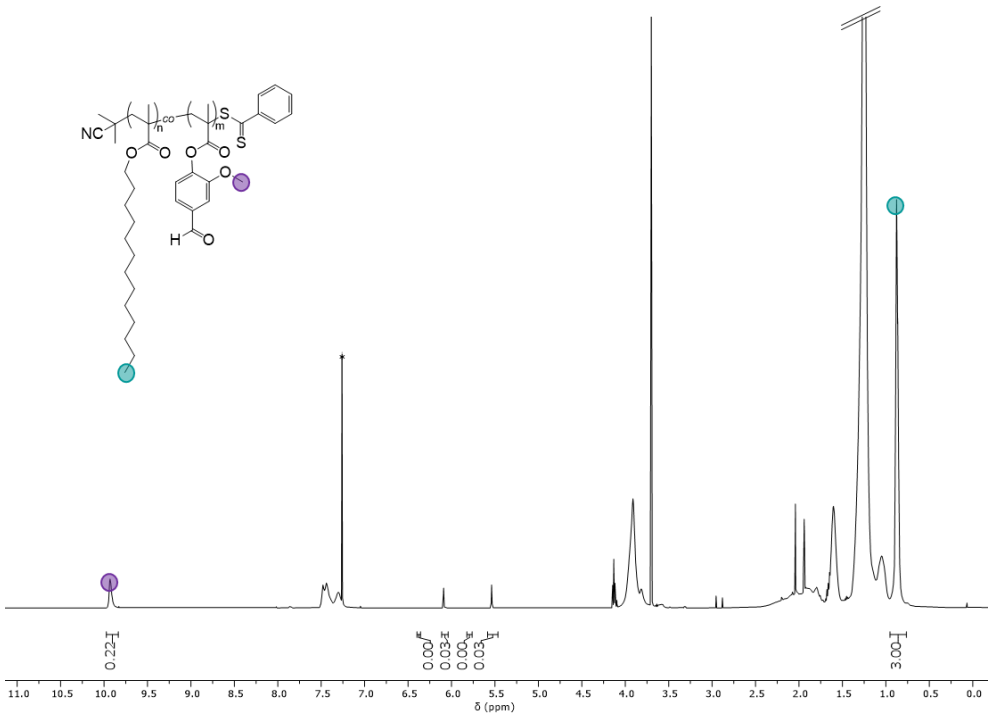

Figure S 5.4 ^{1}H-NMR spectrum of p-s-CV before chain-end removal. The purple circle refers to the methoxy protons (-O-C**H**$_3$) at 9.86 ppm and the green circle refers to the methyl group at the chain-end (-CH_2-C**H**$_3$) at 0.88 ppm. (* $CDCl_3$)

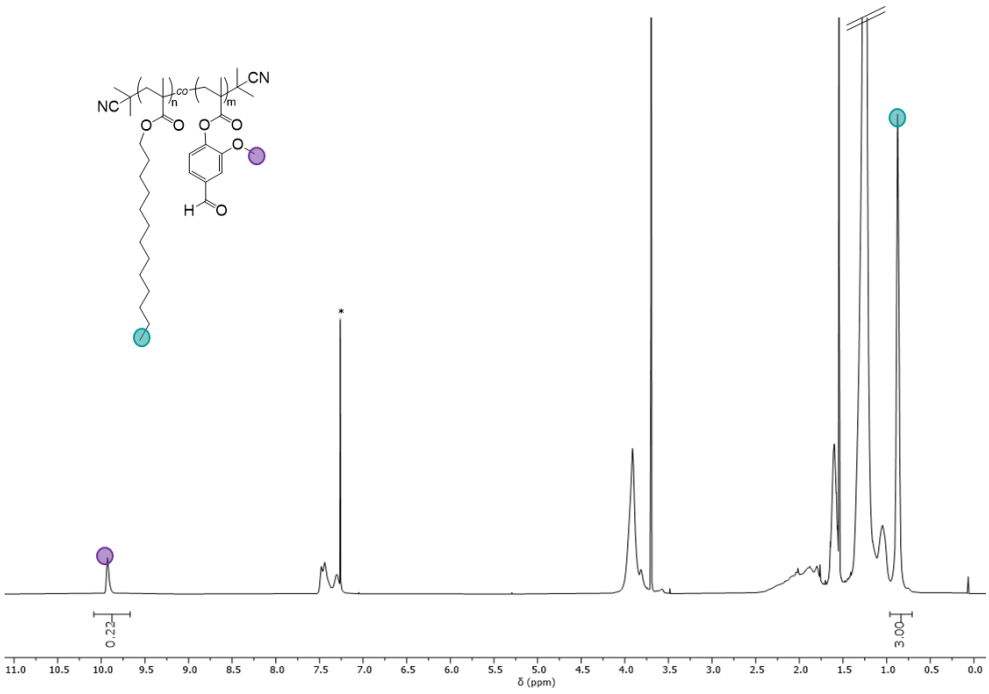

Figure S 5.5 ^{1}H-NMR spectrum of p-s-CV after chain-end removal. The purple circle refers to the methoxy protons (-O-C**H**$_3$) at 9.86 ppm and the green circle refers to the methyl group at the chain-end (-CH_2-C**H**$_3$) at 0.88 ppm. (* $CDCl_3$)

5.6.2.3 Block copolymer: poly(C13MA-*b*-VMA): p-b-CV

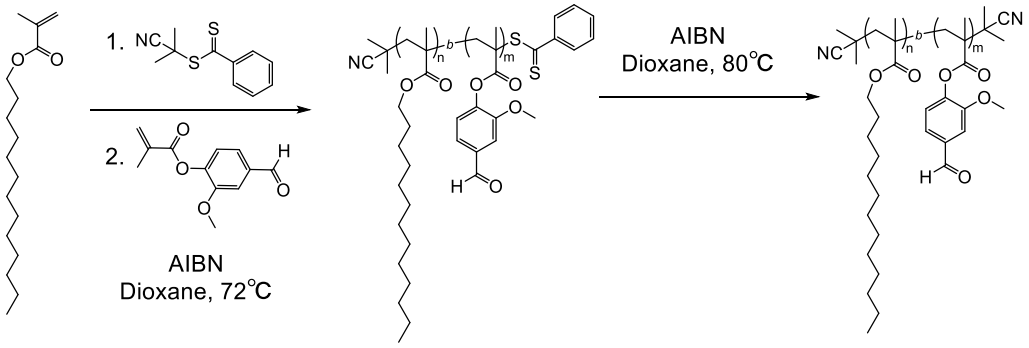

Schematic S 5-3 Two-step synthesis of p-b-CV block copolymer and subsequent chain end removal

C13MA (30 g, 100 eq.), CPB (0.239 g, 0.8 eq.), and AIBN (35.5 mg, 0.12 equiv., $\frac{n_{AIBN}}{n_{CPB}} = 0.2$) were added to a Schlenk flask containing *1,4*-dioxane (32 mL). The solution was purged with nitrogen (N_2) and submerged into a preheated oil bath at 72 °C for 24 h. The obtained polymer homo(C13MA) was precipitated into methanol resulting in a pink viscous liquid (28.8 g, yield = 96%).

Poly(C13MA) (14 g, 1 eq.), which acted as a macro-RAFT agent, VMA (4.92 g, 25 eq.) and AIBN (23 mg, eq.) were added to a Schlenk flask containing 40 mL of 1,4-dioxane. The solution was purged with nitrogen (N_2) and submerged into a preheated oil bath at 72 °C for 7h. The obtained polymer (p-b-CV) was precipitated into methanol resulting in a pink viscous liquid (16.8 g, yield = 88.5%).

p-b-CV (13.5g, 1 eq.) terminated with the benzodithioate moiety was dissolved in 1,4-dioxane (100 mL) prior to the addition of AIBN (1.3 g, 20 eq.). The solution was heated at 80 °C under N_2 overnight, and p-b-CV was precipitated into methanol yielding a white viscous liquid.

5.6.2.4 First block: poly(C13MA) homopolymer

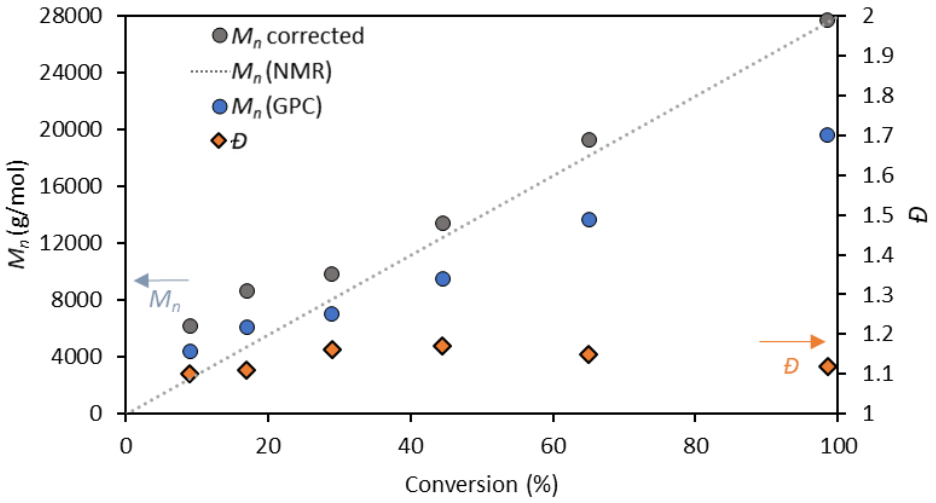

Figure S 5.6 M_n (blue circles), theoretical molecular weight (grey line, calculated from conversion obtained by NMR), corrected molecular weight calculated from Mark-Houwink coefficients of poly(dodecyl methacrylate) (grey circles) and *Đ* (orange diamonds) versus monomer conversion for the polymerization of poly(C13MA).

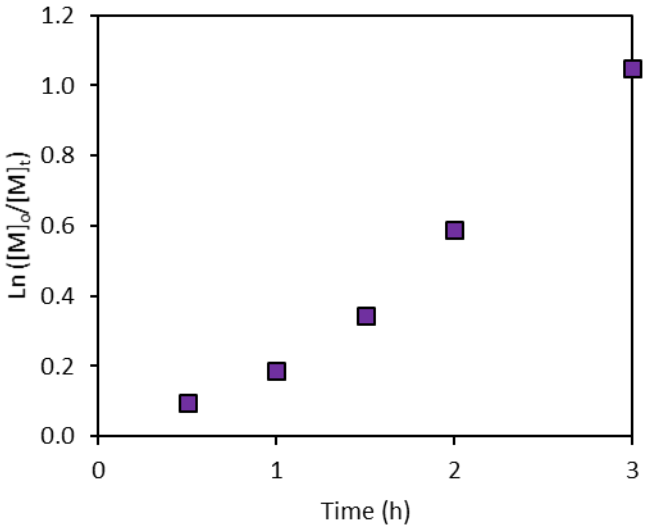

Figure S 5.7 Pseudo-first order kinetics plot for the polymerization of poly(C13MA). Only the first 3 hours of the reactions are plotted.

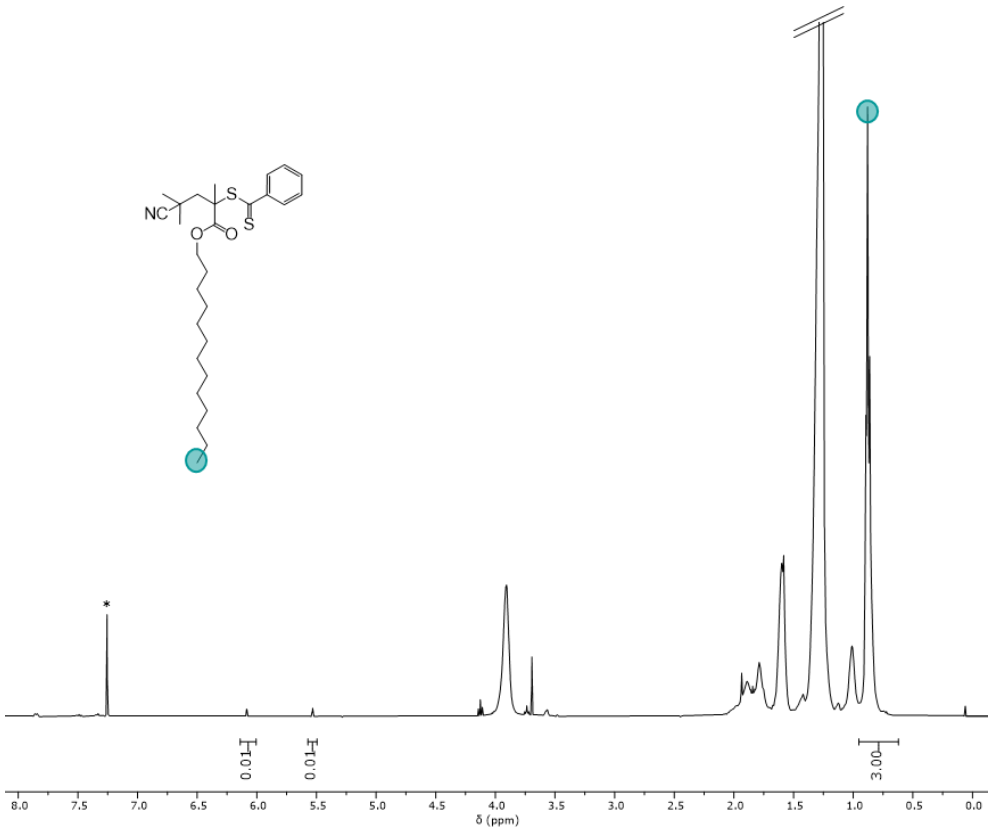

Figure S 5.8 ^{1}H-NMR spectrum of homo(C13MA), first block. The green circle refers to the methyl group at the chain-end (-CH_2-C**H**$_3$) at 0.88 ppm. (* $CDCl_3$)

5.6.2.5 Second block: poly(C13MA-block-VMA): p-b-CV

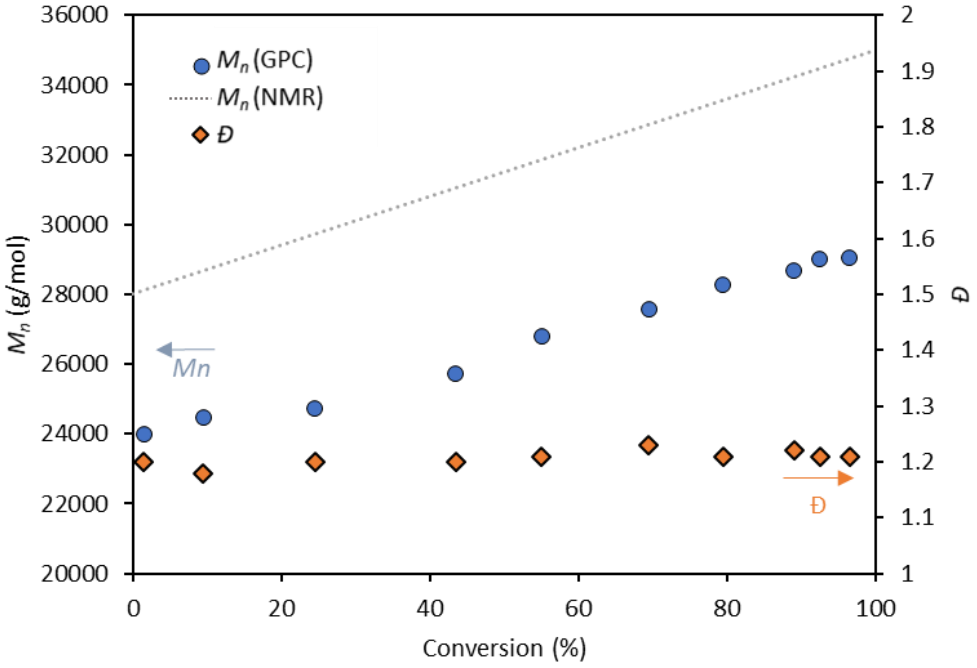

Figure S 5.9 M_n (blue circles), theoretical molecular weight (grey line, calculated from conversion obtained by NMR), and *Đ* (orange diamonds) versus monomer conversion for the polymerization of block copolymer p-b-CV.

The discrepancy between the theorical and the measured M_n is generally decreased when the corrective Mark-Houwink coefficients of poly(dodecyl methacrylate) are applied on the measured M_n, but here the molecular weights obtained from the GPC during the chain-extension were not corrected. Indeed, this correction is only applied when C13MA monomers are involved in the reaction. For the chain-extension reaction, it is only VMA monomers that are used to generate the 2nd block. We consider that the more representative molecular weights are the ones calculated from NMR where we used the corrected M_n of poly(C13MA) homopolymer (1st block) and we add the M_n calculated from the VMA's monomer conversion obtained with NMR. The following equation Eq. S3 shows an example of this calculation.

$$M_{n,t=1h} = M_{n,C13MA\_corrected} + monomer\ conversion_{t=1h} \times M_{n,VMA\_theo} \quad \text{(Eq. S3)}$$

$$M_{n,t=1h} = 28000 + 0{,}245 \times 7000$$

$$M_{n,t=1h} = 29715\ g/mol$$

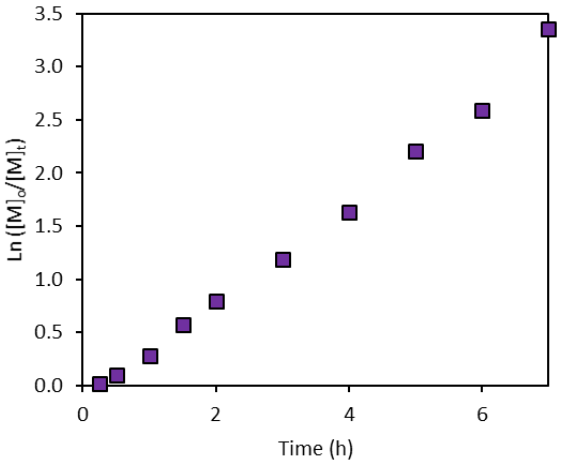

Figure S 5.10 Pseudo-first order kinetics plot for the polymerization of the second block of p-b-CV.

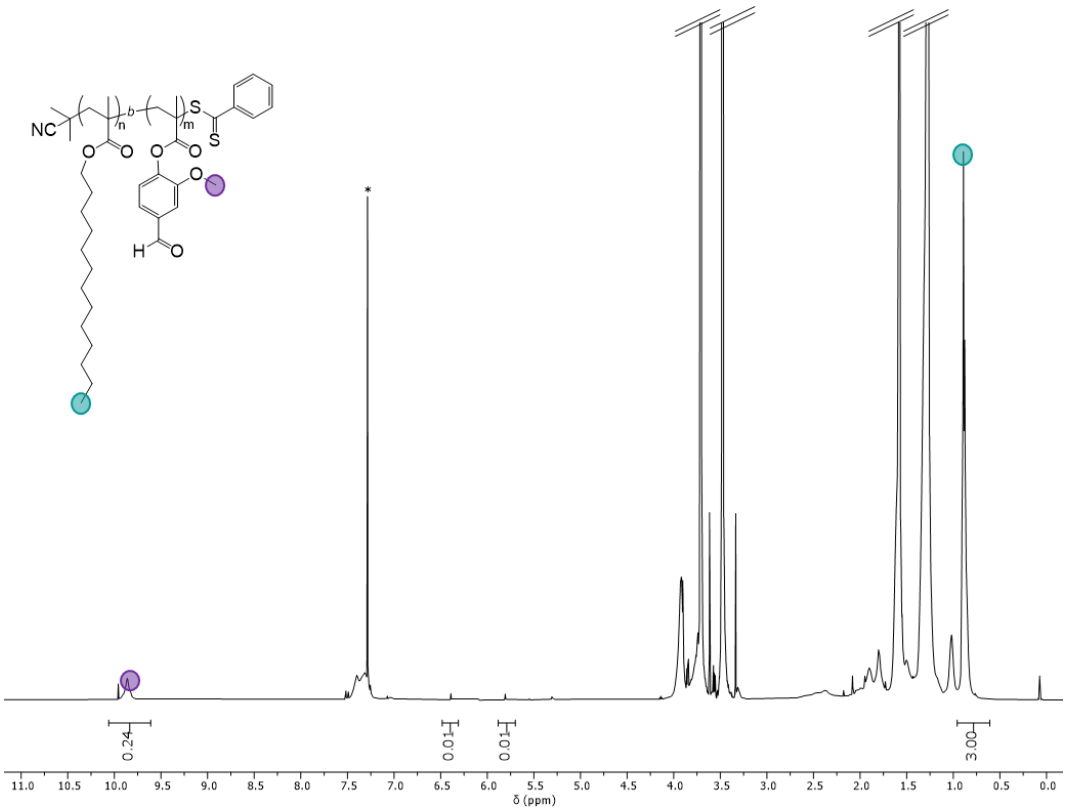

Figure S 5.11 ^{1}H-NMR spectrum of p-b-CV before chain-end removal. The purple circle refers to the methoxy protons (-O-C**H**$_3$) at 9.86 ppm and the green circle refers to the methyl group at the chain-end (-CH$_2$-C**H**$_3$) at 0.88 ppm. (* $CDCl_3$)

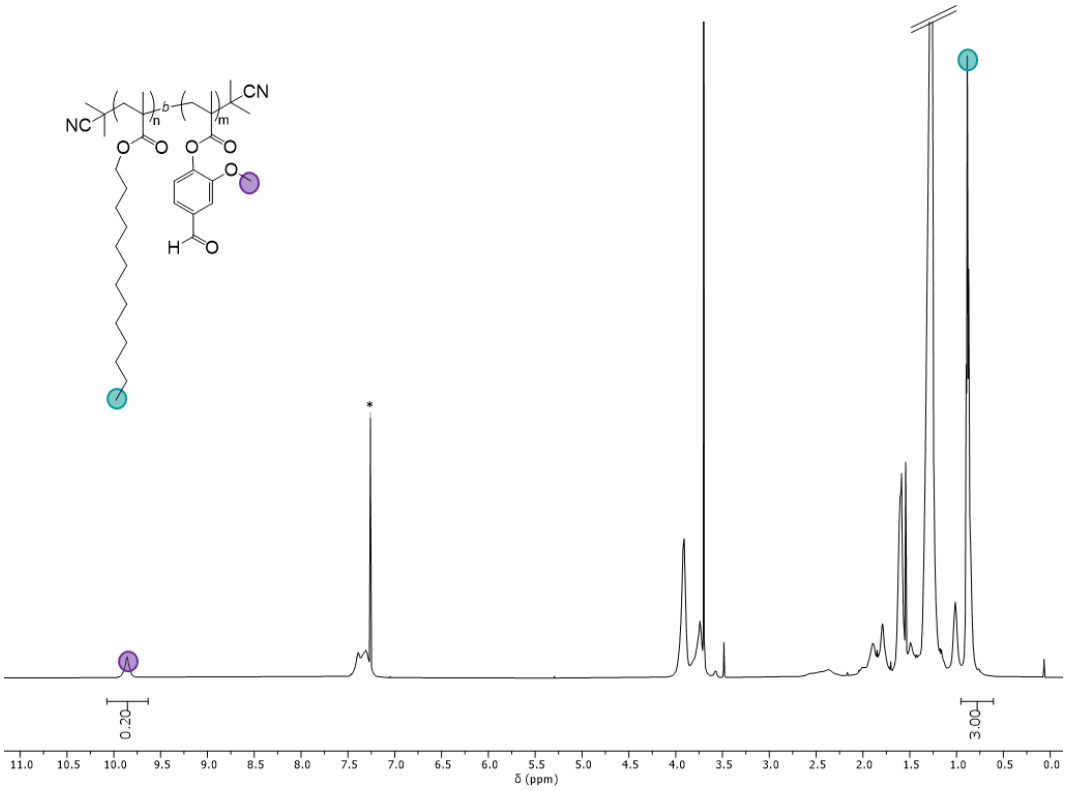

Figure S 5.12 ^{1}H-NMR spectrum of p-b-CV after chain-end removal. The purple circle refers to the methoxy protons (-O-C**H**$_3$) at 9.86 ppm and the green circle refers to the methyl group at the chain-end (-CH$_2$-C**H**$_3$) at 0.88 ppm. (* $CDCl_3$)

5.6.2.6 Statistical tercopolymer of poly(C13MA-*co*-VMA-*co*-GMA): p-s-CVG

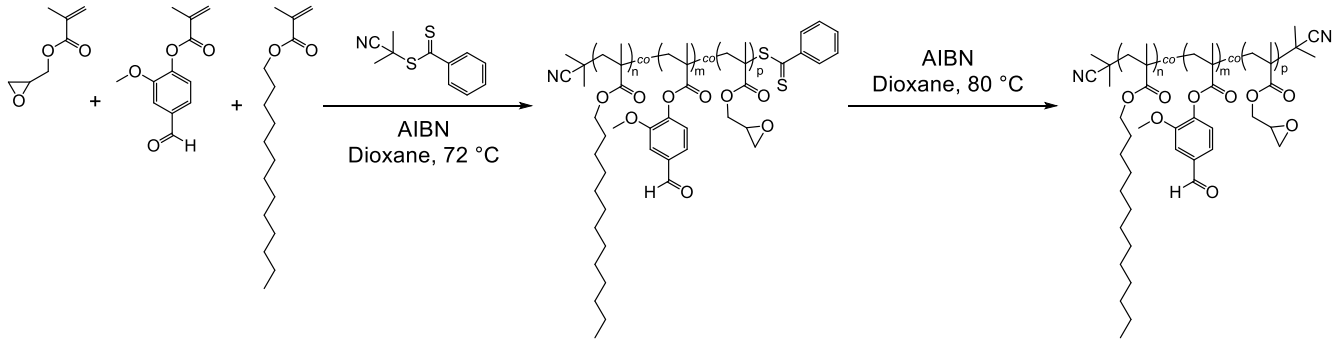

Schematic S 5-4 Synthesis of epoxy-based p-s-CVG statistical terpolymer and subsequent chain end removal.

C13MA (16g, 100 eq.), VMA (3.6g, 22.5 eq.), glycidyl methacrylate (GMA, 0.4g, 2.5eq.), CPB (0.127 g, 0.8 eq.), and AIBN (18.9 mg, 0.12 equiv., $\frac{n_{AIBN}}{n_{CPB}} = 0.2$) were added to a Schlenk flask containing 1,4-dioxane (40 mL). The solution was purged with nitrogen (N_2) and submerged into a preheated oil bath at 72 °C for 24 h. The obtained polymer was precipitated into methanol resulting in a pink viscous liquid (17.9 g, yield = 88%).

p-s-CVG (16 g, 1 eq.) terminated with the benzodithioate moiety was dissolved in 1,4-dioxane (50 mL) prior to the addition of AIBN (1.24 g, 20 eq.). The solution was heated at 80 °C under N_2 overnight, and p-s-CVG was precipitated into methanol yielding a white viscous liquid.

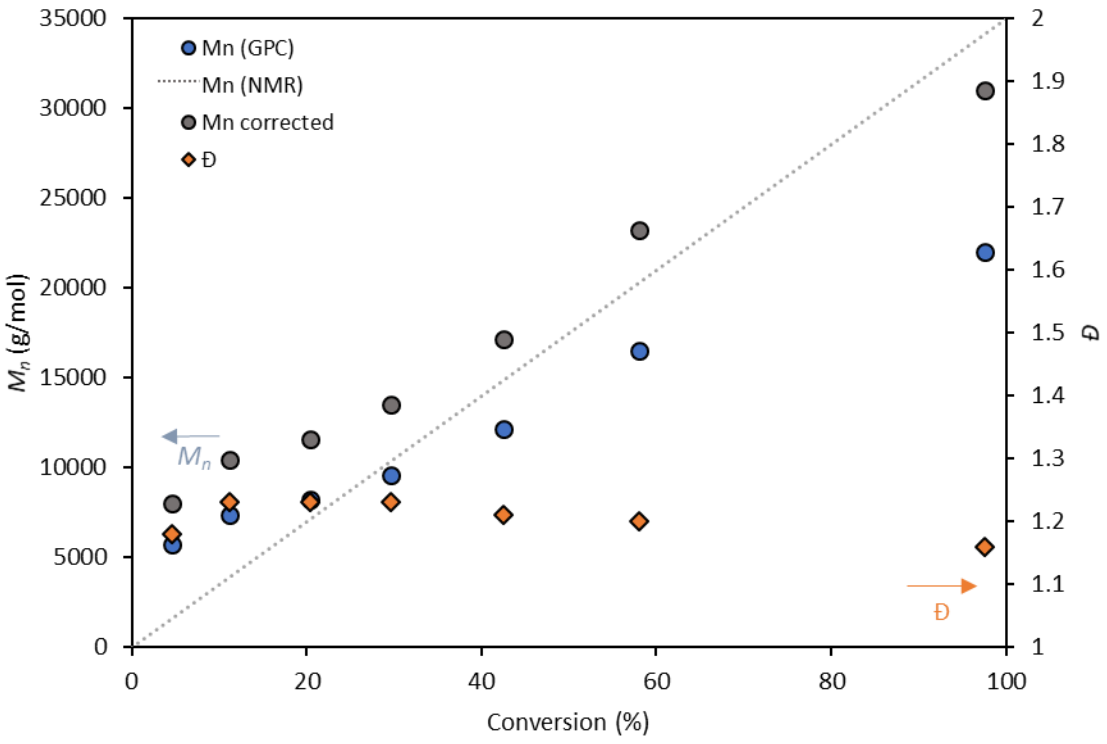

Figure S 5.13 M_n (blue circles), theoretical molecular weight (grey line, calculated from conversion obtained by NMR), corrected molecular weight calculated from Mark-Houwink coefficient of poly(dodecyl methacrylate) (grey circles) and *Đ* (orange diamonds) versus monomer conversion for the polymerization of p-s-CVG.

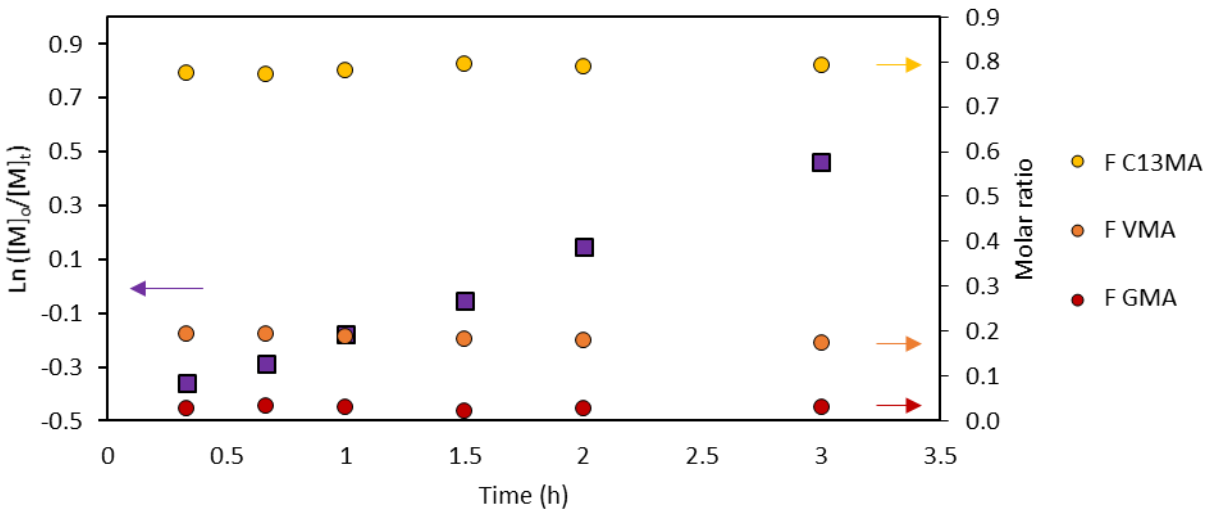

Figure S 5.14 Pseudo-first order kinetics plot for the polymerization of p-s-CVG (purple square), and the molar ratio over time of the different fractions.

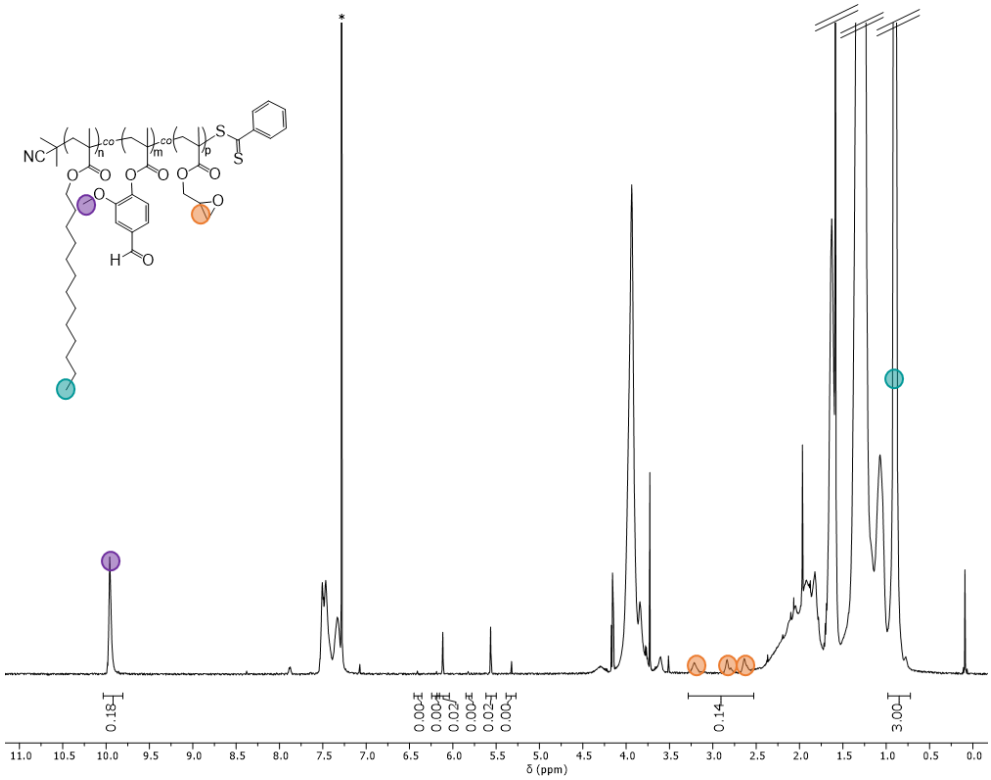

Figure S 5.15 ^{1}H-NMR spectrum of p-s-CVG before chain-end removal. The purple circle refers to the methoxy protons (-O-C**H**$_3$) at 9.86 ppm, the green circle refers to the methyl group at the chain-end (-CH$_2$-C**H**$_3$) at 0.88 ppm and the orange circles refer to the epoxy protons (-CH$_2$-C**H**-C**H**$_2$-O-) between 2.64 and 3.20 ppm. (* $CDCl_3$)

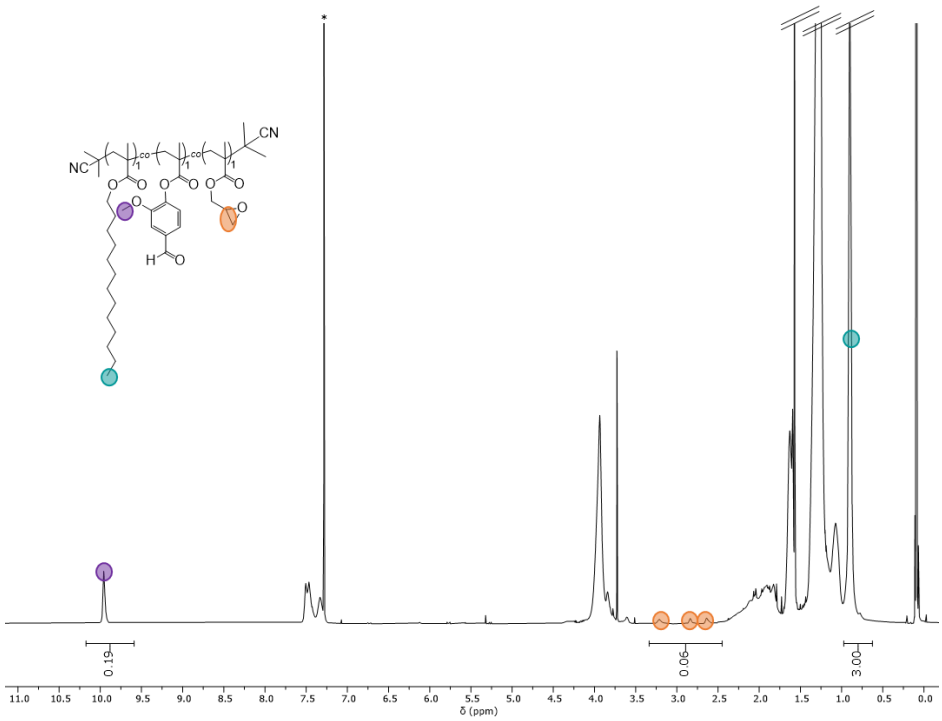

Figure S 5.16 ^{1}H-NMR spectrum of p-s-CVG after chain-end removal. The purple circle refers to the methoxy protons (-O-C**H**$_3$) at 9.86 ppm, the green circle refers to the methyl group at the chain-end (-CH$_2$-C**H**$_3$) at 0.88 ppm and the orange circles refer to the epoxy protons (-CH$_2$-C**H**-C**H**$_2$-O-) between 2.64 and 3.20 ppm. (* $CDCl_3$)

Gel permeation chromatography

Discrepancies between the theoretical and experimental molecular weight measured via GPC due to calibration of the instrument with poly(methyl methacrylate) (PMMA) standards. It is possible to correct the molecular weight by using the appropriate Mark-Houwink coefficients. For the poly(C13MA), the solution properties can be reasonably approximated by poly(dodecyl methacrylate) (a = 0.720, K = 5.18*10-3 mL/g at 30 °C), which structure is much closer than PMMA to our poly(C13MA) based polymer. We decided to use these coefficients to correct the molecular weights for the synthesis where C13MA monomers are involved. The corrected molecular weights are given in the **Table S 5-1**.

$$log_{10}\, M_{pC13MA} = \frac{1+ a_{pMMA}}{1+a_{pDMA}} \times\ log_{10} M_{pMMA}\ + \frac{1}{1+\ a_{pDMA}}\ \times\ log_{10}\left(\frac{K_{pMMA}}{K_{pDMA}}\right) \qquad \text{(Eq. S4)}$$

In the equation Eq. S4, M_{pC13MA} is the corrected molecular weight of poly(C13MA). a_{pMMA} and K_{pMMA} are the Mark-Houwink coefficients for poly(methyl methacrylate) in THF at 30 °C and are

equal to a=0.719 and K=9.44*10^{-3} mL/g. a_{pDMA} and K_{pMMA} are the Mark-Houwink coefficients for poly(dodecyl methacrylate) [212].

Table S 5-1 Molecular weights of the obtained prepolymers

Prepolymers	Targeted M_n (g/mol)	M_n with PMMA calibration (g/mol)	M_n after chain-end removal (PMMA calibration) (g/mol)	Corrected M_n (g/mol)[a]
p-s-C	28,000	19,900	-	28,000
p-s-CV	35,000	24,900	26,400	37,200
p-b-CV	35,000	24,500	25,000	35,200
p-s-CVG	35,000	29,800	28,500	40,200

[a] M_n calculated with Mark-Houwink coefficients of poly(dodecyl methacrylate) [212].

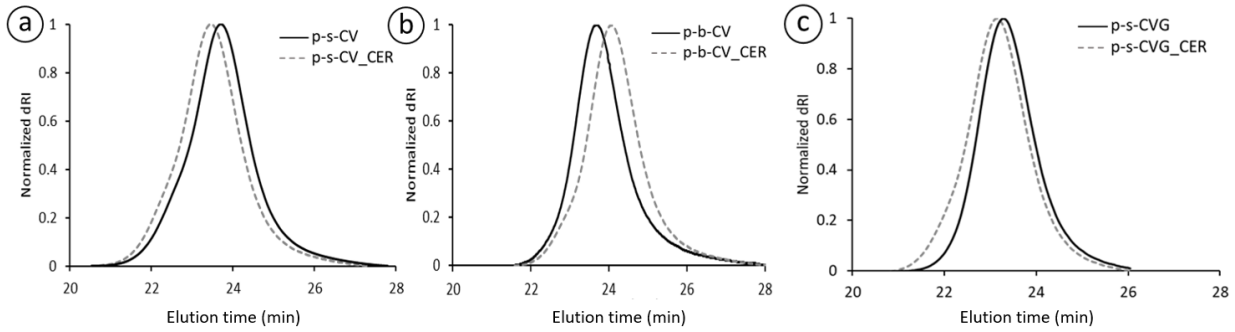

Figure S 5.17 GPC trace of the prepolymers prior to (black solid line) and after (dashed line) chain-end removal. **a.** p-s-CV: before chain-end removal M_n =24,900 g/mol Đ =1.21; after chain-end removal M_n= 26,400 g/mol, Đ= 1.28. **b.** p-b-CV: before chain-end removal M_n =24,5000 g/mol, Đ = 1.24; after chain-end removal M_n = 25,000 g/mol, Đ = 1.25. **c.** p-s-CVG: before chain-end removal M_n =28,000 g/mol, Đ = 1.18; after chain-end removal M_n = 28 500 g/mol, Đ = 1.22.

Ultraviolet-visible spectroscopy

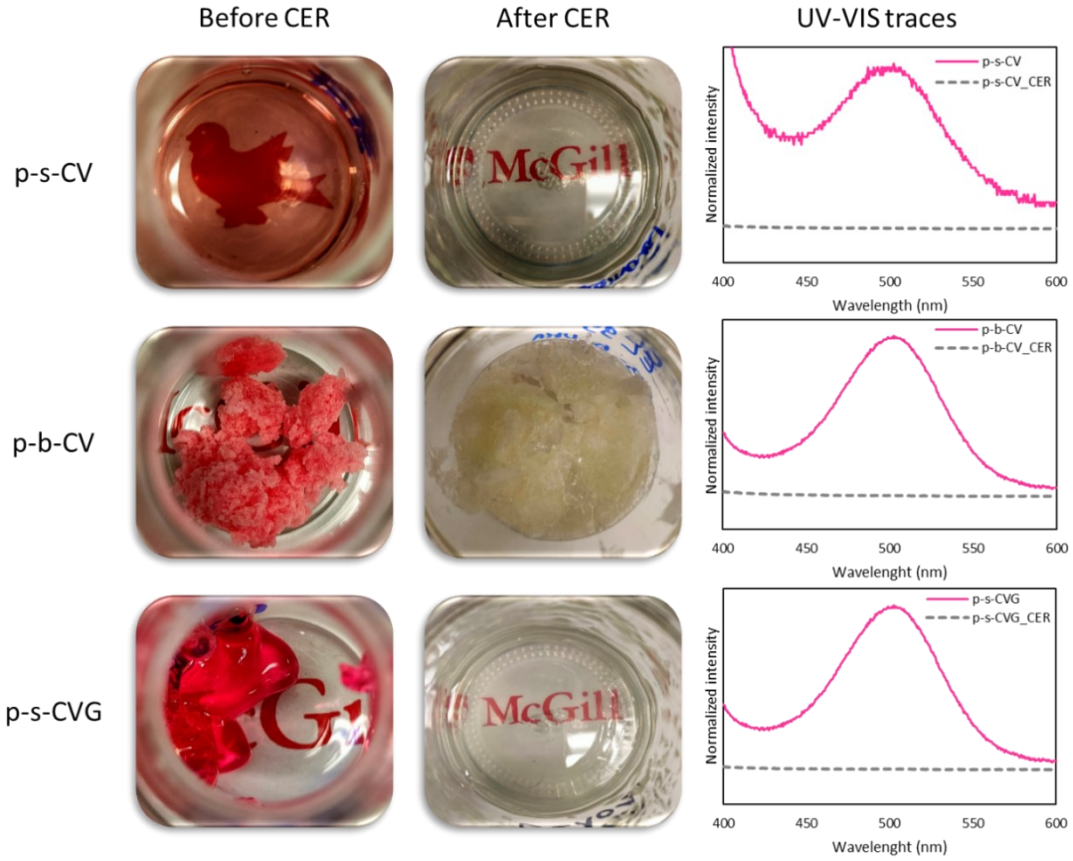

Figure S 5.18 Effect of chain-end removal (CER): before the prepolymers are pink and after the removal of the CTA moiety, the prepolymers become white or colorless. UV-VIS analysis was used to confirm the removal of the chain-end. UV-VIS traces before (pink) and after (dash grey) chain-end removal are showing the detection at 500 nm. Top: p-s-CV. Middle: p-b-CV. Bottom: p-s-CVG.

Fourier transform infrared spectroscopy

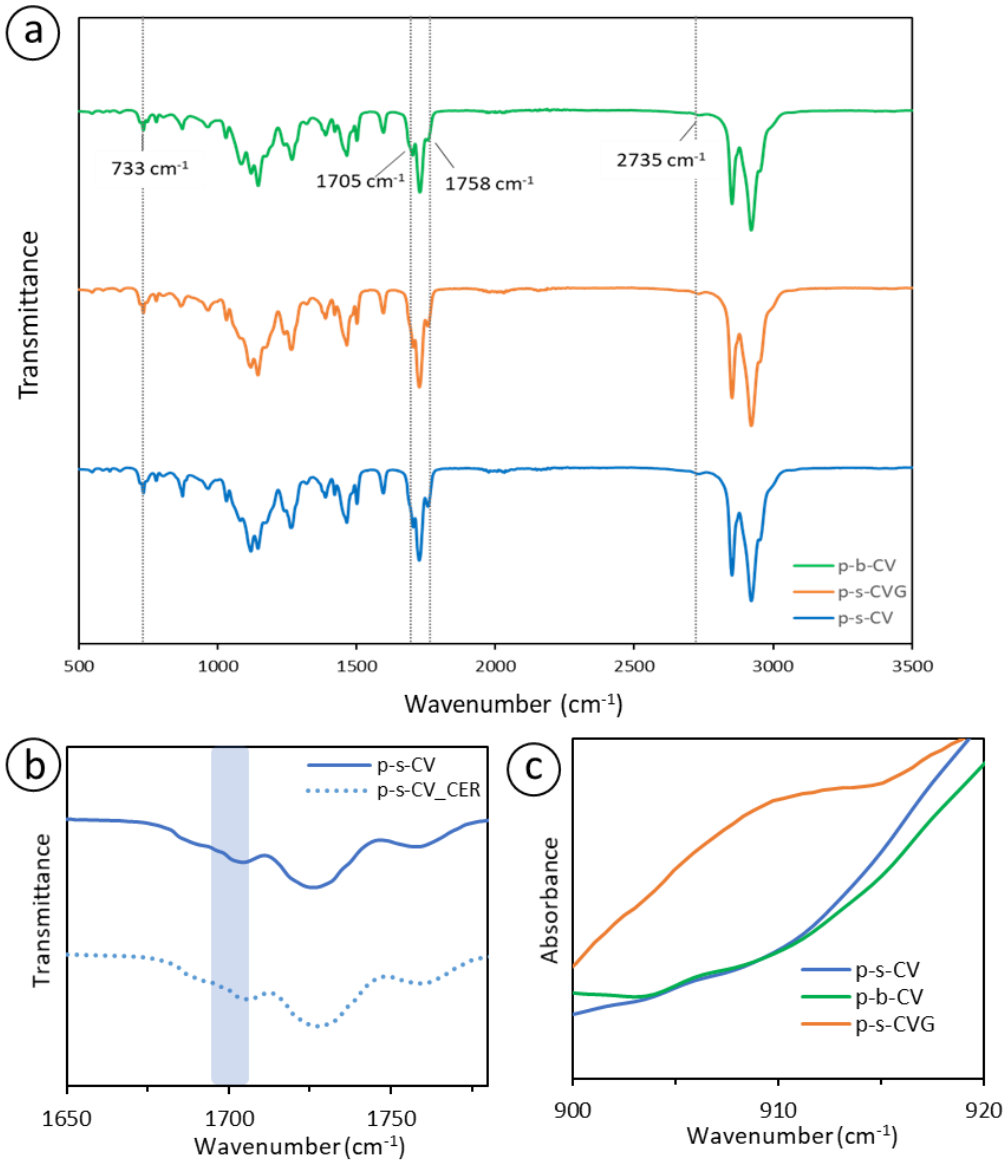

Figure S 5.19 ATR-FTIR spectra of the three polymers: p-s-CV (blue), p-b-CV (green) and p-s-CVG (orange) **a.** Stacked FTIR spectra of the three copolymers is shown with the peaks corresponding to VMA moieties highlighted at 733 cm^{-1} for –C-O-C, 1705 cm^{-1} for the formyl group, 1758 cm^{-1} for -C=O and 2735 cm^{-1} for –CHO. These peaks can be seen on each curve, showing the incorporation of VMA in the copolymers. **b.** Zoom-in on ATR-FTIR spectra shown in a. to visualize the peak at 910 cm^{-1} corresponding to the epoxy ring in GMA only in p-s-CVG. **c.** Stacked ATR-FTIR spectra of p-s-CV before chain-end removal (blue) and after (dash). The peak corresponding to VMA's formyl group at 1758 cm^{-1} has been highlighted showing that the chain-end removal does not have an impact on the presence of the aldehyde function.

5.6.3. Vitrimers synthesis and characterization

5.6.3.1 Synthesis of the vitrimers

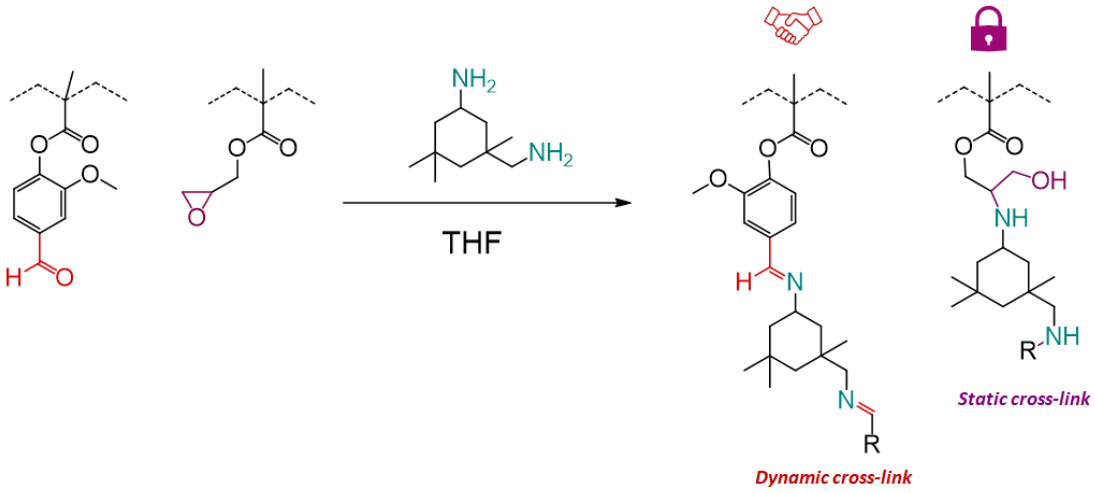

Schematic S 5-5 Cross-linking reactions are shown with the aldehyde group from VMA with IPDA (dynamic bond) and the epoxy group from GMA with IPDA (static bond). The latter only exists in case of v-s-CVG with the hybrid dynamic/static cross-linking network.

Vitrification and network formation started with dissolving the prepolymers in THF (50 w/v%). Then, IPDA diamine crosslinker was added to the solution with 0.9 equivalent of NH_2 to VMA and GMA for p-s-CVG and well mixed. Gelation occurred within minutes, and the solution was capped and placed in a fume hood for overnight. This was followed by vacuum drying at 120 °C for ca 2 hours at 80 °C for 12 hours.

5.6.3.2 Estimation of solubility parameter of VMA using group contribution method

We applied two different algorithmic methods of *Hoftyzer-Van Krevelen* and *Fedor's* for estimation of the VMA's solubility parameter (δ_{VMA}) and used the average value for the calculation of Flory-Huggins parameter (χ) [147].

Table S 5-2 Solubility parameter group contributions [147]

Structural group	Number	Hoftyzer - Van Krevelen			Fedors	
		F_{di} $(MJ/m^3)^{0.5}.mol^{-1}$	F_{pi} $(MJ/m^3)^{0.5}.mol^{-1}$	E_{hi} J /mol	E_{coh} J /mol	V cm^3/mol
-CH3	2	420	0		4,710	33.5
-CH2-	1	270	0		4,940	16.1
>CH-		80	0		3,430	-1
>C<	1	-70	0		1,470	-19.2
=CH2		400	0		4,310	28.5
=CH-		200	0		4,310	13.5
=C<		70	0		4,310	-5.5
-O-	1	100	400	3000	3,350	3.8
-CO-		290	770	2000	17,370	10.8
-COO-	1	390	490	7000	18,000	18
phenyl	1	1430	110	0	31,940	71.4
-CHO-	1	470	800	4500	21,350	22.3

Hoftyzer-Van Krevelen method:

$$\delta_d = \frac{\sum F_{di}}{V} ; \delta_p = \frac{\sqrt{\sum F_{pi}^2}}{V} ; \delta_h = \sqrt{\frac{\sum E_{hi}}{V}}$$

$$\delta^2 = \delta_d^2 + \delta_p^2 + \delta_h^2$$

From the literature V_{VMA} = 173.4 cm^3/mol [195]

$$\delta_{VMA,\ H-V.K} = 22.58\ MPa^{0.5}$$

Fedors' method:

$$\delta = \left(\frac{E_{coh}}{V}\right)^{1/2} \quad \delta_{VMA,Fedors} = 22.46\ MPa^{0.5}$$

Therfore, the average value is: $\delta_{VMA} = 22.52\ MPa^{0.5}$

Since the solubility parameter of C13MA is not available in the literature we used the solubility parameter of lauryl methacrylate instead. From the literature we have: $\delta_{\text{p(lauryl methacrylate)}} = 17.1$ and $V_{\text{p(lauryl methacrylate)}} = 273.8$ cm^3/mol (based on density). Using the group contribution via the Hoftyzer-Van Krevelen method yields $\delta_{\text{C13MA}} = 17.9$ MPa$^{0.5}$ which is close to the reported $\delta_{\text{p(lauryl methacrylate)}}$ [195,213].

5.6.3.3 Estimation of Flory-Huggins interaction parameter

The Flory-Huggins interaction parameter can be estimated as follows, assuming only enthalpic contributions without any entropic contributions:

$$\chi = \frac{\overline{V}}{RT}(\delta_{VMA} - \delta_{C13MA})^2$$

$$\overline{V} = \sqrt{V_{VMA} V_{C13MA}}$$

where δ is the solubility parameter, R is the universal gas contsatant, $\overline{V}$ is the reference molar volume, and T is temperature in K.

For a system of C13MA and VMA with the estimated solubility parameters, the calculated χ was 2.32 and 1.59 at 25 and 160 °C respectievely.

5.6.3.4 Swelling and estimation of cross-linking density

Using the swelling ratio of a cross-linked sample, its cross-linking density can be estimated using the Flory-Rehner equation [14].

$$\nu_e = - \frac{ln(1-V_r) + V_r + \chi_{12} V_r^2}{V_s \left(V_r^{1/3} - \frac{V_r}{2} \right)} \qquad \text{(Eq. S5)}$$

Here, V_s is the molar volume of the THF solvent, 81.3 cm^3/mol, and V_r is the volume fraction of the polymer network in the swollen state, χ_{12} is the Flory-Huggins polymer-solvent interaction parameter using the Flory-Hildebrand equation, similar to eq 1 with V_s instead of $\overline{V}$. The calculated values of the cross-linking densities are summarized in Figure S.20 for the three copolymers studied. While v-s-CV and v-b-CV have similar values, the v-s-CVG has higher density of cross-linking. This agrees with the results of tensile tests in which v-s-CVG exhibited higher stress and lower elongation at break. The observed tighter network in v-s-CVG is a result of static cross-linking from the epoxy-amine reactions.

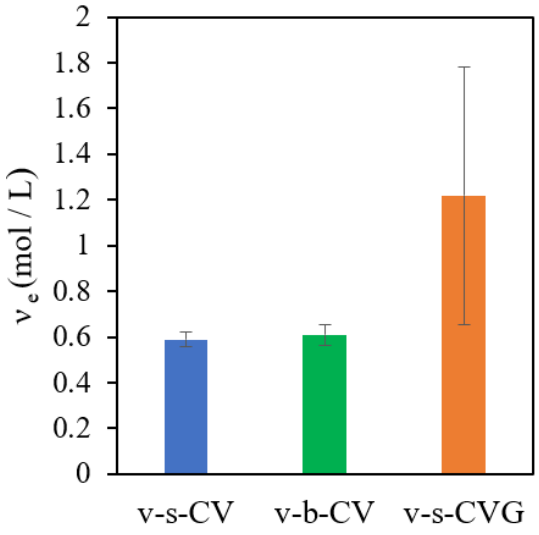

Figure S 5.20 Estimation of cross-linking densities of various vitrimers. While v-s-CV and v-b-CV had similar crosslinking densities, the dual networked v-s-CVG sample had higher cross-linking density.

5.6.3.5 Thermogravimetric analysis

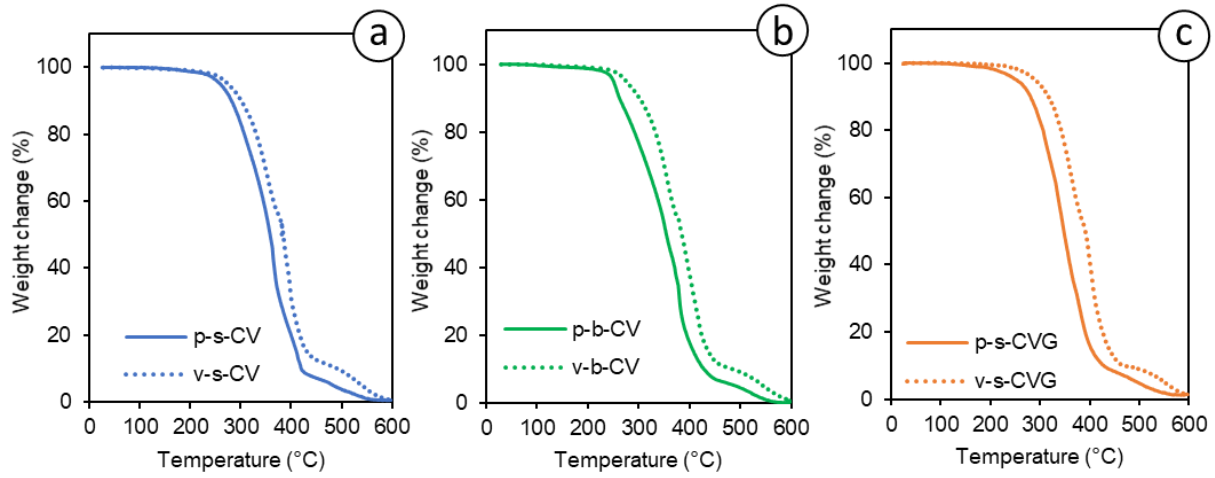

Figure S 5.21 TGA spectra of all prepolymers and their associated vitrimer, a) p-s-CV and v-s-CV, b) p-b-CV and v-b-CVG and c) p-s-CVG and v-s-CVG. In all cases, vitrification slightly enhanced the thermal stability of the samples. The vitrimers showed similar degradation.

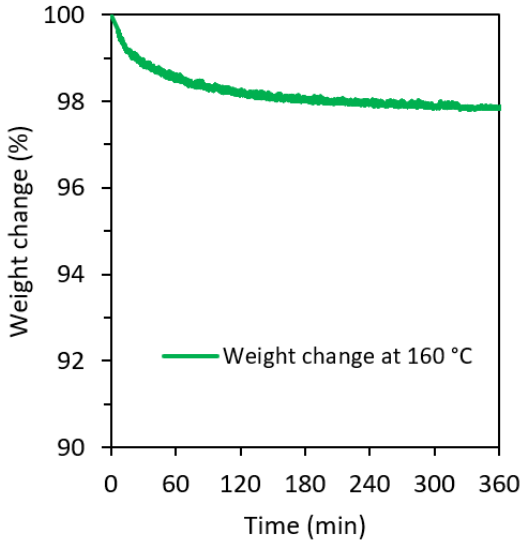

Figure S 5.22 Isothermal TGA experiment at 160 °C for 360 min under nitrogen atmosphere for v-s-CV showing a weight loss of 2.2%. The observed weight loss in the first 30-60 min can be attributed to moisture or any possible remaining THF.

5.6.3.6 Fourier transform infrared spectroscopy

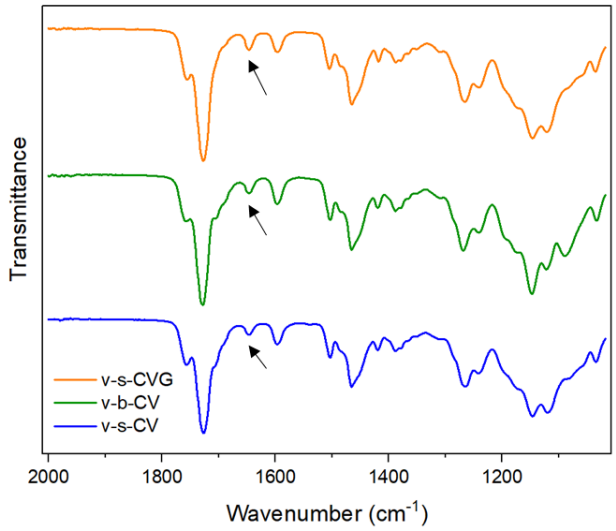

Figure S 5.23 ATR-FTIR of all vitrimers. The peak at 1648 cm^{-1} corresponding to the imine bonds in all vitrimers. In the case of GMA-based vitrimers, the disappearance of the characteristic oxirane peak at 910 cm^{-1} also confirms the reaction of IPDA with GMA [198,202].

5.6.4. Dynamic mechanical analysis and rheology

5.6.4.1 Strain sweep test and linear viscoelastic region (LVR)

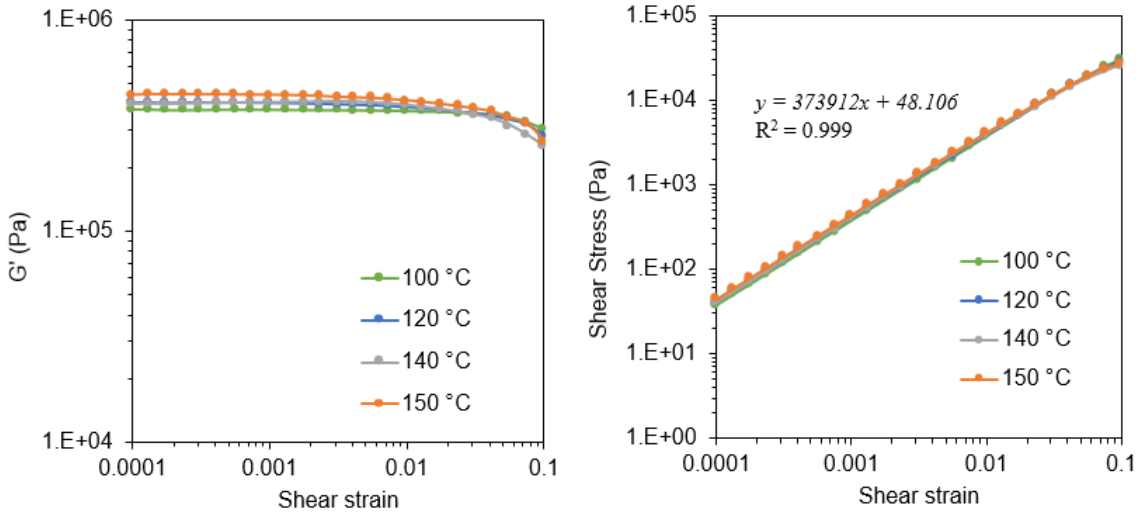

Figure S 5.24 Strain sweep (left) and stress-strain sweep (right) tests at 1Hz of v-s-CV at various temperatures. The linear viscoelastic regions (right) were fitted by linear regression.

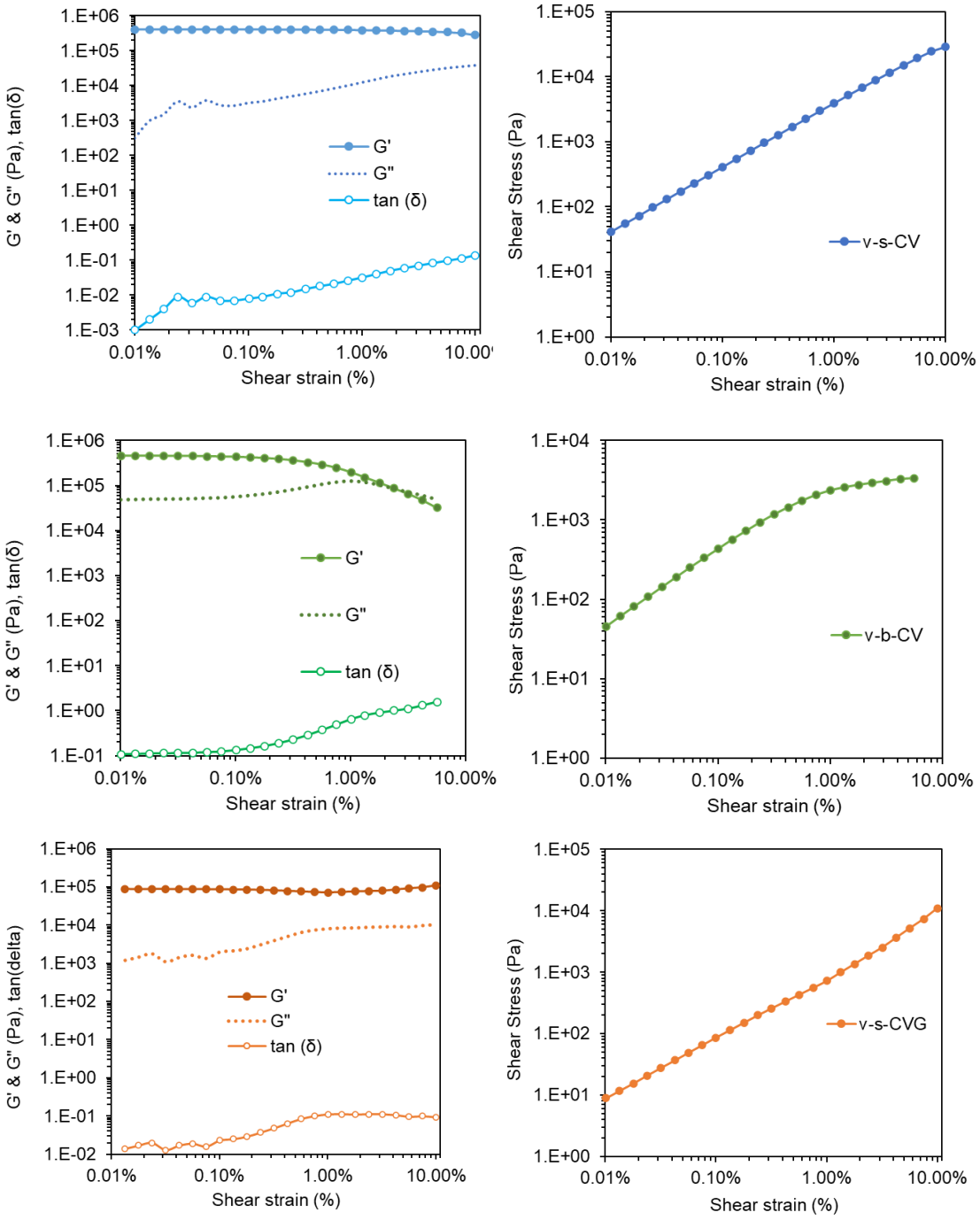

Figure S 5.25 Comparison of strain sweep (left) and stress-strain sweep (right) tests at 1Hz at 120 °C of v-s-CV (blue), v-b-CV (green), and v-s-CVG (orange).

5.6.4.2 Frequency sweep tests

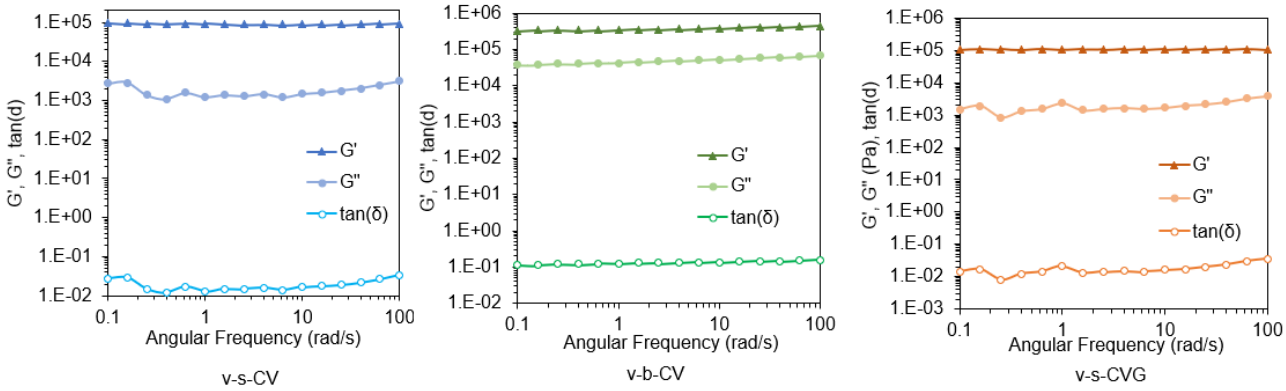

Figure S 5.26 Angular frequency sweep showing G′ and G″ (Pa), of v-s-CV (blue), v-b-CV (green) and v-s-CVG (orange) vitrimers at 120 °C and 0.1 % strain.

5.6.4.3 Stress-Relaxation

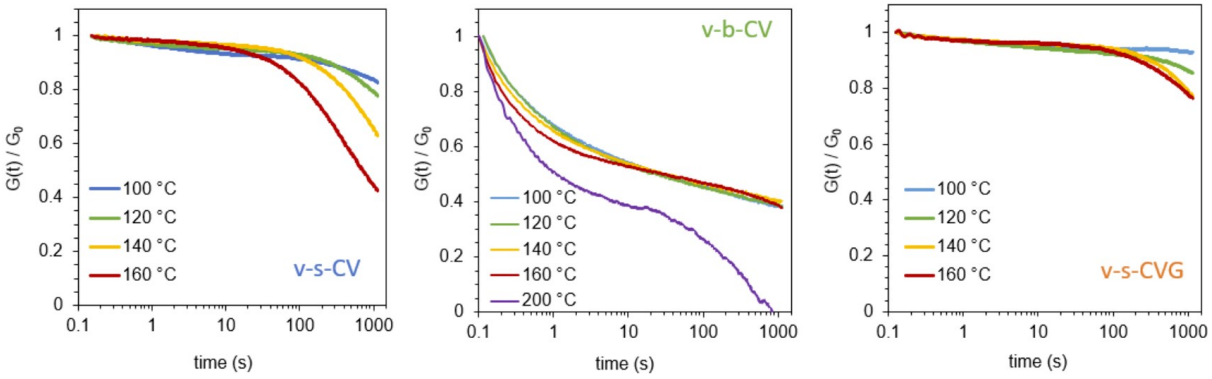

Figure S 5.27 Stress-relaxation of v-s-CV (left), v-b-CV (middle), v-s-CVG (right) vitrimers at various temperatures. The statistical vitrimers follow a Maxwellian stress-relaxation while the block vitrimer does not follow such behavior below the T_g at ~180 ˚C of p(VMA) block. v-b-CV goes under full relaxation at temperatures higher than T_g.

Figure S 5.27 show the normalized stress-relaxation G(t) / G_0 for vitrimers. A stretched exponential decay model was fitted to the data (Eq. S6) and values of characteristic relaxation time (τ^*) and β ($0 < \beta \leq 1$), a parameter related to the breadth of the relaxation distribution, were estimated. The data are summarized in **Table S 5-3**.

$$\frac{G\,(t)}{G_0} = exp\left(-\left(\frac{t}{\tau^*}\right)^{\beta}\right) \qquad \text{(Eq. S6)}$$

Table S 5-3 Stress-relaxation curve fitting

v-s-CV	T (˚C)	τ^* (s)	β
	100	3.34E+06	0.22
	120	1.49E+05	0.38
	140	3.82E+03	0.66
	160	1.24E+03	0.63
v-s-CVG	**T (˚C)**	**τ^* (s)**	**β**
	100	2.22E+08	0.20
	120	1.50E+07	0.21
	140	2.24E+05	0.30
	160	9.66E+03	0.66

$$ln\ \tau^* = \frac{E_a}{RT} + ln\ \tau_0 \qquad \text{(Eq. S7)}$$

In which, E_a is the viscous flow activation energy, R is the universal gas constant, T is the temperature and τ_0 is the Arrhenius pre-factor.

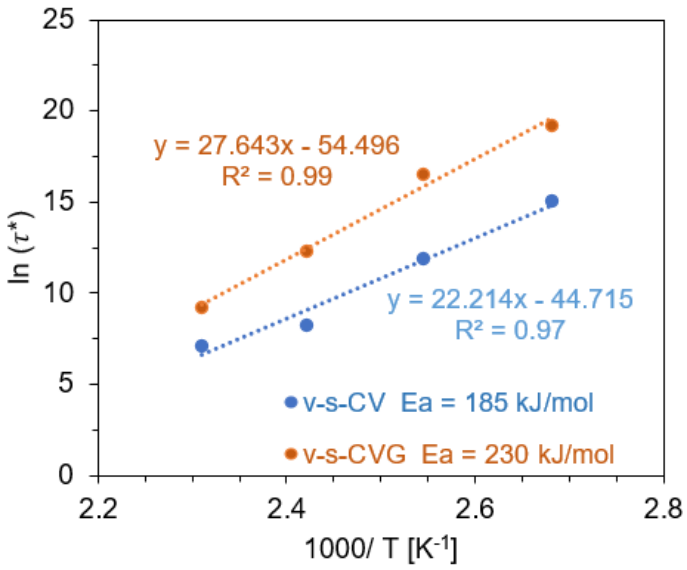

Figure S 5.28 Arrhenius relationship between the relaxation time and the temperature obtained from the stress-relaxation experiment of the statistical vitrimers.

5.6.5. Nanoindentation

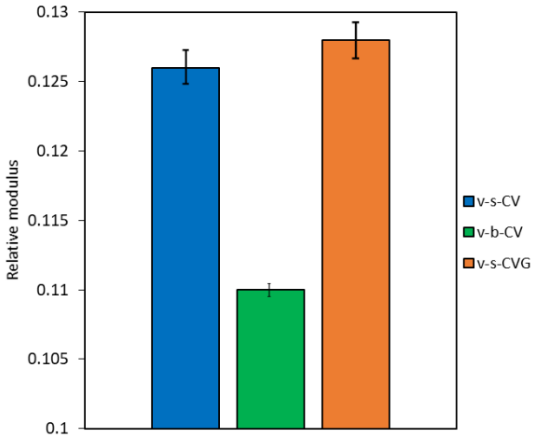

Figure S 5.29 Calculated relative modulus from nanoindentation: v-s-CV (blue), v-b-CV (green) and v-s-CVG (orange).

5.6.6. Tensile properties of reprocessed vitrimers

Table S 5-4 summarizes the tensile data of processed and reprocessed statistical v-s-CV and v-s-CVG vitrimers. Reprocessing by 4 cycles of cutting and hot-pressing did not negatively affect the tensile properties of the vitrimers.

Table S 5-4 Four reprocessing cycles of statistical vitrimer.

Vitrimer	Property *	Processed	Rx1	Rx2	Rx3
v-s-CV	Stress (MPa)	2.7 ± 0.2	2.9 ± 0.2	3.0 ± 0.1	2.7 ± 0.1
	Strain (%)	40 ± 4%	48 ± 1%	46 ± 4%	43 ± 3%
v-s-CVG	Stress (MPa)	3.5 ± 0.1	3.3 ± 0.3	2.9 ± 0.5	3.4 ± 0.4
	Strain (%)	34 ± 2 %	34 ± 4%	29 ± 9%	22 ± 7%

* Stress and stain at break

5.6.7. Estimation of bio-based carbon content

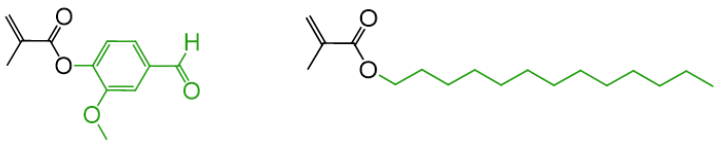

Figure S 5.30 Structure of VMA and C13MA monomers with in green the bio-base atoms.

Table S 5-5 Estimation of the bio-base content of the prepolymers.

Atom / Compound	Carbons			Hydrogens			Oxygens			Total numbers of atoms	Total numbers of bio-sourced atoms	**% total bio-sourced**
	Total	Bio-sourced	% bio-sourced	Total	Bio-sourced	% bio-sourced	Total	Bio-sourced	% bio-sourced			
C13MA	17	13	76.5	32	27	84.4	2	0	0	51	40	**78.4**
VMA	12	8	66.7	12	7	58.3	4	2	50	28	17	**60.7**
p-s-CV	2297	1720	74.9	3713	3281	88.4	349	61	17.4	6359	5062	**79.6**
p-b-CV	3275	2472	75.5	5475	4873	89	456	54	11.9	9206	7400	**80.4**
p-s-CVG	3717	2778	74.7	6208	5488	88.4	525	58	11.1	10451	8325	**79.7**

p-s-CV : DPn = 144 (with 30 VMA units and 114 C13MA units); p-b-CV : DPn = 201 (with 27 VMA units and 173 C13MA units); p-s-CV : DPn = 231 (with 29 VMA units, 196 C13MA units and 6 units of GMA)

Chapter 6: Di-and Tri-Block Copolymer Vitrimers

This chapter is presented as an article published as the following

Farhad Asempour, Eline Laurent, Theo Bride, Milan Maric

Rheological and Mechanical Comparison of Di and Tri-Block Copolymer Vitrimers Using Dynamic Imine Exchange
European Polymer Journal
Volume 219, 16 October 2024, 113402
https://doi.org/10.1016/j.eurpolymj.2024.113402 [214]

6.1. Preamble to Chapter 6

In Chapter 3, we established that vitrification can be used to compensate for the lack of molecular entanglements in brush-like low T_g polymers derived from bio-based monomers. Mechanical properties of such polymers could be enhanced and modulated without sacrificing their recyclability. In Chapter 5 it was found that microphase separation and self-assembly can highly increase the hardness and creep resistance of the vitrimers. However, the hard-soft diblock copolymers of VMA (hard domain) and C13MA (soft domain) exhibited poor tensile strength which was attributed to the high M_e of the C13MA block. In this chapter, we tried to answer the following questions: can we enhance the tensile properties of such hard-soft diblock copolymer vitrimers by incorporating the cross-linkable units within the soft block while still suppressing creep? Thus, prepolymers of PMMA-b-P(C13MA-co-VMA) were synthesized and vitrified. In addition, we investigated the impacts of ABA triblock and AB diblock copolymer precursors on the properties of the vitrimers; here, A stands for the PMMA hard block and B stands for soft and functional P(C13MA-co-VMA) block.

The hypothesis presented in Chapter 6 was verified by the mechanical properties: PMMA-b-P(C13MA-co-VMA) offered much higher tensile strength than P(VMA)-b-P(C13MA). However, it was found that the ABA triblock copolymers offer superior tensile properties to AB diblock while exhibiting similar creep-resistance.

6.2. Abstract

Vitrimers' tendency to creep over time under stress poses a significant challenge to their widespread industrial use. Recently, nanoscale self-assembly has emerged as a promising route to control creep in vitrimers; however, mechanical robustness of such phase-separated materials requires further enhancement and investigation. Herein, we explored the structure-property effects of the prepolymer architectures in statistical, AB hard-soft and ABA hard-soft-hard block copolymers. Reversible addition−fragmentation chain-transfer (RAFT) was employed to precisely control the topology of the precursors. Dynamic imine functionalities were localized within the soft segment made of a bio-based predominantly long chain alkyl methacrylate, copolymerized with an aldehyde-functional vanillin methacrylate, via reaction with amino groups of the Priamine cross-linker. Compared to statistical counterparts, triblock copolymer-based vitrimers not only exhibited superior creep resistance but also had improved hardness, tensile modulus, and stress at break. In contrast, vitrimers from diblock copolymers exhibited much weaker tensile properties. Our findings suggest that by controlling the chain topology in block copolymers and optimizing the order-disorder transition, we can not only enhance vitrimers' creep resistance and tune their viscoelastic properties but also improve their mechanical strength.

6.3. Introduction

Thermosets are permanently cross-linked polymeric networks with exceptional properties such as high dimensional and thermal stability, chemical resistance, and mechanical strength [110,190]. Global production of petroleum-derived thermosetting polymers and their composites has been on the rise [3,4]. However, due to the irreversibility of such covalently bonded networks, thermosets cannot be reshaped, reprocessed, or recycled to high-value products after production [58,150]. This poses a growing environmental and economic challenge. In the quest for more eco-friendly polymeric materials, vitrimers have emerged as a subset of covalent adaptable networks (CANs) [56,61]. Vitrimers employ dynamic associative exchange reactions, allowing their network topology to change and ultimately making them re-moldable under mild stimuli [7,8]. Various associative dynamic bonds such as transesterification [215] boronic ester [73,83], disulfides [92,93], vinylogous urethanes [40,55], α-acetyl cinnamate/acetoacetate [216], and imine [95,133] etc., have been adapted for vitrimers [55,57,58,217,218].

Despite the benefits and promise of vitrimers, balancing vitrimers' reactivity with their dimensional stability at service temperatures remains a challenge [187,190]. Unlike thermosets, which show minimal strain over time under stress (creep), vitrimers exhibit viscoelastic behavior. Controlling creep is vital for scalable industrial applications of vitrimers [150,187]. In an ideal system, bond exchange reactions should be highly activated and occur rapidly during processing at elevated temperatures, while ensuring organic material remains below its degradation point [190]. Conversely, during service temperatures, the exchange should be sufficiently slow and deactivated to effectively suppress creep [187,219].

Many studies have focused on understanding the flow behavior of vitrimers and developing strategies to control creep. These strategies include a spectrum of techniques, such as fine-tuning the cross-linking density and activity [66,208], implementing catalytic control [220], combining dynamic and static bonds [103,109,161,221], adjusting the primary chain length beyond M_e [103,145], controlling the neighboring group participation on the dynamic cross-links (NGP) [69,221–223], protecting reactive groups and temporarily shielded inside the network backbone [71,224], employing highly endothermic bond dissociation chemistries [187,225], and inducing phase separation [90,114,115,161]. Phase separation is particularly interesting since self-assembly is a well-established phenomenon in macromolecular engineering, providing opportunities to

further tune the properties of vitrimers [115]. Despite this, only a handful of works have reported the use of block copolymers in vitrimers [191,192]. Sumerlin and coworkers investigated diblock copolymer vitrimers as precursors for vinylogous urethane networks [114]. The resulting microphase separated networks exhibited lower creep and slower relaxation compared to the statistical ones which were attributed to lower network strand diffusion. Fang et al., introduced vitrimers of boronic transesterification into triblock poly(styrene-*b*-butadiene-*b*-styrene) (SBS) via thiol-ene click chemistry [226]. Compared to neat thermoplastic elastomer SBS, vitrified SBS showed much slower stress-relaxation, improved creep resistance, and 2.8 times higher Young's modulus [226]. In our recent study, we made direct comparisons between two strategies to control creep in imine vitrimers: combining static and dynamic bonds, and utilizing microphase separation in diblock copolymers with contrasting 'soft' and 'hard' segments [161]. Both approaches significantly reduced creep, achieving up to an 84% decrease. The hybrid crosslinking method exhibited a notably slower stress relaxation rate than the self-assembled networks. However, a critical drawback of the microphase-separated vitrimers was their inferior tensile strength, which we attributed to the lack of entanglements within the soft P(C13MA) block. C13MA is a methacrylic ester with an average alkyl side chain length of 13 units whose polymer has entanglement molecular weight (M_e) of > 200,000 g/mol [161,206].

In this contribution, our primary objective is to address the issue of tensile strength of block copolymer vitrimers while also managing their tendency to creep over time. Previously, we demonstrated the effectiveness of vitrification in modulating the properties of brush-like bio-based monomers and compensating for their high M_e and lack of entanglements, while maintaining their re-processability [103].

Building upon this, we propose that by structuring vitrimers into hard-soft block configurations and incorporating dynamic bonds into the soft blocks, we can both suppress creep and enhance their tensile strength. Additionally, inspired by the exceptional properties of ABA-type thermoplastic elastomers, we compared the rheological and mechanical properties of AB diblock and ABA triblock copolymers. To explore this concept further, we synthesized three prepolymers: statistical, AB-type diblock, and ABA-type triblock copolymers. Here, A denotes the hard segment composed of methyl methacrylate (MMA), while B represents the soft block, comprised of C13MA and aldehyde-functional vanillin methacrylate (VMA). These prepolymers had similar

overall compositions and number average molecular weights (M_n). Afterwards, networks were cured by treating the aldehyde from VMA with Priamine 1075 (Priamine), a di-functional amine, at a fixed cross-linking ratio, as seen in **Figure 6.1**. We specifically selected Priamine, C13MA and VMA because of their high bio-based content, all being derived from vegetable oils and lignin.

Atomic force microscopy (AFM) and small angle X-ray scattering (SAXS) confirmed the microphase separation in the prepolymers and cured vitrimers. We further characterized the thermomechanical and viscoelastic properties of the vitrimers by conducting swelling, differential scanning calorimetry (DSC), dynamic thermal mechanical analysis (DMTA), creep rheometry, stress relaxation, and tensile tests. Furthermore, we assessed the re-processability of the vitrimers through multiple grinding and compression molding cycles. This work highlights the versatility of bio-based monomers in fabrication of potentially recyclable polymers with precise architecture which help reduce reliance on petroleum resources and minimize carbon footprints.

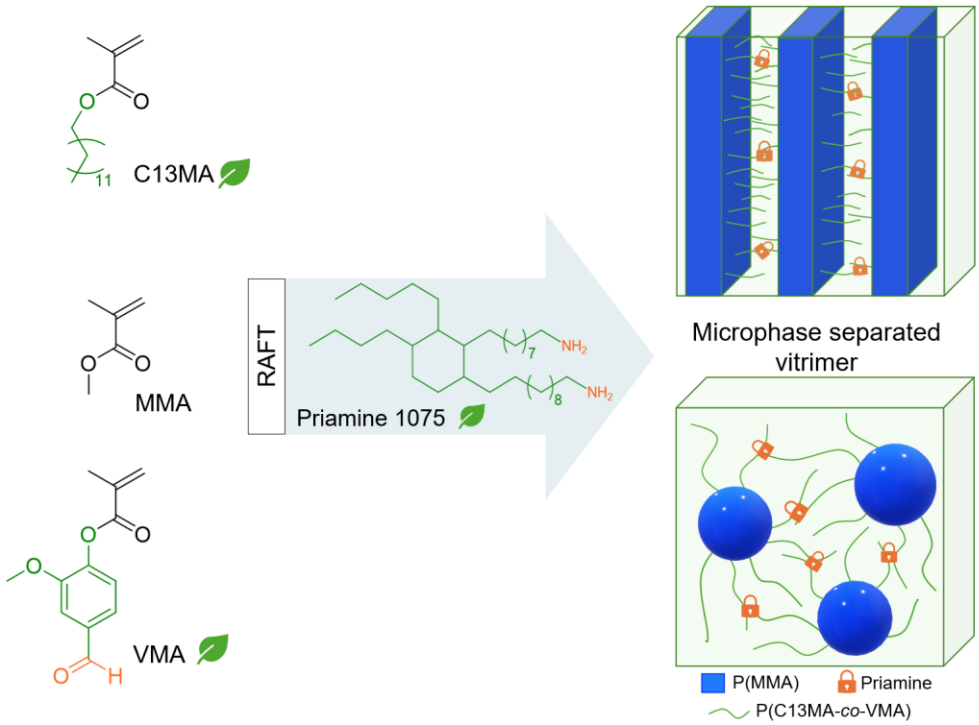

Figure 6.1 Structure of C13MA, MMA, and VMA monomers. Reversible addition fragmentation transfer (RAFT) polymerization was used to form di and tri-block copolymers which formed lamellar and spherical structures. Priamine was used to cross-link the polymers through the reaction of the amines with aldehyde group from VMA (orange). Geen colors represent the bio-based content.

6.4. Results and discussion

6.4.1. Synthesis of prepolymers

We synthesized three prepolymers via reversible addition fragmentation transfer (RAFT) polymerization. RAFT has proven a suitable platform for the synthesis of methacrylate-based vitrimers providing control over composition and molecular architecture [112,145]. The prepolymers were synthesized targeting comparable overall number average molecular weight (M_n ≈ 30,000 g/mol) and similar composition (F_{VMA} ≈ 10%) with different molecular architectures: statistical P(MMA-*co*-C13MA-*co*-VMA), AB-type diblock PMMA-*b*-P(C13MA-*co*-VMA) and ABA-type triblock PMMA-*b*-P(C13MA-*co*-VMA)-*b*-PMMA. The block copolymers were synthesized through the sequential addition of monomers. The polymerization procedures are described in detail in the supporting information as summarized in **Figure S 6.1** - **Figure S6.22**.

The prepolymers are identified as "p-statistical", "p-diblock", and "p-triblock". After the vitrification "p" is replaced by "v". The chemical structures of all monomers and polymers are provided in **Figure 6.1** and **Figure S 6.1**, **Figure S6.3**, **Figure S6.7**, and **Figure S6.16.**

The polymerizations kinetics were followed by ^{1}H NMR spectroscopy and gel permeation chromatography (GPC) to find monomer conversion and M_n and dispersity ($Đ$), respectively. Table 1 summarizes the molecular weight, composition and glass transition temperature (T_g) of all final prepolymers prior to vitrification. A linear increase in M_n versus overall monomer conversion ($X_{overall}$) along with low values of dispersity $Đ$ of ~ 1.20 suggest a well-controlled synthesis of all polymers (**Figure 6.2.h**, **Figure S6.4Figure S6.8Figure S6.10Figure S 6.17**). The synthesis of p-diblock involved two steps. First, a homopolymer of PMMA was synthesized yielding M_n = 10,500 g/mol and $Đ$ = 1.17, after precipitation in methanol. Subsequently, the PMMA macro-chain transfer agent (CTA) was dissolved in ethyl acetate and chain extended with a mixture of C13MA and VMA, resulting in the diblock copolymer with overall M_n = 25,700 g/mol and $Đ$ = 1.27, recovered after precipitation in methanol. The kinetic plots of the synthesis of both blocks are provided in **Figure S6.8** and **Figure S6.10** revealing a linear increase in M_n versus $X_{overall}$. Following the chain extension, a clear monomodal shift towards higher M_n without a significant increase in $Đ$ was observed in the GPC traces. This, alongside the existence of a single population of species seen in DOSY NMR, confirmed a successful chain extension and formation of covalently bonded diblock copolymer. Notably, both the M_n and F_{VMA} of the statistical copolymer

and block copolymer were very similar. This indicates that disparities in material properties should arise solely from variations in the molecular structure and assembly. The third studied prepolymer in this work, p-triblock, was synthesized through chain extension of the p-diblock with MMA using a similar approach. Again, a clear monomodal shift in the GPC traces toward higher M_n with low $Đ$, as illustrated in **Figure 6.2.h**, alongside a single population of species in DOSY NMR, **Figure S6.20**, confirmed a successful covalently bonded chain extension of the third block. After synthesizing well-defined prepolymers, we proceeded to remove the RAFT CTA moieties from the chain ends. The prepolymers were treated with excess free radical initiator at 80 °C to replace the CTAs, as illustrated in **Figure S6.3**, **Figure S6.16**, and **Figure S6.22** [227]. Thiocarbonylthio CTAs are prone to rapid aminolysis upon treatment with primary amines which can later consume the cross-linkers required for vitrification. Moreover, side reactions can result in chain coupling reactions [112] or depolymerization [228] after repeated heating and processing. Characterization by ultraviolet-visible (UV-vis) spectroscopy confirmed the successful removal of chain ends by disappearance of the peak at ~ 500 nm corresponding to the thiocarbonyl moiety (**Figure S6.22.c-e**). Additionally, a noticeable change in the visual appearance of the prepolymers, shifting from pink to white, was indicative of successful chain end removal, please see **Figure S6.22.a-b.** ^{1}H and DOSY NMR as well as GPC revealed minimal to no alterations in the composition and molecular weight distribution of the terpolymers post-chain end removal, as noted in **Figure S6.4, Figure S6.13,** and **Figure S 6.17**. In addition to ^{1}H NMR, attenuated total reflectance–Fourier transform infrared (ATR-FTIR) confirmed the presence of VMA in all prepolymers via the presence of the aldehyde peak at 1600 cm^{-1}, as seen in **Figure 6.3.d** and **Figure S 6.23 a-b** [97,198,229].

Table 6.1 Composition, molecular weight (M_n), and glass transition (T_g) of the chain end removed prepolymers.

	M_n (g/mol) [a]	$Đ$ [a]	F_{MMA} (%) [b]	F_{C13MA} (%) [b]	F_{VMA} (%) [b]	$T_{g,\ prepolymer}$ (°C) [c]	$T_{g,\ vitrimer}$ (°C) [c]	Bio Carbon (%) [d]
p-statistical	24700	1.20	36	53	11	12	22	57
p-diblock	27700	1.23	26	62	12	-75 and 106	-42 and 103	57
p-triblock	41000	1.14	39	52	9	-70 and 111	-45 and 111	55

[a] compared to PMMA standards in THF at 40 °C [b] From ^{1}H NMR analysis [c] From DSC [d] estimation based on bio-based Carbon content of each component and after vitrification with Priamine.

Microphase separation

To ensure microphase separation in the block copolymers, we designed the prepolymers by estimating the segregation strength (χN) at the temperature of the order-disorder transition (ODT) [204]. Here, N represents the total degree of polymerization, and χ is the Flory-Huggins interaction parameter, which roughly quantifies the compatibility between the C13MA-rich and MMA-rich blocks. Assuming only enthalpic contributions are in effect, without any entropic contributions, χ can be estimated through the Hildebrand equation [146,230]:

$$\chi = \frac{\bar{V}}{RT} (\delta_{MMA} - \delta_{C13MA})^2$$

where the reference molar volume ($\bar{V}$) is the geometric average molar volume of the monomers, δ is the solubility parameter of interest, R is the universal gas constant, and T is temperature. Liebler's theory predicts that symmetric diblock copolymers will microphase separate into lamellar geometry at $\chi N > 10.5$ [205]. Our calculation in Supporting Information Section 2.5 roughly estimates ~ 86 and 60 for χN at 25 and 150 °C which suggest a tendency for phase separation of the MMA and C13MA-rich domains. Based on this approximation, we continued to verify the microphase-separation in the block copolymers. Differential scanning calorimetry (DSC) of the prepolymers showed a single T_g at 12 ˚C for p-statistical. However, for p-diblock, two distinct T_g values were observed: -75 °C and 106 °C, while p-triblock exhibited T_g values of -70 °C and 111° C. **Figure 6.3.a-c.** T_g values around -75 °C can be attributed to the C13MA-rich soft block, whereas the T_g values around 106 °C can be attributed to the PMMA hard block(s) [174,231,232]. The presence of such distinct T_g values suggests the existence of microphase separated domains within the diblock and triblock copolymer structures. More importantly, we performed AFM on solvent-cast films of the prepolymers using the phase and amplitude channels from tapping mode, shown in **Figure 6.2.a-f**. Essentially, a uniform morphology was seen for p-statistical while the p-diblock and p-triblock prepolymers exhibited microphase-separated structures. It is noteworthy that the morphology in p-triblock was shifted to a lamellar from spherical morphology in p-diblock, which can be attributed to the higher F_{MMA} and more symmetrical structure of p-triblock [204]. Spherical microdomains for AB type diblock copolymers are typically found with a volume fraction of A block roughly around 0.1–0.2 [233] These results also corroborate with findings of Chatterjee et al., who reported formation of

spherical to lamella microphase separated morphologies for MMA and lauryl methacrylate (LMA)-based di and triblock copolymers [207].

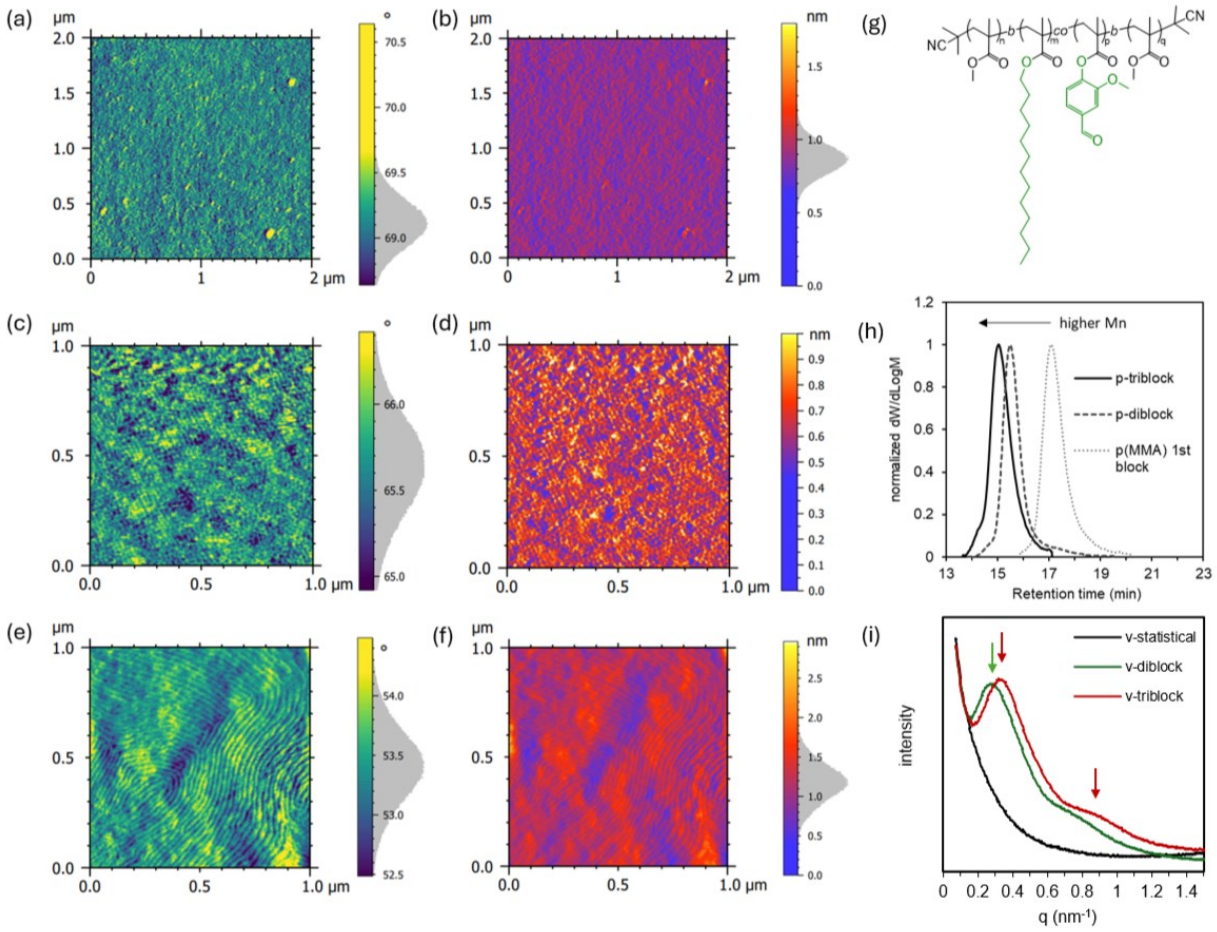

Figure 6.2 AFM images of statistical, diblock, and triblock prepolymers: phase a, c, d and amplitude b, d, f. Molecular structure of p-tiblock (g) , GPC traces of chain extension of di and triblock copolymers (h), and SAXS spectra of vitrimers (i).

6.4.2. Synthesis of vitririmers and their (re)processing

We continued with the vitrification and network formation by dissolving each prepolymer in ethyl acetate (ca 40 wt/v%) and adding the di-functional Priamine 1075 cross-linker from THF (ca 50 wt/v%). The ratio of NH_2 of the crosslinker to the aldehyde group of VMA was 0.9 for all samples. The purpose for the stoichiometry imbalance was to promote dynamic cross-linking exchanges. The gelation occurred within approximately 20 minutes. Afterwards, the organogels were heated to 110 ± 5 °C for 2 h to further push the cross-linking reaction and remove solvents and water followed by overnight heating at 50 ± 5 °C under vacuum. The obtained pale yellowish colored,

optically transparent, and homogenous solid were then hot-pressed at 120 ± 5 °C under 6 ± 0.5 metric tons for 60 ± 5 min to be shaped into disks and dog bone shaped bars for rheological and tensile tests. Exchanges of imine bonds require no catalysts allowing the associated vitrimers to be reprocessed at relatively low temperatures without need of additional chemicals [133,229].

To study the vitrimers' recyclability and reprocessing, each sample was repeatedly chopped into small pieces and pressed under similar conditions. Each sample underwent 4 cycles of cutting and hot-pressing.

6.4.3. Network Characterization

With the vitrimers in hand, we continued with their characterization. Formation of imine cross-links was confirmed via attenuated total reflectance Fourier transform infrared (ATR-FTIR) analysis by the appearance of the corresponding peak at 1645 cm^{-1} for all vitrimers, shown in **Figure 6.3.d** and **Figure S 6.23**. Solubility tests at room temperature after 24 h in ethyl acetate revealed an average of 91 ± 4 % gel content for all vitrimers confirming the formation of cross-linked network. The v-statistical and diblock exhibited the highest, 550 ± 56%, and lowest, 303 ± 59%, swelling ratios, as seen in **Figure 6.3.e.**

The vitrimers' thermal properties were examined using differential scanning calorimetry (DSC) and thermogravimetric analysis (TGA). For the statistical polymer, only one T_g was observed, which showed a slight increase from 12 to 22 °C after vitrification. However, in the case of di- and tri-block copolymer-based networks, cross-linking led to an increase in the T_g of the P(C13MA-co-VMA) soft block from -75 to -40 °C and -70 to -44 °C, respectively. Vitrification had minimal to no effect on the T_g of the PMMA block due to its lack of reactive groups. The observed T_g values from DSC also corroborates with that observed using dynamic thermal mechanical analysis (DMTA), as seen in **Figure 6.4.c** and **Figure S6.28-S6.29.** The presence of distinct low and high T_g values in the blocky vitrimers are again strong indications for microphase separation.

In all cases, vitrification improved thermal stability as evidenced by TGA, **Figure S6.25**. For the statistical terpolymer, the onset of degradation (T_{onset}) increased from 316 to 350 °C while the temperature at which 5% weight loss occurred ($T_{5\%}$) remained at approximately 230 °C. After curing the diblock, both T_{onset} and $T_{5\%}$ rose from 314 to 350 °C and 268 to 305 °C, respectively. Similarly, in the case of the triblock vitrimer, T_{onset} increased from 287 to 378 °C and $T_{5\%}$ increased from 245 to 315 °C. To better understand the thermal stability of the vitrimers at longer time scales,

we performed isothermal TGA on the v-statistical and v-triblock, **Figure S6.24**. Both samples exhibited little thermal degradation with less than 2% weight loss after 3 h at 120 °C under nitrogen flow.

To verify the microphase separation in the cured block vitrimers, we performed small angle X-ray scattering (SAXS) on the bulk vitrimers, shown in **Figure 6.2.i.** The SAXS profile of v-statistical showed no reflections suggesting a disordered morphology with no microphase separation. However, the spectra of block vitrimer exhibited higher order diffraction with no specific pattern. The peaks at q^* at 0.32 (nm^{-1}) suggests interdomain spacing of ~19 nm which agrees well with the AFM images of v-triblock.

To probe the mechanical properties of the vitrimers, we conducted uniaxial tensile tests, illustrated in **Figure 6.3.f.** Despite having similar composition and cross-linking density, the vitrimers displayed distinct mechanical behaviors depending on their prepolymer architecture. The v-statistical exhibited a stress at break (σ_{break}) of 3.1 ± 0.4 MPa, accompanied by the highest elongation at break (ε_{break}) among the vitrimers with ε_{break} of 125 ± 11%. Conversely, v-diblock demonstrated the lowest σ_{break} and ε_{break}, measuring at 2.2 ± 0.5 MPa and 32 ± 1%, respectively.

One of the main motivations for the present work study was to enhance the mechanical properties of block vitrimers. Our group recently studied the tensile properties of PC13MA-*b*-PVMA based vitrimers, which were notably brittle and exhibited significantly inferior tensile properties compared to their statistical counterparts, with approximately 4 and 8 times lower σ_{break} (1 MPa) and ε_{break} (~5%) (Chapter 4). However, herein, v-diblock showcased notably improved tensile properties compared to PC13MA-*b*-PVMA vitrimer, where soft block lacked entanglement, despite PMMA having a lower T_g than PVMA. This improvement is directly attributed to the presence of cross-links in the soft block which compensates for the high M_e of C13MA. Nevertheless, v-triblock demonstrated a significant increase in the elastic modulus and σ_{break}, measuring at 5.2 ± 0.4 MPa, with ε_{break} values comparable to that of v-diblock. This higher σ_{break} can be attributed to both slightly higher F_{MMA} and the ABA morphology which is commonly used in classical thermoplastic elastomers [234,235].

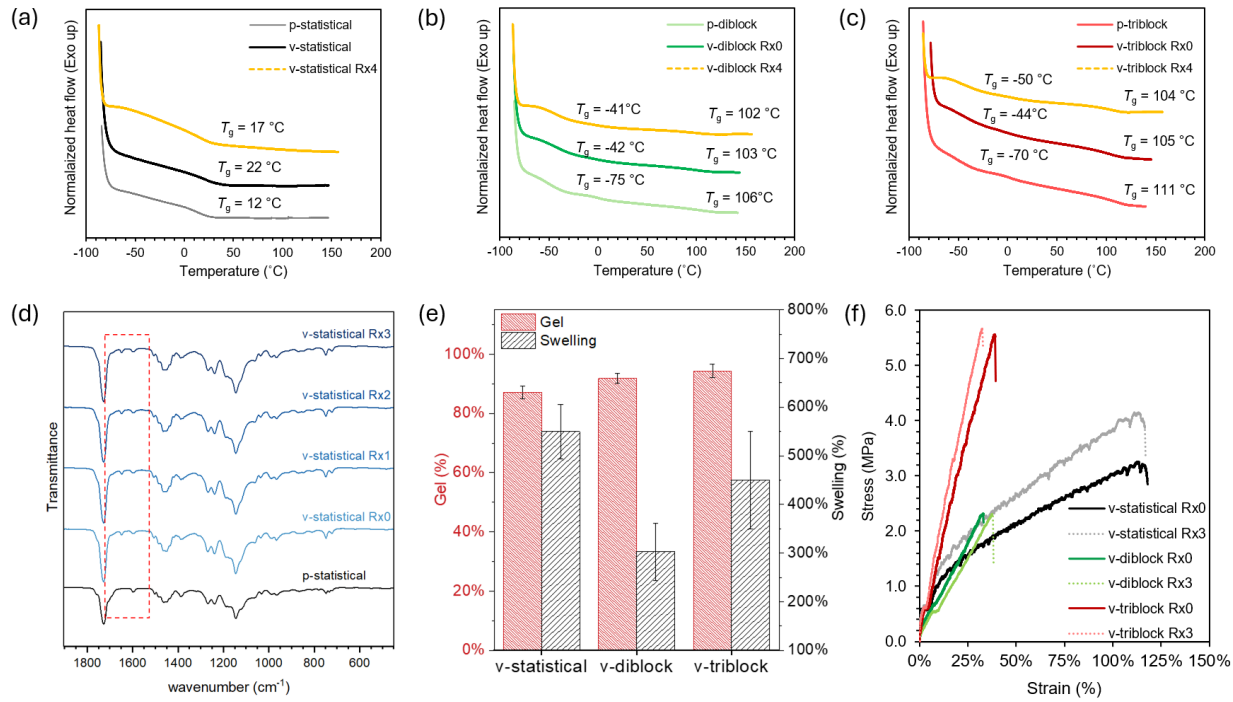

Figure 6.3 DSC traces of prepolymers, in pristine form and 4× recycled vitrimers of a) statistical, b) diblock, c) triblock. d) representative ATR-FTIR spectra of statistical prepolymer, pristine and 4× recycled vitrimers f) Tensile stress-strain curves of statistical, diblock, and triblock after 3× recycling.

We further examined the modulus and hardness of the vitrimers via nanoindentation using a Berkovich tip at room temperature The associated force−displacement curves are provided in **Figure 6.4.a-b.** The vitrimers' moduli followed the same trend as the tensile tests. However, the v-diblock and v-triblock exhibited approximately 1.5- and 4-times enhanced hardness compared to v-statistical, respectively. In addition, the block vitrimers showed significantly smaller creep and higher dimensional stability. It appears that PMMA hard blocks could effectively anchor the networks.

We started the rheological studies by performing strain sweeps at various temperatures to find the linear viscoelastic region (LVR), as seen in **Figure S6.26**. Frequency sweeps, shown in **Figure S 6.27**, were also carried out at 110 °C. In all cases a rubbery plateau was observed with G′ > G″ showed the elastic nature of the vitrimers.

The thermomechanical properties of the vitrimers were further examined using DTMA across a temperature range of 25 to 150 °C. As depicted in **Figure 6.4.c**, all vitrimers displayed a rubbery plateau, indicating their cross-linked nature. v-triblock exhibited the highest modulus at this plateau, while v-statistical showed the lowest value. Notably, the statistical and block vitrimers exhibited different behavior with increasing temperature. The storage (G′) and loss (G″) modulus of the v-statistical vitrimer experienced a sharp decrease starting from 25 °C until approximately 70 °C, reaching the rubbery state, consistent with the T_g of v-statistical. In contrast, both di- and tri-block copolymer vitrimers displayed a T_g in DMTA around 110 ± 10 °C, corresponding to the PMMA block. The T_g values from DMTA align well with the results from DSC. Once again, these findings confirm the presence of microphase-separated domains in the block vitrimers.

Stress Relaxation

To better understand the flow behavior of the networks and the differences between statistical and microphase separated block vitrimers, we carried out stress-relaxation experiments. **Figure 6.4.e** compares the stress relaxation of the three vitrimers at 90 and 120 °C. As evident in **Figure 6.5**, remarkable differences in the stress-relaxation behavior of the statistical and block vitrimers were observed. While v-statistical underwent relatively fast and full relaxation, di- and triblock vitrimers showed a slower overall rate, specially at higher than 10 s time scales, and never reached full relaxation after 1000 s. Notably, the block vitrimers had relatively faster relaxation below 10 s. As expected, the rate of relaxation increased with increasing temperatures for v-statistical and v-triblock. Interestingly, stress-relaxation behavior of block vitrimers becomes more similar to that of v-statistical at higher temperatures beyond > 160 °C. This change in the relaxation behavior can be attributed to a transition from microphase separated microstructure to a disordered one. Further investigation is warranted to determine the phase transition temperature of the block copolymer vitrimers, and to explore its impact on their viscoelastic behavior.

Creep

The susceptibility of vitrimers to creep can significantly restrict their potential applications. Here, we compared the creep-recovery behavior of the statistical and block vitrimers, shown in **Figure 6.4.f.** After 200 s under 1 MPa pressure, v-statistical exhibited 2.5 times higher creep than the blocky networks. Interestingly, v-diblock and v-triblock showed relatively similar behavior. Upon removal of the pressure, v-statistical failed to fully recover, whereas the block copolymer vitrimers

nearly achieved full recovery. The improved dimensional stability in the block vitrimers can be attributed to the presence of microphase separated PMMA hard block which anchors the network. The creep data from rheological studies, which were conducted at elevated temperatures, corroborate with those of the indentation tests, at room temperature.

Reprocessing

One of the most important features of vitrimers is their ability to undergo reshaping and reprocessing via the rearrangement and interchange of crosslinks. All vitrimers in this work could undergo at least 3 cycles of repeated deconstruction and hot-pressing forming new test samples. **Figure 6.3**.d and **Figure S 6.23** display the ATR-FTIR spectra of the prepolymers, comparing the pristine cured networks (R×0), and their subsequent recycles (R×3). No noticeable changes were detected in the spectra, including the peak corresponding to imine cross-links at 1645 cm^{-1}. Furthermore, as displayed in **Figure S6.25**, the thermal properties of the vitrimers after R×4 remained largely intact including the T_g, T_{onset} and $T_{5\%}$. **Figure S6.29** compares the DMTA of v-statistical and v-triblock before and after reprocessing (R×4). Again, no appreciable changes in the modulus and the rubbery plateau were observed over the temperature range of 25 to 150 °C. Finally, we performed tensile tests after each reprocessing cycles. As evident in **Figure 6.3.f** and **Table 6.1**, the Young's modulus and the average values of σ_{break} and ε_{break} of all vitrimers showed no sign of deterioration and remained within the range of the error bar. These findings suggest that the vitrimers can maintain their structural integrity after repeated reprocessing cycles involving deconstruction and compression molding. Microphase separation through the implication of block prepolymers did not influence the vitrimers reprocessing. More importantly, multiple reprocessing of such block vitrimers did not deteriorate their microphase separated structure with the improvements associated with it. The demonstrated recyclability of the studied vitrimers, along with their bio-derived contents, implies promising metrics for enhancing the sustainability of these systems.

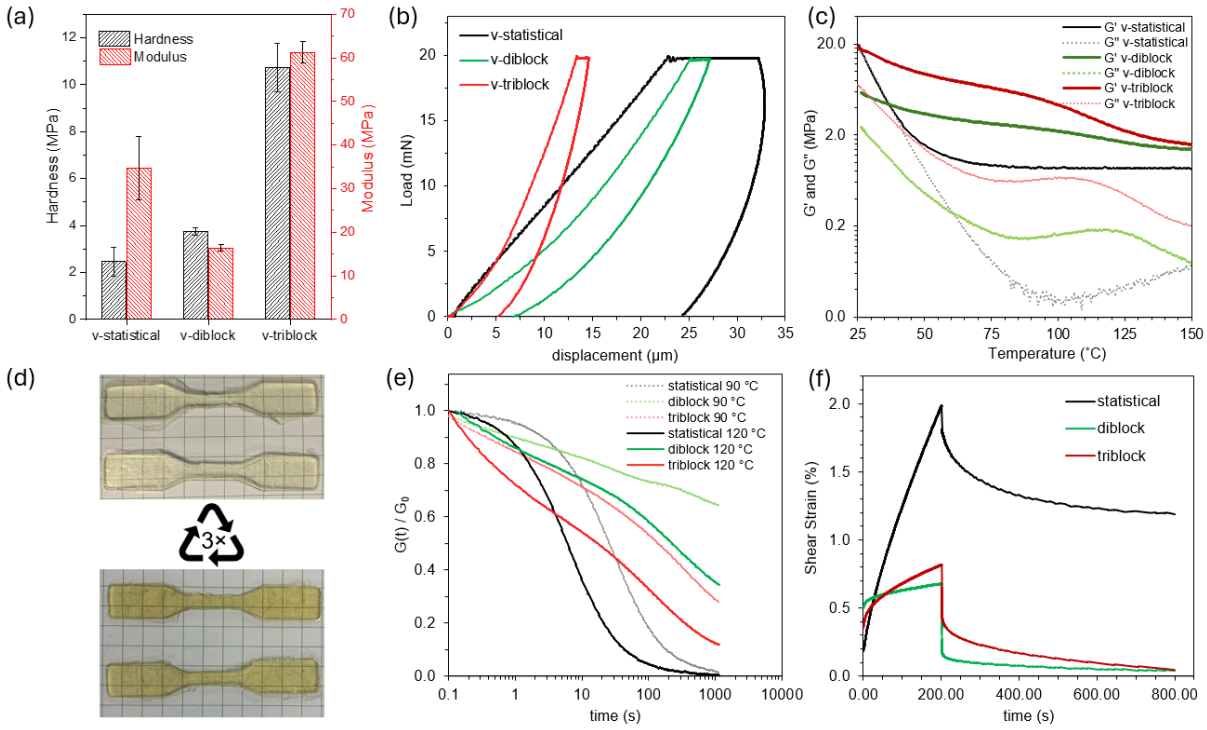

Figure 6.4 a) comparison of hardness and modulus and b) stress-strain behavior and creep from nanoindentation of vitrimers c) comparison of DMTA data of vitrimers d) images of pristine and R×3 v-triblock, e) Comparison of the stress-relaxation of statistical, diblock, and triblock vitrimers at 90 and 120 °C; vitrimers underwent relaxation in the order of v-statistical > v-triblock > v-diblock. f) Comparison of creep-recovery of statistical, diblock, and triblock vitrimers at 130˚C.

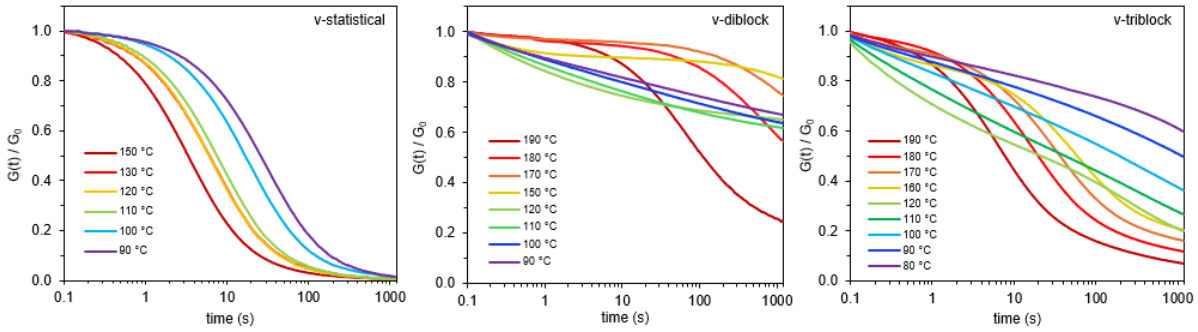

Figure 6.5 Stress relaxation behavior of v-statistical (left), v-diblock (middle) and v-triblock (right) at various temperatures.

6.5. Conclusion

In this work, we investigated the impact of block copolymer precursors and order-disorder transitions as design variables in the development of vitrimers. Specifically, our focus on suppressing creep, a major performance issue in vitrimers, while simultaneously enhancing tensile properties. To achieve this, vitrimer precursors from novel AB-type "*hard-soft"* diblock and ABA-type "*hard-soft-hard*" triblock terpolymers of MMA, C13MA, VMA were synthesized. We employed RAFT polymerization to obtain precursors with comparable molecular weights and compositions, but varying topologies. Vitrimers were cured through a Schiff-based reaction between aldehydes of VMA and the diamine Priamine 1075.

Microphase separation was confirmed via AFM, SAXS, and DSC. Swelling and ATR-FTIR tests, alongside rheological studies verified the formation of networks. The imine bond metathesis facilitated mechanical recyclability, allowing for at least 3 cycles of grinding and hot pressing at 120 °C without compromising the thermomechanical properties. Compared to statistical vitrimers, triblock networks exhibited improved tensile properties while diblock vitrimes showed lower stress and strain at break. More importantly, vitrimers with microphase separated structures, showed approximately 38% smaller creep under constant 1 MPa stress. Based on our findings, we believe that optimizing order disorder transition can be leveraged for the development of creep-resistant and reprocessable dynamic networks.

6.6. Supporting information for Chapter 6

6.6.1. Experimental methods and instrumentation

Materials

All chemicals were of reagent grade and used as received unless otherwise noted. Azobisisobutyronitrile (AIBN, Millipore Sigma, 98%) was recrystallized from methanol (≥99.8%, Millipore Sigma) and dried in vacuum prior to use. 2-cyano-2-propyl benzodithioate (RAFT agent, >97%) was purchased from Sigma Aldrich. C13-methacrylate (C13MA, Evonik) and methyl methacrylate (MMA, Millipore sigma) were passed through a column of basic alumina with 5 wt% calcium hydride (90-95%, Millipore Sigma) to remove inhibitor and stored in a refrigerator under a head of nitrogen prior to use. Ethyl acetate (≥ 99.5%), 1,4-dioxane (≥ 99.0%), dichloromethane (DCM, (≥ 99.0 %), hexanes (≥ 99.0 %), tetrahydrofuran (THF, HPLC grade), anhydrous magnesium sulfate ($MgSO_4$), were purchased from Fisher. 4-dimethylaminopyridine (DMAP), methacrylic anhydride, and vanillin were procured from Millipore Sigma. Priamine 1075 was purchased from Cargill.

6.6.2. Instrumentations and methods

Nuclear Magnetic Resonance (NMR) ^1H NMR analyses were performed in deuterated chloroform ($CDCl_3$) using a Bruker 500 MHz NMR spectrometer at a temperature of 25 °C with 16 scans. DOSY NMR measurements were performed in CDCl3 solution at 25 °C on a Varian Inova 500 MHz NMR spectrometer with a stimulated echo sequence, 15 increments, and 16 scans per increment. The gradient strength of 46.98 G/mm was logarithmically incremented from 2% up to 80% of the maximum gradient strength. The gradient pulse length was 2 ms (one-half of bipolar pulse pair) in order to ensure full signal attenuation. All measurements were performed with a compromise diffusion delay D of 700 ms in order to keep the relaxation contribution to the signal attenuation constant for all samples.

Attenuated total reflection (ATR)-Fourier Transform Infrared (FTIR) was performed on a Thermo Scientific Nicolet iS50 FTIR Spectrometer equipped with a diamond ATR. For each sample, 32 scans were performed over the range of 4000- 400 cm^{-1}.

Atomic Force Microscopy AFM was performed on a Cypher VRS SPM (Asylum Research – Oxford Instruments) in air and tapping mode for phase and amplitude imaging.

Gel Permeation Chromatography (GPC)

The number average molecular weight (M_n) and dispersity ($Đ = M_w/M_n$) of the polymers were estimated with an Agilent 1260 Infinity II SEC using HPLC-grade THF as the eluent at 40 °C and the flow rate of 0.3 mL/min. The GPC system was equipped with a PolyPore guard column (50 x 4.6 mm), an Agilent 1260 Infinity II multi-detector (G7800A) detector, and two PolyPore columns (250 x 4.6 mm). Poly(methyl methacrylate) (PMMA) standards (Varian) were used for the calibration of molecular weights.

Thermogravimetric Analyses (TGA) were carried out on a TA Instrument Discovery 5500 machine with platinum pans. The prepolymers and vitrimers were heated at a rate of 15 ℃/min from 25 ℃ to 700 ℃. TA Instruments TRIOS software was utilized to record and analyze the data.

Differential Scanning Calorimetry (DSC) was carried out on a TA Instruments Discovery 2500 instrument equipped with refrigerated cooling system (RSC 90) using aluminum hermetic pans with a pinhole. Calibrations for temperature and heat flow were conducted using indium and benzoic acid standards, respectively. Samples were analyzed with temperature ramps of -90 ℃ to 150 ℃ using a heat/ cool/ heat procedure with a heating rate of 15 ℃/min and cooling rate of 5 ℃/min. The glass transition temperatures (T_g) were calculated using the curve inflection point of the second heating ramp using the TRIOS sofware.

Dynamic thermal mechanical analysis (DTMA) and Rheology An Anton Paar MCR 302 rheometer was used for all tests. DTMA tests were performed with solid rectangular fixture (SFR 12). Rectangular-shaped neat and 4×recycled vitrimers (60 mm length, 10 mm width, and 2 mm thickness) were heated from room temperature to 150 °C at the rate of 4 °C/min, frequency of 1 Hz, and amplitude of 0.05%. All rheological tests were conducted using a 25 mm parallel plates geometry with the normal force of ~5N. Strain sweep tests were carried out at 90 to 130 °C to determine the linear viscoelastic region (LVR) at 1 Hz. Frequency sweep tests were performed at 120 °C and 0.1% strain. Stress-relaxation experiments were conducted at 0.05% strain at the desired temperatures. Creep-recovery experiments were performed at 1000 Pa for 200 s, followed by 0 Pa for 600 s, total experiment time being 800 s.

Nanoindentation tests were conducted using a Nanovea M1 Hardness Tester instrument equipped with a Berkovich tip. The load of 20 mN was applied at an approaching speed of 2.5 μN/min, with loading and unloading rates of 20 mN/min and 40 mN/min, respectively. A pause of 30 s was

inserted between loading and unloading for creep test. The experiments were carried out at three different locations for each samples. The hardness was calculated using a Nanovea software.

Swelling and gel fractions were determined by immersing the vitrimers in excess ethyl acetate for at least 24 h at room temperature. Subsequently, the swollen samples were filtered, dabbed with delicate task wipes to remove excess solvent and weighed to find the swelling ratio. Afterwards, the samples were dried in a vacuum oven at reduced pressure and ~ 50 °C overnight and weighted again. Gel fraction was calculated using equation S1 where m_0 is the original mass of the sample and m_2 is the mass of dried sample after swelling. The swelling ratio was determined using equation S2 in which m_0 and m_1 are representing the original and swollen mass of the sample, respectively.

$$Gel(\%) = \frac{m_2}{m_0} \times 100\% \qquad (Eq.1)$$

$$Swelling\ ratio(\%) = \frac{m_1 - m_0}{m_0} \times 100\% \qquad (Eq.2)$$

Small-angle X-ray scattering (SAXS) measurements were conducted using a SAXSpoint 2.0 instrument (Anton Paar) equipped with a Cu K-alpha radiation source (wavelength, λ = 1.54 Å) and an Eiger R 1M (Horizontal) detector and distance was 1075.9 mm. Vitrimer samples, ~ 1 mm thick, were positioned on a solid sample holder (10 by 10 mm) provided by Anton Paar, secured with tape. Each experiment was exposed to X-rays for 30 minutes per frame, totaling four frames per experiment.

UV-visible spectrophotometry was carried out using a Thermo Scientific Evolution 300 and the scanning range of 380–780 nm.

6.6.3. Monomers and polymers synthesis and characterizations

6.6.3.1 Synthesis of vanillin methacrylate

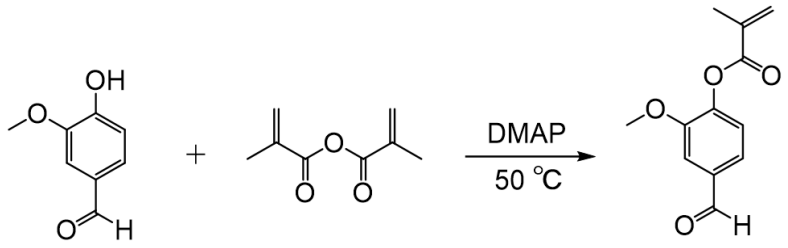

Figure S 6.1 Synthetic route of vanillin methacrylate (VMA) from vanillin and methacrylic anhydride.

Vanillin methacrylate (VMA), was synthesized through a Steglich esterification reaction following a procedure described by Zhang et al. [196]. Accordingly, in a round bottom flask, vanillin (1 eq., 32.8 mmol, 5 g), methacrylic anhydride (1.01 eq., 33.2 mmol, 5.12 g) and 4-dimethylaminopyridine (DMAP, 0.05eq., 9.8 mmol, 0.2g) were added, stirred, and sparged with nitrogen for 2 hours. While still under nitrogen atmosphere, the system was stirred overnight at room temperature. Afterwards, the temperature was increased to 50 °C and the solution was stirred vigorously for 24 additional hours. The final mixture was dissolved in dichloromethane and washed four times with saturated sodium bicarbonate aqueous solution. The separated organic phase was washed with a solution of NaOH (1 M), then with an aqueous solution of HCl at 5 wt% and finally with brine. After drying the organic solution over $MgSO_4$, filtration, concentrate with rotary evaporation and drying in a vacuum oven at 50 °C overnight, the obtained solid was recrystallized in hot hexane to obtain VMA as a white flaky powder.

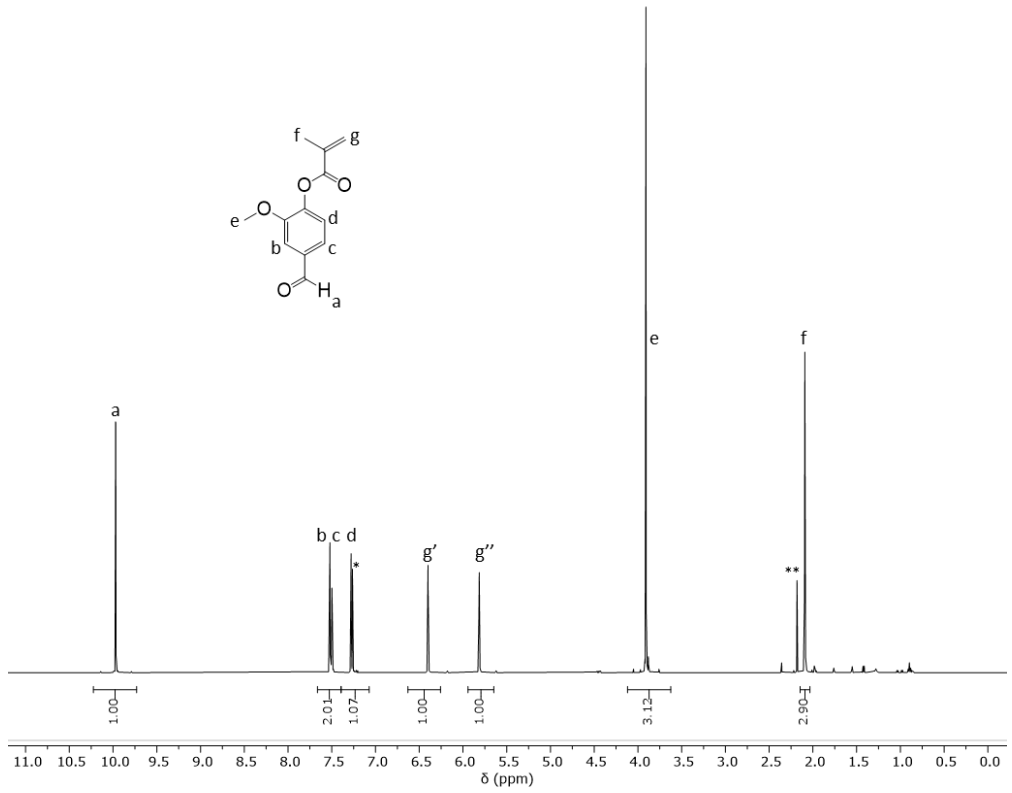

Figure S6.2 ^{1}H-NMR spectrum of vanillin methacrylate (VMA). (* $CDCl_3$, ** acetone, from 0.83 to 2 ppm impurities from methacrylic anhydride).

Polymer synthesis

6.6.3.2 Synthesis of statistical terpolymer p(MMA-co-C13MA-co-VMA): p-statistical

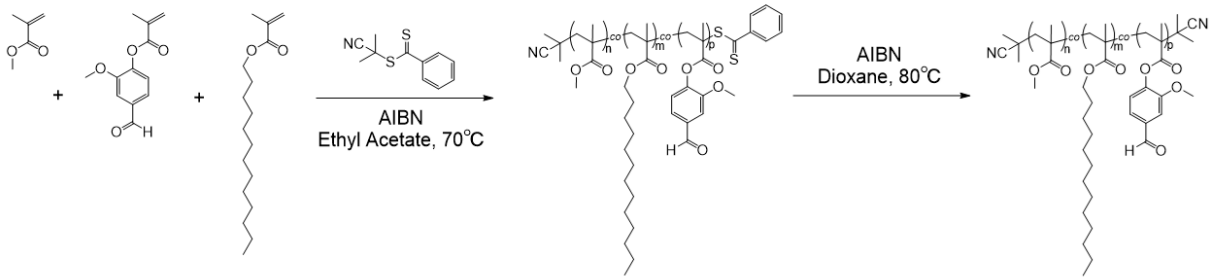

Figure S6.3 Synthesis of p-statistical via RAFT and subsequent chain end removal using AIBN.

MMA (6.80 g, 25.3 mmol) C13MA (11.00 g, 51.3 mmol), VMA (2.20 g, 22.6 mmol), 2-cyano-2-propyl benzodithioate (CPB RAFT CTA, 163.5 mg, 0.74 mmol), and azobisisobutyronitrile (AIBN, 36.39 mg, 0.22mmol, $nAIBN/nCPB$ = 0.3) and ethyl acetate (20 g, 50 wt%) were added

to a 3-neck round bottom flask equipped with a stirring bar and an overhead condenser (kept at 5 ˚C). The solution was purged with nitrogen (N_2) and submerged into a preheated oil bath at 70 °C for 24 h. The targeted M_n at 100% conversion was 27,300 g/mol. The obtained polymer was precipitated into methanol resulting in a pink viscous liquid (15.6 g, yield = 77.4%). The statistical terpolymer (15 g, 1 eq.) terminated with the benzodithioate moiety was dissolved in 1,4-dioxane (60 mL) prior to the addition of AIBN (2.3 g, 20 eq.). The solution was heated to 80 °C under N_2 overnight, and p-stat was precipitated into methanol yielding a white viscous liquid. From ^{1}H NMR, F_{VMA} = 0.11 and from GPC, M_n = 24,700 g/mol with $Đ$ = 1.20.

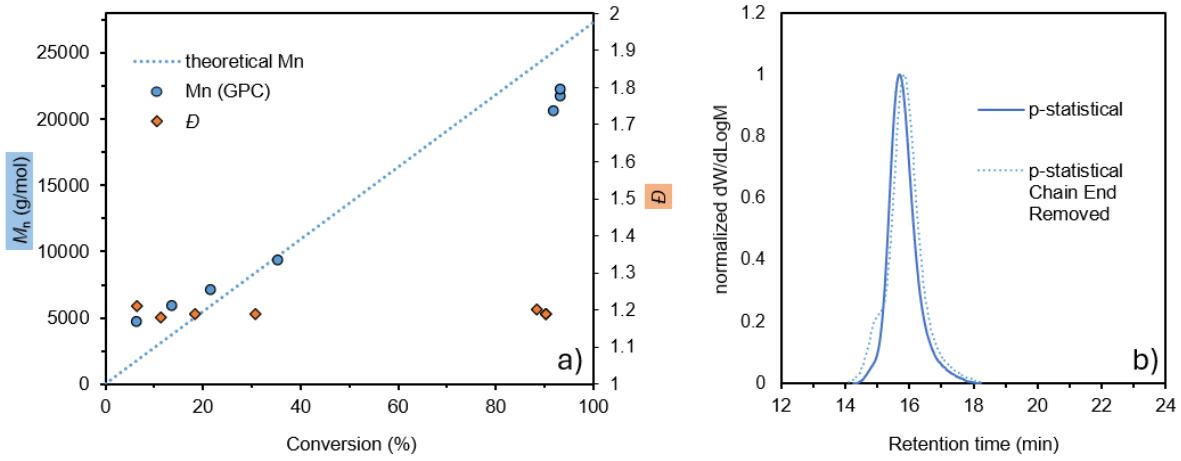

Figure S6.4 a) M_n (blue circles), theoretical M_n line and $Đ$ (orange diamonds) versus monomer conversion for the polymerization of p-statistical. b) GPC traces of p-statistical, before and after removal of the RAFT CTA moiety.

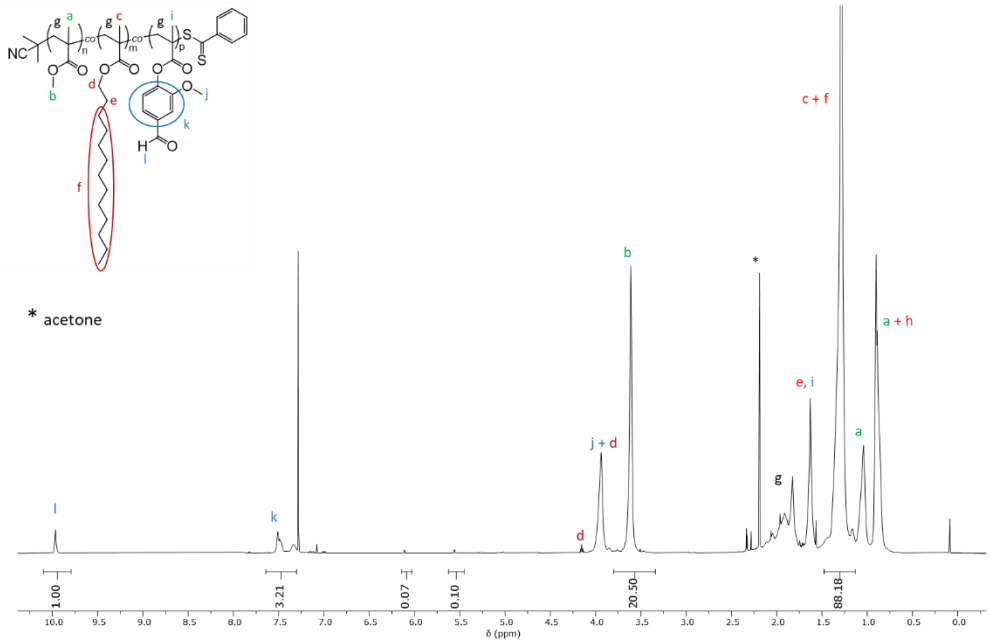

Figure S6.5 ^{1}H-NMR spectrum of p-statistical before chain-end removal in $CDCl_3$.

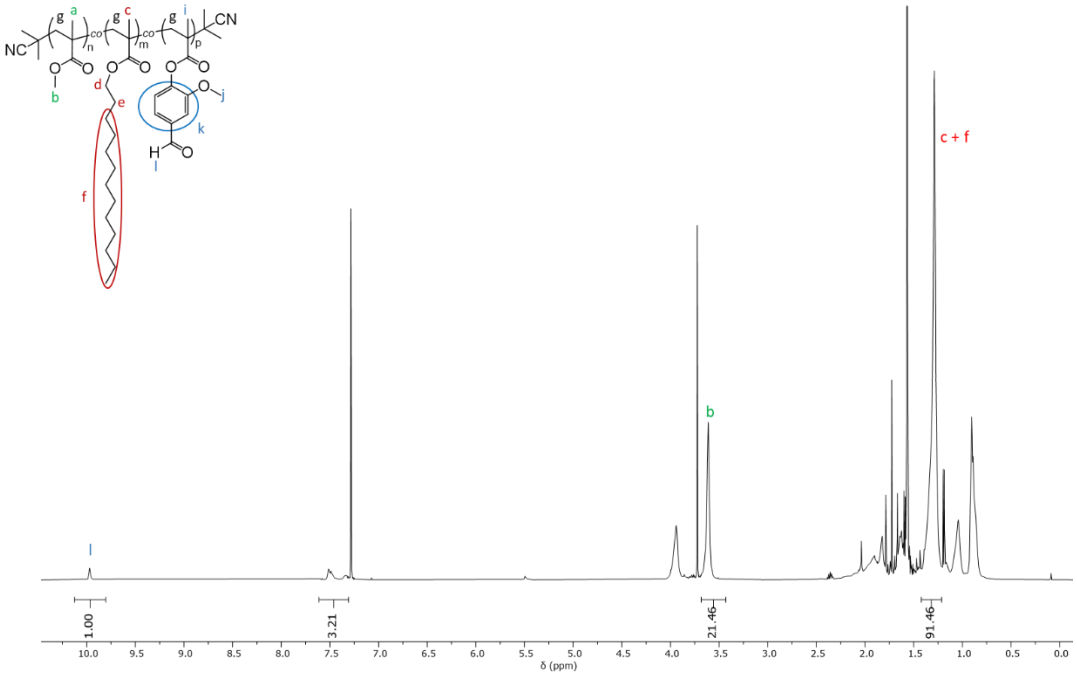

Figure S6.6 ^{1}H-NMR spectrum of p-statistical after chain-end removal in $CDCl_3$.No change in the polymer's composition was observed.

6.6.3.3 Synthesis of p(MMA)-*b*-p(C13MA-*co*-VMA) : p-diblock

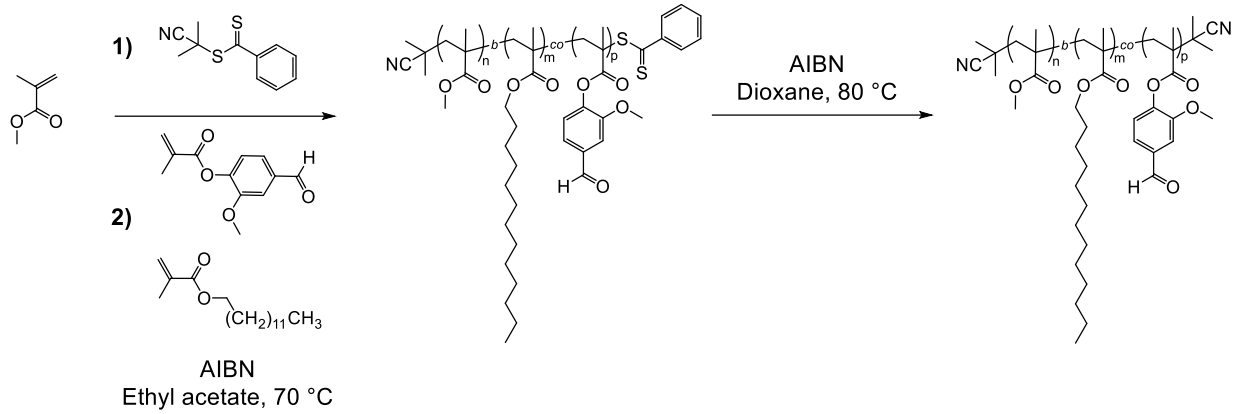

Figure S6.7 Two-step synthesis of p-diblock terpolymer: Two step synthesis of p-diblock terpolymer: 1) homopolymerization of PMMA macroinitiator, 2) chain extinction with VMA and C13MA, and subsequent chain end removal.

MMA (20 g, 199 mmol), CPB (0.453, 2 mmol.), and AIBN (101 mg, 0.61 mmol, $\frac{n_{AIBN}}{n_{CPB}} = 0.3$) were added to a Schlenk flask containing ethyl acetate (40 mL). The solution was purged with nitrogen (N_2) and submerged into a preheated oil bath at 70 °C for 24 h. The obtained PMMA homopolymer was precipitated into methanol resulting in a pink viscous liquid (17.7 g, yield = 88%, M_n = 10,500 g/mol and $Đ$ = 1.17).

PMMA macro-RAFT agent (17.7 g, 2.2 mmol), VMA (6.6 g, 30 mmol), C13MA (37.6, 140 mmol) and AIBN (72.6 mg, 0.44 mmol, $\frac{n_{AIBN}}{n_{CPB}} = 0.2$) were added to a Schlenk flask containing 130 mL of ethyl acetate. The solution was purged with nitrogen (N_2) and submerged into a preheated oil bath at 70 °C for 21h. The obtained polymer p-diblock was precipitated into methanol resulting in a pink viscous liquid (53.14 g, yield = 85.8%).

p-diblock (10, 0.38 mmol) terminated with the benzodithioate moiety was dissolved in 1,4-dioxane (50 mL) prior to the addition of AIBN (1.2 g, 20 eq.). The solution was heated at 80 °C under N_2 overnight, and p-diblock was precipitated into methanol yielding a white viscous liquid. The F_{VMA} = 0.12 and M_n = 27,700 g/mol.

6.6.3.4 Synthesis of first block of PMMA homopolymer

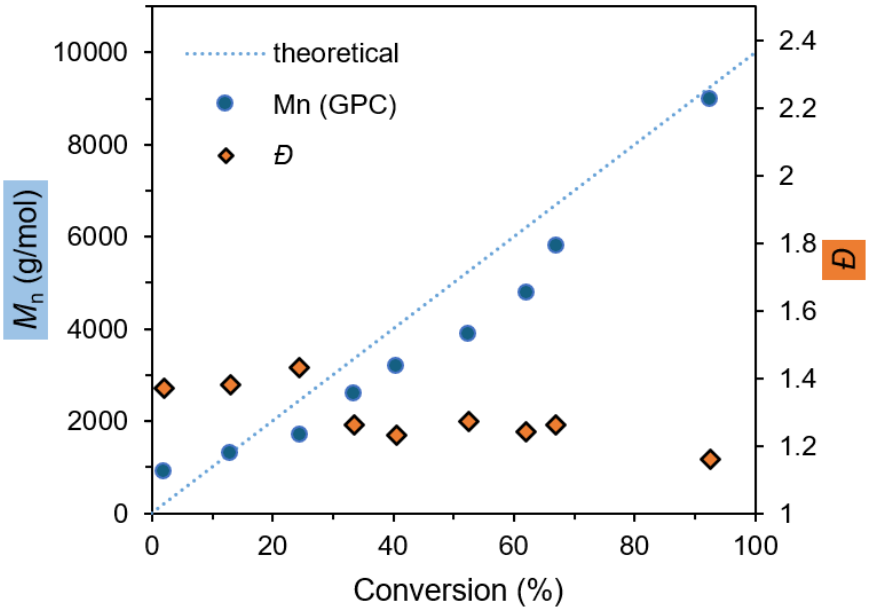

Figure S6.8 M_n (blue circles) and $Đ$ (orange diamonds) from GPC versus monomer conversion from ^{1}H NMR for the photopolymerization MMA macroinitiator block.

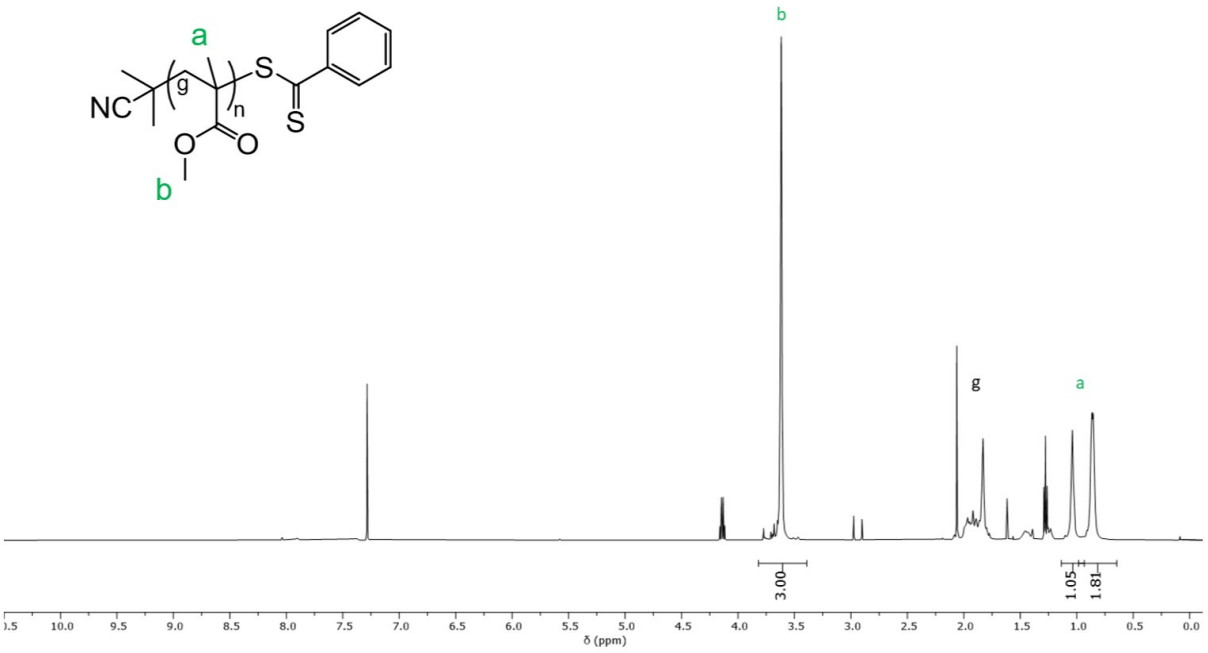

Figure S6.9 ^{1}H-NMR spectrum of PMMA homopolymer, the first block copolymer segment used for subsequent chain extensions, in $CDCl_3$.

6.6.3.5 Second block: PMMA-b-P(C13MA-co-VMA)

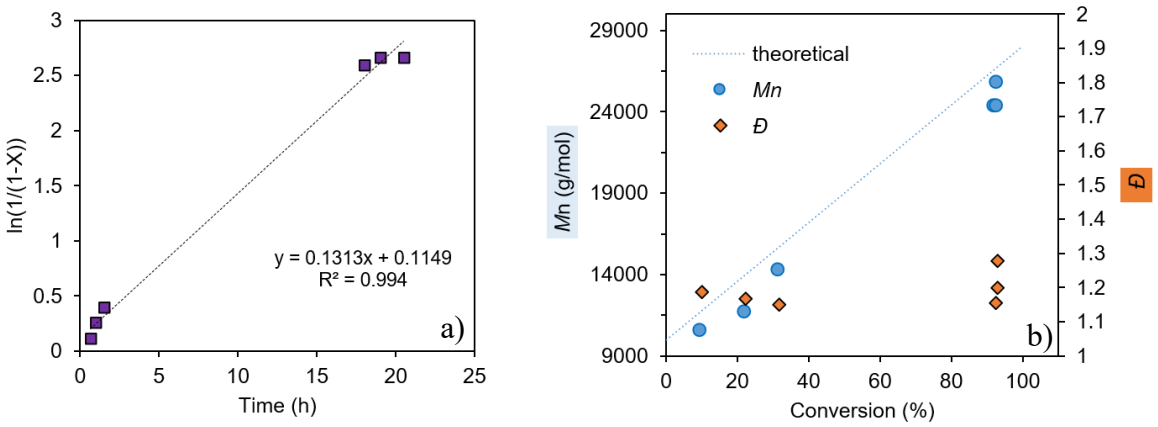

Figure S6.10 . Chain extension polymerization and growth of the second block of p-diblock which was performed over night: a) Pseudo-first order kinetics plot for the polymerization and b) M_n (blue circles), theoretical targeted M_n, and $Đ$ (orange diamonds) versus monomer conversion.

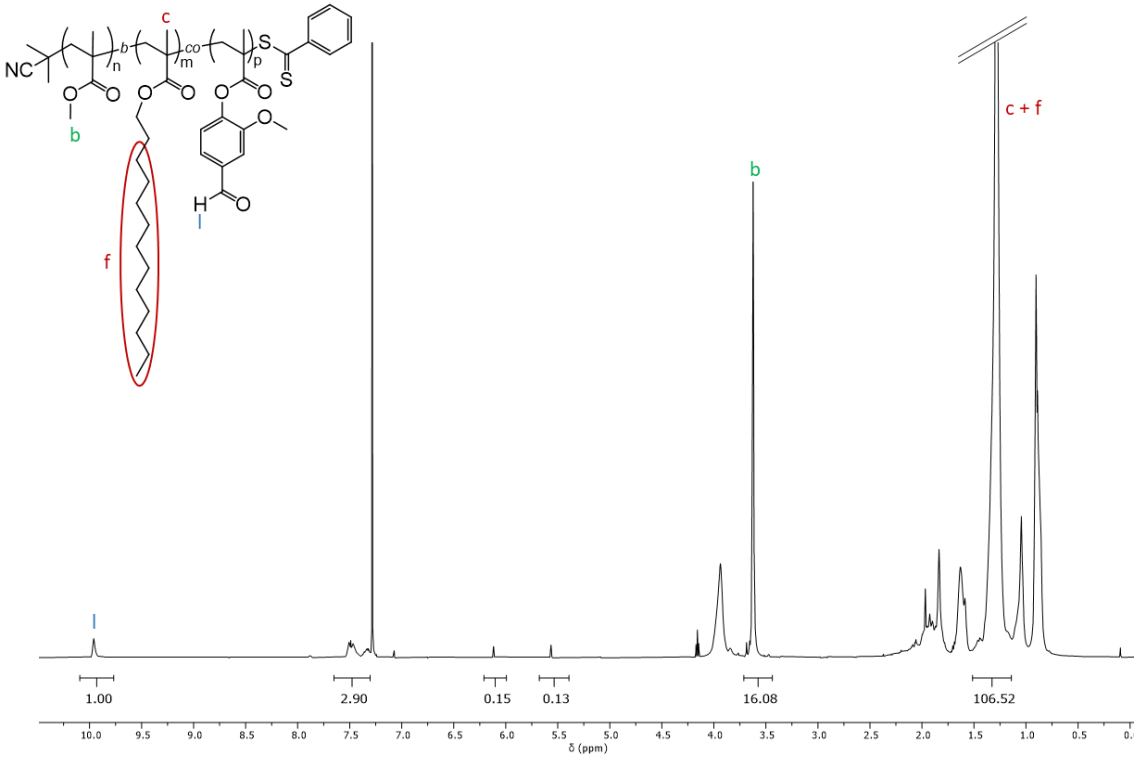

Figure S6.11 ^{1}H-NMR spectrum of p-diblock before chain-end removal in $CDCl_3$.

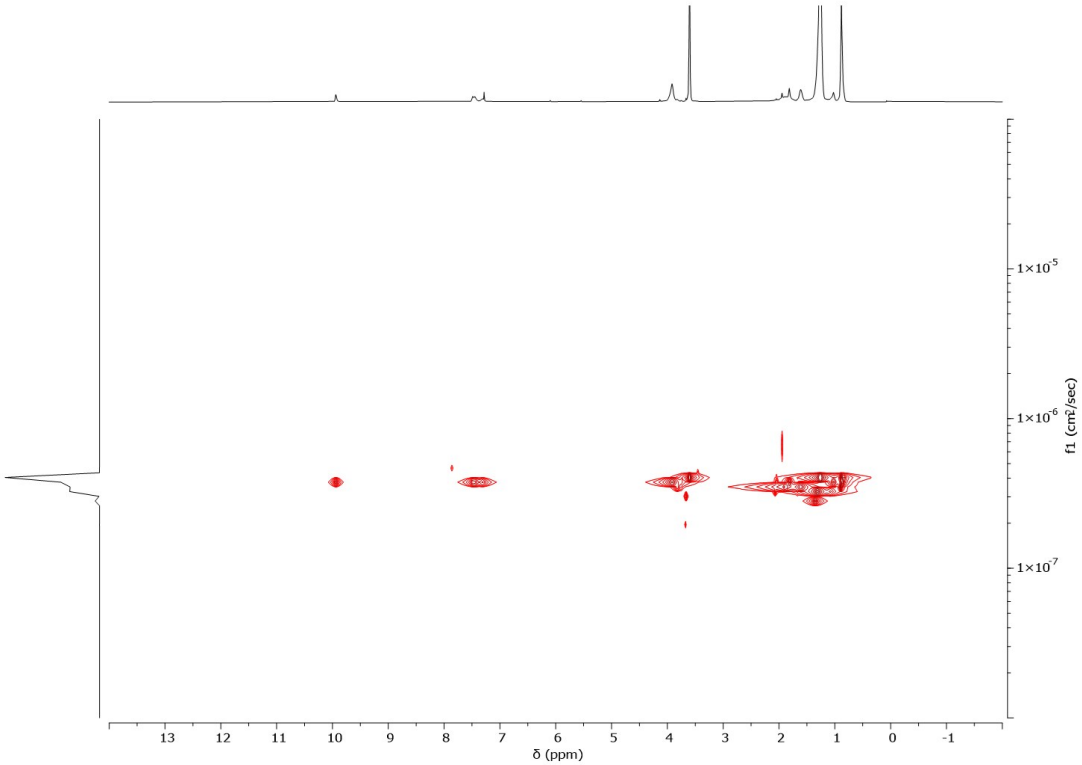

Figure S6.12 DOSY-NMR spectrum of p-diblock before chain-end removal in $CDCl_3$.

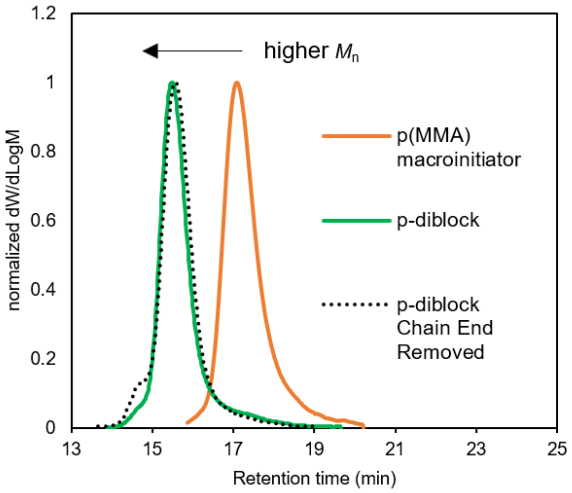

Figure S6.13 GPC traces of chain extension of PMMA macroinitiator (orange line) with C13MA and VMA to form p-diblock (green line), and subsequent removal of RAFT CTA moiety (dotted line); an small shoulder was observed after chain extension which did not affect the overall $Đ$ =1.23 *and* M_n = 27,800 g/mol.

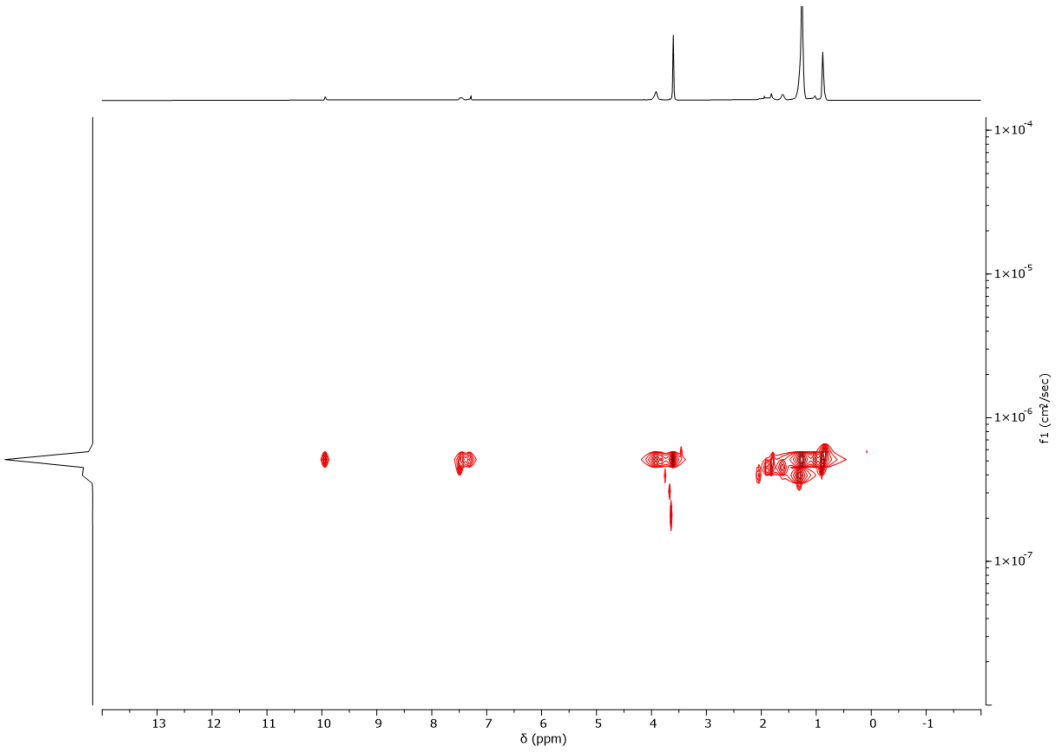

Figure S6.14 DOSY-NMR spectrum of p-diblock after chain-end removal in $CDCl_3$.

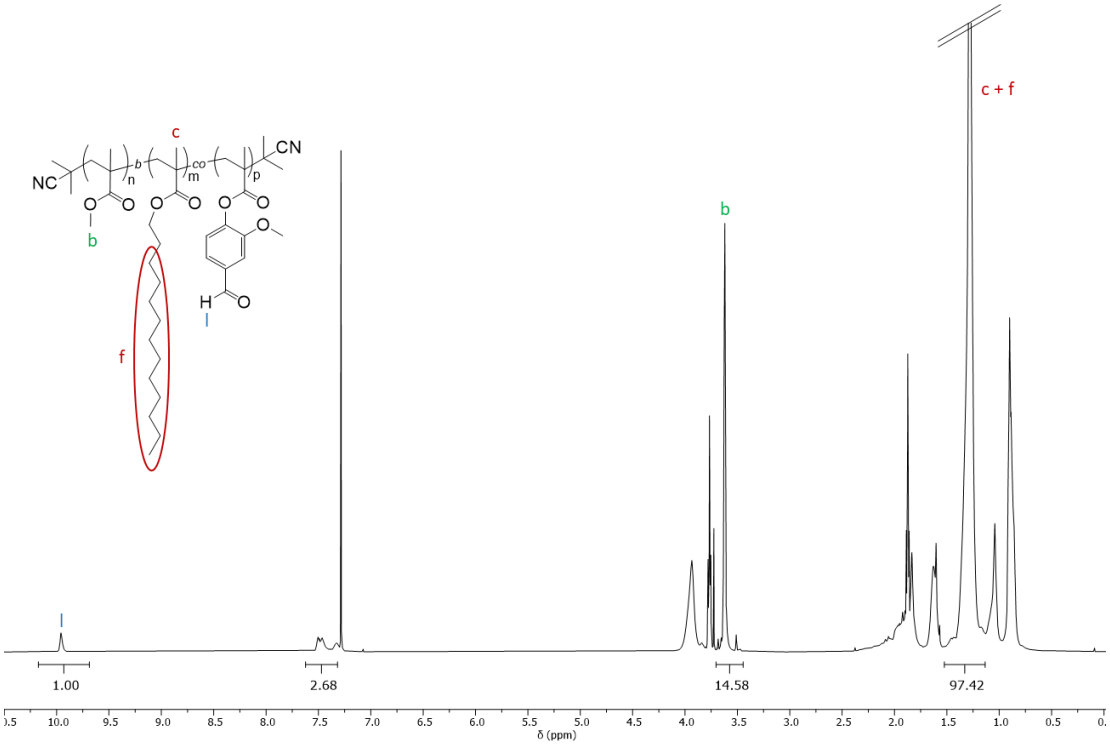

Figure S6.15 ^{1}H-NMR spectrum of p-diblock after chain-end removal in $CDCl_3$.

6.6.3.6 Synthesis of PMMA-*b*-P(C13MA-*co*-VMA)-*b*-PMMA: p-triblock

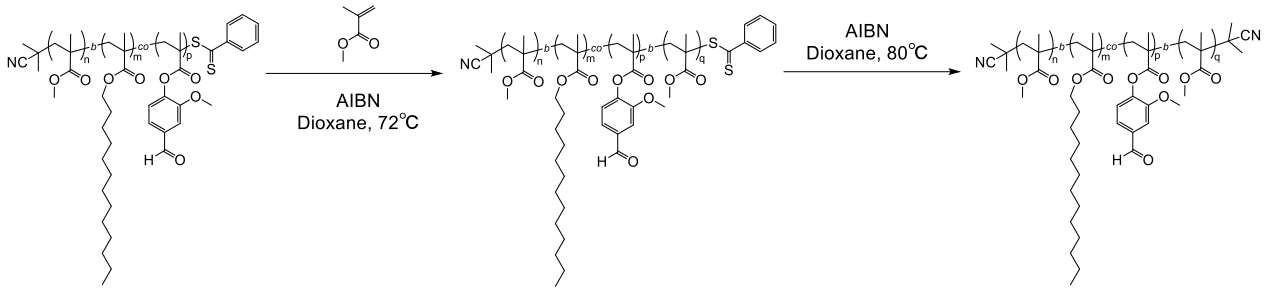

Figure S6.16 Chain extension of p-diblock with MMA to form p-triblock and subsequent chain end removal.

For the synthesis of the triblock p(MMA)-*block*-p(C13MA-*co*-VMA)-*block*-p(MMA), the synthesized p-diblock (10 g, 0.39 mmol), used as a macro-RAFT agent, MMA (3.9 g, 38.9 mmol), and AIBN (19.2 mg, 0.12 mmol, $\frac{n_{AIBN}}{n_{CPB}} = 0.3$) were dissolved in dioxane (30 mL) in Schlenk flask. The solution was purged with nitrogen (N_2) and submerged into a preheated oil bath at 75 °C for 24 h. The obtained p-triblock was precipitated into methanol resulting in a pink viscous liquid (28.8 g, yield = 96%) with M_n = 40,300 g/mol and $Đ$ =1.16 and X_{MMA} = 83%. Successful chain extension was confirmed by a clear monomodal shift of GPC traces towards higher M_n values. Similar to other prepolymers, chain end removal was performed. p-triblock (10, 0.25 mmol) terminated with the benzodithioate moiety was dissolved in 1,4-dioxane (50 mL) prior to the addition of AIBN (0.83 g, 20 eq.). The solution was heated at 80 °C under N_2 overnight, and p-triblock was precipitated into methanol yielding a white viscous liquid. The F_{VMA} =0.09 and M_n = 41000 g/mol and $Đ$ =1.14.

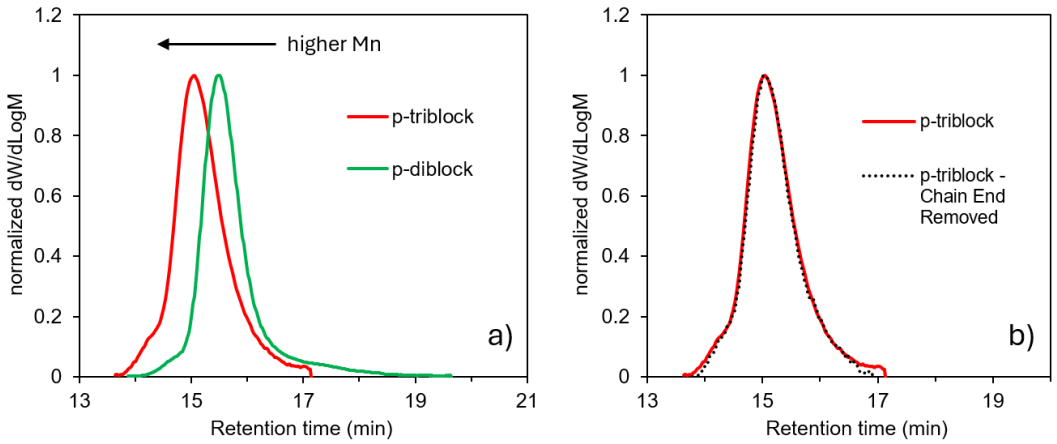

Figure S 6.17 GPC traces of a) p-triblock formed from chain extension of p-diblock a clear monomodal shift towards higher molecular weights was observed. b) comparison of the p-triblock prepolymer before and after removal of the RAFT CTA moiety. Chain end removal did not affect the molecular weight distribution of the p-triblock.

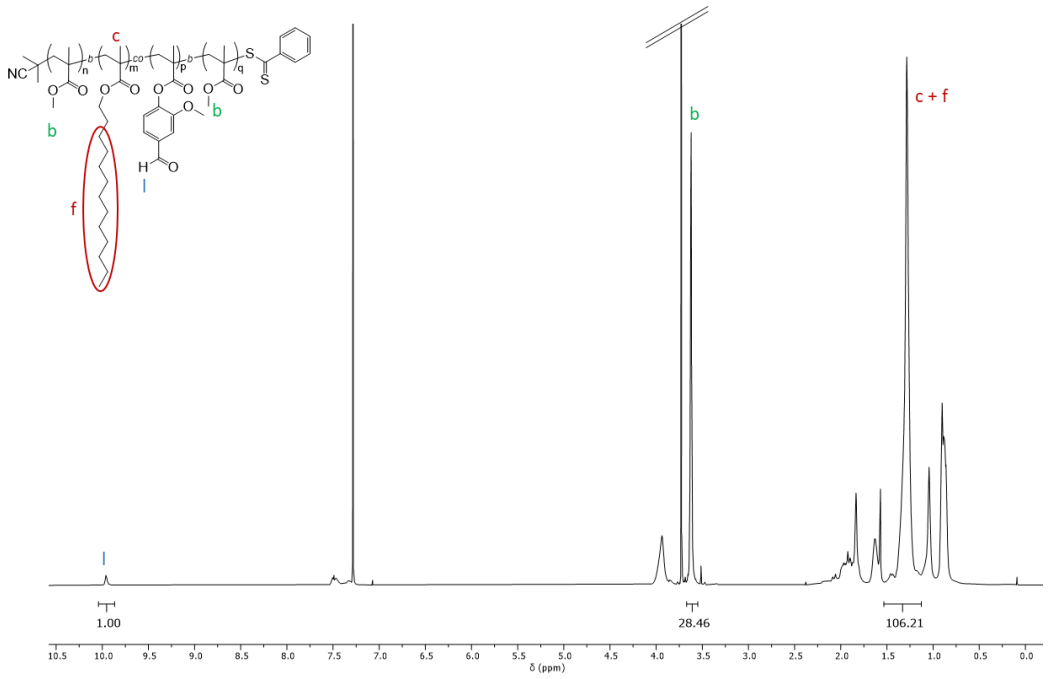

Figure S 6.18 ^{1}H-NMR spectrum of p-triblock before chain-end removal in $CDCl_3$.

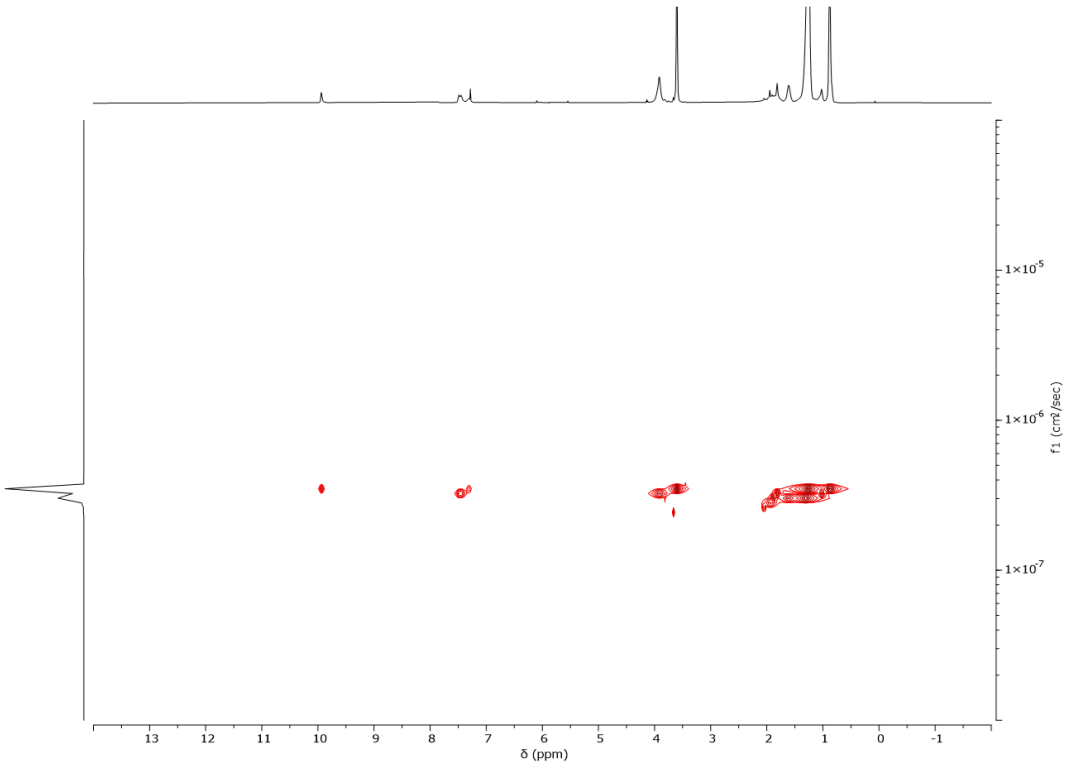

Figure S6.19 DOSY-NMR spectrum of p-triblock before chain-end removal in $CDCl_3$.Only a single distribution of polymers was observed.

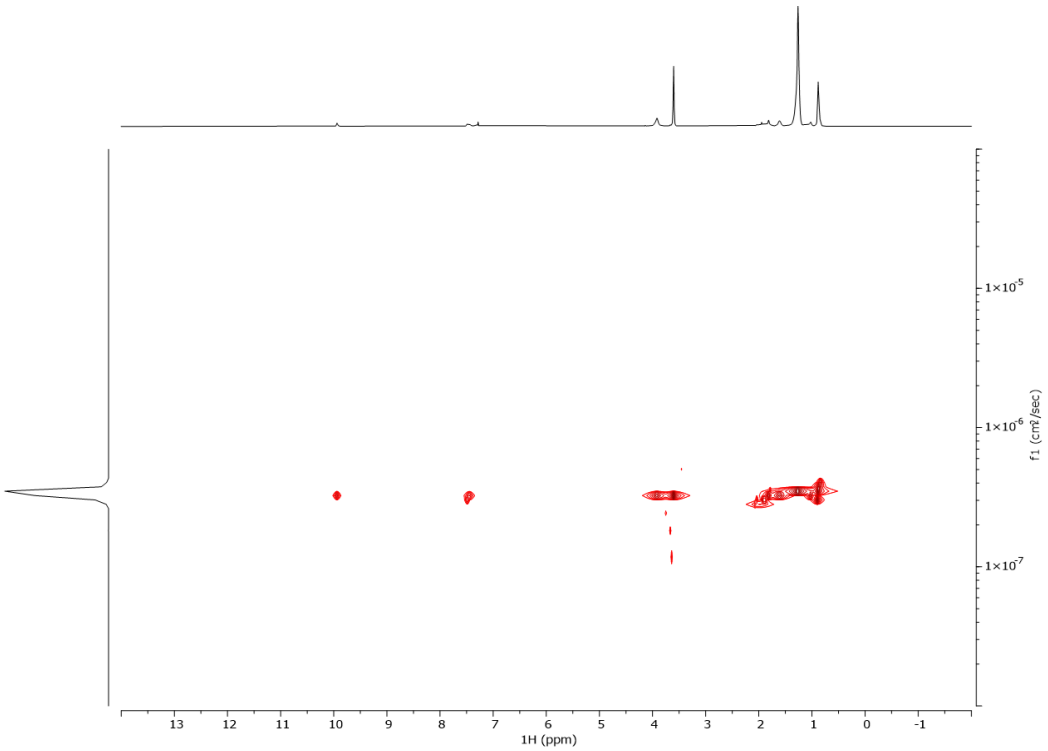

Figure S6.20 DOSY-NMR spectrum of p-triblock after chain-end removal in $CDCl_3$. Only a single distribution of polymers were observed. Proving formation of triblock copolymers an not separate blocks of homo polymers.

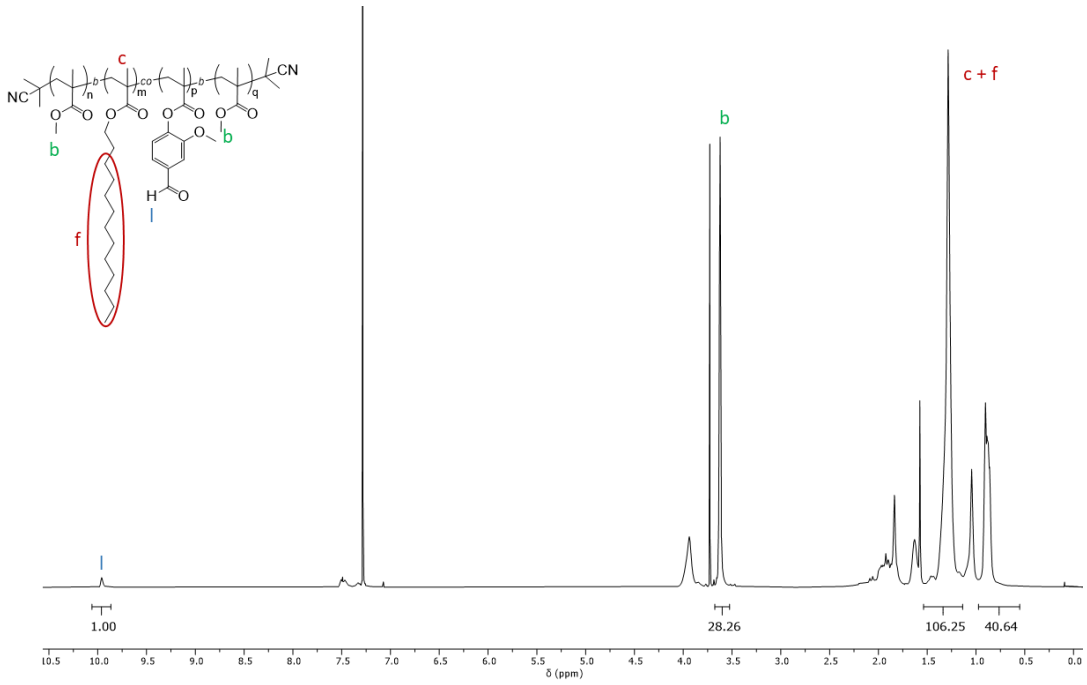

Figure S6.21 ^{1}H-NMR spectrum of p-triblock after chain-end removal in $CDCl_3$.

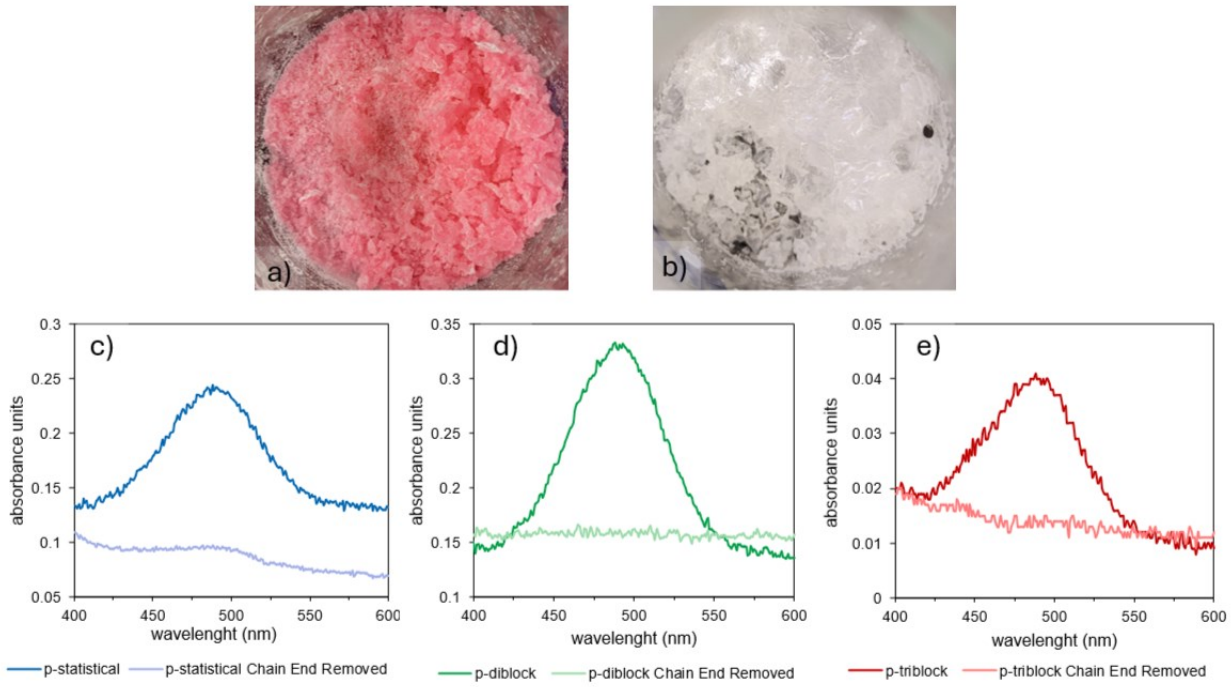

Figure S6.22 Chain-end removal of prepolymers: representative pictures of the a) prepolymers before the RAFT CTA removal (pink colored) and b) after the removal of the chain end moiety, noting the prepolymers become white or colorless. UV-VIS traces of p-statistical (c), p-diblock (d), and p-triblock (e) before (dark color) and after (light colors). Disappearance of the peak at 500 nm confirmed removal of the RAFT-CTA chain-end moiety.

6.6.3.7 ATR-FTIR

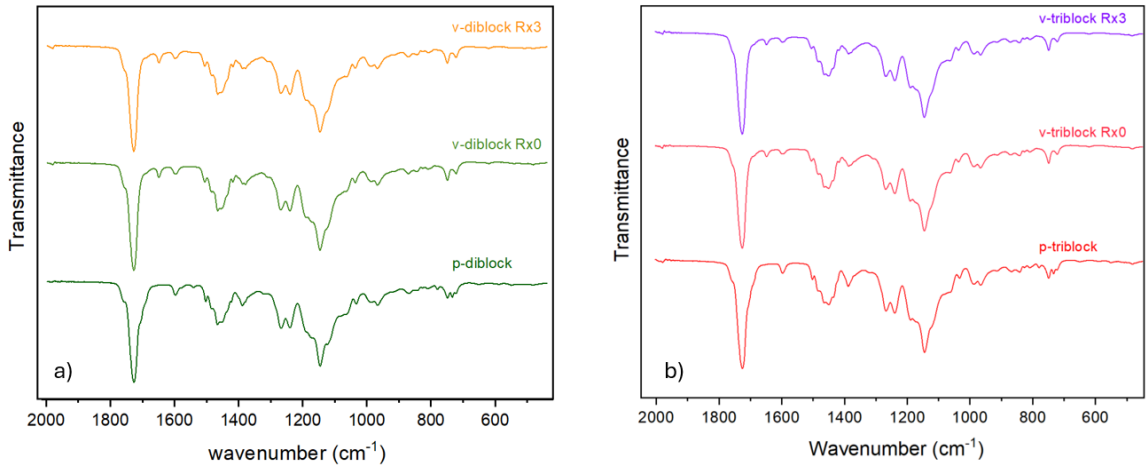

Figure S 6.23 ATR-FTIR spectra of diblock and triblock prepolymer, neat vitrimer, and 3× recycled vitrimer.

6.6.3.8 TGA

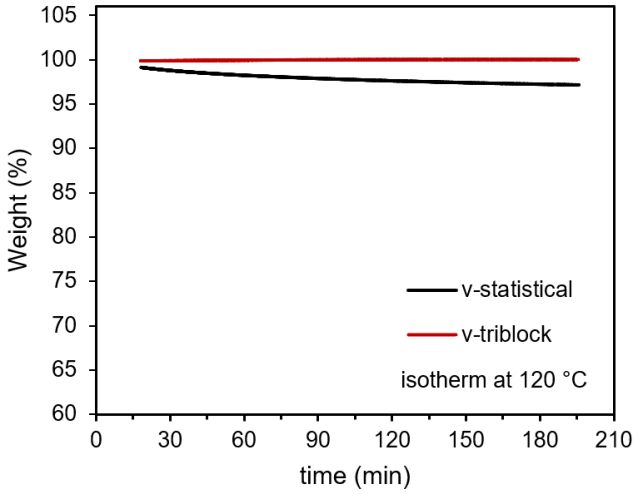

Figure S6.24 Isotherm TGA of the statistical and triblock vitrimers at 120 ˚C, after 3h less than 2% weight change was observed for both samples.

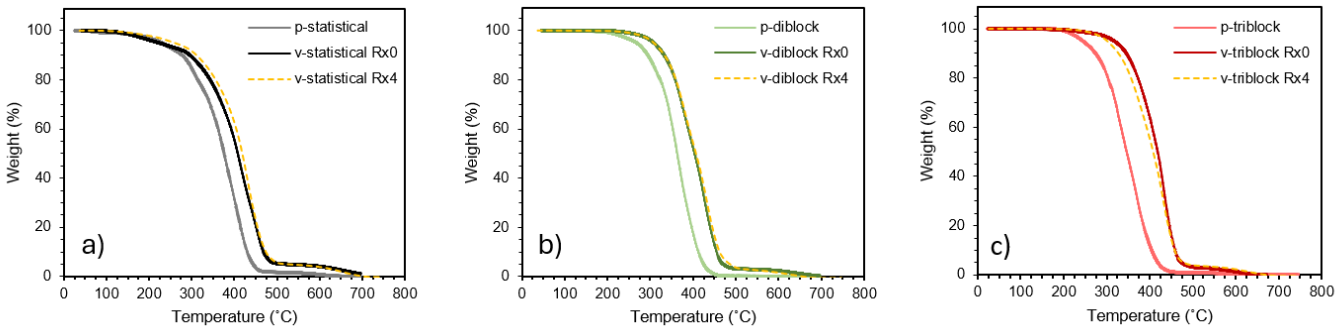

Figure S6.25 TGA of all prepolymer, pristine and ×4 recycled vitrimers.

6.6.3.9 Estimation of Flory-Huggins interaction parameter and order disorder transition

The Flory-Huggins interaction parameter (χ) was estimated to roughly quantify the compatibility of the C13MA-rich and MMA-rich blocks. Assuming that only enthalpic contributions are in effect without any entropic contributions we have:

$$\chi = \frac{\bar{V}}{RT}(\delta_{MMA} - \delta_{C13MA})^2$$

where $\bar{V} = \sqrt{V_{MMA}V_{C13MA}}$ is the reference molar volume, δ is the solubility parameter, R is the universal gas constant and T is temperature (K) [230,236]. The reported value of $\delta_{MMA} \approx 19.3 – 22.7$ MPa $^{0.5}$. δ_{C13MA} is not reported in the literature; however, based on the calculated values reported by Ruzette et al. for poly alkyl methacrylates as well as reported value of $\delta_{lauryl\ methacrylate}$ in the literature, δ_{C13MA} can be estimated to be ≈ 16.8 MPa $^{0.5}$,based on group contribution methods calculated elsewhere and findings of Ruzette et al.[161,174,213]. The reported molar volume for V_{MMA} and $V_{Lauryl\ methacrylate}$ are 106.1 and 293.8 cm^3/mol, respectively [237]. Thus, χ values of the p-diblock at 25 and 150 °C is roughly around 0.22 and 0.33 and the χN, where N is the total degree of polymerization, at 25 and 150 °C are roughly around 86 and 60, respectively [230,238].

6.6.3.10 Rheology

Amplitude sweep

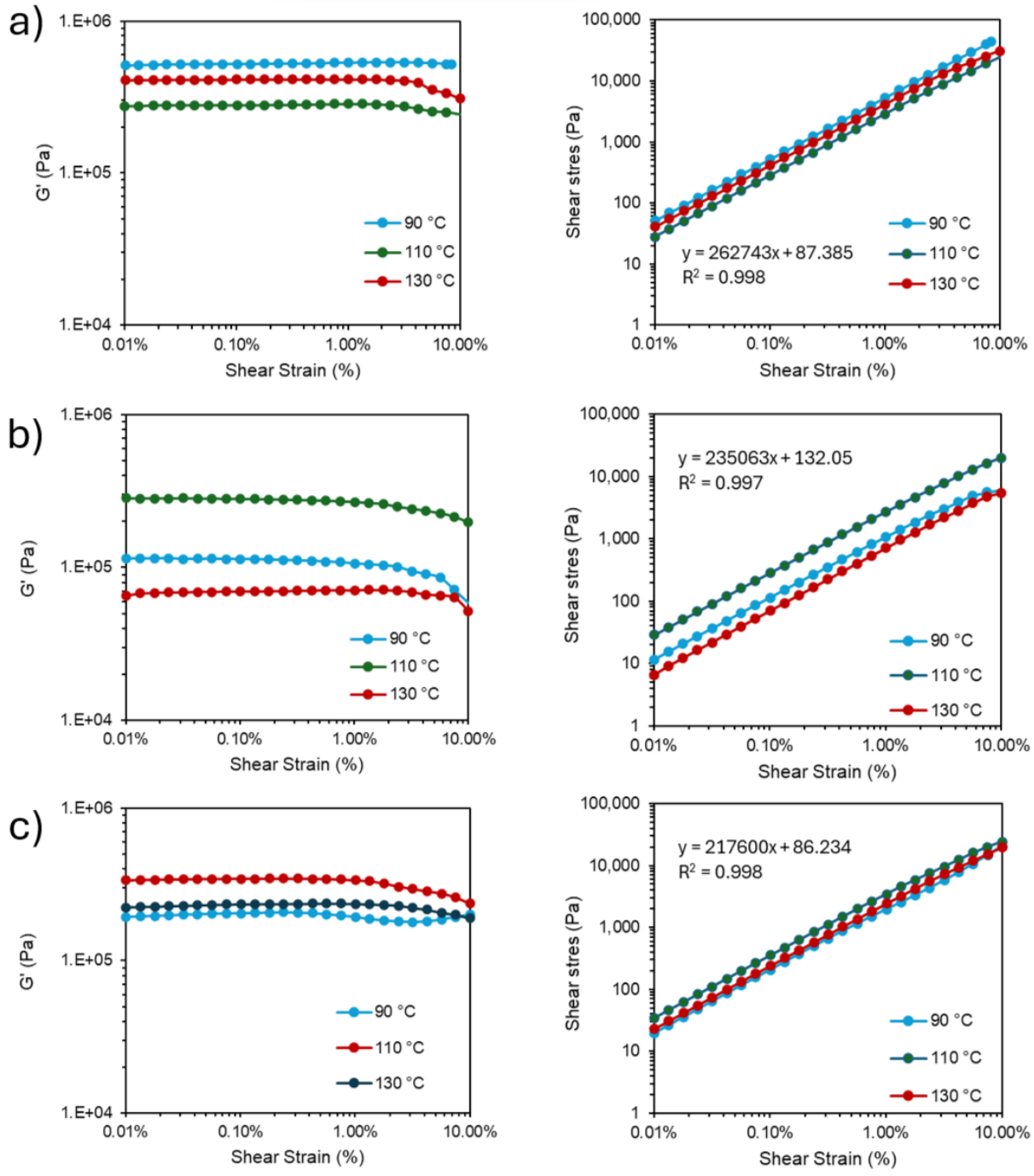

Figure S6.26 Strain sweep and linear viscoelastic region (LVR) of a) v-statistical, b) v-diblock, and c) v-triblock.

Frequency sweeps

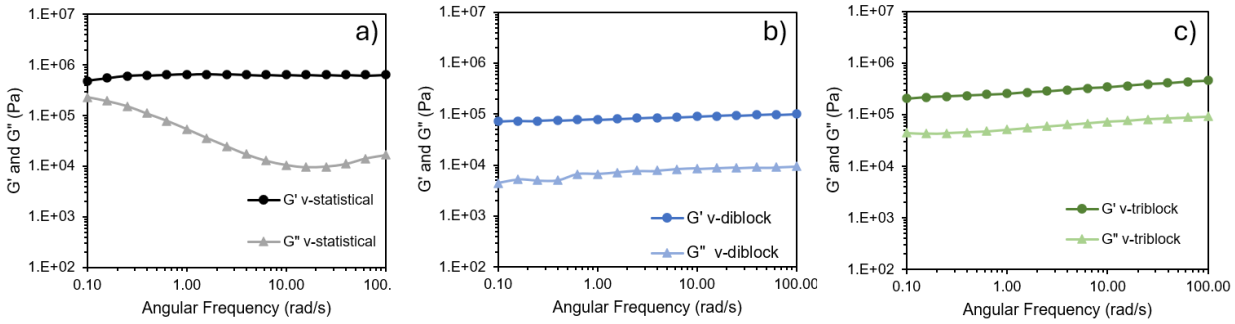

Figure S 6.27 Frequency sweeps of a) v-statistical b) v-diblock and c) v-triblock.

DMTA

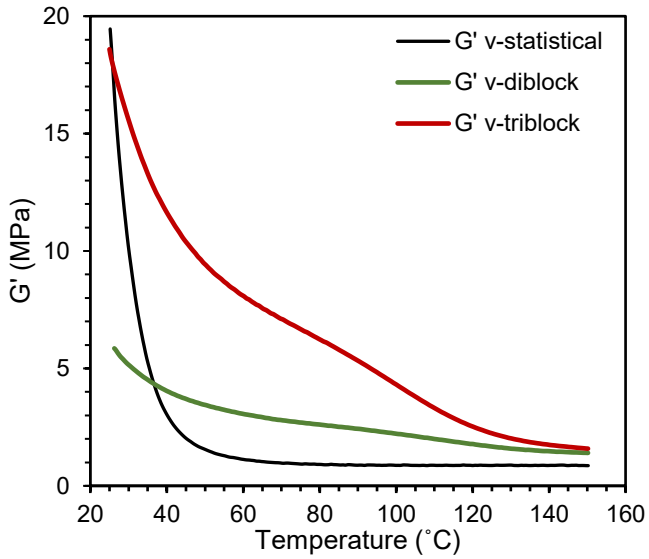

Figure S6.28 Elastic modulus (G') of three vitrimers in linear Y-axis for better presentation of dynamic thermal mechanical analysis (DMTA). The statistical vitrimers shows a sharp decrease in modulus around its $T_g \approx 30$ °C while the diblock and triblock vitrimers show T_g values of around 110 °C attributed to the PMMA microphase separated blocks.

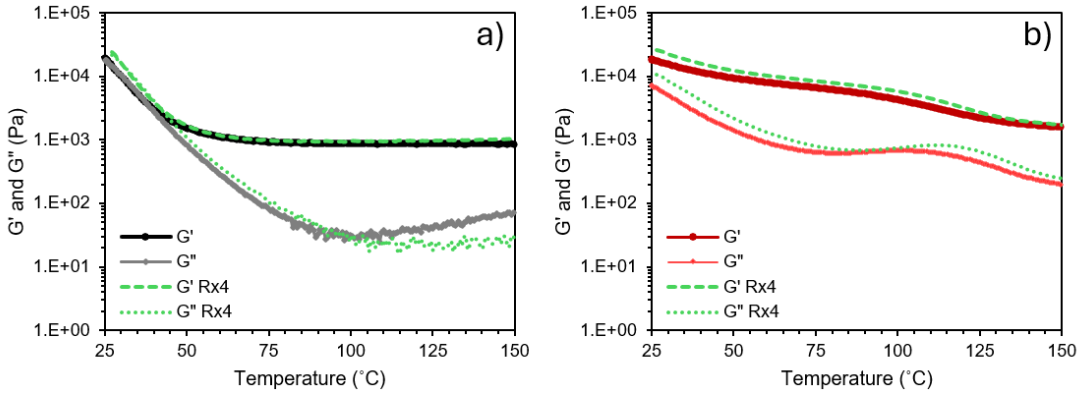

Figure S6.29 DMTA of a) v-statistical and b) v-triblock before and after ×4 recycling

Creep

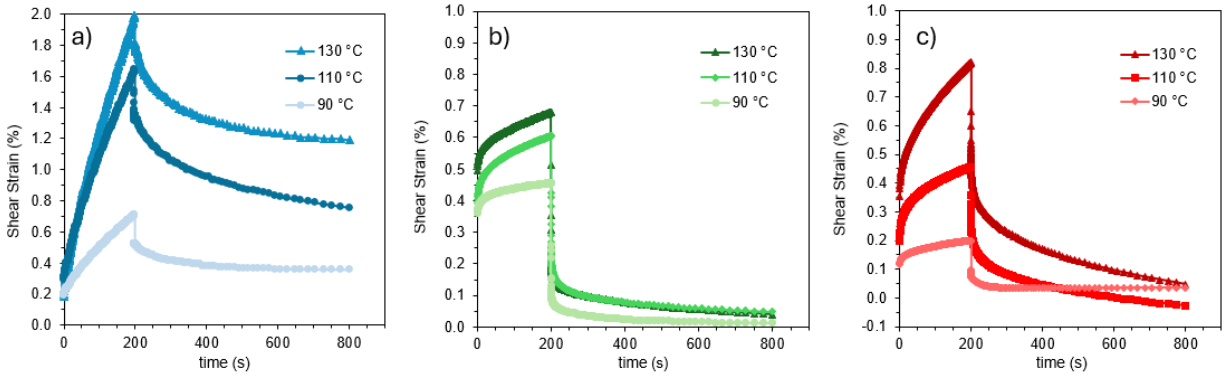

Figure S6.30 Comparison of creep-recovery in a) statistical, b) diblock, c) triblock vitrimers at 90, 110, and 130 °C.

Stress Relaxation

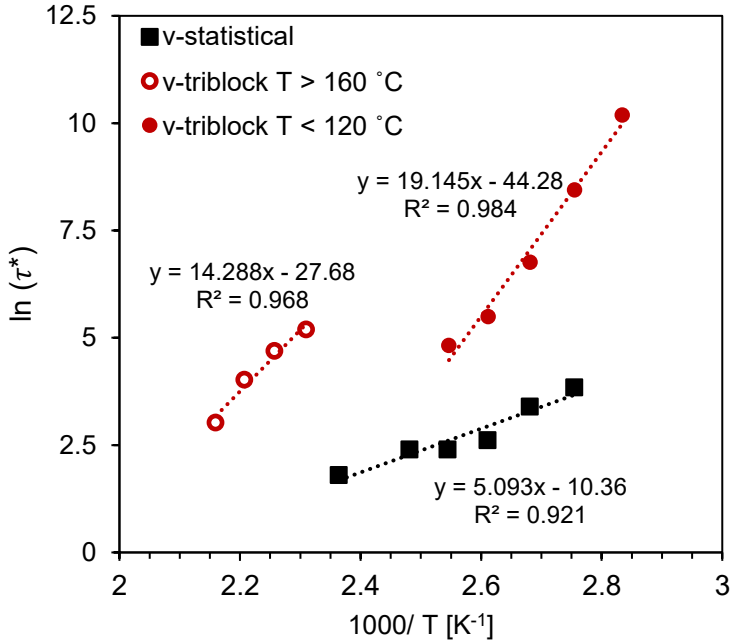

Figure S6.31 Relationship between the relaxation time and the temperature obtained from the stress-relaxation experiment of the v-statistical and v-triblock vitrimers using stretched exponential decay fit.

$$\frac{G(t)}{G_0} = exp\ -(\frac{t}{\tau^*})^{\beta}$$

Where G(t) and G_0 are the relaxation moduli at time t and 0, τ* is the characteristic relaxation time and $0 < \beta \leq 1$ is the breadth of the relaxation distribution.

Table S 6-1 Stress relaxation curve fitting

v-triblock		
T (˚C)	τ*	β
190	**21**	**0.50**
180	56	0.48
170	110	0.44
160	179	0.38
120	124	0.23
110	244	0.23
100	867	0.24
90	4674	0.23
80	26554	0.21

v-statistical		
T (˚C)	τ*	β
150	6	0.74
130	11	0.73
120	11	0.74
110	14	0.74
100	30	0.74
90	47	0.72

Leibler suggested an Arrhenius relationship can model the gradual decrease of viscosity with increasing temperature with E_a the viscous flow activation energy, R the universal gas constant

and T temperature [68,115]. E_a can be roughly estimated 42 kJ/mol for v-statistical, and 102 and 159 kJ/mol for the v-triblock at temperature ranges of T > 160 °C and T < 120 °C respectively.

$$ln\,\tau^* = \frac{E_a}{RT} + ln\,(\tau_0)$$

6.6.3.11 Tensile

Table S6-2 Tensile properties of the vitrimers after 3 reprocessing cycles; stress (σ) and strain (ε) at break did not change significantly.

	R×0		R×1		R×2		R×3	
	σ_{break} (MPa)	ε_{break} (%)	σ_{break} (MPa)	ε_{break} (%)	σ_{break} (MPa)	ε_{break} (%)	σ_{break} (MPa)	ε_{break} (%)
v-statistical	3.3 ± 0.2	123 ± 12	3.5 ± 0.3	119 ± 9	3.7 ± 0.2	121 ± 3	3.8 ± 0.2	123 ± 15
v-diblock	2.3 ± 0.2	32 ± 0.6	2.2 ± 0.2	36 ±2	2.1 ± 0.2	37 ± 1	2.2 ± 0.3	35 ± 2
v-triblock	5.2 ± 0.4	37 ± 3	4.9 ± 1.2	29 ± 7	3.9 ± 0.4	22 ± 5	5.1 ± 0.6	28 ± 5

Chapter 7: Contributions, Conclusions, Discussion, Future Work

7.1. Contributions and conclusions

Plastic waste pollution and climate change are planetary threats [239]. Canada has recently adopted ambitious zero-plastic waste goals by 2050 [5,6]. However, plastics cannot be eliminated from society. To promote and enable a sustainable society we need polymers; these materials increase the fuel efficiency of cars, protect food from pathogens, help cure disease, and enable renewable energy technologies [4].

The overall objective of this doctoral thesis was to develop reprocessable bio-based vitrimers and explore their rheo-mechanical properties, potential applications, and recycling. In recent years, the area of dynamic networks has received considerable attention. However, many examples of bio-derived vitrimers are synthesized via direct formation of networks with largely uncontrolled molecular architecture [1]. In contrast, in this thesis the synthesis of linear polymeric precursors and their subsequent dynamic cross-linking process were decoupled. This approach enabled us to employ controlled radical polymerization for the synthesis of diene and/or vinylic polymers. By using NMP and RAFT methods, we achieved precise control over the molecular weight, composition, and topology of the polymers. Furthermore, this higher level of control facilitated more in-depth exploration of the vitrimers' rheological properties and their shape memory effect.

In Chapters 3 and 4, the focus was on NMP and the development of myrcene (Myr)-based vitrimers. In Chapters 5 and 6, the attention shifted to the development of vitrimers using methacrylic bio-based monomers. Compared to dienes, methacrylic monomer undergo chain polymerization more efficiently and require lower reaction temperatures. In addition, their RAFT polymerization has proved very effective in retaining the chain end fidelity and facilitating formation of block copolymers comprised of multiple segments.

Original contributions to knowledge

Several novel contributions to the field of polymer synthesis and dynamic covalent networks have resulted from this PhD thesis:

1- We demonstrated a straightforward approach to synthesize bio-based vitrimers using commercially available and relatively inexpensive Myr with catalyst-free vinylogous

urethane chemistry and various di and tri-amine cross-linkers. The vitrimers were made with high bio-based contents.

2- It was established that vitrification can be employed as a relatively simple and inexpensive strategy to enhance mechanical properties of brush-like bio-based polymers and compensate for their high M_e while maintaining their processability. Mechanical and rheological properties of the networks could be tuned by adjusting the prepolymers' composition, copolymerization, molecular weight, nature of the cross-linker, and degree of cross-linking.

3- Statistical and diblock copolymers of Myr and β-ketoester functional AAEMA were synthesized for the first time using NMP in a controlled manner with relatively low *Đ*.

4- It was found that 20-30 mol% of Myr can be used as a controlling comonomer of SG1-based NMP of methacrylates (Chapter 3). It was also found that chain extension of p(AAEMA) with Myr is a more effective synthetic route than chain extension of p(Myr) with AAEMA for the synthesis of p(AAEMA)-***b***-p(Myr) (Chapter 4).

5- The reactivity ratios of the Myr/AAEMA pair in xylene solution at 120 °C were found to be $r_{Myr} = 0.20 \pm 0.17$ and $r_{AAEMA} = 0.22 \pm 0.07$, suggesting a nearly alternating microstructure results from this co-monomer pair.

6- It was demonstrated that Myr -based vitrimers could be both mechanically and chemically recycled. Mechanical reprocessing via grinding and hot pressing showed no deterioration of thermomechanical properties for at least 3 recycles. Furthermore, the prepolymers were recovered by addition of excess monofunctional amines at 110 °C and network disintegration without degradation of the prepolymers. (Chapter 3)

7- Increasing the prepolymer's molecular weight beyond its entanglement limit ($M_n > M_e$), and forming hybrid static-dynamic cross-links resulted in significant reductions in creep.

8- Shape memory effects were introduced in Myr-based polymers for the first time. The investigation compared two different structural architectures for triggering the shape recovery:

I. utilizing hybrid static-dynamic networks which resulted in a slow shape recovery over several hours (Chapter 3)

II. employing T_g as a bulk material property for being triggered which led to high shape fixity and rapid shape recovery (< 1 min). In this case, vitrimers could also undergo shape reprogramming through the reconfiguration of dynamic bonds at ~110 °C , a property referred to as Thermadapt. (Chapter 4)

9- In Chapters 5 and 6, vegetable oil-based C13MA was used instead of Myr as the low T_g monomer. The advantages of C13MA over Myr are:

(i.) C13MA is a monofunctional monomer that does not have additional double bonds. Thus, C13MA's simple alkyl pendant chain provides higher thermal stability.

(ii.) C13MA is within the broad portfolio of Evonik's specialty methacrylates and can be purchased in very large quantities from Evonik (standard barrels). In addition, similar and alternatives alkyl methacrylic esters such as lauryl methacrylate and iso-tridecyl methacrylate can be purchased in large commercial scale from BASF.

(iii.) The methacrylic functionality of C13MA allows for achieving high molecular weights and application of RAFT which is commercialized, highly versatile and tolerant to many functional groups, opening the door to the incorporation of other comonomers. RAFT also can allow the use of photo chemistry and photo polymerization.

10- Novel Schiff base vitrimers made of copolymers of VMA and C13MA were synthesized with up to 70% bio-based carbon content and high control over the prepolymer topology, M_n and composition. (Chapter 5)

11- All VMA and C13MA based vitrimers could effectively undergo at least 3× recycling without deterioration of their thermomechanical properties.

12- Four strategies were examined and directly compared for the first time to enhance the mechanical properties of the imine-based vitrimers and improve their creep resistance. All following samples were compared to their statistical vitrimer with solely dynamic cross-links counterpart:

- ***(i)*** hybrid static-dynamic crosslinks via p(C13MA-*co*-VMA-*co*-GMA) (Chapter 5)
- ***(ii)*** hard-soft diblock with cross-links in the hard section via p(VMA)-***b***-p(C13MA) (Chapter 5)
- ***(iii)*** AB type hard-soft diblock copolymer with cross-links in the soft section via p(MMA)-***b***-p(C13MA-*co*-VMA) (Chapter 6)
- ***(iv)*** ABA type triblock copolymer with the cross-links in the soft section via p(MMA)-***b***-p(C13MA-*co*-VMA)-***b***-p(MMA) (Chapter 6)

13- While hybrid network ***(i)*** had comparable tensile properties with the solely dynamic network, the diblock ***(ii)*** tensile tests exhibited a notably weaker modulus. The poor ultimate stress and strain of ***(ii)*** was linked to lack of entanglements in the soft p(C13MA). However, phase separation in ***(ii)*** led to enhanced hardness and reduced creep. In contrast, the drawback of ***(i)*** was its much slower stress-relaxation which makes processing of such networks more difficult. The advantage of ***(i)*** over ***(ii)*** is its simpler one step synthesis.

14- Comparing to ***(ii)***, ***(iii)*** exhibited similar reduction in creep; however, ***(iii)*** had relatively higher tensile strength. In other words, incorporation of dynamic bonds in the soft block was found to be more practical.

15- ***(iii)*** and ***(iv)*** exhibited comparable creep resistance. Conversely, ***(iv)*** had much higher tensile modulus and hardness.

7.2. Discussion and perspective

The findings of the thesis highlight the potential of bio-based vitrimers as a platform for the development of new sustainable polymer. The mechanical and rheological properties of such materials can be highly manipulated and tailored based on the applications. With the plethora of available reversible bonds, CANs and vitrimers have the potential to disrupt the polymer industry not only by enhancing material properties and functionalities but also by providing new pathways for polymer recycling. This could lead to significant advancements in the quality and performance of recycled plastics. By improving the recyclability and upcycling potential of polymers, we can reduce reliance on virgin materials and minimize plastic waste. In addition, as demonstrated in Chapters 3-5, programmable stimuli responsive properties can be imparted further expanding the applications of "smart" bio-based polymers.

Based on the conclusions of this work, several "big picture" points emerge. Here we discuss some of them.

Commercial viability of bio-based polymers

Renewable and bio-based monomers are typically formed by converting and/or cracking bio-feedstocks, including microorganisms and plants such as vegetable oils and lignocellulosic biomass, into functional monomers [240]. For example, lignocellulosic biomass, which includes cellulose, hemicellulose, and lignin, can be fractionated and depolymerized into carbohydrates and aromatic compounds. These compounds are then converted into platform chemicals, which can be further processed into bio-based monomers and solvents [241]. In general, renewable monomers can be categorized into two main groups: (a) those that are chemically identical to fossil-based commodity monomers, and (b) those that posse a unique chemical structure and are not similar to fossil-based monomers [242]. The former group includes familiar monomers such as styrene, ethylene, and bio-based precursors to poly(ethylene terephthalate) (PET) including ethylene glycol [243,244]. This direct replacement strategy makes the replacement of traditional fossil monomers straightforward and is considered commercially viable, especially when petroleum prices are high or additional taxes on fossil carbon are imposed [242]. However, the established markets of petroleum-based polymers make it difficult for new bio-feedstocks and their capital-intensive manufacturing processes to compete with already amortized petrochemical operations on price

alone. Thus, for renewable and plant-based polymers to penetrate the marketplace, they must outcompete traditional materials in both price and performance [4].

In this thesis, the focus was on the latter category of bio-based monomers that possess unique chemical structures. Myr, C13MA, and VMA are processed and converted from biomass and are not identical to commodity monomers; however, they all resemble the functional structure of commodity polymers. The conjugated diene structure of Myr is similar to that of isoprene and butadiene, which are used in synthetic rubbers [245]. Similarly, the methacrylate functional group of C13MA and VMA is identical to the functional groups of commodity methacrylic esters, such as MMA, which are used in Plexiglass and dental fillings [14]. The conjugated diene functionality of Myr, the methacrylic group of C13MA and VMA makes them suitable for chain growth polymerization, a well-established and highly industrialized process. This means they can be easily integrated into existing manufacturing systems. Additionally, their unique chemical structures offer new properties and functionalities, paving the way for innovative applications. The other functional monomers used in this thesis are AAEMA (Chapters 3 and 4) and GMA (Chapters 3 and 5) which are both petroleum derived. These monomers are used in low percentages ~ 5-30 mol%. In addition, AAEMA-related monomers can be partially bio-sourced via the reaction of hydroxyethyl methacrylate (HEMA) with acetoacetate acid or levulinic acid which is derived from the degradation of cellulose and is touted as an important biorefinery feedstock [40,246].

A great advantage of C13MA and Myr over many other bio-based monomers, reported in the literature, is that they are both available commercially. From the chemical point of view, Myr, C13MA, and VMA can be thought of as drop-in solutions for the transition away from petroleum-based monomers towards renewable ones. Myr is a high-value monoterpene that has been widely applied in food, cosmetic, and medicine industry. Myr can be procured in the scale of tens of kilograms and drums. Furthermore, C13MA is part of Evonik's broad portfolio of specialty methacrylic monomers and is available in large quantities (standard barrels). Evonik's VISIOMER® Terra methacrylates are bio-based monomers, made from 70-85% bio-based and recycled materials. Both *VISIOMER® Terra C13-MA* and *VISIOMER® Terra C17,4-MA* (an alkyl methacrylic ester with an average of 17 carbon atoms in the pendant chain) can improve the hydrophobicity of emulsion paints, enhance resin resistance to polar media, and reduce the overall carbon footprint.

Apart from large-scale availability of the bio-based polymers, their cost is also vital for industrial adoption. Currently, renewable bio-based monomers are typically more expensive than their petroleum-based counterparts. As a crude example and as of August 2024, the price of stabilized Myr is at least double the price of isoprene on the website of Millipore-Sigma (this is an ill-comparison as Millipore-Sigma is merely a distributor). Currently, suppliers such as *Vigon* supply Myr for about $100/kg. As the adoption of renewable monomers increases, economies of scale will reduce their production costs and, consequently, their market prices. This trend is driven by several factors, including advancements in biotechnology, increased consumer demand for sustainable products, and supportive government policies [247]. As production volumes rise, manufacturers can achieve greater efficiency and lower costs through optimized processes and bulk purchasing of raw materials [247].

Relatively a small fraction of the commercial polymers used in packaging, coatings, composites and structural materials etc., are bio-sourced, including poly(lactic acid) (PLA), and starch-based polymers and poly(hydroxyalkanoates) (PHAs). Despite the recent increase in production of bio-based polymers due to public demand, biopolymers still face competition from established polymers that have been fine-tuned for decades to achieve desired properties and processing. Like any disruptive technology, it may take time before renewable polymers gain enough traction to be financially viable and widely used [248]. Applications of dynamic covalent bonds and vitrification can play a key role in enhancing the properties of bio-based polymers as showcased in this thesis. This can help further commercialization of bio-based polymers.

Life cycle assessment (LCA)

When evaluating bio-based polymers, it is critical to have a comprehensive understanding of the environmental impacts associated with bio-sourced polymers from cradle to grave. LCA helps towards understanding the energy consumption, water input, carbon emissions, and environmental impact of polymers from raw materials extraction, processing, usage and end-of-life / recycling. This allows drawing fair comparisons between bio-based polymers with fossil-derived ones. Comprehensive LCA allow policymakers and industry leaders in making informed decisions about improvement, optimization, adoption, and promotion of bio-sourced polymers [249].

Commercial viability of RDRP methods

A frequent criticism directed towards controlled radical polymerization is the slow translation into commercial products. It is safe to say that RDRP methods will have very limited application in the production of commodity polymers and high-volume polymers will be dominated by conventional step growth or chain growth polymerizations [23].

With the advancement of the field, modern RDRP methods cover the whole array of radically polymerizable monomers. Copolymers of high structural complexity with controlled architecture, microstructure, functionality and molar mass with low dispersities can be synthesized in bulk, solution and in various dispersed media. RDRP methods have found many uses in niche applications such as emulsifiers, dispersants, rheology and surface modifiers, adhesives, sealants, lubricants, foam control agents, leveling agents, functional binders, electrolytes, blend compatibilizers, thermoplastic elastomers, flexible electronics, textile treatment, nanocontainers for the encapsulation/delivery of active components and polymer bioconjugates [21,44]. It is expected to see an increasing number of novel materials derived from RDRP for new high-valued products, rather than replacement solutions for existing polymers. The main related markets include beauty, health, oil and gas, paints, inks, the space and aircraft industry, automobiles, batteries, energy and electronics [21].

In this context, even though RDRP methods (NMP and RAFT) were used in this thesis they are not an irreplaceable part of vitrimer chemistry. In this work, vitrification was used to enhance the rheo-mechanical properties of p(Myr) and p(C13MA) without sacrificing their sustainability and (re)processability. Conventional free radical (co)polymerization is fully applicable to Myr and C13MA-based systems. Another possible synthetic route for Myr-based CANs is to homopolymerize Myr using living ionic methods and graft dynamic bonds onto the polymer backbone using its double bonds. Ionic polymerization methods have proven very successful in terms of formation of high molecular weight p(Myr) with high conversions [20,167].

Block copolymers vitrimers

The potential of self-assembly was demonstrated in Chapters 5 and 6 for tailoring the properties of vitrimers. This thesis demonstrated that the combination of dynamic chemistries and hard-soft microphase-separated block copolymers can effectively modulate the rheo-mechanical properties

of vitrimers. Specifically, we showed that in hard-soft AB and ABA type block copolymers, the incorporation of dynamic cross-links in the rubbery "B" domain enhances tensile properties and elongation. Meanwhile, the glassy "A" domain acts as anchors, reducing creep at service temperatures and increase hardness. Additionally, above the T_g of the "A" domain, the vitrimers can be easily (re)processed while compression molding.

In this context, a particularly intriguing area of research involves comparing the rheological properties of vitrimers made from ABA-type and ABC triblock copolymers. In ABC triblock terpolymer, microphase separation occurs between the A and C domains with minimal to no loops since A blocks are not miscible with C domains as shown in **Figure 7.1** [250].

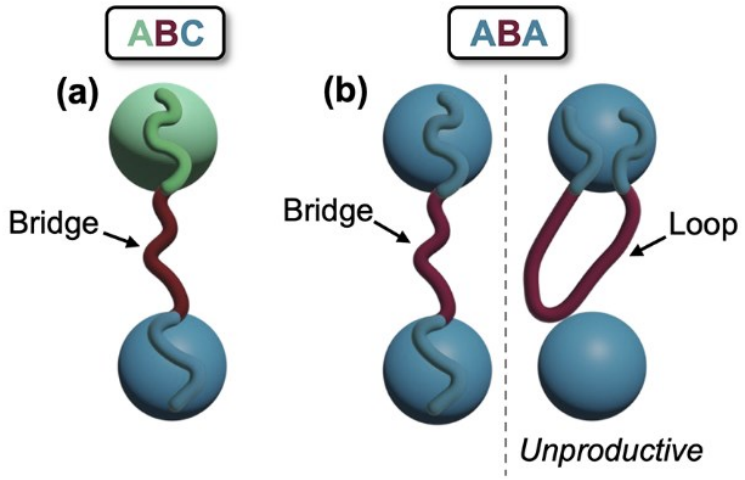

Figure 7.1 Comparison of ABC with ABA triblock copolymers (a) In case of ABC sequence, the chemical immiscibility of A and C domains leads to nearly a full molecular bridging between the two discrete hard domains. In contrast, in ABA sequence (b) both bridge and loop chain configurations forms [250].

Recently, Bates' and Hawker's groups showed the potential of ABC triblock terpolymers in enhancing the mechanical properties of thermoplastic elastomers [250]. By comparing symmetric ABA/CBC analogs of similar molecular weights and volume fractions of B and A/C domains, they found that the ABC architecture significantly improves elasticity, achieving up to 98% recovery over 10 cycles. This improvement was attributed to the nearly complete chain bridging between discrete hard domains, which minimizes mechanically unproductive loops [250].

In the context of this thesis, ABC triblock copolymers such as p(MMA)-b-p(AAEMA)-b-p(Sty) with 3 microphase separated domains can provide better bridging between the glassy MMA and Sty domains. Key questions include: How do polymer chain loops influence macro-level properties and stress-relaxation and creep behaviour? Additionally, how do the various microstructural morphologies that are achievable with ABC triblock terpolymers impact the properties of vitrimers?

Furthermore, the literature currently lacks comprehensive studies on the use of order-disorder transitions (ODT) and lower critical solution temperature (LCST) for controlling creep in vitrimers. Addressing this gap could open new avenues for developing creep-resistant yet highly processable vitrimers, making this an exciting and promising field for future research.

Vitrimers made of ABC triblock terpolymers have the potential to offer a versatile platform for developing materials with practical applications and easy re-processibility. Additionally, studying ABC triblock terpolymers, their morphologies, and ODT advances our understanding of chain conformation and structure-property relationships in microphase-separated block copolymer vitrimers.

Application of nitroxides and other stable radicals to form dynamic networks

In Chapters 3 and 4, NMP was used to grow polymer chains via RDRP. However, beyond applications in RDRP, the stable radical effect in nitroxides can be harnessed to form reversible covalent cross-links [251,209]. As illustrated in Chapter 2, NMP uses nitroxides to regulate the polymerization process through a thermally reversible capping and uncapping reaction. When capped, the polymer forms a covalent bond between a nitroxide and a carbon atom. When uncapped, this alkoxyamine bond breaks, creating a polymeric free radical, **Schematic 7.1**. The nitroxide radical does not react with other nitroxide radicals but only with other types of radicals [252]. Due to the thermal stability of TEMPO and SG1-based nitroxides, monomers with pendant TEMPO or SG1 side groups can be copolymerized via low temperature free radical or RAFT methods to form CANs. For example, Jin et al. utilized commercially available TEMPO-substituted methacrylate to cross-link styrene−butadiene rubber (SBR) in a one-step controlled curing process [252]. The resulting rubbers showed good reprocessing efficiencies over multiple compression molding cycles. Nitroxide-based dynamic cross-linking can be applied to a wide range of polymers based on acrylic, styrenic, and other olefinic monomers. In addition, this method

has the advantage of reducing discoloration, increased E_a of viscous flow resulting reduce creep at service temperature and bio-compatibility [252–254]. So far, mostly commercially available TEMPO based alkoxyamines have been used as dynamic cross-links or grafting agents in combination of other dynamic covalent bonds including boronic esters and disulfides, **Schematic 7.1**. NMP-based dynamic cross-linking approach has some limitations as well. That is, it does not fully recover the network's cross-link density after reprocessing [209,252]. This issue arises in CANs due to the loss of reactivity of carbon-based radicals during reprocessing. However, enhancing these NMP-based dynamic networks with additives and advancing the chemistry of persistent radicals could potentially address these challenges. One interesting avenue can be the development of nitroxide cross-linkers based on TIPNO-based alkoxyamine chemistry.

Thyil radicals are another form of stable radicals which have recently been used in CANs, **Schematic 7.1** [209]. Otsuka's group showed that dialkylamino disulfide reversibly dissociates homolytically when heated above 80°C, forming stable piperidine-based sulfur radicals (TEMPS) that are resistant to disproportionation and oxygen sensitivity [255]. Aiba et al., demonstrated that BiTEMPS-containing molecules with a trisulfide bridge (dialkylamino trisulfide) could be used as dynamic cross-linkers in polymethacrylate CANs [256]. Dialkylamino trisulfides dissociate asymmetrically upon heating into stable thiyl and dithiyl radicals, **Schematic 7.1**. Torkelson's group also developed a simple, catalyst-free, one-pot reactive process using dialkylamino disulfide dynamic chemistry for upcycling of PE [257]. Bin Rusayyis et al., developed a non-piperidine dialkylamino disulfide-based cross-linker bis(tert-butyl-3-ethylamino methacrylate) disulfide (BiTEBES methacrylate) from commercially available starting materials in short synthetic steps [225]. They showed that BiTEBES methacrylate can be used as a dynamic cross-linker in the conventional FRP of catalyst-free, reprocessable networks that can be recycled multiple times with complete retention of cross-link density within experimental uncertainty.

Indeed, stable free radicals, such as nitroxide-based TEMPO and dialkylamino disulfides-based TEMPS or TEBES, have shown great promise in the formation of dynamic networks. These radicals can function both as grafting agents and reversible cross-links. When combined with bio-based monomers or the upcycling of polyolefins, these chemistries can lead to a plethora of more sustainable polymeric materials.

reversible capping of alkoxyamines

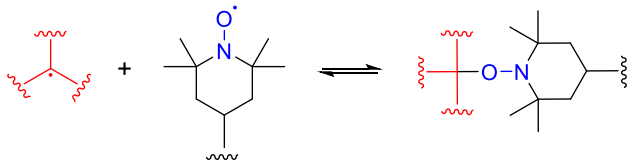

nitroxide mediate radical cross-linking

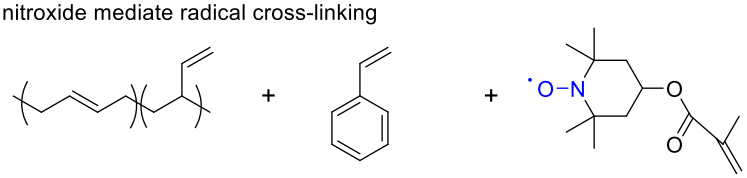

TEMPO-based cross-linked polyurethanes

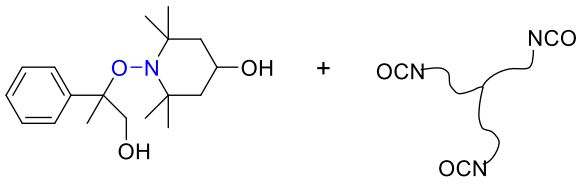

TEMPO-based grafting of reversible cross-links with bis-dioxaborolane

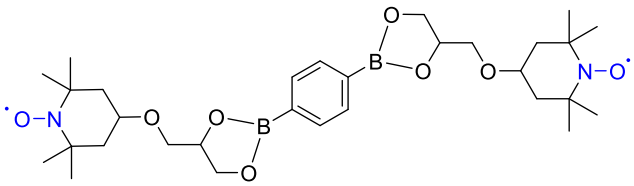

dialkylamino disulfides and homolytic dissociation of stable thyil radicals (TEMPS)

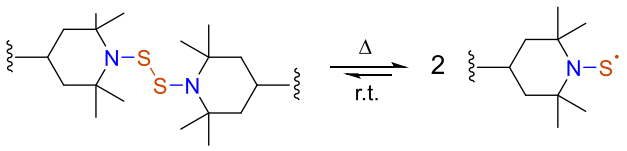

dialkylamino trisulfide reversible homolytic dissociation of stable thyil and dithyil radicals

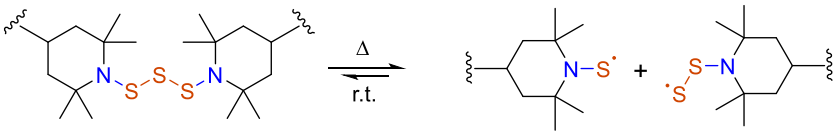

non-piperidine-based dialkylamino disulfide cross-linker (BiTEBES methacrylate)

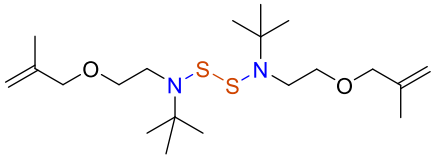

Schematic 7-1 Applications of stable free radicals in dynamic cross-linking [209,251,255–261].

Continuous extrusion-based processing for upcycling of vitrimers

In this thesis, vitrimers were formed using compression molding, which is the most common laboratory-scale method in the literature for shaping vitrimers and CANs. However, to achieve commercial and large-scale viability for closed-loop recycling of vitrimers, it is crucial to develop continuous flow re-processing/upcycling methods, including extrusion-based processes. A significant challenge with current dynamic networks is the trade-off between dimensional stability of the vitrimers and their processability. To achieve industrial closed-loop recycling, the vitrimers must maintain their shape and functionality at service temperature and yet when heated have sufficiently low viscosity to be able to be processed by extruders.

Given the wide range of dynamic chemistries available for fabricating vitrimers, it is essential to apply them beyond compression molding processing and focus on improving the upcycling and processability using continuous flow methods. In this context, several innovative research works recently focused on using reactive extrusion to develop vitrimers. For example, Demongeot et al. prepared p(butylene terephthalate) (PBT) vitrimers using reactive extrusion of industrial PBT thermoplastics with Zn(II)-catalyzed addition and transesterification [262]. Maaz et al reported a dimaleimide bis(dioxaborolane) dynamic cross-linking agent that allows for commercial polyethylene (PE) to be transformed into a vitrimer using a batch twin-screw microcompounder, shown in **Figure 7.2** [263]. They found that the miscibility of the grafting agent with the PE melt plays a critical role for the grafting, as efficient mixing is essential for achieving quantitative grafting and a high gel content. More importantly, Qiu et al., studied upcycling of PET via combining polyols with a tertiary amine structure and diepoxy to transform PET to continuously reprocessable vitrimers through a twin-screw extruder [264]. In addition to compression molding, they reported extrusion molding of the networked PET vitrimers [264].

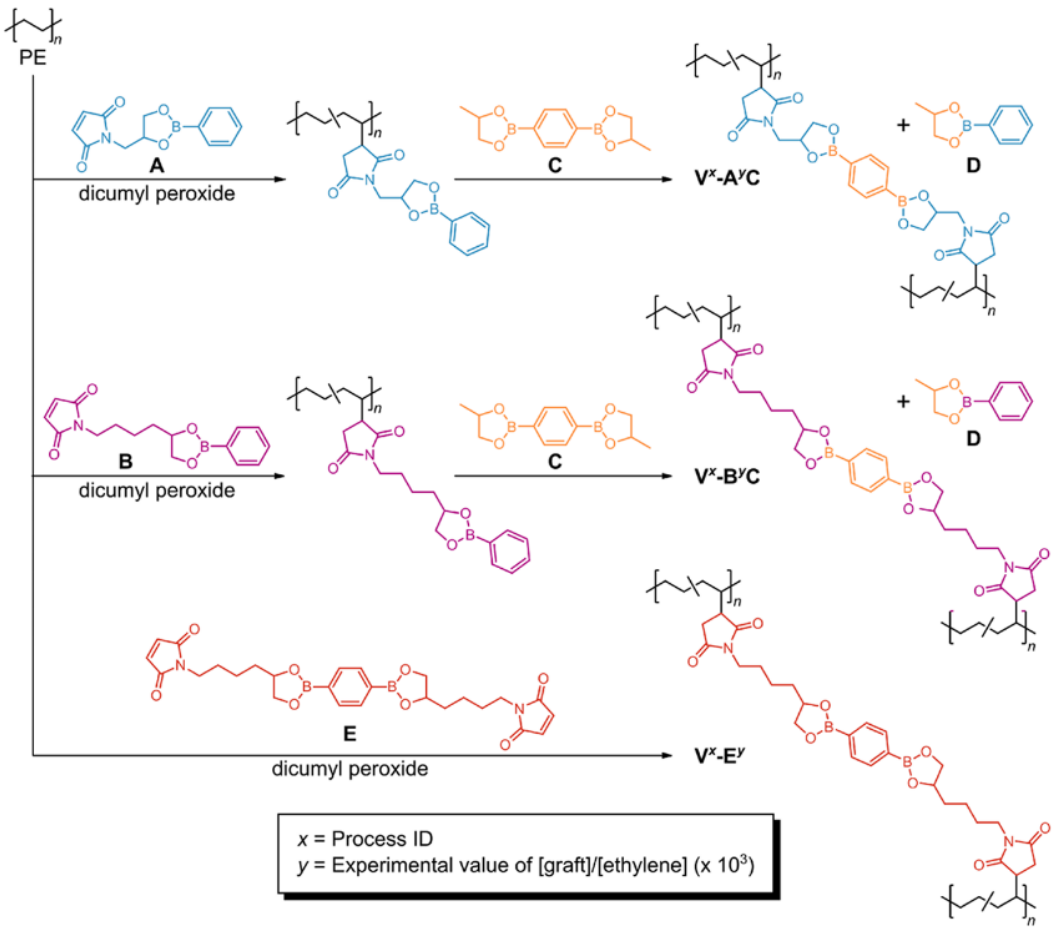

Figure 7.2 Synthesis of polyethylene (PE) vitrimers using maleimide-based grafting agents and dioxaborolane dynamic chemistry [263].

In addition to continuous forming and recycling of vitrimers, extrusion-based fused filament fabrication (FFF) 3D printing of dynamic networks is particularly interesting for innovative high-added value application of vitrimers. FFF is one of the most common methods of additive manufacturing of polymers owing to its cost-effectiveness and relatively simple setup [265,266]. FFF is based on the extrusion of materials through a heated nozzle, followed by a layer-by-layer deposition and fusing of the extruded melt. Melt-processable thermoplastic polymers such as p(lactic acid) (PLA), p(acrylonitrile butadiene styrene) (ABS), and p(carbonate) (PC) are the materials mainly used for FFF [267]. Recently few studies have investigated FFF of vitrimers. Choi et al., reported epoxy vitrimers with controlled and optimized rheological properties for extrusion-based FFF with shape memory effect [267]. The epoxy-based vitrimeric filaments were

prepared using bisphenol A diglycidyl ether (DGEBA) and dodecanedioic acid (DA) with triazabicyclodecene (TBD) as a catalyst for transesterification. They showed the stress relaxation and modulus of the vitrimers could be effectively tuned to ensure that the rheological properties are suitable for FFF. The vitrimer filaments for printing were fabricated using a filament extruder, and 4D printing, i.e. with stimuli responsive shape memory effect, was performed using a portable, handheld FFF printer for prototyping.

Another example of vitrimer upcycling and FFF 3D printing is illustrated in the work of Kim et al [266]. They reported a scalable closed-loop manufacturing of acrylonitrile butadiene styrene (ABS) thermoplastics into re-printable vitrimers, **Figure 7.3**. They used thiol-ene "click" chemistry to functionalize butadiene segments with cysteamine, followed by reacting the pendant amine with a short-chain dialdehyde (i.e., glutaraldehyde) to produce imine-based ABS vitrimers. In their system, the free amine groups allowed facile and fast imine bond exchanges rendering the vitrimers applicable for filament extrusion, loading, feeding, and printing without any postprocessing [266].

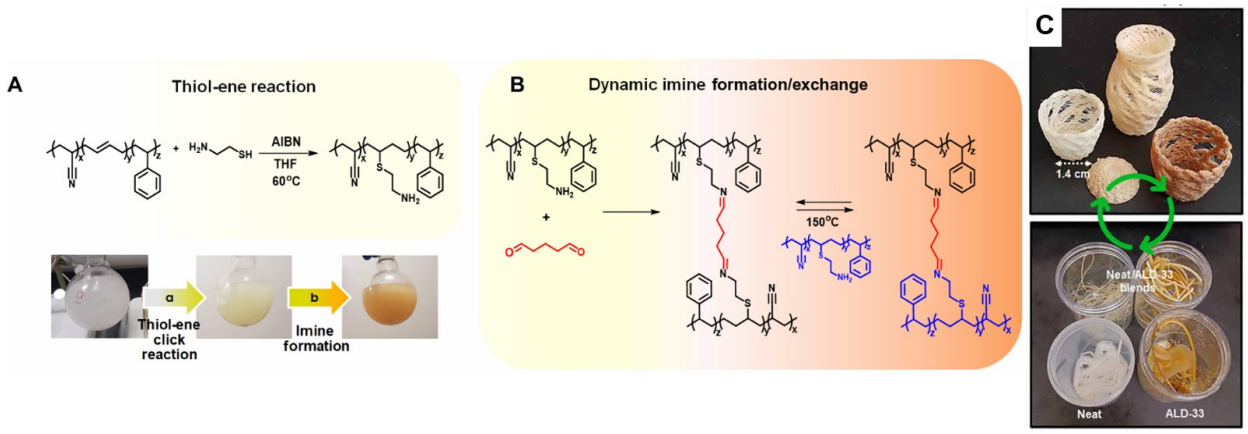

Figure 7.3 3D printing of acrylonitrile butadiene styrene (ABS) vitrimers. A) Grafting to ABS polymer backbone by thiol-ene clicking. B) Imine-based dynamic crosslinking. C) FFF of neat-ABS, ABS-vitrimer, or their blends upcycled into 3D-printed baskets with different colors by iterating the same FFF protocols [266].

Dynamic covalent bonds for compatibilization of recycled polymers

Polymer recycling streams are often comprised of a diverse array of materials with different chemical compositions and properties. In addition, these streams are subjected to significant content variability from differences in polymer types, additives, contaminants, and degradation products. This composition variability poses challenges for efficient recycling processes, as it can affect the quality and performance of the recycled materials. That is why often polymer materials are recycled into low-value materials. Chemical incompatibility in recycling feed streams leads to macro-phase separation and low mechanical properties [206,239].

In this thesis, the welding tests conducted in Chapter 3 demonstrated that dynamic covalent bonds offer a robust and cost-effective method for compatibilizing polymers with varying compositions. This approach can enhance the properties of recycled plastics, providing a viable pathway for their upcycling. By leveraging the reversible nature of these bonds, it is possible to improve the mechanical strength, thermal stability, and overall performance of recycled materials. This not only addresses the challenges associated with polymer recycling streams but also opens new opportunities for creating high-value products from recycled plastics. For example, the weldability has the potential to alleviate the inherent anisotropic mechanical properties of 3D printed materials using FFF by chemically bonding the deposited layers [266,268].

Can vitrification broaden polylactide's applications and boosts industrial adoption of degradable polymers?

Given polylactide's significance as a commercially viable and sustainable thermoplastic, this section will focus on the applications of vitrimers with PLA.

Polylactide (PLA), also known as p(lactic acid), is arguably one of the most important bio-based polymers [269]. It has been widely studied and successfully commercialized. PLA has the potential to replace petroleum-based polymers such as p(Sty) and PET [270]. It has been proven that vitrimers have the potential to further increase the range of PLA applications by enhancing and tailoring its thermos-mechanical properties [70]. The successful integration of PLA and vitrimer chemistry could pave the way for a wide array of sustainable, recyclable, bio-based, and degradable products. This advancement represents a milestone towards a sustainable plastics industry and the commercialization of vitrimeric materials.

PLA is an aliphatic polyester that is bio-based, compostable, and eco-friendly [271]. Its monomer, lactic acid, is derived from renewable resources like corn starch and sugarcane. Unlike many bio-based polymers with a C–C backbone, the ester groups in PLA enable its degradability. PLA degrades within months in industrial composting, enabling a circular life cycle [124,271]. Thanks to its easy processing, biocompatibility, and degradability, PLA has diverse commercial applications such as packaging materials, biomedical devices, and 3D printing [272]. Driven by the soaring demand for sustainable materials, the global market for PLA is rapidly expanding, expected to grow from 2.16 million tons in 2024 to 5.5 million tons by 2029 [273].

Despite its promise, PLA has significant shortcomings, including its brittleness and low thermal resistance [269]. These restrict PLA's use in applications requiring ductility and heat tolerance. Addressing these challenges will derive significant economic and environmental benefits. Several strategies have been developed to enhance the thermomechanical properties of PLA, such as blending, adding plasticizers and fillers [269]. However, such methods often result in limited improvements and issues like macro phase separation, reduced thermochemical stability, limiting their large-scale adoption [271,274,275].

In this thesis, vitrification and dynamic networks were applied to compensate for the performance deficiencies of the bio-based polymers. It was shown that rheo-mechanical properties of p(Myr) and p(C13MA) could be enhanced by tuning the dynamic cross-linking density as well as incorporation of hybrid static/dynamic network. Similarly, vitrification and dynamic bonds can be applied to PLA-based materials to improve their properties. There are a few studies that have applied vitrification to PLA [70,276]. For example, Brutman et al., prepared vitrimers from hydroxyl-terminated 4-arm star-shaped racemic PLA [70]. The samples were cross-linked with methylenediphenyl diisocyanate (MDI) and stannous(II) octoate [$Sn(Oct)_2$] as both the cross-linking and transesterification catalyst. The isocyanate reacts with hydroxyl groups of PLA to form urethane linkages providing toughness while the $Sn(Oct)_2$ catalyst facilitates transesterification reactions within the ester bonds of the PLA, as shown in Schematic 7.2. This dynamic exchange allows the material to exhibit vitrimeric properties. They reported that the PLA vitrimers healed fractures by compression molding with up to 67% recovery of ultimate elongation, up to 102% recovery of tensile strength, and up to 133% recovery of tensile modulus values [70].

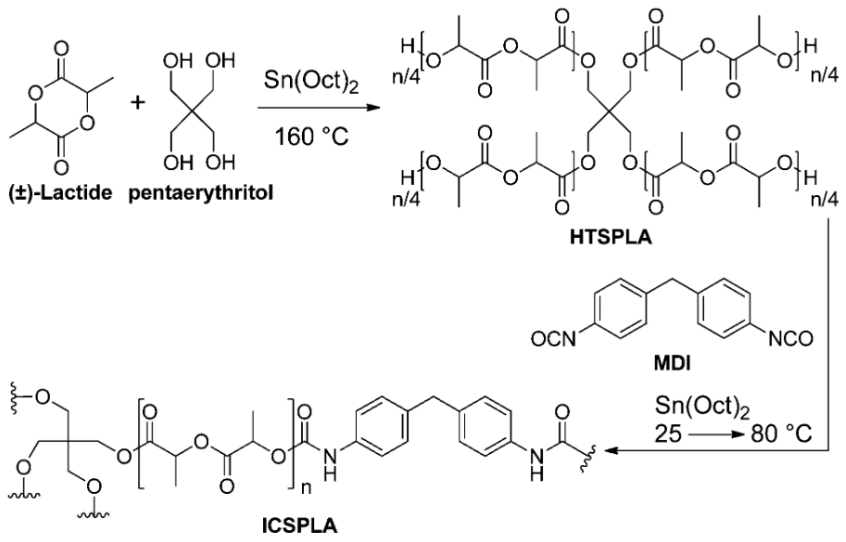

Schematic 7-2 Synthesis of hydroxylterminated 4-arm star-shaped poly((±)-lactide) (HTSPLA) based vitrimers. A tetraol was used as the initiator and $Sn(Oct)_2$ was used as the catalyst for the ring opening of lactide monomer. Cross-linking of HTSPLA with diisocyanate MDI forming urethane linkages and transesterification with $Sn(Oct)_2$ (ICSPLA) [70].

In this context, terpenoids such as Myr and Farnesene have shown significant potential in enhancing the tensile strength, ductility, and impact resistance of PLA. These improvements are achieved through both conventional and reactive extrusion processes. For instance, Halloran et al. demonstrated that rubber-toughened PLA can be obtained by incorporating poly(farnesene) copolymers containing moderate amounts (10 mol%) of epoxy-based GMA and methacrylic acid (MAA) [124]. These copolymers undergo cross-linking via acid-epoxy or transesterification reactions during reactive blending. Therefore, the integration of vitrimers and reactive blending with rubbery bio-based polymer into PLA can further enhance its mechanical strength, thermal stability, reusability [276]. Similar improvements are crucial for applications of PLA in automotive parts, consumer electronics, medical devices, etc. This strategy has the potential to pave the way for the development of a wide range of degradable bio-based polymers.

7.3. Recommendations for future work

This thesis has answered several questions and tackled numerous issues within the field of bio-based vitrimers. However, there are many topics that warrant further investigation. Currently there are several upcoming collaborative projects based on the findings of this thesis.

- Block copolymers and NMP can be applied to Myr and other terpenes such as Farnesene as well. Diblock (AB: hard-soft) and triblock copolymers (ABA: hard-soft-hard and BAB: soft-hard-soft) with dynamic bonds within the soft domains can enhance the rheo-mechanical properties of these bio-based polymers as proposed in **Schematics 7.3** to **5**. Acrylates, styrene and dienes work very well with SG1-based NMP. Studying the structure-property relationships in these polymers would be particularly interesting.

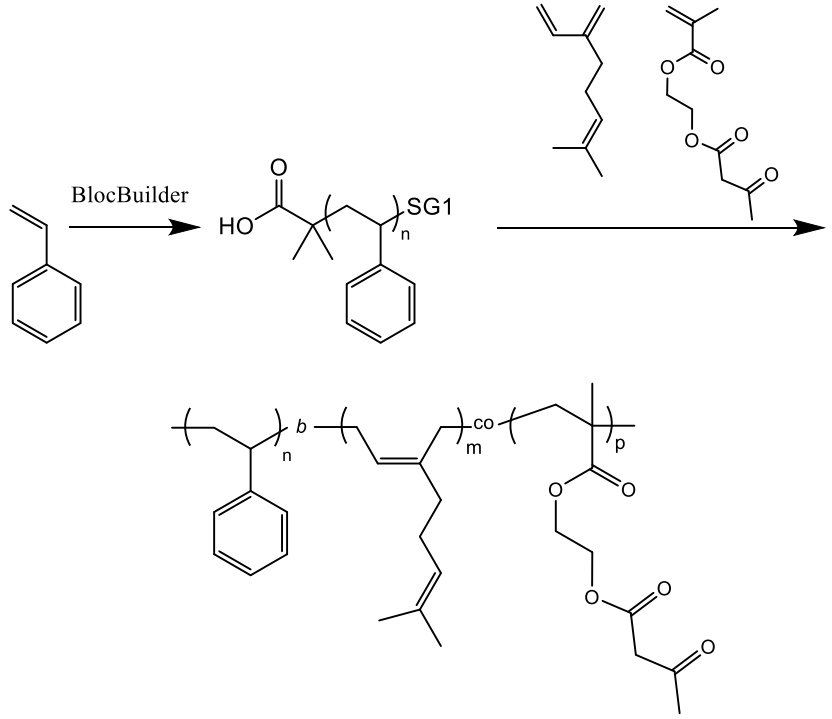

Schematic 7-3 Proposed synthesis of p(Sty)-*b*-p(Myr-co-AAEMA) diblock copolymer. AAEMA can be later used for cross-linking

For the synthesis of ABA triblock copolymers using NMP, a telechelic SG1-based initiator can be made by following the suggested method below or similar to previously reported works [277,278]. The synthesis starts by making a p(Myr-co-AAEMA) macroinitiator

middle block followed by a chain extension with styrene. In this synthesis isobornyl acrylate (IBOA) can replace styrene and vanillin methacrylate (VMA) can replace AAEMA to increase the bio-based content, shown in **Schematic 7-5**.

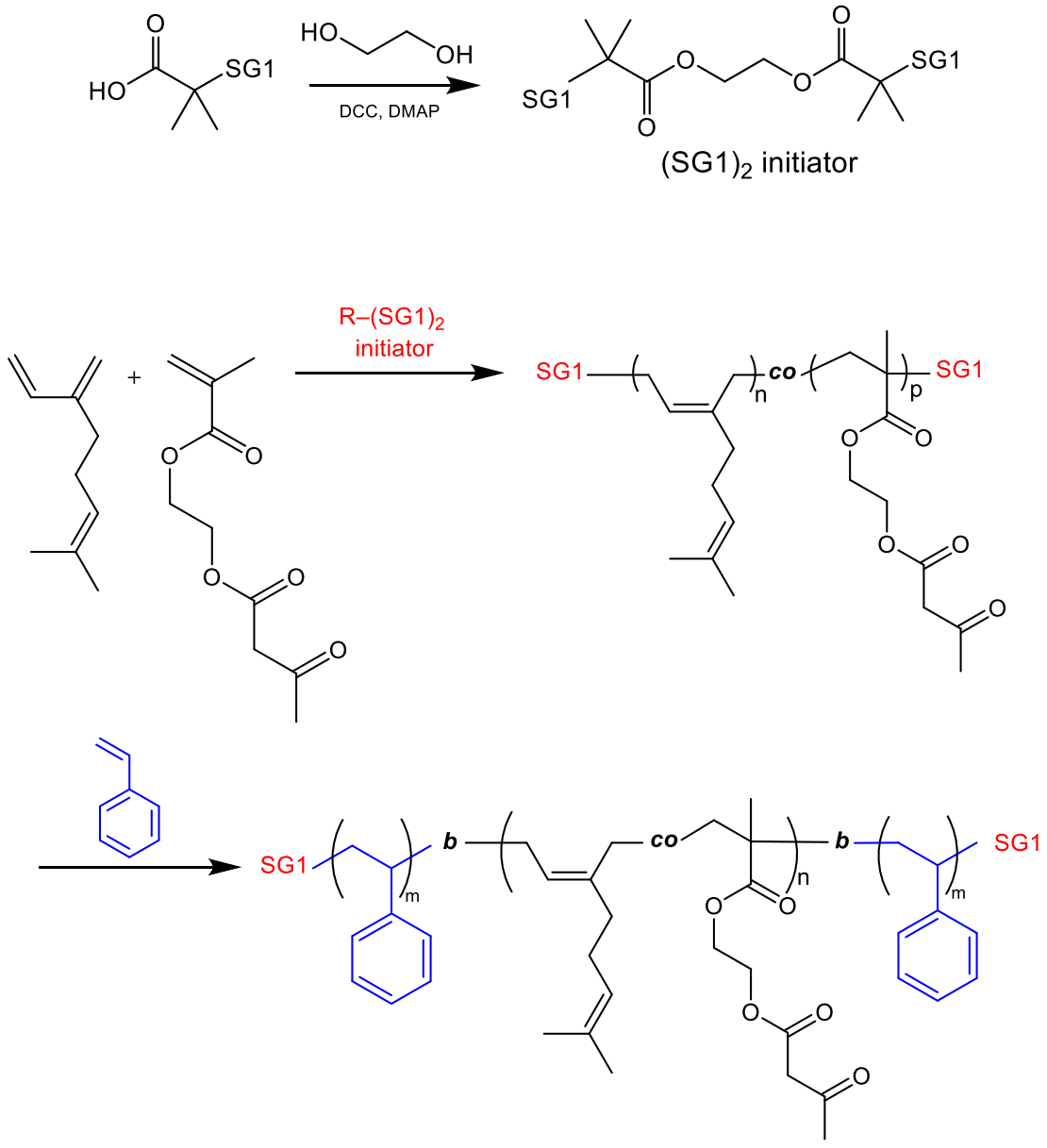

Schematic 7-4 Suggested telechelic synthesis of p(Sty)-*block*-p(Myr/AAEMA)-*block*-p(Sty). First, the middle block of p(Myr-co-AAEMA) difunctional $(SG1)_2$ macroinitiator is synthesized. Then, it is chain extended with Sty to form triblock terpolymer. The AAEMA can be used to dynamically cross-link the polymer.

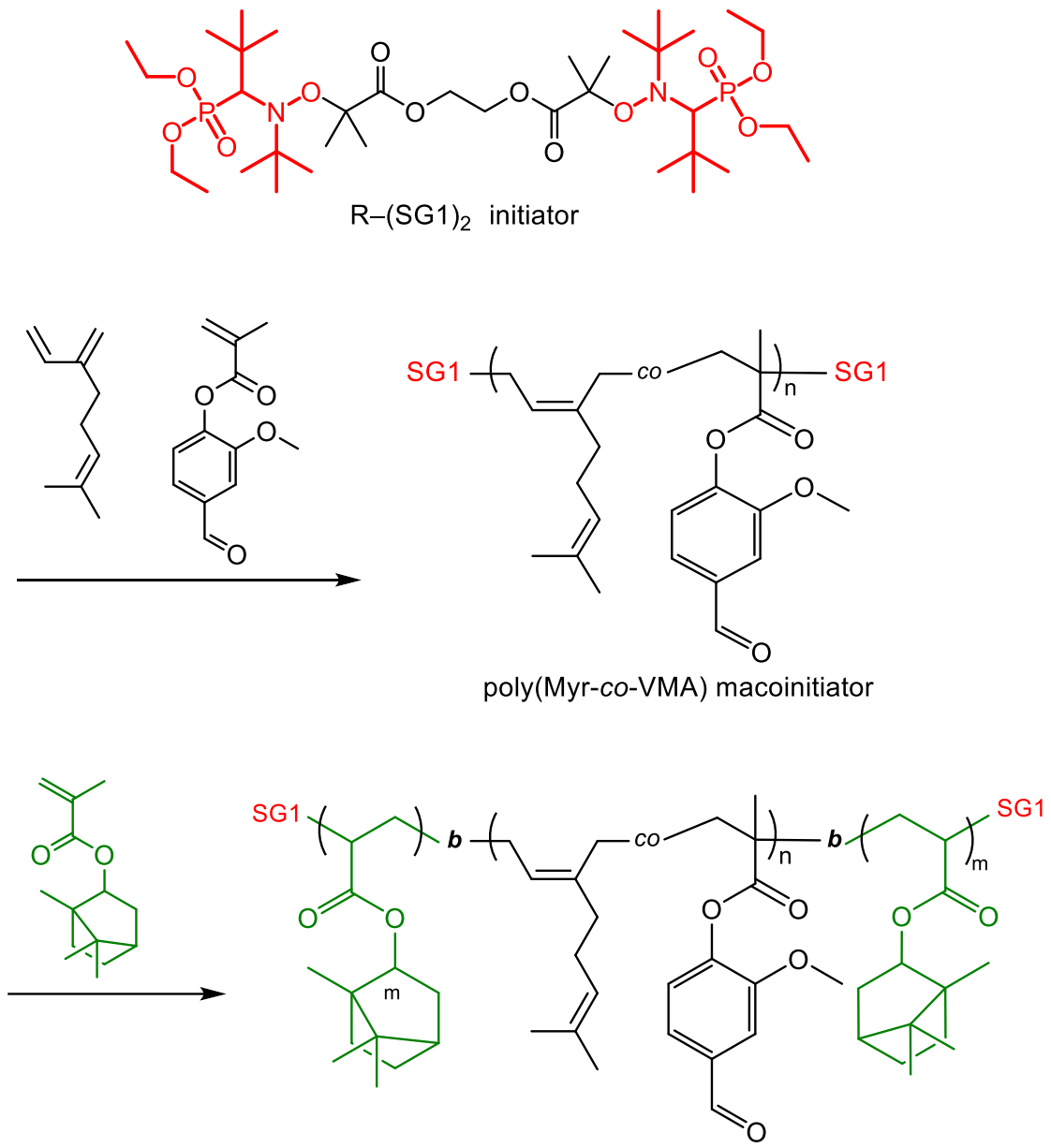

Schematic 7-5 Suggested telechelic synthesis of bio-based p(iBOA)-*block*-p(Myr/VMA)-*block*-p(iBOA). The aldehyde functionality of vanillin methacrylate (VMA) can be used to form dynamic imine cross-links.

- The synthesis of bio-based statistical and block copolymers using alternative monomers, such as methacrylated terpenes, via sulfur-free RAFT or low copper ATRP methods like ARGET, ICAR, or photoinduced ATRP, promises not only novel polymers but also a pathway for greener vitrimers with controlled architecture [142,279,280].

- Exploring the vitrification for compatibilization of polymer blends is also very intriguing. For example, can we use vitrification for reactive blending and rubber toughening? Separation of mixed post-consumer plastic waste streams is difficult and expensive. Is it possible to use dynamic bonds as compatibilizers of different polymers and enhance recyclability?
- Exploring other dynamic chemistries with higher activation energy E_a can reduce the creep at the service temperature. Can we use nitroxides for dynamic cross-linking [225,281]? There are few examples of application of alkoxyamines as crosslinkers in the development of CANs. However, nitroxides are typically sensitive to oxygen and protecting the alkoxyamine is required.

  In addition to the use of nitroxides as the reversible cross-linkers, nitroxides can be used as grafting agents for polymer upcycling. Nicolaÿ's group reported upcycling of commercial high-density polyethylene (HDPE) by grafting it with nitroxide (TEMPO) carrying dioxaborolane moieties via reactive extrusion followed by crosslinking with bis-dioxaborolane [261]. Building on this concept, can acetoacetate bearing TEMPO be used for upcycling PE via reactive extrusion, as shown in **Schematic 7.6**, followed by cross-linking with diamines?

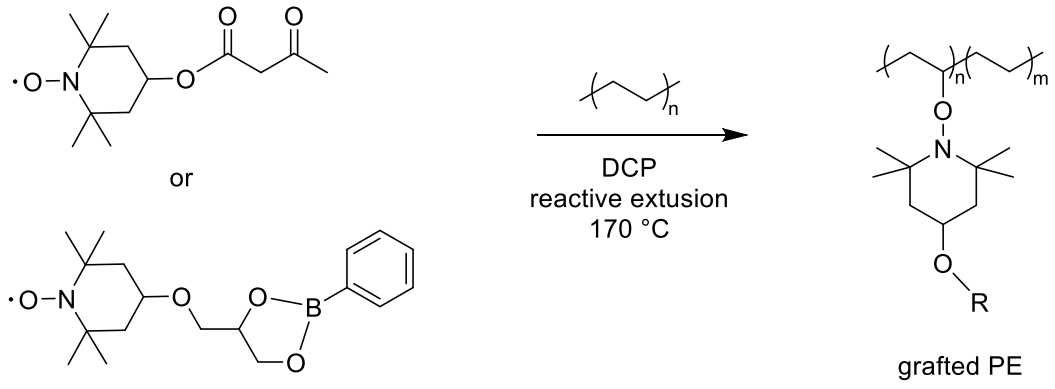

Schematic 7-6 Two proposed synthesis of grafted PE using TEMPO based nitroxides. The dynamic cross-linking can be based on vinylogous urethane exchanges or dioxaborolanes. The grafting agents start from 4-hydroxy-TEMPO similar to the previous literature [261,282].

- Polymer biodegradation is very important to tackle the plastic waste issue. One possible route is to explore vitrimeric systems that can undergo controlled degradation by manipulation of the C-C backbone. Copolymerization with lipoic acid can be an intriguing avenue to incorporate S-S bonds and use dynamic cross-links to compensate for their potential weaker thermomechanical properties [283]. **Schematic 7.6** illustrates a proposed copolymerization of Myr with lipoic acid (or functionalized lipoic acid). The S-S dyads can be used for depolymerization using mild reducing agents such as tris(2-carboxyethyl)phosphine (TCEP) [284,285].

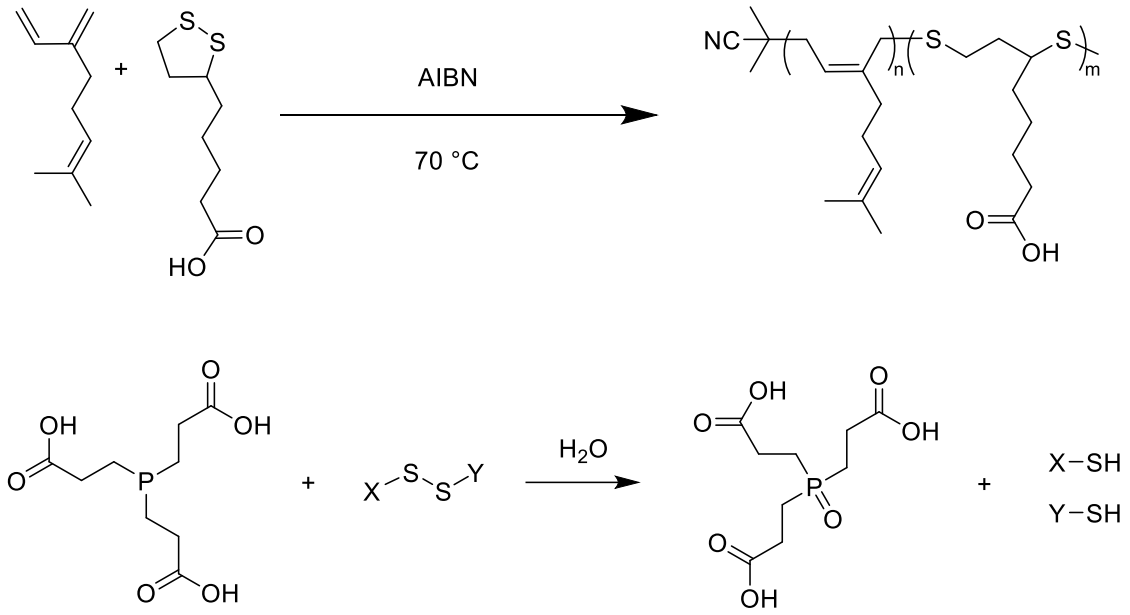

Schematic 7-7 Proposed copolymerization of Myr with lipoic acid. The imparted S-S dyads in the polymer backbone can be targeted for depolymerization using TCEP

- Inter-disciplinary applications of functional dynamic networks are remarkably interesting. One example can be using dynamic bonds for the synthesis of polymeric membranes for separation processes used in water purification. Can we make dynamically cross-linked ultra/nanofiltration membranes that are fully recyclable?

7.4. Summary

In conclusion, controlled radical polymerization was employed to fabricate novel linear copolymers of terpene-based Myr with acetoacetate methacrylate (Chapters 3 and 4) as well as copolymers of vegetable oil-based alkyl methacrylate and vanillin methacrylate (Chapters 5 and 6). Dynamic networks based on vinylogous urethanes (Chapter 3 and 4) and Schiff base (Chapter 5 and 6) were synthesized by crosslinking with multifunctional amines. The properties of the vitrimers could be highly customized by manipulation of the type of functional comonomer and loading, nature of the cross-linker molecule, and degree of cross-linking, as well as microstructure of the prepolymer. All synthesized vitrimers were highly re-processable and mechanically recyclable. This work shows the adaptability of bio-based vitrimeric polymers for the development of more sustainable elastomers. Dynamic bonds can tailor and enhance the rheo-mechanical properties of the polymers without sacrificing their renewability and re-processability. This approach can be used as a platform to develop customized recyclable bio-based elastomers with applications in rubbers, smart materials, wearable electronics, to name but a few.

Indeed, there is so much work left to do and possibilities for applications of dynamic networks are endless, and we are limited only by our own imagination!

References

[1] R. Mülhaupt, Hermann Staudinger and the Origin of Macromolecular Chemistry, Angewandte Chemie International Edition 43 (2004) 1054–1063. https://doi.org/10.1002/ANIE.200330070.

[2] M. Shen, W. Huang, M. Chen, B. Song, G. Zeng, Y. Zhang, (Micro)plastic crisis: Un-ignorable contribution to global greenhouse gas emissions and climate change, Journal of Cleaner Production 254 (2020) 120138. https://doi.org/10.1016/j.jclepro.2020.120138.

[3] S.B. Borrelle, J. Ringma, K.L. Law, C.C. Monnahan, L. Lebreton, A. McGivern, E. Murphy, J. Jambeck, G.H. Leonard, M.A. Hilleary, M. Eriksen, H.P. Possingham, H. De Frond, L.R. Gerber, B. Polidoro, A. Tahir, M. Bernard, N. Mallos, M. Barnes, C.M. Rochman, Predicted growth in plastic waste exceeds efforts to mitigate plastic pollution, Science 369 (2020) 1515–1518. https://doi.org/10.1126/science.aba3656.

[4] M.A. Hillmyer, The promise of plastics from plants, Science 358 (2017) 868–870. https://doi.org/10.1126/science.aao6711.

[5] T.R. Walker, D. Xanthos, A call for Canada to move toward zero plastic waste by reducing and recycling single-use plastics, Resources, Conservation and Recycling 133 (2018) 99–100. https://doi.org/10.1016/j.resconrec.2018.02.014.

[6] Canadian Council of Ministers of the Environment, Strategy on Zero Plastic Waste (PN 1583), 2018. https://ccme.ca/en/current-activities/waste.

[7] B.D. Vogt, K.K. Stokes, S.K. Kumar, Why is Recycling of Postconsumer Plastics so Challenging?, ACS Applied Polymer Materials 3 (2021) 4325–4346. https://doi.org/10.1021/acsapm.1c00648.

[8] Z. Wang, M.S. Ganewatta, C. Tang, Sustainable polymers from biomass: Bridging chemistry with materials and processing, Progress in Polymer Science 101 (2020) 101197. https://doi.org/10.1016/J.PROGPOLYMSCI.2019.101197.

[9] R.M. Cywar, N.A. Rorrer, C.B. Hoyt, G.T. Beckham, E.Y.X. Chen, Bio-based polymers with performance-advantaged properties, Nature Reviews Materials 2021 7:2 7 (2021) 83–103. https://doi.org/10.1038/s41578-021-00363-3.

[10] N.D. Fitzgerald, Chemistry challenges to enable a sustainable bioeconomy, Nature Reviews Chemistry 2017 1:10 1 (2017) 1–3. https://doi.org/10.1038/s41570-017-0080.

[11] M.A. Lucherelli, A. Duval, L. Avérous, Biobased vitrimers: Towards sustainable and adaptable performing polymer materials, Progress in Polymer Science 127 (2022) 101515. https://doi.org/10.1016/j.progpolymsci.2022.101515.

[12] F. Rodriguez, C. Cohen, C.K. Ober, L.A. Archer, Principles of polymer systems, CRC Press, 2015. https://www.routledge.com/Principles-of-Polymer-Systems/Rodriguez-Cohen-Ober-Archer/p/book/9781482223781 (accessed January 2, 2024).

[13] R.J. Young, P.A. Lovell, Introduction to polymers, CRC Press, 2011.

[14] T.P. Lodge, P.C. Hiemenz, Polymer Chemistry, CRC Press, 2020. https://doi.org/10.1201/9780429190810.

[15] Paul J. Flory, The Mechanism of Vinyl Polymerizations, Journal of the American Chemical Society 59 (1937) 241–253.

[16] A. Anastasaki, Shining a Light on Copper Mediated Living Radical Polymerisation: Maximising End-group Fidelity, (2014). http://go.warwick.ac.uk/wraphttp://go.warwick.ac.uk/wrap/65614 (accessed January 1, 2024).

[17] F. Hajiali, Designing polymer coatings for aerospace industry, McGill University, 2021. https://escholarship.mcgill.ca/concern/theses/tm70n108g.

[18] M. Szwarc, M. Levy, R. Milkovich, Polymerization initiated by electron transfer to monomer. A new method of formation of block polymers, Journal of the American Chemical Society 78 (1956) 2656–2657. https://doi.org/10.1021/ja01592a101.

[19] W.A. Braunecker, K. Matyjaszewski, Controlled/living radical polymerization: Features, developments, and perspectives, Progress in Polymer Science 32 (2007) 93–146. https://doi.org/10.1016/j.progpolymsci.2006.11.002.

[20] J. Zhang, C. Aydogan, G. Patias, T. Smith, L. Al-Shok, H. Liu, A.M. Eissa, D.M. Haddleton, Polymerization of Myrcene in Both Conventional and Renewable Solvents: Postpolymerization Modification via Regioselective Photoinduced Thiol–Ene Chemistry for Use as Carbon Renewable Dispersants, ACS Sustainable Chemistry & Engineering 10 (2022) 9654–9664. https://doi.org/10.1021/acssuschemeng.2c03755.

[21] M. Destarac, Industrial development of reversible-deactivation radical polymerization: is the induction period over?, Polymer Chemistry 9 (2018) 4947. https://doi.org/10.1039/c8py00970h.

[22] S. Penczek, G. Moad, Glossary of terms related to kinetics, thermodynamics, and mechanisms of polymerization (IUPAC Recommendations 2008), Pure and Applied Chemistry 80 (2008) 2163–2193. https://doi.org/10.1351/pac200880102163.

[23] N. Corrigan, K. Jung, G. Moad, C.J. Hawker, K. Matyjaszewski, C. Boyer, Reversible-deactivation radical polymerization (Controlled/living radical polymerization): From discovery to materials design and applications, Progress in Polymer Science 111 (2020) 101311. https://doi.org/10.1016/j.progpolymsci.2020.101311.

[24] D.A. Shipp, Reversible-Deactivation Radical Polymerizations, Polymer Reviews 51 (2011) 99–103. https://doi.org/10.1080/15583724.2011.566406.

[25] K. Matyjaszewski, Lifetimes of polystyrene chains in atom transfer radical polymerization, Macromolecules 32 (1999) 9051–9053. https://doi.org/10.1021/MA991145X/ASSET/IMAGES/MEDIUM/MA991145XE00011.GIF.

[26] C.J. Hawker, A.W. Bosman, E. Harth, New polymer synthesis by nitroxide mediated living radical polymerizations, Chemical Reviews 101 (2001) 3661–3688. https://doi.org/10.1021/CR990119U.

[27] D. Benoit, V. Chaplinski, R. Braslau, C.J. Hawker, Development of a universal alkoxyamine for “living” free radical polymerizations, Journal of the American Chemical Society 121 (1999) 3904–3920. https://doi.org/10.1021/ja984013c.

[28] D. Solomon, E. Rizzardo, P. Cacioli, Polymerization process and polymers produced thereby, 1986.

[29] M.K. Georges, R.P.N. Veregin, P.M. Kazmaier, G.K. Hamer, Narrow Molecular Weight Resins by a Free-Radical Polymerization Process, 1993. https://doi.org/10.1021/ma00063a054.

[30] H. Fischer, The Persistent Radical Effect in Controlled Radical Polymerizations, J Polym Sci A: Polym Chem 37 (1999) 1885–1901. https://doi.org/10.1002/(SICI)1099-0518(19990701)37:13.

[31] M. Maric, Application of Nitroxide Mediated Polymerization in Different Monomer Systems, Current Organic Chemistry 22 (2018) 1264–1284. https://doi.org/10.2174/1385272822666180404144327.

[32] D. Benoit, S. Grimaldi, S. Robin, J.P. Finet, P. Tordo, Y. Gnanou, Kinetics and mechanism of controlled free-radical polymerization of styrene and n-butyl acrylate in the presence of an acyclic β-phosphonylated nitroxide, Journal of the American Chemical Society 122 (2000) 5929–5939. https://doi.org/10.1021/ja991735a.

[33] S. Grimaldi, J.P. Finet, F. Le Moigne, A. Zeghdaoui, P. Tordo, D. Benoit, M. Fontanille, Y. Gnanou, Acyclic β-phosphonylated nitroxides: a new series of counter-radicals for 'living'/controlled free radical polymerization, Macromolecules 33 (2000) 1141–1147. https://doi.org/10.1021/MA9913414.

[34] J. Nicolas, Y. Guillaneuf, D. Bertin, D. Gigmes, B. Charleux, Nitroxide-Mediated Polymerization, in: Polymer Science: A Comprehensive Reference, 10 Volume Set, Elsevier, 2012: pp. 277–350. https://doi.org/10.1016/B978-0-444-53349-4.00069-8.

[35] J. Ruehl, C. Morimoto, D.J. Stevens, R. Braslau, Carboxylic acid- and hydroxy-functionalized alkoxyamine initiators for nitroxide mediated radical polymerization, Reactive and Functional Polymers 68 (2008) 1563–1577. https://doi.org/10.1016/j.reactfunctpolym.2008.08.010.

[36] J. Nicolas, S. Brusseau, B. Charleux, A minimal amount of acrylonitrile turns the nitroxide-mediated polymerization of methyl methacrylate into an almost ideal controlled/living system, Journal of Polymer Science Part A: Polymer Chemistry 48 (2010) 34–47. https://doi.org/10.1002/pola.23749.

[37] N. Ballard, M. Aguirre, A. Simula, A. Agirre, J.R. Leiza, J.J. Asua, S. Van Es, † Polymat, K.A. Saila, New Class of Alkoxyamines for Efficient Controlled Homopolymerization of Methacrylates, 5 (2016) 23. https://doi.org/10.1021/acsmacrolett.6b00547.

[38] A. Simula, N. Ballard, M. Aguirre, J.R. Leiza, S. van Es, J.M. Asua, Nitroxide mediated copolymerization of acrylates, methacrylates and styrene: The importance of side reactions in the polymerization of acrylates, European Polymer Journal 110 (2019) 319–329. https://doi.org/10.1016/j.eurpolymj.2018.11.041.

[39] A. Simula, M. Aguirre, N. Ballard, A. Veloso, J.R. Leiza, S. Van Es, J.M. Asua, Novel alkoxyamines for the successful controlled polymerization of styrene and methacrylates, Polymer Chemistry 8 (2017) 1728–1736. https://doi.org/10.1039/c6py02190e.

[40] F. Hajiali, S. Tajbakhsh, M. Marić, Thermally reprocessable bio-based polymethacrylate vitrimers and nanocomposites, Polymer 212 (2021) 123126. https://doi.org/10.1016/j.polymer.2020.123126.

[41] S.B. Luk, M. Marić, Nitroxide-Mediated Polymerization of Bio-Based Farnesene with a Functionalized Methacrylate, Macromolecular Reaction Engineering 13 (2019) 1800080. https://doi.org/10.1002/mren.201800080.

[42] H.R. Lamontagne, B.H. Lessard, Nitroxide-Mediated Polymerization: A Versatile Tool for the Engineering of Next Generation Materials, ACS Applied Polymer Materials 2 (2020) 5327–5344. https://doi.org/10.1021/acsapm.0c00888.

[43] J. Chiefari, Y.K. Chong, F. Ercole, J. Krstina, J. Jeffery, T.P.T. Le, R.T.A. Mayadunne, G.F. Meijs, C.L. Moad, G. Moad, E. Rizzardo, S.H. Thang, Living free-radical polymerization by reversible addition - Fragmentation chain transfer: The RAFT process, Macromolecules 31 (1998) 5559–5562. https://doi.org/10.1021/ma9804951.

[44] M. Destarac, Controlled Radical Polymerization: Industrial Stakes, Obstacles and Achievements, Macromolecular Reaction Engineering 4 (2010) 165–179. https://doi.org/10.1002/mren.200900087.

[45] G. Moad, An Industrial History of RAFT Polymerization, RAFT Polymerization: Methods, Synthesis and Applications: Volume 1 and 2 1–2 (2021) 1077–1169. https://doi.org/10.1002/9783527821358.CH24.

[46] S. Perrier, 50th Anniversary Perspective: RAFT Polymerization - A User Guide, Macromolecules 50 (2017) 7433–7447. https://doi.org/10.1021/acs.macromol.7b00767.

[47] G. Moad, E. Rizzardo, RAFT Polymerization: Methods, Synthesis and Applications: Volume 1 and 2, RAFT Polymerization: Methods, Synthesis and Applications: Volume 1 and 2 1–2 (2021) 1–1240. https://doi.org/10.1002/9783527821358.

[48] A.H.E. Müller, K. (Krzysztof) Matyjaszewski, Controlled and Living Polymerizations, Wiley, 2009. https://doi.org/10.1002/9783527629091.

[49] J. Xu, S. Shanmugam, N.A. Corrigan, C. Boyer, Catalyst-Free Visible Light-Induced RAFT Photopolymerization, (2015). https://pubs.acs.org/sharingguidelines (accessed January 24, 2024).

[50] G. Moad, E. Rizzardo, S.H. Thang, Fundamentals of RAFT Polymerization, Fundamentals of Controlled/Living Radical Polymerization (2013) 205–249. https://doi.org/10.1039/9781849737425-00205.

[51] C.L. Moad, G. Moad, Fundamentals of reversible addition-fragmentation chain transfer (RAFT), Chemistry Teacher International 3 (2021) 3–17. https://doi.org/10.1515/CTI-2020-0026/MACHINEREADABLECITATION/RIS.

[52] X. Tian, J. Ding, B. Zhang, F. Qiu, X. Zhuang, Y. Chen, Recent Advances in RAFT Polymerization: Novel Initiation Mechanisms and Optoelectronic Applications, Polymers 10 (2018). https://doi.org/10.3390/POLYM10030318.

[53] D.J. Keddie, G. Moad, E. Rizzardo, S.H. Thang, RAFT agent design and synthesis, Macromolecules 45 (2012) 5321–5342. https://doi.org/10.1021/MA300410V.

[54] S. Bastien Perrier, P. Takolpuckdee, J. Westwood, D.M. Lewis, Versatile Chain Transfer Agents for Reversible Addition Fragmentation Chain Transfer (RAFT) Polymerization to Synthesize Functional Polymeric Architectures, (2004). https://doi.org/10.1021/ma035468b.

[55] W. Denissen, G. Rivero, R. Nicolaÿ, L. Leibler, J.M. Winne, F.E. Du Prez, Vinylogous Urethane Vitrimers, Advanced Functional Materials 25 (2015) 2451–2457. https://doi.org/10.1002/adfm.201404553.

[56] C.N. Bowman, C.J. Kloxin, Covalent Adaptable Networks: Reversible Bond Structures Incorporated in Polymer Networks, Angewandte Chemie International Edition 51 (2012) 4272–4274. https://doi.org/10.1002/anie.201200708.

[57] J. Zheng, Z.M. Png, S.H. Ng, G.X. Tham, E. Ye, S.S. Goh, X.J. Loh, Z. Li, Vitrimers: Current research trends and their emerging applications, Materials Today (2021). https://doi.org/10.1016/j.mattod.2021.07.003.

[58] W. Denissen, J.M. Winne, F.E. Du Prez, Vitrimers: permanent organic networks with glass-like fluidity, Chemical Science 7 (2016) 30–38. https://doi.org/10.1039/C5SC02223A.

[59] N.J. Van Zee, R. Nicolaÿ, Vitrimers: Permanently crosslinked polymers with dynamic network topology, Progress in Polymer Science 104 (2020) 101233. https://doi.org/10.1016/j.progpolymsci.2020.101233.

[60] A.M. Wemyss, C. Bowen, C. Plesse, C. Vancaeyzeele, G.T.M. Nguyen, F. Vidal, C. Wan, Dynamic crosslinked rubbers for a green future: A material perspective, Materials Science and Engineering: R: Reports 141 (2020) 100561. https://doi.org/10.1016/j.mser.2020.100561.

[61] C. Bowman, F. Du Prez, J. Kalow, Introduction to chemistry for covalent adaptable networks, Polymer Chemistry 11 (2020) 5295–5296. https://doi.org/10.1039/D0PY90102D.

[62] K.M. Lindenmeyer, R.D. Johnson, K.M. Miller, Self-healing behaviour of furan–maleimide poly(ionic liquid) covalent adaptable networks, Polymer Chemistry 11 (2020) 5321–5326. https://doi.org/10.1039/d0py00016g.

[63] M.A. Tasdelen, Diels–Alder “click” reactions: recent applications in polymer and material science, Polymer Chemistry 2 (2011) 2133–2145. https://doi.org/10.1039/C1PY00041A.

[64] C.J. Kloxin, T.F. Scott, B.J. Adzima, C.N. Bowman, Covalent Adaptable Networks (CANs): A Unique Paradigm in Cross-Linked Polymers, Macromolecules 43 (2010) 2643–2653. https://doi.org/10.1021/ma902596s.

[65] D. Montarnal, M. Capelot, F. Tournilhac, L. Leibler, Silica-Like Malleable Materials from Permanent Organic Networks, Science 334 (2011) 965–968. https://doi.org/10.1126/science.1212648.

[66] B.M. El-Zaatari, J.S.A. Ishibashi, J.A. Kalow, Cross-linker control of vitrimer flow, Polymer Chemistry 11 (2020) 5339–5345. https://doi.org/10.1039/D0PY00233J.

[67] L.E. Porath, C.M. Evans, Importance of Broad Temperature Windows and Multiple Rheological Approaches for Probing Viscoelasticity and Entropic Elasticity in Vitrimers, 12 (2021) 43. https://doi.org/10.1021/acs.macromol.0c02800.

[68] M.L. Martins, X. Zhao, Z. Demchuk, J. Luo, G.P. Carden, G. Toleutay, A.P. Sokolov, Viscoelasticity of Polymers with Dynamic Covalent Bonds: Concepts and Misconceptions, Macromolecules 56 (2023) 8688–8696. https://doi.org/10.1021/ACS.MACROMOL.3C01545.

[69] D.J. Fortman, J.P. Brutman, C.J. Cramer, M.A. Hillmyer, W.R. Dichtel, Mechanically Activated, Catalyst-Free Polyhydroxyurethane Vitrimers, J. Am. Chem. Soc. 137 (2015) 14019–14022. https://doi.org/10.1021/jacs.5b08084.

[70] J.P. Brutman, P.A. Delgado, M.A. Hillmyer, Polylactide vitrimers, ACS Macro Letters 3 (2014) 607–610. https://doi.org/10.1021/MZ500269W.

[71] Y. Zhou, J.G.P. Goossens, S. van den Bergen, R.P. Sijbesma, J.P.A. Heuts, In Situ Network Formation in PBT Vitrimers via Processing-Induced Deprotection Chemistry, Macromolecular Rapid Communications 39 (2018) 1800356. https://doi.org/10.1002/marc.201800356.

[72] Y.X. Lu, F. Tournilhac, L. Leibler, Z. Guan, Making insoluble polymer networks malleable via olefin metathesis, Journal of the American Chemical Society 134 (2012) 8424–8427. https://doi.org/10.1021/JA303356Z

[73] M. Röttger, T. Domenech, R. van der Weegen, A. Breuillac, R. Nicolaÿ, L. Leibler, High-performance vitrimers from commodity thermoplastics through dioxaborolane metathesis, Science 356 (2017) 62–65. https://doi.org/10.1126/science.aah5281.

[74] S. Wu, H. Yang, W.-S. Xu, Q. Chen, Thermodynamics and Reaction Kinetics of Symmetric Vitrimers Based on Dioxaborolane Metathesis, Macromolecules 54 (2021) 6799–6809. https://doi.org/10.1021/acs.macromol.1c00697.

[75] A. Breuillac, A. Kassalias, R. Nicolaÿ, Polybutadiene Vitrimers Based on Dioxaborolane Chemistry and Dual Networks with Static and Dynamic Cross-links, Macromolecules 52 (2019) 7102–7113. https://doi.org/10.1021/acs.macromol.9b01288.

[76] F. Caffy, R. Nicolaÿ, Transformation of polyethylene into a vitrimer by nitroxide radical coupling of a bis-dioxaborolane, Polymer Chemistry 10 (2019) 3107–3115. https://doi.org/10.1039/C9PY00253G.

[77] S. Tajbakhsh, F. Hajiali, K. Guinan, M. Marić, Highly reprocessable, room temperature self-healable bio-based materials with boronic-ester dynamic cross-linking, Reactive and Functional Polymers 158 (2021) 104794. https://doi.org/10.1016/j.reactfunctpolym.2020.104794.

[78] A.P. Bapat, D. Roy, J.G. Ray, D.A. Savin, B.S. Sumerlin, Dynamic-Covalent Macromolecular Stars with Boronic Ester Linkages, Journal of the American Chemical Society 133 (2011) 19832–19838. https://doi.org/10.1021/ja207005z.

[79] M. Gosecki, M. Gosecka, Boronic Acid Esters and Anhydrates as Dynamic Cross-Links in Vitrimers, Polymers 14 (2022) 842. https://doi.org/10.3390/polym14040842.

[80] J.J. Cash, T. Kubo, A.P. Bapat, B.S. Sumerlin, Room-Temperature Self-Healing Polymers Based on Dynamic-Covalent Boronic Esters, Macromolecules 48 (2015) 2098–2106. https://doi.org/10.1021/acs.macromol.5b00210.

[81] A. Zych, J. Tellers, L. Bertolacci, L. Ceseracciu, L. Marini, G. Mancini, A. Athanassiou, Biobased, Biodegradable, Self-Healing Boronic Ester Vitrimers from Epoxidized Soybean Oil Acrylate, Cite This: ACS Appl. Polym. Mater 2021 (2020) 1135–1144. https://doi.org/10.1021/acsapm.0c01335.

[82] O.R. Cromwell, J. Chung, Z. Guan, Malleable and Self-Healing Covalent Polymer Networks through Tunable Dynamic Boronic Ester Bonds, Journal of the American Chemical Society 137 (2015) 6492–6495. https://doi.org/10.1021/jacs.5b03551.

[83] L. Huang, Y. Yang, Z. Niu, R. Wu, W. Fan, Q. Dai, J. He, C. Bai, Boronic ester bonds crosslinked vitrimer elastomers with mechanical robustness, shape memory, self-healing and recyclability properties, Composites Science and Technology 228 (2022) 109621. https://doi.org/10.1016/j.compscitech.2022.109621.

[84] Z.H. Zhao, D.P. Wang, J.L. Zuo, C.H. Li, A Tough and Self-Healing Polymer Enabled by Promoting Bond Exchange in Boronic Esters with Neighboring Hydroxyl Groups, ACS Materials Letters 3 (2021) 1328–1338. https://doi.org/10.1021/ACSMATERIALSLETT.1C00314

[85] R. Guo, Q. Su, J. Zhang, A. Dong, C. Lin, J. Zhang, Facile Access to Multisensitive and Self-Healing Hydrogels with Reversible and Dynamic Boronic Ester and Disulfide Linkages, Biomacromolecules 18 (2017) 1356–1364. https://doi.org/10.1021/acs.biomac.7b00089.

[86] C.A. Tretbar, J.A. Neal, Z. Guan, Direct Silyl Ether Metathesis for Vitrimers with Exceptional Thermal Stability, Journal of the American Chemical Society 141 (2019) 16595–16599. https://doi.org/10.1021/jacs.9b08876.

[87] Y. Nishimura, J. Chung, H. Muradyan, Z. Guan, Silyl Ether as a Robust and Thermally Stable Dynamic Covalent Motif for Malleable Polymer Design, Journal of the American Chemical Society 139 (2017) 14881–14884. https://doi.org/10.1021/jacs.7b08826.

[88] W. Denissen, M. Droesbeke, R. Nicolaÿ, L. Leibler, J.M. Winne, F.E. Du Prez, Chemical control of the viscoelastic properties of vinylogous urethane vitrimers, Nature Communications 8 (2017) 14857. https://doi.org/10.1038/ncomms14857.

[89] Y. Spiesschaert, J. Danneels, N. Van Herck, M. Guerre, G. Acke, J. Winne, F. Du Prez, Polyaddition Synthesis Using Alkyne Esters for the Design of Vinylogous Urethane Vitrimers, Macromolecules 54 (2021) 7931–7942. https://doi.org/10.1021/acs.macromol.1c01049.

[90] S. Weerathaworn, V. Abetz, Tailor-Made Vinylogous Urethane Vitrimers Based on Binary and Ternary Block and Random Copolymers: An Approach toward Reprocessable Materials, Macromolecular Chemistry and Physics 224 (2023) 2200248. https://doi.org/10.1002/macp.202200248.

[91] Z. Liu, C. Zhang, Z. Shi, J. Yin, M. Tian, Tailoring vinylogous urethane chemistry for the cross-linked polybutadiene: Wide freedom design, multiple recycling methods, good shape memory behavior, Polymer 148 (2018) 202–210. https://doi.org/10.1016/j.polymer.2018.06.042.

[92] A. Roig, V. D'Agostino, À. Serra, S. De la Flor, Towards fast relaxation rates and creep resistance in disulfide vitrimer-like materials, Reactive and Functional Polymers 193 (2023) 105764. https://doi.org/10.1016/J.REACTFUNCTPOLYM.2023.105764.

[93] L. Imbernon, E.K. Oikonomou, S. Norvez, L. Leibler, Chemically crosslinked yet reprocessable epoxidized natural rubber via thermo-activated disulfide rearrangements, Polym. Chem 6 (2015) 4271. https://doi.org/10.1039/c5py00459d.

[94] S.K. Schoustra, M.H.P. de Heer Kloots, J. Posthuma, D. van Doorn, J.A. Dijksman, M.M.J. Smulders, Raman Spectroscopy Reveals Phase Separation in Imine-Based Covalent Adaptable Networks, Macromolecules 55 (2022) 10341–10355. https://doi.org/10.1021/acs.macromol.2c01595.

[95] A. Liguori, M. Hakkarainen, Designed from Biobased Materials for Recycling: Imine-Based Covalent Adaptable Networks, Macromolecular Rapid Communications 43 (2022) 2100816. https://doi.org/10.1002/marc.202100816.

[96] Y. Xu, K. Odelius, M. Hakkarainen, Photocurable, Thermally Reprocessable, and Chemically Recyclable Vanillin-Based Imine Thermosets, ACS Sustainable Chemistry & Engineering 8 (2020) 17272–17279. https://doi.org/10.1021/acssuschemeng.0c06248.

[97] S. Guggari, F. Magliozzi, S. Malburet, A. Graillot, M. Destarac, M. Guerre, Vanillin-Based Epoxy Vitrimers: Looking at the Cystamine Hardener from a Different Perspective, ACS Sustainable Chemistry & Engineering 11 (2023) 6021–6031. https://doi.org/10.1021/acssuschemeng.3c00379.

[98] M. Guerre, C. Taplan, J.M. Winne, F.E. Du Prez, Vitrimers: directing chemical reactivity to control material properties, (2020). https://doi.org/10.1039/d0sc01069c.

[99] L. Porath, B. Soman, B.B. Jing, C.M. Evans, Vitrimers: Using Dynamic Associative Bonds to Control Viscoelasticity, Assembly, and Functionality in Polymer Networks, ACS Macro Letters 11 (2022) 475–483. https://doi.org/10.1021/acsmacrolett.2c00038.

[100] J. Luo, Z. Demchuk, X. Zhao, T. Saito, M. Tian, A.P. Sokolov, P.F. Cao, Elastic vitrimers: Beyond thermoplastic and thermoset elastomers, Matter 5 (2022) 1391–1422. https://doi.org/10.1016/J.MATT.2022.04.007.

[101] J. Xia, J.A. Kalow, M. Olvera de la Cruz, Structure, Dynamics, and Rheology of Vitrimers, Macromolecules 56 (2023) 8080–8093. https://doi.org/10.1021/acs.macromol.3c01366.

[102] H. Fang, H. Fang, H. Fang, W. Ye, Y. Ding, Y. Ding, H.H. Winter, Rheology of the Critical Transition State of an Epoxy Vitrimer, Macromolecules 53 (2020) 4855–4862. https://doi.org/10.1021/ACS.MACROMOL.0C00843/ASSET/IMAGES/MEDIUM/MA0C00843_M004.GIF.

[103] F. Asempour, M. Marić, Vitrification: Versatile Method To Modulate Properties of Myrcene-Based Rubbers, ACS Applied Polymer Materials 5 (2023) 6364–6376. https://doi.org/10.1021/acsapm.3c00914.

[104] J.J. Lessard, G.M. Scheutz, R.W. Hughes, B.S. Sumerlin, Polystyrene-Based Vitrimers: Inexpensive and Recyclable Thermosets, ACS Applied Polymer Materials 2 (2020) 3044–3048. https://doi.org/10.1021/acsapm.0c00523.

[105] S. Wang, M.W. Urban, Self-healing polymers, Nature Reviews Materials 5 (2020) 562–583. https://doi.org/10.1038/s41578-020-0202-4.

[106] G.M. Scheutz, J.J. Lessard, M.B. Sims, B.S. Sumerlin, Adaptable Crosslinks in Polymeric Materials: Resolving the Intersection of Thermoplastics and Thermosets, Journal of the American Chemical Society 141 (2019) 16181–16196. https://doi.org/10.1021/jacs.9b07922.

[107] J.M. Winne, L. Leibler, F.E. Du Prez, Dynamic covalent chemistry in polymer networks: a mechanistic perspective, Polymer Chemistry 10 (2019) 6091–6108. https://doi.org/10.1039/C9PY01260E.

[108] P. Taynton, K. Yu, R.K. Shoemaker, Y. Jin, H.J. Qi, W. Zhang, Heat- or Water-Driven Malleability in a Highly Recyclable Covalent Network Polymer, Advanced Materials 26 (2014) 3938–3942. https://doi.org/10.1002/adma.201400317.

[109] J.J. Cash, T. Kubo, D.J. Dobbins, B.S. Sumerlin, Maximizing the symbiosis of static and dynamic bonds in self-healing boronic ester networks, Polymer Chemistry 9 (2018) 2011–2020. https://doi.org/10.1039/c8py00123e.

[110] S. Yu, S. Wu, C. Zhang, Z. Tang, Y. Luo, B. Guo, L. Zhang, Catalyst-Free Metathesis of Cyclic Acetals and Spirocyclic Acetal Covalent Adaptable Networks, ACS Macro Letters 9 (2020) 1143–1148. https://doi.org/10.1021/acsmacrolett.0c00527.

[111] M. Ahmadi, A. Hanifpour, S. Ghiassinejad, E. van Ruymbeke, Polyolefins Vitrimers: Design Principles and Applications, Chemistry of Materials 34 (2022) 10249–10271. https://doi.org/10.1021/acs.chemmater.2c02853.

[112] J.J. Lessard, L.F. Garcia, C.P. Easterling, M.B. Sims, K.C. Bentz, S. Arencibia, D.A. Savin, B.S. Sumerlin, Catalyst-Free Vitrimers from Vinyl Polymers, Macromolecules 52 (2019) 2105–2111. https://pubs.acs.org/doi/abs/10.1021/acs.macromol.8b02477.

[113] A. Perego, F. Khabaz, Creep and Recovery Behavior of Vitrimers with Fast Bond Exchange Rate, Macromolecular Rapid Communications 44 (2023) 2200313. https://doi.org/10.1002/marc.202200313.

[114] J.J. Lessard, G.M. Scheutz, S.H. Sung, K.A. Lantz, T.H. Epps, B.S. Sumerlin, Block Copolymer Vitrimers, Journal of the American Chemical Society 142 (2020). https://doi.org/10.1021/jacs.9b10360.

[115] J.S.A. Ishibashi, I.C. Pierce, A.B. Chang, A. Zografos, B.M. El-Zaatari, Y. Fang, S.J. Weigand, F.S. Bates, J.A. Kalow, Mechanical and Structural Consequences of Associative Dynamic Cross-Linking in Acrylic Diblock Copolymers, Macromolecules 54 (2021) 3972–3986. https://doi.org/10.1021/acs.macromol.0c02744.

[116] F. Van Lijsebetten, K. De Bruycker, Y. Spiesschaert, J.M. Winne, F.E. Du Prez, Suppressing Creep and Promoting Fast Reprocessing of Vitrimers with Reversibly Trapped Amines, Angewandte Chemie International Edition 61 (2022) e202113872. https://doi.org/10.1002/anie.202113872.

[117] Chuanbing Tang, Chang Y. Ryu, Sustainable Polymers from Biomass, Wiley-VCH Verlag GmbH & Co. KGaA, Weinheim, Germany, 2017. https://doi.org/10.1002/9783527340200.

[118] N. Bauer, J. Brunke, G. Kali, Controlled Radical Polymerization of Myrcene in Bulk: Mapping the Effect of Conditions on the System, ACS Sustainable Chemistry and

Engineering 5 (2017) 10084–10092. https://pubs.acs.org/doi/abs/10.1021/acssuschemeng.7b02091.

[119] P. Sarkar, A.K. Bhowmick, Terpene Based Sustainable Elastomer for Low Rolling Resistance and Improved Wet Grip Application: Synthesis, Characterization and Properties of Poly(styrene-co-myrcene), ACS Sustainable Chemistry & Engineering 4 (2016) 5462–5474. https://doi.org/10.1021/acssuschemeng.6b01038.

[120] S.B. Luk, L.A. Azevedo, M. Maric, Reversible deactivation radical polymerization of bio-based dienes, Reactive and Functional Polymers 162 (2021) 104871. https://doi.org/10.1016/j.reactfunctpolym.2021.104871.

[121] I. Magaña, R. López, F.J. Enríquez-Medrano, S. Kumar, A. Aguilar-Sanchez, R. Handa, R. Díaz de León, L. Valencia, Bioelastomers: current state of development, Journal of Materials Chemistry A 10 (2022) 5019–5043. https://doi.org/10.1039/D1TA09404A.

[122] S.B. Luk, A. Métafiot, J. Morize, E. Edeh, M. Marić, Hydrogenation of poly(myrcene) and poly(farnesene) using diimide reduction at ambient pressure, Journal of Polymer Science 59 (2021) 2140–2153. https://doi.org/10.1002/POL.20210479.

[123] A. Behr, L. Johnen, Myrcene as a Natural Base Chemical in Sustainable Chemistry: A Critical Review, ChemSusChem 2 (2009) 1072–1095. https://doi.org/10.1002/CSSC.200900186.

[124] M.W. Halloran, J.A. Nicell, R.L. Leask, M. Marić, Toughening Poly(lactide) with Bio-Based Poly(farnesene) Elastomers, ACS Applied Polymer Materials 4 (2022) 6276–6287. https://doi.org/10.1021/acsapm.2c01183.

[125] A. Métafiot, Y. Kanawati, J.-F. Gérard, B. Defoort, M. Marić, Synthesis of β-Myrcene-Based Polymers and Styrene Block and Statistical Copolymers by SG1 Nitroxide-Mediated Controlled Radical Polymerization, Macromolecules 50 (2017) 3101–3120. https://doi.org/10.1021/acs.macromol.6b02675.

[126] C. Wahlen, H. Frey, Anionic Polymerization of Terpene Monomers: New Options for Bio-Based Thermoplastic Elastomers, Macromolecules 54 (2021) 7323–7336. https://doi.org/10.1021/acs.macromol.1c00770.

[127] P. Sahu, A.K. Bhowmick, G. Kali, Terpene Based Elastomers: Synthesis, Properties, and Applications, Processes 8 (2020) 553. https://doi.org/10.3390/pr8050553.

[128] S. Zhang, L. Han, H. Ma, P. Liu, H. Shen, L. Lei, C. Li, L. Yang, Y. Li, Investigation on Synthesis and Application Performance of Elastomers with Biogenic Myrcene, Industrial & Engineering Chemistry Research 58 (2019) 12845–12853. https://doi.org/10.1021/acs.iecr.9b02010.

[129] A. Métafiot, L. Gagnon, S. Pruvost, P. Hubert, J.-F. Gérard, B. Defoort, M. Marić, β-Myrcene/isobornyl methacrylate SG1 nitroxide-mediated controlled radical polymerization: synthesis and characterization of gradient, diblock and triblock copolymers, RSC Advances 9 (2019) 3377–3395. https://doi.org/10.1039/C8RA09192G.

[130] P. Sarkar, A.K. Bhowmick, Synthesis, characterization and properties of a bio-based elastomer: polymyrcene, RSC Adv. 4 (2014) 61343–61354. https://doi.org/10.1039/C4RA09475A.

[131] P. Sahu, A.K. Bhowmick, Sustainable self-healing elastomers with thermoreversible network derived from biomass via emulsion polymerization, Journal of Polymer Science Part A: Polymer Chemistry 57 (2019) 738–751. https://doi.org/10.1002/pola.29320.

[132] W. Luo, P. Yang, Q. Gan, Z. Zhao, F. Tang, Y. Xu, X. Jia, D. Gong, Reversible addition–fragmentation chain transfer polymerization of myrcene derivatives: an efficient access to fully bio-sourced functional elastomers with recyclable, shape memory and self-healing properties, Polymer Chemistry 12 (2021) 3677–3687. https://doi.org/10.1039/D1PY00549A.

[133] P. Li, C. Hao, H. Wang, T. He, T. Shu, C. Li, L. Yu, N. Yan, Eco-friendly recyclable high performance ramie yarn reinforced polyimine vitrimer composites, Chemical Engineering Journal 457 (2023) 141341. https://doi.org/10.1016/j.cej.2023.141341.

[134] J.C. Kölsch, C.M. Berač, F. Lossada, O.S. Stach, S. Seiffert, A. Walther, P. Besenius, Recyclable Vitrimers from Biogenic Poly(itaconate) Elastomers, Macromolecules 55 (2022) 8032–8039. https://doi.org/10.1021/acs.macromol.2c00825.

[135] Z. Feng, J. Hu, H. Zuo, N. Ning, L. Zhang, B. Yu, M. Tian, Photothermal-Induced Self-Healable and Reconfigurable Shape Memory Bio-Based Elastomer with Recyclable Ability, ACS Applied Materials & Interfaces 11 (2019) 1469–1479. https://doi.org/10.1021/acsami.8b18002.

[136] W. Liu, J. Huang, Z. Gong, J. Fan, Y. Chen, Healable, recyclable and mechanically robust elastomers with multiple dynamic cross-linking bonds, Polymer 252 (2022) 124900. https://doi.org/10.1016/j.polymer.2022.124900.

[137] J. Vinas, N. Chagneux, D. Gigmes, T. Trimaille, A. Favier, D. Bertin, SG1-based alkoxyamine bearing a N-succinimidyl ester: A versatile tool for advanced polymer synthesis, Polymer 49 (2008) 3639–3647. https://doi.org/10.1016/j.polymer.2008.06.017.

[138] A. Moayeri, B. Lessard, M. Maric, Nitroxide mediated controlled synthesis of glycidyl methacrylate-rich copolymers enabled by SG1-based alkoxyamines bearing succinimidyl ester groups, Polymer Chemistry 2 (2011) 2084. https://doi.org/10.1039/c1py00190f.

[139] Á. Pablo-Morales, M.E. Treviño,, E. Saldívar-Guerra, Toward Bio-Sourced Elastomers with Reactive/Polar Groups. Myrcene – Glycidyl Methacrylate Copolymerization: Reactivity Ratios, Properties, and Preliminary RAFT Emulsion Polymerization, Macromolecular Reaction Engineering 16 (2022) 2200007. https://doi.org/10.1002/mren.202200007.

[140] J. Hilschmann, G. Kali, Bio-based polymyrcene with highly ordered structure via solvent free controlled radical polymerization, European Polymer Journal 73 (2015) 363–373. https://doi.org/10.1016/J.EURPOLYMJ.2015.10.021.

[141] A. Métafiot, J.F. Gérard, B. Defoort, M. Marić, Synthesis of β-myrcene/glycidyl methacrylate statistical and amphiphilic diblock copolymers by SG1 nitroxide-mediated controlled radical polymerization, Journal of Polymer Science Part A: Polymer Chemistry 56 (2018) 860–878. https://doi.org/10.1002/POLA.28963.

[142] S. Noppalit, A. Simula, L. Billon, J.M. Asua, On the nitroxide mediated polymerization of methacrylates derived from bio-sourced terpenes in miniemulsion, a step towards sustainable products, Polymer Chemistry 11 (2020) 1151–1160. https://doi.org/10.1039/C9PY01667H.

[143] C. Iacob, M. Heck, M. Wilhelm, Molecular Dynamics of Polymyrcene: Rheology and Broadband Dielectric Spectroscopy on a Stockmayer Type A Polymer, Macromolecules 56 (2023) 188–197. https://doi.org/10.1021/acs.macromol.2c01884.

[144] L.H. Sperling, Introduction to Physical Polymer Science, Wiley, 2005. https://doi.org/10.1002/0471757128.

[145] J.J. Lessard, K.A. Stewart, B.S. Sumerlin, Controlling Dynamics of Associative Networks through Primary Chain Length, Macromolecules 55 (2022) 10052–10061. https://doi.org/10.1021/acs.macromol.2c01909.

[146] S.B. Luk, M. Maric, Farnesene and norbornenyl methacrylate block copolymers: Application of thiol-ene clicking to improve thermal and mechanical properties, Polymer 230 (2021) 124106. https://doi.org/10.1016/j.polymer.2021.124106.

[147] D.W. Van Krevelen, K. Te Nijenhuis, Cohesive Properties and Solubility, in: Properties of Polymers, Elsevier, 2009: pp. 189–227. https://doi.org/10.1016/B978-0-08-054819-7.00007-8.

[148] M.A. Bin Rusayyis, L.M. Fenimore, N.S. Purwanto, J.M. Torkelson, Reprocessable, creep-resistant covalent adaptable networks synthesized using conventional free-radical polymerization conditions with piperidine-based and non-piperidine-based dynamic dialkylamino disulfide chemistry, Polym. Chem. 14 (2023) 3519–3534. https://doi.org/10.1039/D3PY00498H.

[149] J.L. Self, N.D. Dolinski, M.S. Zayas, J. Read De Alaniz, C.M. Bates, Brønsted-Acid-Catalyzed Exchange in Polyester Dynamic Covalent Networks, ACS Macro Lett 7 (2018) 821. https://doi.org/10.1021/acsmacrolett.8b00370.

[150] L. Li, X. Chen, K. Jin, J.M. Torkelson, Vitrimers Designed Both To Strongly Suppress Creep and To Recover Original Cross-Link Density after Reprocessing: Quantitative Theory and Experiments, Macromolecules 51 (2018) 5537–5546. https://doi.org/10.1021/acs.macromol.8b00922.

[151] M.D. Hager, S. Bode, C. Weber, U.S. Schubert, Shape memory polymers: Past, present and future developments, Progress in Polymer Science 49–50 (2015) 3–33. https://doi.org/10.1016/j.progpolymsci.2015.04.002.

[152] D. Horák, P. Shapoval, Reactive poly(glycidyl methacrylate) microspheres prepared by dispersion polymerization, (n.d.). https://onlinelibrary.wiley.com/doi/10.1002/1099-0518(20001101)38:21%3C3855::AID-POLA20%3E3.0.CO;2-2 (accessed August 13, 2024).

[153] P. Sarkar, A.K. Bhowmick, Green Approach toward Sustainable Polymer: Synthesis and Characterization of Poly(myrcene- co-dibutyl itaconate), ACS Sustainable Chemistry & Engineering 4 (2016) 2129–2141. https://doi.org/10.1021/acssuschemeng.5b01591.

[154] F. Asempour, R. Yang, M. Maric, Thermadapt shape memory vitrimeric polymyrcene elastomer, Reactive and Functional Polymers 201 (2024) 105941. https://doi.org/10.1016/j.reactfunctpolym.2024.105941.

[155] L. Imbernon, S. Norvez, From landfilling to vitrimer chemistry in rubber life cycle, European Polymer Journal 82 (2016) 347–376. https://doi.org/10.1016/J.EURPOLYMJ.2016.03.016.

[156] J. Ye, S. Tan, H. Deng, W. Huang, H. Jin, L. Zhang, H. Xiang, M. Zhang, Self-healing and reprocessing of reclaimed rubber prepared by re-crosslinking waste natural rubber powders, Green Chemistry 25 (2023) 6327–6335. https://doi.org/10.1039/D3GC01652H.

[157] C. Ma, W. Liu, X. Zhou, J. He, Z. Wang, Z. Wang, Dynamic Chemical Cross-Linking and Mechanical Training of Bio-Based Polyamides Fabricate Strong and Recyclable Elastomers, ACS Sustainable Chemistry & Engineering 10 (2022) 6775–6783. https://doi.org/10.1021/acssuschemeng.2c01145.

[158] B. Krishnakumar, A. Pucci, P.P. Wadgaonkar, I. Kumar, W.H. Binder, S. Rana, Vitrimers based on bio-derived chemicals: Overview and future prospects, Chemical Engineering Journal 433 (2022) 133261. https://doi.org/10.1016/J.CEJ.2021.133261.

[159] C.-C. Wang, M.-J. Xie, R. Zhang, J. Cao, M.-Z. Tang, Y.-X. Xu, Improved strength, creep resistance and recyclability of polyisoprene vitrimers by bottom-up construction of inhomogeneous network, Polymer 273 (2023) 125854. https://doi.org/10.1016/j.polymer.2023.125854.

[160] D. Hassanian-Moghaddam, N. Asghari, M. Ahmadi, Circular Polyolefins: Advances toward a Sustainable Future, Macromolecules (2023). https://doi.org/10.1021/ACS.MACROMOL.3C00872.

[161] F. Asempour, E. Laurent, Y. Ecochard, M. Maric, Reprocessable Biobased Statistical and Block Copolymer Methacrylic-Based Vitrimers with a Shape Memory Effect, ACS Applied Polymer Materials 6 (2024) 956–966. https://doi.org/10.1021/acsapm.3c02515.

[162] F. Chen, Q. Cheng, F. Gao, J. Zhong, L. Shen, C. Lin, Y. Lin, The effect of latent plasticity on the shape recovery of a shape memory vitrimer, European Polymer Journal 147 (2021) 110304. https://doi.org/10.1016/J.EURPOLYMJ.2021.110304.

[163] J.-C. Lai, J.-F. Mei, X.-Y. Jia, C.-H. Li, X.-Z. You, Z. Bao, A Stiff and Healable Polymer Based on Dynamic-Covalent Boroxine Bonds, Advanced Materials 28 (2016) 8277–8282. https://doi.org/10.1002/adma.201602332.

[164] H. Zhang, D. Wang, N. Wu, C. Li, C. Zhu, N. Zhao, J. Xu, Recyclable, Self-Healing, Thermadapt Triple-Shape Memory Polymers Based on Dual Dynamic Bonds, ACS Applied Materials & Interfaces 12 (2020) 9833–9841. https://doi.org/10.1021/acsami.9b22613.

[165] S. Zhang, L. Pan, L. Xia, Y. Sun, X. Liu, Dynamic polysulfide shape memory networks derived from elemental sulfur and their dual thermo-/photo-induced solid-state plasticity, Reactive and Functional Polymers 121 (2017) 8–14. https://doi.org/10.1016/J.REACTFUNCTPOLYM.2017.10.005.

[166] I.M. Alarifi, A comprehensive review on advancements of elastomers for engineering applications, Advanced Industrial and Engineering Polymer Research 6 (2023) 451–464. https://doi.org/10.1016/J.AIEPR.2023.05.001.

[167] J.M. Bolton, M.A. Hillmyer, T.R. Hoye, Sustainable Thermoplastic Elastomers from Terpene-Derived Monomers, ACS Macro Letters 3 (2014) 717–720. https://doi.org/10.1021/mz500339h.

[168] L.J. Fetters, D.J. Lohse, R.H. Colby, Chain Dimensions and Entanglement Spacings, Physical Properties of Polymers Handbook (2007) 447–454. https://doi.org/10.1007/978-0-387-69002-5_25.

[169] X. Ren, F. Guo, H. Fu, Y. Song, Y. Li, Z. Hou, Scandium-catalyzed copolymerization of myrcene with ethylene and propylene: convenient syntheses of versatile functionalized polyolefins, Polymer Chemistry 9 (2018) 1223–1233. https://doi.org/10.1039/C8PY00039E.

[170] E. Grune, J. Bareuther, J. Blankenburg, M. Appold, L. Shaw, A.H.E. Müller, G. Floudas, L.R. Hutchings, M. Gallei, H. Frey, Towards bio-based tapered block copolymers: the behaviour of myrcene in the statistical anionic copolymerisation, Polymer Chemistry 10 (2019) 1213–1220. https://doi.org/10.1039/C8PY01711E.

[171] J. Zhang, J. Lu, K. Su, D. Wang, B. Han, Bio-based β-myrcene-modified solution-polymerized styrene–butadiene rubber for improving carbon black dispersion and wet skid resistance, Journal of Applied Polymer Science 136 (2019) 48159. https://doi.org/10.1002/app.48159.

[172] D.L. Trumbo, Free radical copolymerization behavior of myrcene I. Copolymers with styrene, methyl methecrylate orp-fluorostyrene, Polymer Bulletin 31 (1993) 629–636.

[173] S. Tajbakhsh, F. Hajiali, M. Marić, Nitroxide-Mediated Miniemulsion Polymerization of Bio-Based Methacrylates, Industrial & Engineering Chemistry Research 59 (2020) 8921–8936. https://doi.org/10.1021/acs.iecr.0c00840.

[174] F. Hajiali, A. Métafiot, L. Benitez-Ek, L. Alloune, M. Marić, Nitroxide mediated polymerization of sustainably sourced isobornyl methacrylate and tridecyl methacrylate with acrylonitrile co-monomer, Journal of Polymer Science Part A: Polymer Chemistry 56 (2018) 2422–2436. https://doi.org/10.1002/pola.29216.

[175] N.A. Lynd, R.C. Ferrier, B.S. Beckingham, Recommendation for Accurate Experimental Determination of Reactivity Ratios in Chain Copolymerization, Macromolecules 52 (2019) 2277–2285. https://doi.org/10.1021/acs.macromol.8b01752.

[176] V.E. Meyer, G.G. Lowry, Integral and differential binary copolymerization equations, Journal of Polymer Science Part A: General Papers 3 (1965) 2843–2851. https://doi.org/10.1002/POL.1965.100030811.

[177] K. Farajzadehahary, X. Telleria-Allika, J.M. Asua, N. Ballard, An artificial neural network to predict reactivity ratios in radical copolymerization, Polymer Chemistry 14 (2023) 2779–2787. https://doi.org/10.1039/D3PY00246B.

[178] S. Robin, Y. Gnanou, Synthesis of Polystyrene—Polyacrylate Block Copolymers by Nitroxide-Mediated Radical Polymerization, in: ACS Symposium Series, Oxford University Press, 2000: pp. 334–346. https://doi.org/10.1021/bk-2000-0768.ch023.

[179] M. Fache, C. Montérémal, B. Boutevin, S. Caillol, Amine hardeners and epoxy cross-linker from aromatic renewable resources, European Polymer Journal 73 (2015) 344–362. https://doi.org/10.1016/J.EURPOLYMJ.2015.10.032.

[180] U. Kalita, S. Samanta, S.L. Banerjee, N.C. Das, N.K. Singha, Biobased Thermoplastic Elastomer Based on an SMS Triblock Copolymer Prepared *via* RAFT Polymerization in

Aqueous Medium, Macromolecules 54 (2021) 1478–1488. https://doi.org/10.1021/acs.macromol.0c02169.

[181] T. Yan, A.H. Balzer, K.M. Herbert, T.H. Epps, L.S.T.J. Korley, Circularity in polymers: addressing performance and sustainability challenges using dynamic covalent chemistries, Chemical Science 14 (2023). https://doi.org/10.1039/d3sc00551h.

[182] C.C. Hornat, M.W. Urban, Shape memory effects in self-healing polymers, Progress in Polymer Science (2020) 101208. https://doi.org/10.1016/j.progpolymsci.2020.101208.

[183] F. Pilate, A. Toncheva, P. Dubois, J.-M. Raquez, Shape-memory polymers for multiple applications in the materials world, European Polymer Journal 80 (2016) 268–294. https://doi.org/10.1016/j.eurpolymj.2016.05.004.

[184] M. Qi, L. Zheng, C. Li, Y. Xiao, J. Liu, S. Wu, B. Zhang, The yellowing mechanism of polyesteramide based on poly(ethylene terephthalate) and polyamide 6, Journal of Applied Polymer Science 138 (2021) 49986. https://doi.org/10.1002/APP.49986.

[185] R.A. Newmark, R.N. Majumdar, 13 C-NMR spectra of cis -polymyrcene and cis -polyfarnesene, Journal of Polymer Science Part A: Polymer Chemistry 26 (1988) 71–77. https://doi.org/10.1002/pola.1988.080260107.

[186] S. Zhang, Q. Hu, Y.-X. Zhang, H. Guo, Y. Wu, M. Sun, X. Zhu, J. Zhang, S. Gong, P. Liu, Z. Niu, Depolymerization of polyesters by a binuclear catalyst for plastic recycling, Nature Sustainability 6 (2023) 965–973. https://doi.org/10.1038/s41893-023-01118-4.

[187] L. Li, X. Chen, K. Jin, M.B. Rusayyis, J.M. Torkelson, Arresting Elevated-Temperature Creep and Achieving Full Cross-Link Density Recovery in Reprocessable Polymer Networks and Network Composites via Nitroxide-Mediated Dynamic Chemistry, Macromolecules 54 (2021) 1452–1464. https://doi.org/10.1021/acs.macromol.0c01691.

[188] D.K. Schneiderman, M.A. Hillmyer, 50th Anniversary Perspective: There Is a Great Future in Sustainable Polymers, Macromolecules 50 (2017) 3733–3749. http://dx.doi.org/10.1021/acs.macromol.7b00293.

[189] S. Wang, L. Li, Q. Liu, M.W. Urban, Self-Healable Acrylic-Based Covalently Adaptable Networks, Macromolecules 55 (2022) 4703–4709. https://doi.org/10.1021/acs.macromol.2c00739.

[190] F. Van Lijsebetten, T. Debsharma, J.M. Winne, F.E. Du Prez, A Highly Dynamic Covalent Polymer Network without Creep: Mission Impossible?, Angewandte Chemie - International Edition 61 (2022). https://doi.org/10.1002/ANIE.202210405.

[191] R.G. Ricarte, F. Ois Tournilhac, M. Cloître, L. Leibler, Linear Viscoelasticity and Flow of Self-Assembled Vitrimers: The Case of a Polyethylene/Dioxaborolane System, Macromolecules 53 (2020) 1852–1866. https://doi.org/10.1021/acs.macromol.9b02415.

[192] M.H.P. de Heer Kloots, S.K. Schoustra, J.A. Dijksman, M.M.J. Smulders, Phase separation in supramolecular and covalent adaptable networks, Soft Matter 19 (2023) 2857–2877. https://doi.org/10.1039/D3SM00047H.

[193] M. W. Halloran, L. Danielczak, J. A. Nicell, R. L. Leask, M. Marić, Highly Flexible Polylactide Food Packaging Plasticized with Nontoxic, Biosourced Glycerol Plasticizers,

ACS Applied Polymer Materials 4 (2022) 3608–3617. https://doi.org/10.1021/acsapm.2c00172.

[194] B.L. Tardy, E. Lizundia, C. Guizani, M. Hakkarainen, M.H. Sipponen, Prospects for the integration of lignin materials into the circular economy, Materials Today 65 (2023) 122–132. https://doi.org/10.1016/J.MATTOD.2023.04.001.

[195] A.L. Holmberg, J.F. Stanzione, R.P. Wool, T.H. Epps, A Facile Method for Generating Designer Block Copolymers from Functionalized Lignin Model Compounds, ACS Sustainable Chemistry & Engineering 2 (2014) 569–573. https://doi.org/10.1021/sc400497a.

[196] C. Zhang, S.A. Madbouly, M.R. Kessler, Renewable Polymers Prepared from Vanillin and Its Derivatives, Macromolecular Chemistry and Physics 216 (2015) 1816–1822. https://doi.org/10.1002/macp.201500194.

[197] J. S. Mahajan, R. M. O'Dea, J. B. Norris, L. T. J. Korley, T. H. Epps III, Aromatics from Lignocellulosic Biomass: A Platform for High-Performance Thermosets, ACS Sustainable Chemistry & Engineering 8 (2020) 15072–15096. https://doi.org/10.1021/acssuschemeng.0c04817.

[198] S. Subramaniyan, M. Bergoglio, M. Sangermano, M. Hakkarainen, Vanillin-Derived Thermally Reprocessable and Chemically Recyclable Schiff-Base Epoxy Thermosets, Global Challenges 7 (2023). https://doi.org/10.1002/gch2.202200234.

[199] A. Liguori, S. Subramaniyan, J.G. Yao, M. Hakkarainen, Photocurable extended vanillin-based resin for mechanically and chemically recyclable, self-healable and digital light processing 3D printable thermosets, European Polymer Journal 178 (2022) 111489. https://doi.org/10.1016/j.eurpolymj.2022.111489.

[200] S. Gao, Z. Cheng, X. Zhou, Y. Liu, J. Wang, C. Wang, F. Chu, F. Xu, D. Zhang, Fabrication of lignin based renewable dynamic networks and its applications as self-healing, antifungal and conductive adhesives, Chemical Engineering Journal 394 (2020) 124896. https://doi.org/10.1016/j.cej.2020.124896.

[201] X. Gong, Z. Cheng, S. Gao, D. Zhang, Y. Ma, J. Wang, C. Wang, F. Chu, Ethyl cellulose based self-healing adhesives synthesized via RAFT and aromatic schiff-base chemistry, Carbohydrate Polymers 250 (2020) 116846. https://doi.org/10.1016/J.CARBPOL.2020.116846.

[202] M.G. González, J.C. Cabanelas, J. Baselga, Applications of FTIR on Epoxy Resins - Identification, Monitoring the Curing Process, Phase Separation and Water Uptake, in: T. Theophanides (Ed.), Infrared Spectroscopy - Materials Science, Engineering and Technology, InTech, Rijeka, 2012: p. Ch. 13. https://doi.org/10.5772/36323.

[203] A. Roig, A. Petrauskaité, X. Ramis, S. De la Flor, À. Serra, Synthesis and characterization of new bio-based poly(acylhydrazone) vanillin vitrimers, Polymer Chemistry 13 (2022) 1510–1519. https://doi.org/10.1039/D1PY01694F.

[204] F.S. Bates, G.H. Fredrickson, Block Copolymer Thermodynamics: Theory and Experiment, Annual Review of Physical Chemistry 41 (1990) 525–557. https://doi.org/10.1146/annurev.pc.41.100190.002521.

[205] L. Leibler, Theory of Microphase Separation in Block Copolymers, Macromolecules 13 (1980) 1602–1617. https://doi.org/10.1021/ma60078a047.

[206] W. Ding, M.L. Robertson, Sustainable thermoplastic elastomers with a transient network, European Polymer Journal 113 (2019) 411–423. https://doi.org/10.1016/j.eurpolymj.2019.01.010.

[207] D.P. Chatterjee, B.M. Mandal, Triblock Thermoplastic Elastomers with Poly(lauryl methacrylate) as the Center Block and Poly(methyl methacrylate) or Poly(tert-butyl methacrylate) as End Blocks. Morphology and Thermomechanical Properties, Macromolecules 39 (2006) 9192–9200. https://doi.org/10.1021/ma061391q.

[208] R.G. Ricarte, S. Shanbhag, Unentangled Vitrimer Melts: Interplay between Chain Relaxation and Cross-link Exchange Controls Linear Rheology, Macromolecules 54 (2021) 3304–3320. https://doi.org/10.1021/acs.macromol.0c02530.

[209] D.J. Fortman, J.P. Brutman, G.X. De Hoe, R.L. Snyder, W.R. Dichtel, M.A. Hillmyer, Approaches to Sustainable and Continually Recyclable Cross-Linked Polymers, ACS Sustainable Chemistry & Engineering 6 (2018) 11145–11159. https://doi.org/10.1021/acssuschemeng.8b02355.

[210] A. Adjaoud, L. Puchot, P. Verge, High- Tg and Degradable Isosorbide-Based Polybenzoxazine Vitrimer, ACS Sustainable Chemistry & Engineering 10 (2022) 594–602. https://doi.org/10.1021/acssuschemeng.1c07093.

[211] C.C. Hornat, Y. Yang, M.W. Urban, Quantitative Predictions of Shape-Memory Effects in Polymers, Advanced Materials 29 (2017) 1603334. https://doi.org/10.1002/adma.201603334.

[212] M. Buback, U. Geers, C.H. Kurz, J. Heyne, Propagation rate coefficients in free-radical homopolymerizations of butyl methacrylate and dodecyl methacrylate, Macromolecular Chemistry and Physics 198 (1997) 3451–3464. https://doi.org/10.1002/MACP.1997.021981110.

[213] A.-V.G. Ruzette, P. Banerjee, A.M. Mayes, M. Pollard, T.P. Russell, R. Jerome, T. Slawecki, R. Hjelm, P. Thiyagarajan, Phase Behavior of Diblock Copolymers between Styrene and n-Alkyl Methacrylates, Macromolecules 31 (1998) 8509–8516. https://doi.org/10.1021/ma981055c.

[214] F. Asempour, E. Laurent, T. Bride, M. Maric, Rheological and mechanical comparison of di-and tri-block copolymer imine vitrimers, European Polymer Journal 219 (2024) 113402. https://doi.org/10.1016/j.eurpolymj.2024.113402.

[215] M. Capelot, M.M. Unterlass, F. Tournilhac, L. Leibler, Catalytic Control of the Vitrimer Glass Transition, ACS Macro Lett. 1 (2012) 789–792. https://doi.org/10.1021/mz300239f.

[216] H. Feng, S. Wang, J.Y.C. Lim, B. Li, W. Rusli, F. Liu, N. Hadjichristidis, Z. Li, J. Zhu, Catalyst-Free α-Acetyl Cinnamate/Acetoacetate Exchange to Enable High Creep-Resistant Vitrimers, Angewandte Chemie International Edition n/a (n.d.) e202400955. https://doi.org/10.1002/anie.202400955.

[217] P. Chakma, D. Konkolewicz, Dynamic Covalent Bonds in Polymeric Materials, Angewandte Chemie International Edition 58 (2019) 9682–9695. https://doi.org/10.1002/anie.201813525.

[218] Z.P. Zhang, M.Z. Rong, M.Q. Zhang, Polymer engineering based on reversible covalent chemistry: A promising innovative pathway towards new materials and new functionalities, Progress in Polymer Science 80 (2018) 39–93. https://doi.org/10.1016/j.progpolymsci.2018.03.002.

[219] M.M. Obadia, A. Jourdain, P. Cassagnau, D. Montarnal, E. Drockenmuller, Tuning the Viscosity Profile of Ionic Vitrimers Incorporating 1,2,3-Triazolium Cross-Links, Advanced Functional Materials 27 (2017) 1703258. https://doi.org/10.1002/adfm.201703258.

[220] W. Liu, D.F. Schmidt, E. Reynaud, Catalyst Selection, Creep, and Stress Relaxation in High-Performance Epoxy Vitrimers, Ind. Eng. Chem. Res. 56 (2017) 2667–2672. https://doi.org/10.1021/acs.iecr.6b03829.

[221] Q.-A. Poutrel, J.J. Blaker, C. Soutis, F. Tournilhac, M. Gresil, Dicarboxylic acid-epoxy vitrimers: influence of the off-stoichiometric acid content on cure reactions and thermo-mechanical properties, Polym. Chem. 11 (2020) 5327–5338. https://doi.org/10.1039/D0PY00342E.

[222] M. Kathan, P. Kovaříček, C. Jurissek, A. Senf, A. Dallmann, A.F. Thünemann, S. Hecht, Control of Imine Exchange Kinetics with Photoswitches to Modulate Self-Healing in Polysiloxane Networks by Light Illumination, Angewandte Chemie International Edition 55 (2016) 13882–13886. https://doi.org/10.1002/anie.201605311.

[223] F. Van Lijsebetten, Y. Spiesschaert, J.M. Winne, F.E. Du Prez, Reprocessing of Covalent Adaptable Polyamide Networks through Internal Catalysis and Ring-Size Effects, J. Am. Chem. Soc. 143 (2021) 15834–15844. https://doi.org/10.1021/jacs.1c07360.

[224] F.V. Lijsebetten, K.D. Bruycker, E.V. Ruymbeke, J.M. Winne, F.E.D. Prez, Characterising different molecular landscapes in dynamic covalent networks, Chem. Sci. 13 (2022) 12865–12875. https://doi.org/10.1039/D2SC05528G.

[225] M.A.B. Rusayyis, L. M. Fenimore, N. S. Purwanto, J. M. Torkelson, Reprocessable, creep-resistant covalent adaptable networks synthesized using conventional free-radical polymerization conditions with piperidine-based and non-piperidine-based dynamic dialkylamino disulfide chemistry, Polymer Chemistry 14 (2023) 3519–3534. https://doi.org/10.1039/D3PY00498H.

[226] H. Fang, X. Gao, F. Zhang, W. Zhou, G. Qi, K. Song, S. Cheng, Y. Ding, H.H. Winter, Triblock Elastomeric Vitrimers: Preparation, Morphology, Rheology, and Applications, Macromolecules 55 (2022) 10900–10911. https://doi.org/10.1021/acs.macromol.2c01711.

[227] S. Perrier, P. Takolpuckdee, C.A. Mars, Reversible Addition−Fragmentation Chain Transfer Polymerization: End Group Modification for Functionalized Polymers and Chain Transfer Agent Recovery, Macromolecules 38 (2005) 2033–2036. https://doi.org/10.1021/ma047611m.

[228] H.S. Wang, N.P. Truong, Z. Pei, M.L. Coote, A. Anastasaki, Reversing RAFT Polymerization: Near-Quantitative Monomer Generation Via a Catalyst-Free Depolymerization Approach, Journal of the American Chemical Society 144 (2022) 4678–4684. https://doi.org/10.1021/jacs.2c00963.

[229] J. Stouten, M.K.N. de Roy, K.V. Bernaerts, Synthesis and characterization of water-borne vanillin derived copolymers containing dynamic imine cross-links, Materials Today Sustainability 22 (2023) 100396. https://doi.org/10.1016/J.MTSUST.2023.100396.

[230] A.V. Ruzette, S. Tencé-Girault, L. Leibler, F. Chauvin, D. Bertin, O. Guerret, P. Gérard, Molecular Disorder and Mesoscopic Order in Polydisperse Acrylic Block Copolymers Prepared by Controlled Radical Polymerization, Macromolecules 39 (2006) 5804–5814. https://doi.org/10.1021/MA060541U.

[231] M. Fernández-García, J.L. De La Fuente, M. Fernández-Sanz, E.L. Madruga, Synthesis and characterization of PMMA-b-PBMA block copolymers by atom transfer radical polymerization, Journal of Applied Polymer Science 84 (2002) 2683–2691. https://doi.org/10.1002/app.10471.

[232] C. György, T.J. Neal, T. Smith, D.J. Growney, S.P. Armes, Tuning the Glass Transition Temperature of a Core-Forming Block during Polymerization-Induced Self-Assembly: Statistical Copolymerization of Lauryl Methacrylate with Methyl Methacrylate Provides Access to Spheres, Worms, and Vesicles, Macromolecules 16 (2022) 25. https://doi.org/10.1021/ACS.MACROMOL.2C00475/ASSET/IMAGES/LARGE/MA2C00475_0009.JPEG.

[233] C. Choi, S. Ahn, J.K. Kim, Diverse Morphologies of Block Copolymers by Blending with Homo (and Co) Polymers, Macromolecules 53 (2020) 4577–4580. https://doi.org/10.1021/ACS.MACROMOL.0C00545.

[234] K.R. Albanese, J.R. Blankenship, T. Quah, A. Zhang, K.T. Delaney, G.H. Fredrickson, C.M. Bates, C.J. Hawker, Improved Elastic Recovery from ABC Triblock Terpolymers, ACS Polym. Au 3 (2023) 376–382. https://doi.org/10.1021/acspolymersau.3c00012.

[235] H. Schmalz, A. Böker, R. Lange, G. Krausch, V. Abetz, Synthesis and Properties of ABA and ABC Triblock Copolymers with Glassy (A), Elastomeric (B), and Crystalline (C) Blocks, Macromolecules 34 (2001) 8720–8729. https://doi.org/10.1021/ma010875d.

[236] F.S. Bates, G.H. Fredrickson, Block Copolymers—Designer Soft Materials, Physics Today 52 (1999) 32–38. https://doi.org/10.1063/1.882522.

[237] C.M. Hansen, Hansen Solubility Parameters: A User's Handbook, Second Edition, 2nd ed., CRC Press, Boca Raton, 2007. https://doi.org/10.1201/9781420006834.

[238] S. Jiang, T.Y. Huang, K.M. Wang, B.Z. Tang, Q. Yu, A New Determination Method of the Solubility Parameter of Polymer Based on AIE, Molecules 22 (2017) 54. https://doi.org/10.3390/molecules22010054.

[239] R. Geyer, J.R. Jambeck, K.L. Law, Production, use, and fate of all plastics ever made, Sci. Adv. 3 (2017) e1700782. https://doi.org/10.1126/sciadv.1700782.

[240] C. Chen, X. Chen, L. Liu, J. Wu, C. Gao, Engineering Microorganisms to Produce Bio-Based Monomers: Progress and Challenges, Fermentation 9 (2023) 137. https://doi.org/10.3390/fermentation9020137.

[241] F. Pei, L. Liu, H. Zhu, H. Guo, Recent Advances in Lignocellulose-Based Monomers and Their Polymerization, Polymers 15 (2023) 829. https://doi.org/10.3390/polym15040829.

[242] R.M. Cywar, N.A. Rorrer, C.B. Hoyt, G.T. Beckham, E.Y.-X. Chen, Bio-based polymers with performance-advantaged properties, Nat Rev Mater 7 (2022) 83–103. https://doi.org/10.1038/s41578-021-00363-3.

[243] Q. Zhang, M. Song, Y. Xu, W. Wang, Z. Wang, L. Zhang, Bio-based polyesters: Recent progress and future prospects, Progress in Polymer Science 120 (2021) 101430. https://doi.org/10.1016/j.progpolymsci.2021.101430.

[244] J. van Schijndel, D. Molendijk, K. van Beurden, L.A. Canalle, T. Noël, J. Meuldijk, Preparation of bio-based styrene alternatives and their free radical polymerization, European Polymer Journal 125 (2020) 109534. https://doi.org/10.1016/j.eurpolymj.2020.109534.

[245] W. Zeng, Y. Jiang, X. Shan, J. Zhou, Engineering Saccharomyces cerevisiae for synthesis of β-myrcene and (E)-β-ocimene, 3 Biotech 13 (2023) 384. https://doi.org/10.1007/s13205-023-03818-2.

[246] J. Liu, R.C. Li, G.J. Sand, V. Bulmus, T.P. Davis, H.D. Maynard, Keto-Functionalized Polymer Scaffolds as Versatile Precursors to Polymer Side-Chain Conjugates, Macromolecules 46 (2013) 8–14. https://doi.org/10.1021/ma302183g.

[247] S.V. Suba, P. Sangavi, K. Nachammai, K. Langeswaran, Economics of Bioplastics and Biobased Products, in: Biodegradable Polymers, Blends and Biocomposites, CRC Press, 2024.

[248] B.A. Morris, The Science and Technology of Flexible Packaging, William Andrew Publishing, Oxford, 2022. https://doi.org/10.1016/B978-0-323-85435-1.00008-9.

[249] O. Adekomaya, T. Majozi, S. Adedoyin, Bio-based and Biodegradable Plastic Materials: Life Cycle Assessment, Springer International Publishing, Cham, 2020. https://doi.org/10.1007/978-3-030-11155-7_180-1.

[250] K.R. Albanese, J.R. Blankenship, T. Quah, A. Zhang, K.T. Delaney, G.H. Fredrickson, C.M. Bates, C.J. Hawker, Improved Elastic Recovery from ABC Triblock Terpolymers, ACS Polymers Au 3 (2023) 376–382. https://doi.org/10.1021/ACSPOLYMERSAU.3C00012/ASSET/IMAGES/LARGE/LG3C00012_0009.JPEG.

[251] C. Yuan, M.Z. Rong, M.Q. Zhang, Z.P. Zhang, Y.C. Yuan, Self-Healing of Polymers via Synchronous Covalent Bond Fission/Radical Recombination, Chem. Mater. 23 (2011) 5076–5081. https://doi.org/10.1021/cm202635w.

[252] K. Jin, L. Li, J. Torkelson, Recyclable Crosslinked Polymer Networks via One-Step Controlled Radical Polymerization, Advanced Materials 28 (2016). https://doi.org/10.1002/adma.201600871.

[253] T. Maeda, H. Otsuka, A. Takahara, Dynamic covalent polymers: Reorganizable polymers with dynamic covalent bonds, Progress in Polymer Science 34 (2009) 581–604. https://doi.org/10.1016/j.progpolymsci.2009.03.001.

[254] Y. Jia, G. Delaittre, M. Tsotsalas, Covalent Adaptable Networks Based on Dynamic Alkoxyamine Bonds, Macromolecular Materials and Engineering 307 (2022) 2200178. https://doi.org/10.1002/mame.202200178.

[255] A. Takahashi, R. Goseki, H. Otsuka, Thermally Adjustable Dynamic Disulfide Linkages Mediated by Highly Air-Stable 2,2,6,6-Tetramethylpiperidine-1-sulfanyl (TEMPS) Radicals, Angewandte Chemie International Edition 56 (2017) 2016–2021. https://doi.org/10.1002/anie.201611049.

[256] M. Aiba, T. Koizumi, K. Okamoto, M. Yamanaka, M. Futamura, Y. Ishigaki, M. Oda, C. Ooka, A. Takahashi, H. Otsuka, Effect of bulky 2,6-bis(spirocyclohexyl)-substituted piperidine rings in bis(hindered amino)trisulfide on thermal healability of polymethacrylate networks, Materials Advances 2 (2021) 7709–7714. https://doi.org/10.1039/D1MA00811K.

[257] L.M. Fenimore, B. Chen, J.M. Torkelson, Simple upcycling of virgin and waste polyethylene into covalent adaptable networks: catalyst-free, radical-based reactive processing with dialkylamino disulfide bonds, J. Mater. Chem. A 10 (2022) 24726–24745. https://doi.org/10.1039/D2TA06364F.

[258] A. Tsuruoka, A. Takahashi, D. Aoki, H. Otsuka, Fusion of Different Crosslinked Polymers Based on Dynamic Disulfide Exchange, Angewandte Chemie International Edition 59 (2020) 4294–4298. https://doi.org/10.1002/anie.201913430.

[259] H. Yokochi, R. Takashima, D. Aoki, H. Otsuka, Using the dynamic behavior of macrocyclic monomers with a bis(hindered amino)disulfide linker for the preparation of end-functionalized polymers, Polym. Chem. 11 (2020) 3557–3563. https://doi.org/10.1039/D0PY00366B.

[260] H. Sakai, T. Sumi, D. Aoki, R. Goseki, H. Otsuka, Thermally Stable Radical-Type Mechanochromic Polymers Based on Difluorenylsuccinonitrile, ACS Macro Lett. 7 (2018) 1359–1363. https://doi.org/10.1021/acsmacrolett.8b00755.

[261] F. Caffy, R. Nicolaÿ, Transformation of polyethylene into a vitrimer by nitroxide radical coupling of a bis-dioxaborolane, Polymer Chemistry 10 (2019) 3107–3115. https://doi.org/10.1039/C9PY00253G.

[262] A. Demongeot, R. Groote, H. Goossens, T. Hoeks, F. Tournilhac, L. Leibler, Cross-Linking of Poly(butylene terephthalate) by Reactive Extrusion Using Zn(II) Epoxy-Vitrimer Chemistry, Macromolecules 50 (2017) 6117–6127. https://doi.org/10.1021/acs.macromol.7b01141.

[263] M. Maaz, A. Riba-Bremerch, C. Guibert, N.J. Van Zee, R. Nicolaÿ, Synthesis of Polyethylene Vitrimers in a Single Step: Consequences of Graft Structure, Reactive Extrusion Conditions, and Processing Aids, Macromolecules 54 (2021) 2213–2225. https://doi.org/10.1021/acs.macromol.0c02649.

[264] J. Qiu, S. Ma, S. Wang, Z. Tang, Q. Li, A. Tian, X. Xu, B. Wang, N. Lu, J. Zhu, Upcycling of Polyethylene Terephthalate to Continuously Reprocessable Vitrimers through Reactive Extrusion, Macromolecules 54 (2021) 703–712. https://doi.org/10.1021/acs.macromol.0c02359.

[265] Y. Jia, H. Xie, J. Qian, Y. Zhang, H. Zheng, F. Wei, Y. Li, Z. Zhao, Recent Progress on the 3D Printing of Dynamically Cross-Linked Polymers, Advanced Functional Materials 34 (2024) 2307279. https://doi.org/10.1002/adfm.202307279.

[266] S. Kim, M.A. Rahman, M. Arifuzzaman, D.B. Gilmer, B. Li, J.K. Wilt, E. Lara-Curzio, T. Saito, Closed-loop additive manufacturing of upcycled commodity plastic through dynamic cross-linking, Science Advances 8 (2022) eabn6006. https://doi.org/10.1126/sciadv.abn6006.

[267] S. Choi, B. Park, S. Jo, J.H. Seo, W. Lee, D.-G. Kim, K.B. Lee, Y.S. Kim, S. Park, Weldable and Reprocessable Shape Memory Epoxy Vitrimer Enabled by Controlled Formulation for Extrusion-Based 4D Printing Applications, Advanced Engineering Materials 24 (2022) 2101497. https://doi.org/10.1002/adem.202101497.

[268] J.J. Schwartz, Additive manufacturing: Frameworks for chemical understanding and advancement in vat photopolymerization, MRS Bulletin 47 (2022) 628–641. https://doi.org/10.1557/s43577-022-00343-0.

[269] K.S. Anderson, K.M. Schreck, M.A. Hillmyer, Toughening Polylactide, Polymer Reviews 48 (2008) 85–108. https://doi.org/10.1080/15583720701834216.

[270] A. Zografos, E.M. Maines, J.F. Hassler, F.S. Bates, M.A. Hillmyer, Preparation and Characterization of H-Shaped Polylactide, ACS Macro Lett. 13 (2024) 695–702. https://doi.org/10.1021/acsmacrolett.4c00217.

[271] M.T. Martello, M.A. Hillmyer, Polylactide–Poly(6-methyl-ε-caprolactone)–Polylactide Thermoplastic Elastomers, Macromolecules 44 (2011) 8537–8545. https://doi.org/10.1021/ma201063t.

[272] K. Masutani, Y. Kimura, PLA Synthesis. From the Monomer to the Polymer, in: Poly(Lactic Acid) Science and Technology: Processing, Properties, Additives and Applications, The Royal Society of Chemistry, 2014: pp. 1–36. https://doi.org/10.1039/9781782624806-00001 (accessed December 7, 2024).

[273] Polylactic Acid Market Size, Share & Growth Report, 2030, Grand View Research (2024). https://www.grandviewresearch.com/industry-analysis/polylactic-acid-pla-market (accessed December 7, 2024).

[274] K. Masutani, Y. Kimura, PLA Synthesis. From the Monomer to the Polymer, (n.d.). https://books.rsc.org/books/edited-volume/1100/chapter/915860/PLA-Synthesis-From-the-Monomer-to-the-Polymer (accessed October 10, 2024).

[275] M.T. Martello, D.K. Schneiderman, M.A. Hillmyer, Synthesis and Melt Processing of Sustainable Poly(ε-decalactone)-block-Poly(lactide) Multiblock Thermoplastic Elastomers, ACS Sustainable Chem. Eng. 2 (2014) 2519–2526. https://doi.org/10.1021/sc500412a.

[276] Y.-B. Liu, L.-M. Peng, R.-Y. Bao, M.-B. Yang, W. Yang, Vitrimeric Polylactide by Two-step Alcoholysis and Transesterification during Reactive Processing for Enhanced Melt Strength, ACS Appl. Mater. Interfaces 14 (2022) 45966–45977. https://doi.org/10.1021/acsami.2c15595.

[277] B. Lessard, M. Marić, One-step poly(styrene-alt-maleic anhydride)-block-poly(styrene) copolymers with highly alternating styrene/maleic anhydride sequences are possible by nitroxide-mediated polymerization, Macromolecules 43 (2010) 879–885. https://doi.org/10.1021/MA902234T/ASSET/IMAGES/LARGE/MA-2009-02234T_0003.JPEG.

[278] D. Gigmes, J. Vinas, N. Chagneux, C. Lefay, T.N.T. Phan, T. Trimaille, P.-E. Dufils, Y. Guillaneuf, G. Carrot, F. Boué, D. Bertin, SG1 and BLOCBUILDER® technology: a versatile toolbox for the elaboration of complex macromolecular architectures, in: Controlled/Living Radical Polymerization: Progress in RAFT, DT, NMP & OMRP, American Chemical Society, 2009: pp. 245–262. https://doi.org/10.1021/bk-2009-1024.ch016.

[279] C. Veith, F. Diot-Néant, S. A. Miller, F. Allais, Synthesis and polymerization of bio-based acrylates: a review, Polymer Chemistry 11 (2020) 7452–7470. https://doi.org/10.1039/D0PY01222J.

[280] M.A. Droesbeke, R. Aksakal, A. Simula, J.M. Asua, F.E. Du Prez, Biobased acrylic pressure-sensitive adhesives, Progress in Polymer Science 117 (2021) 101396. https://doi.org/10.1016/j.progpolymsci.2021.101396.

[281] K. Jin, L. Li, J.M. Torkelson, Recyclable Crosslinked Polymer Networks via One-Step Controlled Radical Polymerization, Advanced Materials 28 (2016) 6746–6750. https://doi.org/10.1002/adma.201600871.

[282] K. Matsumoto, T. Iwata, M. Suenaga, M. Okudomi, M. Nogawa, M. Nakano, A. Sugahara, Y. Bannai, K. Baba, Mild Oxidation of Alcohols Using Soluble Polymer-Supported TEMPO in Combination with Oxone: Effect of a Basic Matrix of TEMPO Derivatives, HETEROCYCLES 81 (2010) 2539. https://doi.org/10.3987/COM-10-12027.

[283] K.R. Albanese, P.T. Morris, J.R. de Alaniz, C.M. Bates, C.J. Hawker, Controlled-Radical Polymerization of α-Lipoic Acid: A General Route to Degradable Vinyl Copolymers, Journal of the American Chemical Society 145 (2023) 22728–22734. https://doi.org/10.1021/jacs.3c08248.

[284] P.T. Morris, K. Watanabe, K.R. Albanese, G.T. Kent, R. Gupta, M. Gerst, J. Read de Alaniz, C.J. Hawker, C.M. Bates, Scalable Synthesis of Degradable Copolymers Containing α-Lipoic Acid via Miniemulsion Polymerization, J. Am. Chem. Soc. 146 (2024) 30662–30667. https://doi.org/10.1021/jacs.4c12438.

[285] K.R. Albanese, Y. Okayama, P.T. Morris, M. Gerst, R. Gupta, J.C. Speros, C.J. Hawker, C. Choi, J.R. de Alaniz, C.M. Bates, Building Tunable Degradation into High-Performance Poly(acrylate) Pressure-Sensitive Adhesives, ACS Macro Lett. 12 (2023) 787–793. https://doi.org/10.1021/acsmacrolett.3c00204.